Nonlinear Adaptive Estimation with Application To Sinusoidal Identification

Boli Chen

Department of Electrical and Electronic Engineering

Imperial College London

This dissertation is submitted for the degree of

Doctor of Philosophy

November 2015

I would like to dedicate this thesis to my loving parents and my wife

Declaration of Originality

I hereby declare that this thesis is the result of my own work, all material in this dissertation which is not my own work has been properly acknowledged.

Boli Chen
November 2015

Declaration of Copyright

Boli Chen
November 2015

Acknowledgements

This thesis is the result of research work carried out at the Department of Electrical and Electronic Engineering, Imperial College London. First and foremost, I would like to express deepest gratitude to my supervisor, Prof. Thomas Parisini, for giving me the opportunity to learn substantially from him the passion for science and for his excellent guidance, caring, patience, and providing me with an excellent atmosphere for doing research. Without his direction and persistent help this dissertation would not have been completed.

I wish to thank Gilberto Pin from Electrolux Professional S.p.A. for sharing his inspiration for the topic and for his invaluable advice throughout my works. I am very fortunate to have had him as a collaborator since the beginning of my PhD. I am indebted to Prof. Shu-Yuen Ron Hui and Wai Man Ng from Hong Kong University for their collaboration, priceless advice and assistance in practical implementations. They warmly welcomed me in Hong Kong when I visited and made a perfect environment for me to perform particular real-time experiments. A very special thank you to my friend Gabriele Donati from Danieli Automation S.p.A. where I worked for a very short duration but I gained precious experience on the steel making industry. I would not have been able to get through to the end of my PhD without the help I received from all of them.

Thanks to my friends and colleagues, Jingjing Jiang, Yilun Zhou, Yang Wang, Cheng Cheng, together with all the people of the control and power research group for the perfect environment you created and the fun we had in the spare times. I strongly believe that this work would have not been possible without them with whom I shared joyful moments as well as hard times in the past years.

Finally, I owe deepest gratitude towards my family, for their unceasing encouragement and support. Without them I could have never achieved any of these results.

Abstract

Parameter estimation of a sinusoidal signal in real-time is encountered in applications in numerous areas of engineering. Parameters of interest are usually amplitude, frequency and phase wherein frequency tracking is the fundamental task in sinusoidal estimation. This thesis deals with the problem of identifying a signal that comprises n ($n \geq 1$) harmonics from a measurement possibly affected by structured and unstructured disturbances. The structured perturbations are modeled as a time-polynomial so as to represent, for example, bias and drift phenomena typically present in applications, whereas the unstructured disturbances are characterized as bounded perturbation. Several approaches upon different theoretical tools are presented in this thesis, and classified into two main categories: asymptotic and non-asymptotic methodologies, depending on the qualitative characteristics of the convergence behavior over time.

The first part of the thesis is devoted to the asymptotic estimators, which typically consist in a pre-filtering module for generating a number of auxiliary signals, independent of the structured perturbations. These auxiliary signals can be used either directly or indirectly to estimate—in an adaptive way—the frequency, the amplitude and the phase of the sinusoidal signals. More specifically, the direct approach is based on a simple gradient method, which ensures Input-to-State Stability of the estimation error with respect to the bounded-unstructured disturbances. The indirect method exploits a specific adaptive observer scheme equipped with a switching criterion allowing to properly address in a stable way the poor excitation scenarios. It is shown that the adaptive observer method can be applied for estimating multi-frequencies through an augmented but unified framework, which is a crucial advantage with respect to direct approaches. The estimators' stability properties are also analyzed by Input-to-State-Stability (ISS) arguments.

In the second part we present a non-asymptotic estimation methodology characterized by a distinctive feature that permits finite-time convergence of the estimates. Resorting to the Volterra integral operators with suitably designed kernels, the measured signal is processed, yielding a set of auxiliary signals, in which the influence of the unknown initial conditions is annihilated. A sliding mode-based adaptation law, fed by the aforementioned auxiliary signals, is proposed for deadbeat estimation of the frequency and amplitude, which are dealt

with in a step-by-step manner. The worst case behavior of the proposed algorithm in the presence of bounded perturbation is studied by ISS tools.

The practical characteristics of all estimation techniques are evaluated and compared with other existing techniques by extensive simulations and experimental trials.

Table of contents

Notation

$\exists$	there exists
$\forall$	for all
$\in$	is an element of
$/'.$	define
!	factorial
$\mathbb{R}$	real numbers
$\mathbb{R}_{\geq 0}$	non-negative real numbers
$\mathbb{R}_{>0}$	strictly positive real numbers
$\mathbb{R}^n$	real valued n-vectors
$\mathbb{R}^{m \times n}$	real valued $m \times n$-matrices
$\mathbb{C}$	complex numbers
$\mathbb{Z}$	the set of integers
$\mathbb{Z}_{\geq 0}$	non-negative integers
$\mathbb{Z}_{>0}$	strictly positive integers
$\emptyset$	empty set
$\imath$	imaginary unit, $\sqrt{-1}$
$\|x\|$	Euclidean norm of x
$\|x\|_1$	L_1 norm $\sum_{i=1}^{n} \|x_i\|$
$\|x\|_\infty$	sup norm over a time-varying vector, $\sup_{t \geq 0} \|x(t)\|$
inf	infimum or greatest lower bound
sup	supremum or greatest upper bound
arg	argument or solution of an optimization problem
P	projection operator
I	the identity matrix
0	the null matrix
$\frac{d^i}{dt^i} u(t)$	i-th derivative of $u(t)$

Symbols used in the text

$v(t)$	a measurement perturbed by a structured and unstructured disturbance
$y(t)$	a measurement perturbed by a structured disturbance only
$\breve{y}(t)$	a stationary single sinusoidal signal
ω	angular frequency of a sinusoidal signal
Ω	square of the true frequency ω^2
a	amplitude of a sinusoidal signal
ϕ	phase of a sinusoidal signal
$d(t)$	an unstructured disturbance
ω_c	pre-filter coefficient related to the cutoff frequency of a low-pass filter
K_c	damping coefficient of the pre-filter
T_s	sampling period

Subscripts, superscripts and accents

$\hat{x}$	estimate
$\tilde{x}$	estimation error
x_0	initial state
$\breve{x}$	steady state, stationary signal
x_i	i-th component of the vector x

Acronyms and Abbreviation

AFP	Amplitude, frequency and phase
FFT	Fast Fourier transform
DFT	Discrete Fourier transform
PLL	Phase-locked-loop
ANF	Adaptative notch filtering
KF	Kalman filtering
EKF	Extended Kalman filtering
SOGI	Second order generalized integrator
OSG	Orthogonal signal generator
FLL	Frequency locked loop
SVF	State-variable filtering
AO	Adaptative observer
ISS	Input-to-State Stable
B-G	Bellman Gronwall (lemma)
LTI	Linear time invariant
LTV	Linear time varying SISO
	Single input single output MIMO Multi-input multi-output PE Persistently exciting
MF	Modulating function
BIBO	Bounded-input bounded-output
PE	Persistency of excitation
SVD	Singular value decomposition
w.r.t.	With respect to

List of figures

Chapter 1

INTRODUCTION

1.1 Background and Motivations

Consider the signal

$$\begin{cases} y(t) = \sum_{i=1}^{n} a_i \sin(\phi_i(t)) + \sum_{k=1}^{n_d} b_k t^{k-1} + d(t) \\ \dot{\phi}_i(t) = \omega_i \\ \phi_i(0) = \phi_{i0} \end{cases} \tag{1.1}$$

where for a given positive and known integer n_d, the term $\sum_{k=1}^{n_d} b_k t^{k-1}$ represents a time-polynomial structured exogenous measurement perturbation [1], with b_k unknown for any $k \in \{1, \ldots, n_d\}$, and where $d(t)$ characterizes an unstructured perturbation (referred to as *measurement noise* in the thesis). The structured measurement disturbances have a practical interest because they may incorporate bias and measurement drift up to any given order, the presence of which are commonly acknowledged in several practical applications (see [35]). For example, physical transducers and A/D converters are often affected by offsets that correspond to $n_d = 1$, while several sensing devices are influenced by temperature variations that cause drift phenomena (i.e., $n_d = 2$). Note that in principle n_d is the expected order of the structured perturbations, chosen a-priori by the designer (see Figure 1.1 for examples with $n_d = 1$ and $n_d = 2$, respectively).

The problem of estimating the amplitudes $a_i \in \mathbb{R}_{>0}$, the frequencies $\omega_i \in \mathbb{R}_{>0}$ and the phases $\phi_i(t) \in \mathbb{R}, t \in \mathbb{R}_{\geq 0}$ on the basis of the perturbed measurement (1.1) has drawn

[1] The given time-polynomial representation includes all the possible structured perturbation in a unified way. A reasonable SNR within a bounded time interval is ensured by proper weighting factors b_k. In the following chapters, we will show that the influence of the structured uncertainty (though unbounded as $t \to \infty$) is removable.

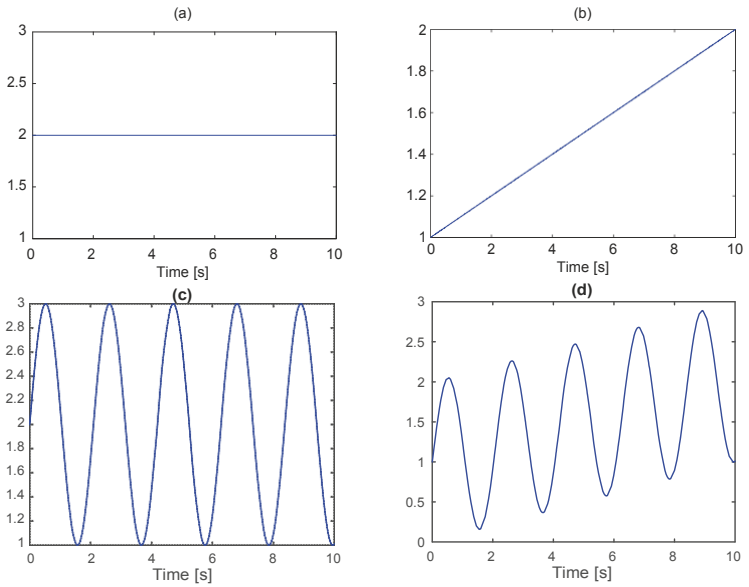

Fig. 1.1 Examples of structured perturbations: (a) $n_d = 1$, $b_1 = 2$ (i.e., Bias). (b) $n_d = 2$, $b_1 = 1$, $b_2 = 0.1$ (i.e., Drift). (c) A sinusoidal signal affected by the bias (a). (d) A signal affected by the drift (b).

considerable attention in the past few decades (see, for instance, the recent contributions [2, 8, 18, 28, 106]). In Fig. 1.2, this task of detecting the characteristics of sinusoidal signals, which is also referred to as an *AFP* problem in this thesis is illustrated. In the majority

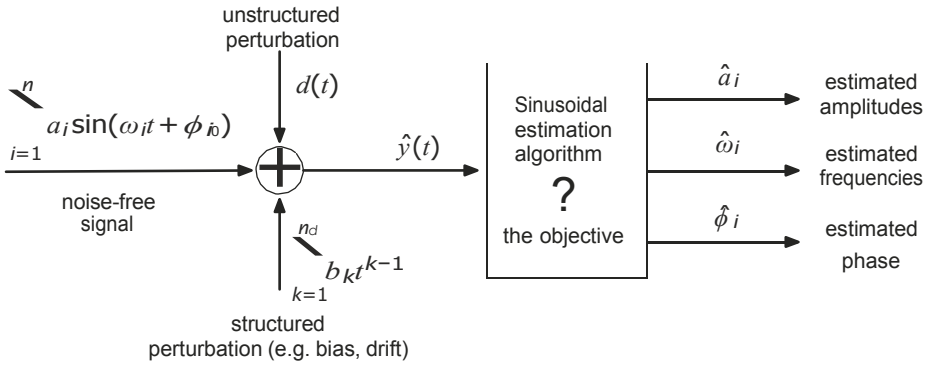

Fig. 1.2 Basic scheme of the sinuosidal estimation.

of the AFP problems, real-time frequency estimation is the fundamental issue since the amplitude and the phase can be identified afterwards. Contributions can be found with impact on specific application domains like vibrations suppression (see for example [10] and the references therein) and periodic disturbance rejection (see [9, 13, 68, 82, 109]) and power quality assessment (see for example [91] and the references cited therein). Specific examples of application can be found in the system of micro-power grids, the control units need to track

the frequency and phase variations of electrical signals with fast dynamics in order to ensure effective synchronization of the distributed power generators [11, 25, 26]. Moreover, the massive use of switched-mode power electronics circuits—that inject higher-order harmonics in the system—requires the development of phase-frequency-tracking techniques that, besides being fast compared to the time constants of the micro-generators, are robust with respect to large harmonic distortion and measurement noise. Another example is continuous casting which is a very important stage of the process of steel manufacturing. A typical setup of the control architecture in continuous casting plants is depicted in Fig. 1.3 (see [40]). One

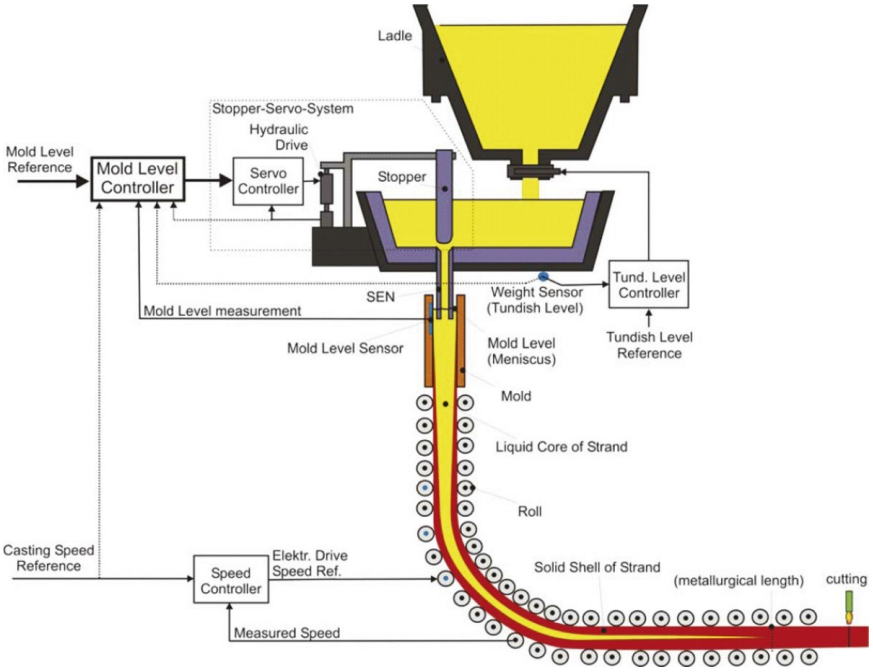

Fig. 1.3 Mould level control scheme in a steel continuous casting process (drawn from [40]).

of the most significant control problems in this setup concerns mould level control against disturbances that may affect the quality of the final products. In particular, the disturbance caused by the bulging phenomenon generates serious periodic level fluctuation, especially at high casting speed (see [40] and the references cited therein). Substantial research has been recently carried on in terms of advanced control schemes improving the rejection of bulging disturbance. An important component of these control architectures is the estimator of the bulging disturbance exploiting on-line measurement of the mold level fluctuations. In this thesis, we concentrate on the design of AFP estimators that are robust against various disturbances appear in the highlighted challenges, such as structured perturbations modeled as time-polynomial functions, harmonics and unstructured noises.

In the signal processing community there is a rich literature on the problem of frequencies detection, among which the Prony method, Fourier transform (e.g. FFT and DFT), Chirp Z transform, the contraction mapping method, adaptive least square methods and subspace method represent frequently used tools. The principles behind the methods are conceptually off-line in most cases or are devised for complex exponential sinusoidal signals, hence a detailed discussion of these methodologies is beyond the scope of the present work and the reader is referred to [39, 93, 102] and the references cited therein.

On the other hand, a wide variety of approaches for sinusoidal parameter estimation are already available in the systems and control community. These exploit concepts and tools such as phase-locked-loop (PLL), state-variable filtering, adaptive observers, adaptive notch filters (ANF) or Kalman/extended Kalman filters (KF/EKF). A comprehensive review of some techniques in these categories is carried out in next section.

1.2 Literature review

1.2.1 Kalman Filtering

The Kalman filter appears as one of the most attractive solutions, which has numerous applications in entire areas of engineering. Ever since the KF and EKF were applied in the field of frequency detection [101], a large amount of EKF-based frequency trackers have been proposed in the literature (see, for example [6, 97, 99] and the references cited therein). In principle, EKF is the nonlinear version of the KF, whereas its process essentially linearizes the nonlinear dynamics around the previous state estimates without any stability guarantee. As an example, a representation of the stochastic model for the parametric estimation of a single sinusoidal signal may be written as

$$\begin{bmatrix} a(k+1) \\ \phi(k+1) \\ \omega(k+1) \end{bmatrix} = \begin{bmatrix} 1 & 0 & 0 \\ 1 & T_s & \\ 0 & 0 & 1 \end{bmatrix} \begin{bmatrix} a(k) \\ \phi(k) \\ \omega(k) \end{bmatrix} + w_1(k)$$
$$y(k) = a(k)\sin(\phi(k)) + w_2(k) \tag{1.2}$$

where k denotes the discrete time step index with sampling period T_s, $a(k)$, $\phi(k)$, $\omega(k)$ and $y(k)$ represents the amplitude, phase, angular frequency and the extracted sinusoid at the time step index k. The random process $w_1(k)$ and $w_2(k)$ within the state and output equations are usually white noise characterized by their covariance matrices. In view of (1.2), the sinusoidal parameters can be retrieved iteratively by implementing the extended Kalman filter in a straightforward way.

Since the Kalman filter is extremely susceptible to model parameters, the relationship between its behavior and the tunable parameters has been investigated in [6, 97] to gain some heuristic guidelines. In the power system community, the KF or EKF still remain the preferred choice in several applications [91]. For instance, the EKF algorithms proposed in [50, 95] are shown to be effective in coping with the severely distorted signal in power systems, although the EKF frequency estimators are characterized by local stability only (see [98]). Recently, a new EKF-based frequency identifier that relies on a higher order state space representation, embedding the dynamics of amplitudes is presented in [44]. Compared to the standard EKF models, the integration of the amplitude's dynamics significantly improves the frequency tracking accuracy, especially in the case of a time-varying amplitudes. Last but not least, structured uncertainties, such as bias or drift, have not been addressed so far in the context of KF or EKF algorithms.

1.2.2 Phase-Locked-Loop

The Phase-Locked-Loop method and its many variants still represent the most used approach in many application contexts of electrical and electronic engineering for its ease of implementation in digital signal processing platforms and its robustness to environmental and measurement noise (see [3, 41, 48, 103] and the references cited therein). However, the conventional PLL exhibits the well-known double-frequency ripple phenomenon, which causes undesired oscillations on the reconstructed signal. In this connection, several modified PLL architectures are devised in the literature with the aim of improving the conventional PLL, such as magnitude PLL (MPLL) [110], enhanced PLL (EPLL) [59] and quadrature-PLL (QPLL) [57]. More specifically, the MPLL consists in providing the PLL of an outer adaptation loop which is in charge of estimating the amplitude of the input signal, while the QPLL is based on a mechanism that estimates quadrature amplitudes and frequency of the input signal. The applicability and benefits of the QPLL in the power and communication systems are surveyed in [53]. On the other hand, the enhanced PLL (EPLL) [59] along with its variants [62, 116] represents another class of successful approaches with particular focus on power and energy applications. A block diagram of the EPLL architecture is shown in Fig. 1.4, highlighted by the dashed rectangle. The dynamics of the amplitude, frequency and phase-angle estimates of the EPLL are given equations:

$$\begin{aligned} \dot{\hat{a}}(t) &= \mu_1 \sin(\hat{\phi}(t))\, e(t), \\ \dot{\Delta}_\omega(t) &= \mu_2 \cos(\hat{\phi}(t))\, e(t), \\ \dot{\hat{\phi}}(t) &= \omega_0 + \Delta_\omega(t) + \mu_3 \cos(\hat{\phi}(t))\, e(t), \\ e(t) &= v(t) - \hat{a}(t) \sin(\hat{\phi}(t)), \end{aligned} \tag{1.3}$$

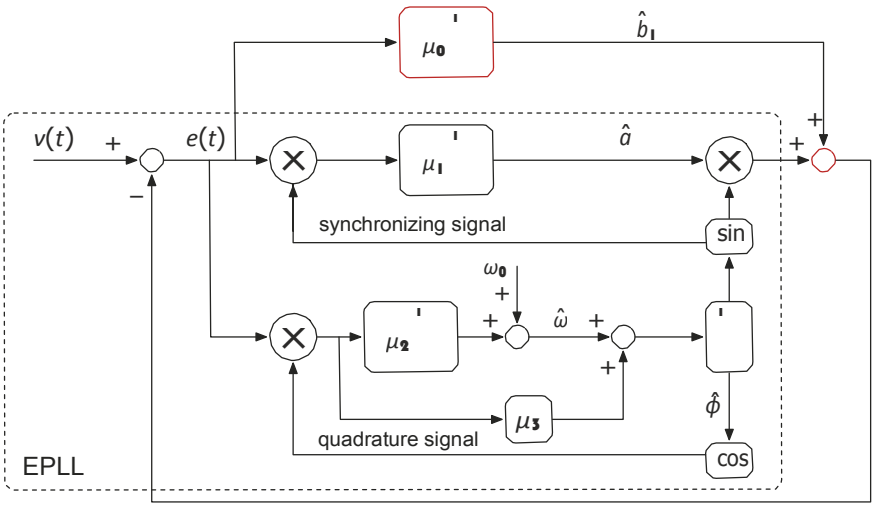

Fig. 1.4 Detailed scheme of the modified EPLL. Compared to the nominal EPLL scheme it contains an additional integrator for estimation of the DC component (highlighted by the red rectangles).

with the initial conditions $\hat{a}(0)$, $\hat{\phi}(0)$, $\Delta_\omega(0)$ and where $\Delta_\omega(t)$ represents the frequency correction term generated by the algorithm with respect to the nominal frequency ω_0, such that the estimated frequency is given by $\hat{\omega}(t) = \Delta_\omega(t) + \omega_0$. Substantial evaluations involving simulations and experiments can be found in [54] and [60], which justify their effectiveness in practical implementation. The stability properties of the EPLL dynamics have been studied in [61] resorting to the periodic orbit analysis by which *local stability* is proved. It is worth noting that in [115], mathematical analysis has been performed to evidence that the three PLL approaches emerging from different areas (see [110], [59] and [70] respectively) are intrinsically equivalent.

To address the structured disturbance shown in Fig. 1.2, the nominal EPLL has been augmented in [58] by another outer loop to estimate and reject the bias term through an additional integrator designed by (see Fig. 1.4):

$$\dot{\hat{b}}_1(t) = \mu_0\, e(t), \tag{1.4}$$

where $e(t) = v(t) - \hat{a}(t)\sin(\hat{\phi}(t)) - \hat{b}_1(t)$.

Finally, in multi-sinusoidal scenarios, a chain of PLLs are usually used. In [55], the devised multi-EPLL methodology that links n EPLL units within one “external" loop succeeds in extracting the harmonics and inter-harmonics from a multi-sinusoidal measurement. The problem becomes more challenging in case of an input with two frequencies that are close to each other. It has been shown in [88] that any two nearby frequencies can be discriminated by a two PLL configuration that is equipped with a de-correlator module. An alternative

solution is given in [43], where the estimates from two identifiers are separated by enforcing a minimum frequency interval. However, such de-correlation methods are hardly applicable for a number of harmonics larger than two. In spite of the popularity of the PLL techniques, the stability results available for the PLL nonlinear AFP algorithms provide, in most cases, only local stability guarantees, or, when averaging analysis is used, global results are valid only for small adaptation gains [61, 82, 110].

1.2.3 Adaptive Notch Filtering

Another significant category of techniques is the one concerning algorithms based on the adaptive notch filtering model that is characterized by constrained poles and zeros. In [92], a very important ANF estimator is proposed in a lattice-based discrete-time form, while the continuous time version is introduced in [9] for a typical application to sinusoidal disturbance rejection with unknown frequency. As reported in [5], the standard ANF model is either sensitive to the initial condition or subject to biased estimates depending on the positions of the poles and zeros. To remove such restrictions, a modified ANF-based frequency estimator that is capable to provide reliable estimates in the presence of colored noise, is presented in [5]. Thereafter, on the basis of [92], the first globally convergent ANF estimator (i.e., scaled normalized ANF) has been developed in [49], although the global property is guaranteed only for sufficiently small adaptation gain. In [71, 72], an improved version of the scaled normalized ANF that is also known as a second order generalized integrator (SOGI)-based frequency-locked-loop (FLL) is discussed. The stability results obtained by averaging theory only ensure local convergence. As can be seen in Fig. 1.5, the DC bias in the measurement can be handled by an augmented integral loop in addition to the nominal FLL, the revised ANF turn out to be a SOGI-based orthogonal signal generator (OSG-SOGI) [34, 58]), the associated frequency adaptation law of which is given by:

$$\begin{aligned}
\dot{\hat{b}}_1(t) &= k_0\,\hat{\omega}(t)\,e(t),\\
\dot{v}_1(t) &= -\hat{\omega}(t)v_2(t) + k\,\hat{\omega}(t)\,e(t),\\
\dot{v}_2(t) &= \hat{\omega}(t)\,v_1(t),\\
\dot{\hat{\omega}}(t) &= -\gamma e(t)v_2(t),\\
e(t) &= v(t) - v_1(t) - \hat{b}_1(t).
\end{aligned} \tag{1.5}$$

The OSG-SOGI structure is also studied in [28] and [31] for biased sinusoidal signals. In particular, the frequency adaptation law is integrated into the OSG-SOGI in [31], thus leading to a new extension, namely a third order generalized integrator-based OSG (OSG-TOGI). Moreover, the estimation problem for a multi-sinusoidal signal is addressed in [29] resorting

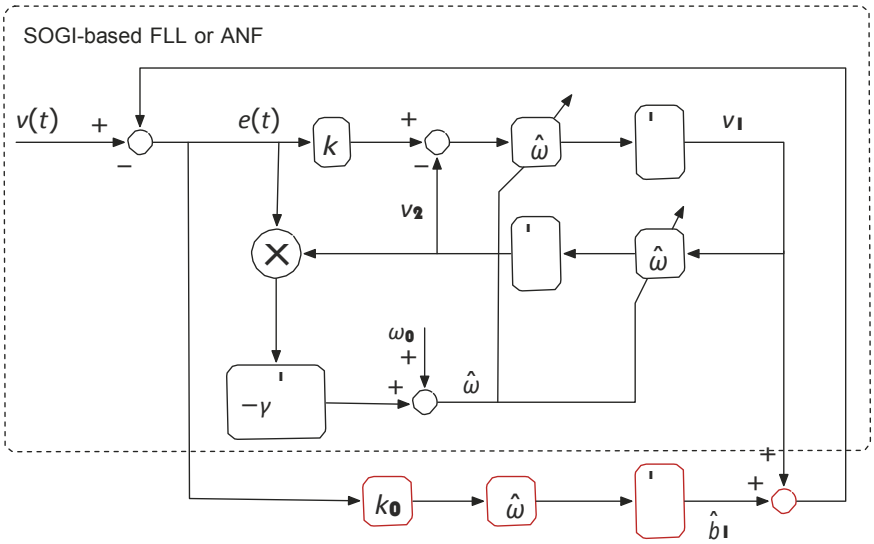

Fig. 1.5 Detailed scheme of the enhanced ANF. Compared to the nominal ANF scheme it contains the an additional integrator for estimation of the dc component (highlighted by red rectangles).

to a bank of such FLL filters, which ensures unbiased frequency estimates in the presence of a white noise.

It has been recently shown that the ANF is an effective alternative of PLL in many applications. More specifically, in [74] the ANF approach reported in [71, 72] is numerically evaluated and compared with the QPLL [53] in terms of some typical power system signals. To address a three phase system, three identical ANFs reported in [74] are combined in [77], the integrated architecture permits the use of all three-phase signals together, thus achieving a unique and accurate estimation of the frequency. It has been evidenced that such a new ANF based scheme significantly improves the performance of the conventional three-PLL mechanism (see [56, 94] and the references cited therein). Following the preliminary work (see [73, 75]), an improved work reported in [76] concerning a bank of ANF schemes has been shown advantageous from a computational perspective in comparison with the counterpart with respect to the PLL (see [55]). In order to avoid the interference, frequency limiters that determine the range of individual frequencies are exploited based on the a priori informations (i.e., precise bound of the frequencies) which, however, impose additional restrictions thus limiting the generality. Moreover, in [64, 81], multiple ANFs are linked in series rather than in parallel in order to prevent two or more estimators to converge to the same frequency. It is worth noting that this cascaded architecture works only when the amplitudes of the sinusoids can be sorted hierarchically, and it suffers from a so called "beating phenomena", due to the mutual interaction between the estimators.

For the sake of digital implementation, the discrete-time versions of the continuous-time FLL filters is introduced in [30] and [105], where the influences of sampling periods and discretization policies are studied. Although the discretization from a continuous-time algorithm is a fairly straightforward task, such an analysis is instrumental for the practical implementation in embedded systems.

1.2.4 State-Variable Filtering

In recent years, significant research activities have been devoted to nonlinear AFP algorithms involving the use of state-variable filtering (SVF) techniques. The SVF technique can be illustrated as follows. Consider a linear oscillator generating a single sinusoidal signal:

$$\ddot{y}(t) = -\Omega y(t), \tag{1.6}$$

where $y(t) := A\sin(\omega t + \phi_0)$ and $\Omega := \omega^2$. Auxiliary filtering techniques are used to generate the filtered input's derivatives for the construction of the frequency adaptation mechanisms. In this respect, the squared angular frequency is adapted, and then the frequency is estimated according to

$$\hat{\omega}(t) = \sqrt{\max\{0, \hat{\Omega}(t)\}}. \tag{1.7}$$

A simple third-order estimator is presented in [1] for pure sinusoidal signals, and later it was modified in [2] by adding a leakage correction term to the adaptation law (i.e., the so-called switching σ modification technique) to prevent estimation drifts in case of perturbed input. The main drawback of this approach is that the boundedness in a predetermined set is not guaranteed ("soft projection" is used [51, Chapter 3]). In [90], a minimum-order frequency estimator for biased sinusoidal signals is introduced; the method offers attenuation of the high-frequency noise in steady state thanks to the use of switching strategies. However, the switching algorithm has to be reset if the nominal frequency changes. Finally, in [8], the same research group presented a fourth-order frequency estimator bringing significant improvements in robustness compared to [90].

Another class of approaches based on SVF techniques concerns a specific pre-filtering module composed of a set of identical-cascaded first-order low pass filters. A method coping with a large class of structured perturbations parameterized in the family of time-polynomial functions is proposed in [86]. In the spirit of previous work on estimation of unbiased harmonic signals (see [89]), the robustness of the method against bounded unstructured perturbations (noise or additive exogenous signals having bounded amplitude) is characterized by Input-to-State-Stability analysis (also referred to ISS in this thesis). The ISS-Lyapunov tool also allows to assess the influences of the tunable parameters on the

transient performance of the frequency-estimator and on the practical convergence of the estimates toward a neighborhood of the true values in presence of non-fading perturbations. In [19, 23], a parallel pre-filtering system (extending the pre-filter used in [86, 89]) is designed. This enhanced structure allows to simplify the adaptation law introduced in [21, 86], while maintaining the stability properties.

1.2.5 Adaptive Observers

Methods based on adaptive observers yielding the simultaneous estimation of states and parameters constitute valid alternatives to the aforementioned techniques. The theoretical properties of these observers have been extensively characterized leading to global or semi-global stability results (see [7, 45] and the references therein). For example, the recent paper [20] extends the results presented in [21] (where both structured and unstructured uncertainties are addressed using suitable pre-filtering techniques) and deals with a "dual-mode" estimation scheme, in which a switching algorithm (depending on the real-time excitation level) is integrated into an adaptive observer-based sinusoidal estimator. In addition, the robustness against bounded unstructured disturbance is proved resorting to ISS arguments. The dynamic order of this estimator is equal to $6 + n_d$ with n_d the order of the time-polynomial structured perturbations (see (1.1)) that are assumed to possibly affect the input signal.

It is worth noting that the approaches based on adaptive observers can be extended to address multi-sinusoidal signals by state augmentation. Specifically, the frequency estimation problem is addressed by introducing a state space representation of the measured signal, in which the unknown frequencies are incorporated by a suitable linear parameterization. Typically, these algorithms do not provide direct estimates of the frequencies. Instead, the parameter adaptation laws are applied to a set of coefficients of the characteristic polynomial of the autonomous signal generator system:

$$P(s) = \prod_{k=1}^{n} (s^2 + \omega_i^2) = s^{2n} + \theta_{n-1} s^{2n-2} + \cdots + \theta_1 s^2 + \theta_0 \tag{1.8}$$

where s is the Laplace variable and $(\theta_0, \theta_1, \cdots, \theta_{n-1})$ are the parameters undergoing adaptation. The frequency estimates are determined as the zeros of the characteristic polynomial. The first global adaptive observer-based estimator for estimating n frequencies is proposed in [67] with dynamic order $5n - 1$ ($5n$ for the biased case), whereas the dimension of the adaptive observer is reduced to $3n$ ($3n+1$ for the biased case) in [46, 47, 80, 111] at the price of a slight degradation of the convergence properties. Moreover, on the basis of the algorithm

given in [15] dealing with a methodology with minimum order $3n - 1$ ($3n$ with bias), the frequency estimation problems of single sinusoidal signals [16] and multi-frequency signals [17, 18] with saturated amplitudes are addressed via hybrid systems tools (see [42]).

Alternative schemes in multi-frequency estimation are based on multiple ANFs and PLLs in parallel. The major issue of such schemes based on banks of adaptive filters in parallel is the interference between estimators. The adaptive observer approach circumvents this restriction by estimating the frequencies in a single adaptive system framework, thereby resulting in an indirect frequency adaptation. The drawback is the computational burden in the presence of a large number of sinusoids, thus restricting the application in practice. In this respect, a direct adaptation scheme is designed in [22] with semi-globally exponential convergence guaranteed thanks to an adaptive observer framework with state-affine linear parameterization (see [84]).

Theoretically, an arbitrarily large number of sinusoids can be handled by multi-sinusoidal estimators with properly set order. However, it is commonly acknowledged that the performance deteriorates as the number of sinusoids grows. In addition to the above limitation in multi-sinusoidal estimation, the parameter estimation (e.g. frequencies) problem of a generic periodic signal with a possibly infinite number of harmonics can not be recast in a traditional adaptive observer or be solved by multiple PLLs and ANFs. In this respect, most research efforts only focus on the detection of the fundamental frequency. The PLL and ANF tools, that are originally conceived for parameter extraction of a single sinusoid, are shown also to be effective in the presence of a generic periodic signal comprised of arbitrary (possibly infinite) number of harmonics (see [71, 72, 110]). On the other hand, the internal model principle proposed by Francis and Wonham [37, 38] also plays an important role in periodic signal estimation. In [12], an adaptive internal model parametrized by the frequency of the periodic input is embedded in a fictitious closed-loop system, giving rise to a novel estimation algorithm. Moreover, the stochastic analysis performed in [113] verifies the robustness of [12] with respect to additive white noise. Alternatively, [32] deals with an adaptive 'quasi' repetitive control (RC) scheme for asymptotic tracking of the fundamental frequency of a periodic signal. The time-delay of the RC is steered on-line to the period of the input by a FLL, thereby improving the accuracy by mitigating the effect of the harmonics other than the fundamental. Nevertheless, the stability analysis of the aforementioned methods is local and is based on singular perturbation or averaging theory. Recently, a globally convergent fundamental frequency estimator is proposed [69] using an adaptive observer of order 10 (see [67]). Moreover, it is shown in [24] that another adaptive observer framework presented in [21] can be generalized, producing a valid alternative for global frequency estimation where the minimum-dynamic order is reduced to 8.

1.2.6 Estimators with Finite-Time Convergence

Despite the numerous sinusoidal estimators available in the literature, only a few of them can drive the estimation error to 0 within a finite time, which is a desirable feature in control applications. A deadbeat frequency estimation method is first proposed in [107] based on the concept of algebraic derivatives, and this methodology is extended in [106] by processing a measured signal corrupted by an unknown bias. Although the method in [106] is capable to address the AFP problem with instantaneous convergence by taking quotients, re-initialization may needed due to the presence of singularities at certain time instants. This issue has been tackled in [65] and [66] by means of recursive least squares algorithms, while preserving the deadbeat property. In [108], the algebraic identification approach [107] is further extended to address the parameter estimation of two sinusoidal signals from a perturbed measurement. Besides, a modulating function (MF)-based approach is presented in [33], which allows non-asymptotic frequency detection by processing the input with suitably truncated periodic functions. Moreover, it has been shown in a recently proposed FLL framework [34] that the convergence speed and steady state accuracy are enhanced by employing the MF method [33] for the adjustment of the resonant frequency.

As shown in the very recent papers [83, 87] (dealing with non-asymptotic continuous-time systems identification), Volterra operators turn out to be an effective tool for finite-time estimation. Resorting to such kernel based-linear integral operators, a novel finite-time frequency identifier is presented in [85], implementing a variable-structure adaptation law based on a sliding mode technique. Instantaneous convergence gets lost in this way, but a major improvement in robustness to measurement noise is attained while keeping the deadbeat property with tunable finite-time convergence rate. This is the first finite-time convergent frequency estimator, the behavior of which is analyzed also in the presence of unstructured (though bounded) measurement perturbations.

1.3 Aims and Contributions

1.3.1 Research Challenges in Sinusoidal Estimation

We now list the most significant challenges in sinusoidal estimation that this thesis will address.

- *Global stability*. Global stability is an important property for sinusoidal estimators. Although global or semi-global stability has been theoretically proved in methods based on adaptive observers, this property is not available in some practical AFP tools, e.g., PLL and ANF due to the use of averaging analysis.

- *Robustness and accuracy*. The works concerning the AFP estimation in the presence of bias is vast, yet there is a lack of a comprehensive investigation for the perturbations other than the bias, e.g. drifts, harmonics and unstructured perturbations, which are also often encountered in practice.
- *Digital implementation*. In most cases, AFP methods are devised in a continuous-time setting which is useful in terms of a possible analog implementation in electronics and power engineering application contexts. In this connection, one of the issues that deserve further investigation from a practical perspective is the steady-state bias in the frequency estimate caused by the discretization of the continuous-time algorithms.
- *Persistency of excitation*. The persistency of excitation (PE) assumption usually plays a key role in AFP estimation. It is assumed in standard estimation tools to guarantee that the estimated sinusoids are sufficiently informative in the presence of additive disturbances. The loss of excitation is a phenomenon that has not been widely addressed.
- *Multi-sinusoidal signal estimation*. Existing methods in the literature are either *locally* convergent (refer to PLLs and ANFs in parallel) or less efficient due the *indirect* estimation (refer to AO methods).
- *Finite-time (instantaneous) estimation* . Despite the large number of AFP techniques, the currently available literature is still short of the deadbeat AFP estimators. This type of estimators are needed in typical scenarios where the estimates are required to converge in a neighborhood of the true values within a predetermined finite time, independently from the unknown initial conditions.

1.3.2 Contribution of the Thesis

The main objective of this thesis consists in providing reliable tools to estimate the amplitude, frequency and phase of sinusoidal signals in real time from a given perturbed measurement (1.1) with known n. This includes AFP estimation of a single (i.e., $n = 1$ in (1.1)) or multiple sinusoidal signal (i.e., $1 < n < +\infty$), and even fundamental frequency tracking of a generic periodic signal that is the sum of an arbitrary (possibly infinite) number of sinusoids (i.e., $n \to \infty$). The thesis consists of two main parts. Part I regards estimators with asymptotic convergence property, whereas Part II is devoted to the non-asymptotic detection of a sinusoidal signal. The contribution of each chapter is briefly outlined in the following.

In Chapter 2, a specific state variable filtering tool, which plays an important role in the presented AFP approaches, is introduced (see for example [20, 86]). Thanks to the

pre-filtering stage that is configured by cascaded 1-st order low-pass filters, structured perturbations with arbitrary order are addressed in a consistent way. Thereafter, we propose a fundamental frequency estimator that is based on a suitable adaptive observer, which is characterized by ISS properties in the presence of a class of disturbances, such as structured perturbations modeled as time-polynomial functions, harmonics and unstructured disturbances [20, 24]. The estimator is equipped with a switching criterion enabling the adaptation only when the excitation condition is fulfilled, thus preventing a possible drift of the estimates in poor excitation conditions. Although the discretization gives rise to a biased equilibrium, a post-correction scheme for the proposed methodology is proposed.

In Chapter 3, the basic AO method is extended to identify n unknown frequencies embedded in a biased signal. In contrast with existing methods, the nonlinear AO allows the frequency estimates to be updated *directly* while guaranteeing *semi-global* stability property (proved resorting to ISS tools). Moreover, the proposed algorithm is able to tackle the problem of overparametrization (when the internal model accounts for a number of sinusoids that is greater than the actual spectral content) or temporarily fading sinusoidal components by a specific switching criterion: the parameter adaptation scheme with respect to n frequencies is controlled by an n-dimensional excitation-based switching logic, that enables the update of a parameter only when the measured signal is sufficiently informative.

Chapter 4 deals with an enhanced pre-filtering configuration, in which the signals produced by the pre-filtering modules are employed directly for constructing estimation algorithms. In contrast with the AO approach illustrated in Chapter 2, this simplified algorithm relieves the computation burden whilst still enjoying ISS stability properties with respect to bounded measurement perturbations.

Finally, in Chapter 5, a deadbeat parametric identifier for biased and perturbed sinusoidal signals is presented (see [85]). Thanks to Volterra integral operators with suitably designed kernels, a set of auxiliary signals (regardless of the unknown initial conditions) are produced by processing the measured signal. These auxiliary signals are exploited for the amplitude and frequency adaptation, yielding a sliding mode-based methodology that ensures finite-time convergence of the estimation error. It is worth noting that another significant contribution consists in the investigation for the worst case behavior of the algorithm in the presence of bounded additive disturbances; this analysis is currently missing in the literature.

1.3.3 Publications

The research results illustrated in the thesis have been published or are currently under review in several archival journals . These results have been also presented in several international conferences. The list of these publications is reported in the following.

- Papers in international journals

  1. G. Pin, B. Chen, T. Parisini, and M. Bodson, "*Robust Sinusoid Identification with Structured and Unstructured Measurement Uncertainties*," IEEE Trans. Automatic Control, vol. 59, no. 6, 2014, pp. 1588-1593.
  2. B. Chen, G. Pin, W. M. Ng, C. K. Lee, S. Y. R. Hui, and T. Parisini, "*An Adaptive Observer-based Switched Methodology for Identification of a Perturbed Sinusoidal Signal: Theory and Experiments*," IEEE Trans. Signal Processing, vol. 62, no. 24, 2014, pp. 6355-6365
  3. B. Chen, G. Pin, W. M. Ng, S. Y. R. Hui, and T. Parisini, "*A Parallel Pre-filtering Approach for the Identification of a Biased Sinusoid Signal: Theory and Experiments*," International Journal of Adaptive Control and Signal Processing, 2015

- Papers included in proceedings of international conferences

  1. B. Chen, G. Pin, and T. Parisini, "*Adaptive observer-based sinusoid identification: structured and bounded unstructured measurement disturbances*," in Proc. of the European Control Conference, Zurich, 2013, pp. 2645-2650.
  2. G. Pin, B. Chen and T. Parisini, "*A Nonlinear Adaptive Observer with Excitation-based Switching*," in Proc. of the Conference on Decision and Control, Florence, 2013, pp. 4391-4398.
  3. B. Chen, G. Pin, and T. Parisini, "*An adaptive observer-based estimator for multi-sinusoidal signals*," in Proc. of the American Control Conference, Portland, OR, 2014, pp. 3450–3455.
  4. B. Chen, G. Pin and T. Parisini, "*Robust Parametric Estimation of Biased Sinusoidal Signals: a Parallel Pre-filtering Approach*," in Proc. of the Conference on Decision and Control, Los Angeles, California, 2014.
  5. B. Chen, G. Pin, and T. Parisini, "*Frequency Estimation of Periodic Signals: an Adaptive Observer approach*," in Proc. of the American Control Conference, Chicago, IL, 2015.
  6. G. Pin, B. Chen and T. Parisini, "*The Modulation Integral Observer for Linear Continuous-Time Systems*," in Proc. of the European Control Conference, Linz, 2015.

7. G. Pin, B. Chen and T. Parisini, "*Deadbeat Kernel-based Frequency Estimation of a Biased Sinusoidal Signal*," in Proc. of the European Control Conference, Linz, 2015.
8. G. Pin, Yang Wang, Boli Chen, and Thomas Parisini, "*Semi-Global Direct Estimation of Multiple Frequencies with an Adaptive Observer having Minimal Parameterization*," in Proc. of the Conference on Decision and Control, Osaka, Japan, 2015.

- Papers currently under review

1. B. Chen, G. Pin, W. M. Ng, S. Y. R. Hui, and T. Parisini, "*An Adaptive Observer-based Estimator for Multi-sinusoidal Signals*," IEEE Trans. Automatic Control.
2. G. Pin, B. Chen, and T. Parisini, "*Robust Finite-Time Estimation of Biased Sinusoidal Signals: A Volterra Operators Approach*," Automatica.
3. B. Chen, G. Pin, W. M. Ng, T. Parisini, and S. Y. R. Hui, "*A Fast-Convergent Modulation integral Observer for Online Detection of the Fundamental and Harmonics in Active Power Filters*," IEEE Trans. on Power Electronics.

1.4 Preliminaries

The purpose of this section is to provide the reader with the basic notations, definitions and assumptions that are employed throughout the thesis, in order to set a consistent framework. More specific definitions and assumptions that are not included in this section will be introduced in the relevant parts of the thesis.

Let $M \in \mathrm{R}^{n\times m}$ be a matrix. M^{T} denotes the transpose of M while $\sigma(M)$ denotes the set of singular values of M. Let $\overline{\sigma}(M)$ be the maximum singular value of M, whereas $\underline{\sigma}(M)$ be the minimum singular value of M, then $\|M\|$ denotes the induced 2-norm of M, that is $\|M\| = \overline{\sigma}(M)$.

Let $M \in \mathrm{R}^{n\times n}$ be a symmetric matrix, such that $M^{\mathsf{T}} = M$. The notations M^{-1}, $\det(M)$ and $\mathrm{tr}(M)$ are used to respectively denote the inverse, determinant and trace of M. The set of eigenvalues values of M is denoted by $\lambda(M)$. Similarly, $\overline{\lambda}(M)$ is the maximum eigenvalues value of M, whereas $\underline{\lambda}(M)$ is the minimum eigenvalues value of M.

Definition 1.4.1 (Positive Definite Matrix) *[96] A symmetric matrix $M \in \mathrm{R}^{n\times n}$ is positive definite if and only if any one of the following conditions holds:*

1. $\lambda_i(M) > 0,\ i = 1, 2, \cdots, n.$

2. *There exists a nonsingular matrix* M_1 *such that* $M = M_1 M_1^\top$.

3. *Every principal minor of M is positive.*

4. $x^\top M x \geq \alpha |x|^2$ *for some* $\alpha > 0$ *and* $\forall\, x \in \mathrm{R}^n$

A symmetric matrix $M \in \mathrm{R}^{n\times n}$ has n orthogonal eigenvectors and can be decomposed as

$$M = U^\top \Lambda U \tag{1.9}$$

where U is a unitary (orthogonal) matrix (i.e., $U^\top U = I$) with the eigenvectors of M and Λ is a diagonal matrix composed of the eigenvalues of M. Moreover, a matrix M is negative definite if $-M$ is positive definite.

Theorem 1.4.1 *[52] Let* $M \in \mathrm{R}^{n\times n}$. *The following statements are equivalent:*

1. *all the eigenvalues of* M *have negative real part;*

2. *for all matrices* $Q = Q^\top > 0$ *there exists an unique solution* $P = P^\top > 0$ *to the following (Lyapunov) equation:*

$$M^\top P + PM + Q = 0$$

Definition 1.4.2 *[63] A continuous function* $\alpha(r) : \mathrm{R}_{\geq 0} \to \mathrm{R}_{\geq 0}$ *belongs to the class* K *if it is continuous, strictly increasing and* $\alpha(0) = 0$. *If, in addition* $\lim_{r\to\infty} \alpha(r) = \infty$ *then it belongs to the class* K_∞.

Definition 1.4.3 *[63] A continuous function* $\beta : \mathrm{R}_{\geq 0} \times \mathrm{R}_{\geq 0} \to \mathrm{R}_{\geq 0}$ *belongs to the class* KL *if, for any fixed* $t \in \mathrm{R}_{\geq 0}$, *the function* $\beta(\cdot\,, t)$ *is a* K*-function with respect to the first argument and if, for any fixed* $r \in \mathrm{R}_{\geq 0}$, *the function* $\beta(r, t)$ *is monotonically decreasing with respect to* t *and* $\lim_{t\to\infty} \beta(r, t) = 0$.

Definition 1.4.4 (Piecewise Continuity) *[63] A function* $f : [0, \infty) \to \mathrm{R}$ *is piecewise continuous on* $[0, \infty)$ *if* f *is continuous on any finite interval* $[t_0, t_1] \subset [0, \infty)$ *except for a finite number of points.*

Definition 1.4.5 (Lipschitz) *[96] A function* $f : [\underline{x}, \overline{x}] \to \mathrm{R}$ *is Lipschitz on* $[\underline{x}, \overline{x}]$ *if* $|f(x_1) - f(x_2)| \leq \kappa |x_1 - x_2|$, $\forall\, x_1, x_2 \in [\underline{x}, \overline{x}]$, *where* $\kappa \geq 0$ *is a constant referred to as the Lipschitz constant.*

Consider the following dynamical system

$$\dot{x} = f(x, u) \tag{1.10}$$

with $x \in \mathbb{R}^n, u \in \mathbb{R}^m, f(0,0) = 0$ and $f(x,u)$ locally Lipschitz in $\mathbb{R}^n \times \mathbb{R}^m$.

Definition 1.4.6 (ISS) *[63] The system (1.10) is ISS (Input-to-State Stable) if there exist a* $\mathcal{KL}$*-function* $\beta(\cdot,\cdot)$ *and a class* $\mathcal{K}$*-function such that, for any input* $u \in \mathbb{R}^m$ *and any initial condition* $x_0 \in \mathbb{R}^n$*, the trajectory of the system verifies*

$$|x(t)| \leq \beta(|x_0|, t) + \gamma(\|u\|_\infty) \tag{1.11}$$

Definition 1.4.7 (ISS-Lyapunov Function) *[63] A function* $V : \mathbb{R}^n \to \mathbb{R}_{\geq 0}$ *of class* $\mathcal{C}^1$ *is an ISS-Lyapunov function for (1.10) if there exist three* $\mathcal{K}_\infty$*-functions* $\underline{\alpha}(\cdot)$, $\overline{\alpha}(\cdot)$, $\alpha(\cdot)$ *and a* $\mathcal{K}$*-function* $\chi(\cdot)$ *such that*

$$\underline{\alpha}(|x|) \leq V(x) \leq \overline{\alpha}(|x|), \quad \forall x \in \mathbb{R}^n \tag{1.12}$$

and

$$|x| \geq \chi(|u|) \Rightarrow \frac{\partial V}{\partial x} f(x,u) \leq -\alpha(|x|), \ \forall x \in \mathbb{R}^n, \ \forall u \in \mathbb{R}^m \tag{1.13}$$

Theorem 1.4.2 ([63]) *The system (1.10) is ISS if and only if it admits an ISS-Lyapunov function.* □

Definition 1.4.8 *[96] The set* $\mathcal{L}_q$, $q \in \{1, 2, \cdots\}$, $q < \infty$, *consists of all the measurable functions* $f : \mathbb{R}_{\geq 0} \to \mathbb{R}$ *that satisfy*

$$\int_0^\infty \|f(t)\|^q dt < \infty$$

Moreover $\left(\int_0^\infty \|f(t)\|^q dt\right)^{\frac{1}{q}}$ *is the* $\mathcal{L}_q$ *norm of the function* $f \in \mathcal{L}_q$. *If* $q = \infty$, *the set* $\mathcal{L}_\infty$ *consists of all measurable functions* $f : \mathbb{R}_{\geq 0} \to \mathbb{R}$ *which are bounded, namely*

$$\sup_{t \in \mathbb{R}_{>0}} \|f(t)\| < \infty$$

with norm $\|f\|_\infty = \sup_{t \in \mathbb{R}_{>0}} \|f(t)\|$

Lemma 1.4.1 (Bellman-Gronwall's Inequality-differential form) *Let* $\mathcal{T} = [t_0, t_1]$. *Suppose* g*:* $\mathcal{T} \to \mathbb{R}$ *and* h*:* $\mathcal{T} \to \mathbb{R}$ *are continuous, and suppose* u*:* $\mathcal{T} \to \mathbb{R}$ *is in* $\mathcal{C}^1(\mathcal{T})$ *and*

satisfies

$$\dot{u}(t) \leq g(t)u(t) + h(t) \text{ for } t \in \mathsf{T}, \text{ and } u(t_0) = u_0.$$

Then

$$u(t) \leq u_0 e^{\int_{t_0}^{t} g(s)ds} + \int_{t_0}^{t} e^{\int_{s}^{t} g(\tau)d\tau} h(s)ds \tag{1.14}$$

Moreover, let us introduce following assumptions on the main problem formulated in (1.1):

Assumption 1 (Boundedness of the Disturbance) *The unstructured measurement noise* $d(t)$ *defined in (1.1) is subject to an a-priori known bound* $\bar{d}$*, that is*

$$|d(t)| \leq \bar{d}, \quad t \in \mathsf{R}_{\geq 0}. \tag{1.15}$$

Assumption 2 (Boundness and Uniqueness of the Frequencies) *The frequencies of the sinusoids in (1.1) are all unique strictly-positive time-invariant parameters, bounded by a positive constant* $\bar{\omega}$*, such that* $\omega_i > 0$*,* $\omega_i \neq \omega_j$ *for* $i \neq j$ *and*

$$\omega_i < \bar{\omega}, \ \forall i \in \{1, \cdots, n\}. \tag{1.16}$$

Part I

ASYMPTOTIC ESTIMATORS

Chapter 2

ADAPTIVE OBSERVER APPROACH: THE SINGLE SINUSOIDAL CASE

2.1 Introduction

In this chapter, the AFP estimation of a single sinusoidal signal from a measurement affected by structured and unstructured disturbances is addressed. Let us recall the generic sinusoidal measurement (1.1) and let $n = 1$, consequently forming the available signal as follows:

$$v(t) = y(t) + \sum_{k=1}^{n_d} b_k t^{k-1} + d(t), \quad t \in \mathbb{R}_{\geq 0}, \tag{2.1}$$

where $y(t)$ represents the stationary sinusoidal signal described by

$$\begin{cases} y(t) = a \sin(\phi(t)), \\ \dot{\phi}(t) = \omega, & t \in \mathbb{R}_{\geq 0}, \\ \phi(0) = \phi_0, \end{cases} \tag{2.2}$$

with unknown amplitude, angular frequency and phase respectively denoted by a, ω, and ϕ, wherein $\omega < \bar{\omega}$ according to Assumption 2. Note that the choice of n_d is not unique. For instance, a bias is involved with all $n_d \geq 1$. Therefore, in case of a sensing devise affected by uncertain perturbations, a proper choice of n_d has to be carried out depending on the a-priori knowledge about the possible structured uncertainties in the specific application. In addition, $d(t)$ is subject to the constraint (1.15) given in Assumption 1.

In the works [21, 86, 89], a set of cascaded first-order low-pass (LP) filters, called "pre-filter" is exploited with the aim of both canceling the effect of structured "time-polynomial" perturbations (such as bias and linear drift) and obtaining auxiliary signals for AFP detection.

The said signals can be used either *directly* (see [89] and [86]) or *indirectly* (see [21]) to estimate the unknown parameters of the measured sinusoid with high noise immunity.

This chapter deals with a class of sinusoidal estimators that employ the auxiliary pre-filtered signal *indirectly* resorting to a specific adaptive observer system. The behavior of the approach against various types of disturbances is characterized by a comprehensive robustness analysis. In Sec. 2.3, we will start from a problem formulated by (2.1) based on some preliminary results in [21], a "dual-mode" estimation scheme is dealt with by incorporating a switching algorithm (depending on the real-time excitation level) into an adaptive observer-based sinusoidal estimator. In comparison with the typical adaptive estimators relying on an integral-type persistency of excitation condition (see, for instance, [8, 67, 111]), the devised method allows to check the excitation level in real-time which might be advantageous from a computational perspective. The stability properties of the devised method are rigorously analyzed in terms of ISS arguments thus coping with bounded measurement noise.

In Sec. 2.4, we study the behavior of the introduced AO estimator in the scenario where the input is corrupted by a series of harmonics of the fundamental. Consider a bounded piecewise continuous periodic signal $y(t)$ of unknown frequency ω, that can be expressed in terms of its Fourier harmonic components as follows:

$$\begin{aligned} y(t) &= \frac{a_0}{2} + \sum_{n=1}^{\infty} [a_{1,n}\cos(n\omega t) + a_{2,n}\sin(n\omega t)] \\ &\quad \frac{a_0}{2} + a_{1,n}\cos(\omega t) + a_{2,n}\sin(\omega t) + h(t) \\ &= \frac{a_0}{2} + \sum_{n=1}^{\blacksquare} \sqrt{a_{1,n}^2 + a_{2,n}^2}\sin(\omega t + \phi_0) + h(t), \quad t \in \mathbb{R}_{\geq 0} \end{aligned} \tag{2.3}$$

in which $\phi_0 = \arctan(a_{1,n}/a_{2,n})$ and $h(t)$ collects all the high order harmonics of $y(t)$. We assume that $a_{1,n}^2 + a_{2,n}^2 > 0$. Our objective consists in estimating the fundamental frequency of $y(t)$ from a noisy measurement $v(t) = y(t) + d(t)$, which can be subsumed into (1.1) with the number of the frequencies tend to infinity: $n \to +\infty$. Assuming that the amplitude of the fundamental is *larger* than that of the high-order harmonics, we will investigate the convergence of the AO technique by considering the high-frequency content as a bounded perturbation (i.e., $\|h\|_\infty \leq \bar{h}$, $\bar{h} \in \mathbb{R}_{\geq 0}$) whose effect on the estimated frequency can be bounded by adopting a deterministic worst-case viewpoint. Compared with [69], where the availability of a pure periodic signal $y(t)$ is assumed, the ISS analysis performed in this work encompasses also the presence of a bounded measurement noise, i.e., $d(t)$ other than the harmonics. By explicitly expressing the ISS asymptotic gains of the estimator in terms of the tuning parameters of the algorithm, it is possible to highlight the influence of each parameter

on the accuracy of the estimates. The practical characteristics of the estimator are evaluated and compared with other existing tools by extensive simulation trials in Sec. 2.6.

2.2 The Pre-Filtering Scheme

2.2.1 Nominal Pre-Filtering System

To deal with the structured perturbation term $\sum_{k=1}^{n_d} b_k t^{k-1}$ appearing in (2.1), we extend the state variable filtering tool proposed in [89] (see also the alternative GPI observer approach [27]) to compute the unavailable time-derivatives of $y(t)$ that are needed to remove the effect of structured perturbations from the AFP estimates. To this end, we first address the problem for the noise-free signal

$$y(t) = \breve{y}(t) + \sum_{k=1}^{n_d} b_k t^{k-1}, \quad t \in \mathbb{R}_{\geq 0}\,. \tag{2.4}$$

A block diagram of the proposed pre-filter's architecture [86] is shown in Fig. 2.1. In the

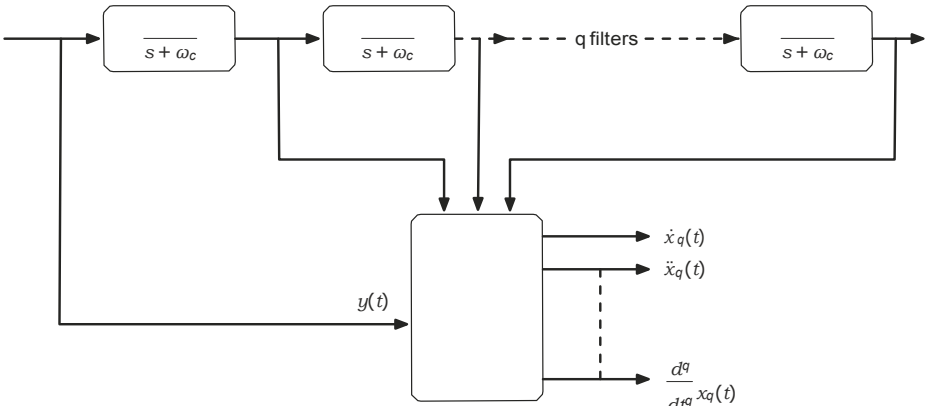

Fig. 2.1 Detailed scheme of the proposed pre-filtering system.

simplified setting given by (2.4), we adopt a n_p-th order pre-filter, the dynamics of which obey

$$\begin{cases} \dot{x}_1(t) = \omega_c(K_c y(t) - x_1(t)) \\ \dot{x}_k(t) = \omega_c(K_c x_{k-1}(t) - x_k(t)), \ \forall k \in \{2, \ldots, n_p\}, \end{cases} \tag{2.5}$$

where $x_k(0) = x_{k0}$, $k \in \{1, \ldots, n_p\}$; ω_c and K_c are positive parameters to be selected by the designers. In qualitative terms, ω_c determines the cut-off frequency while $K_c \in (0, 1]$ acts as a damping coefficient. More details of parameter tuning and the benefit of using a non-unity DC gain K_c will be discussed in Sec. 2.6 (see Fig. 2.5). In the following, we will

show that for all $n_p \geq n_d$, there exists a class of computable auxiliary signals derivatives that are independent of the structured disturbance in steady state.

Defining $x(t) \triangleq [x_1(t) \ \dots \ x_{n_p}(t)]^\top$, a state-space realization of the filter evolving from arbitrary initial conditions $x_0 \triangleq [x_{1_0} \ \dots \ x_{n_p 0}]^\top \in \mathbb{R}^{n_p}$ is

$$\begin{cases} \dot{x}(t) = Ax(t) + B\,y(t) \\ x_{n_p}(t) = Cx(t) \end{cases} \tag{2.6}$$

where

$$A = \begin{bmatrix} -\omega_c & 0 & \cdots & \cdots & 0 \\ K_c\omega_c & -\omega_c & \ddots & \ddots & \vdots \\ 0 & \ddots & \ddots & \ddots & \vdots \\ \vdots & \ddots & \ddots & \ddots & 0 \\ 0 & \cdots & 0 & K_c\omega_c & -\omega_c \end{bmatrix} \quad B = \begin{bmatrix} K_c\omega_c \\ 0 \\ \vdots \\ 0 \end{bmatrix}, \tag{2.7}$$

and

$$C = \begin{bmatrix} 0 & \cdots & 0 & 1 \end{bmatrix}. \tag{2.8}$$

In view of the proposed filter's structure, it follows that

$$CA^k B = 0, \ \ \forall k \in \{0, \dots, n_p - 2\}.$$

Then, the time-derivatives $\dot{x}_{n_p}(t)$, $\frac{d^2}{dt^2}x_{n_p}(t)$, $\cdots$, $\frac{d^{n_p}}{dt^{n_p}}x_{n_p}(t)$ can be computed as follows:

$$\begin{aligned} \frac{d^k}{dt^k}x_{n_p}(t) &= CA^k x(t), \ \ \forall k \in \{1, \dots, n_p - 1\}, \\ \frac{d^{n_p}}{dt^{n_p}}x_{n_p}(t) &= CA^{n_p-1}(Ax(t) + By(t)). \end{aligned} \tag{2.9}$$

Now, the Laplace transform of $x_k, \ \forall k \in \{1, 2, \cdots, n_p\}$ is

$$\mathcal{L}[x_k](s) = H_k(s)\mathcal{L}[y](s) \text{ with } H_k(s) = \frac{\omega_c^k K_c^k}{(s+\omega_c)^k}.$$

Neglecting the initial conditions of the internal filter's states, the Laplace transform of the auxiliary signal is:

$$\mathcal{L}[x_{n_p}](s) = H_{n_p}(s)a\frac{s\sin(\phi_0) + \omega\cos(\phi_0)}{s^2+\omega^2} + H_{n_p}(s)\sum_{k=1}^{n_d} b_k(k-1)!\frac{1}{s^k}$$

and hence

$$\mathcal{L}\left\{\frac{d^i x_{n_p}}{dt^i}\right\}(s) = H_{n_p}(s)a\frac{s\sin(\phi_0)+\omega\cos(\phi_0)}{s^2+\omega^2}s^i + H_{n_p}(s)\sum_{k=1}^{n_d} b_k(k-1)!s^{i-k}.$$

which implies that for all $n_d \le i \le n_p$ the time-polynomial perturbation vanishes asymptotically due to the time-derivative operations. Clearly, $\frac{d^i}{dt^i}x_{n_p}(t)$ tends asymptotically to a sinusoidal regime $\frac{d^i}{dt^i}\bar{x}_{n_p}(t)$ given by

$$\frac{d^i}{dt^i}\bar{x}_{n_p}(t) = a_i\sin(\phi_i(t)),$$

where

$$a_i = a\omega^i|H_{n_p}(\mathrm{j}\omega)|,\quad \phi_i(t) = \phi(t) + \angle H_{n_p}(\mathrm{j}\omega) + \frac{\pi}{2}i. \tag{2.10}$$

It is worth noting that the order of the pre-filter n_p (subject to $n_p \ge n_d$) can be set arbitrarily, whereas the use of higher-order filters is not encouraged mainly due to following reasons: 1) higher complexity; 2) decrease in convergence speed (the pre-filter is a cascade of scalar low-pass filters); 3) excessive attenuation that may lead to numerical issues. In this respect, the filter's order is fixed at the minimum value in the rest of this section, that is $n_p = 1 + n_d$, and then we introduce a pair of auxiliary derivatives for the sake of further discussion:

$$z(t) = \begin{bmatrix} z_1(t) & z_2(t) \end{bmatrix}^\top := \begin{bmatrix} \frac{d^{n_d}}{dt^{n_d}}x_{1+n_d}(t) & \frac{d^{1+n_d}}{dt^{1+n_d}}x_{1+n_d}(t) \end{bmatrix}^\top,$$

in which $z(t)$ tends asymptotically to a sinusoidal regime $\bar{z}(t) = [\bar{z}_1(t)\ \bar{z}_2(t)]^\top$ given by

$$\begin{aligned} \bar{z}_1(t) &= \frac{d^{n_d}}{dt^{n_d}}\bar{x}_{1+n_d}(t) = a_z\sin(\phi_z(t)),\\ \bar{z}_2(t) &= a_z\omega\cos(\phi_z(t)), \end{aligned}$$

with

$$a_z = a\omega^{n_d}|H_{1+n_d}(\mathrm{j}\omega)|,\quad \phi_z(t) = \phi(t) + \angle H_{1+n_d}(\mathrm{j}\omega) + \frac{\pi}{2}n_d. \tag{2.11}$$

In view of (2.9), the auxiliary derivatives $z(t)$ can be written in a compact form $z(t) = \Phi\begin{bmatrix} y(t) & x(t)^\top \end{bmatrix}^\top$, with Φ given by

$$\Phi = \begin{bmatrix} 0 & CA^{n_d} \\ CA^{n_d}B & CA^{1+n_d} \end{bmatrix}.$$

As a final remark, it is immediate to see that the sinusoidal regime $z(t)$ can be described in terms of the following simple state equations:

$$\begin{cases} \dot{z}(t) = A_z z(t) + \Omega G_z z(t) \\ z_1(t) = C_z z(t) \end{cases} \tag{2.12}$$

by setting the initial conditions as

$$z(0) = \begin{bmatrix} a_z \sin\left(\phi_0 + \angle H_{1+n}(j\omega) + \frac{\pi}{2} n_d\right) & a_z \omega \cos\left(\phi_0 + \angle H_{1+n}(j\omega) + \frac{\pi}{2} n_d\right) \end{bmatrix}^\top,$$

with $\Omega = \omega^2$, $A_z = \begin{bmatrix} 0 & 1 \\ 0 & 0 \end{bmatrix}$, $G_z = \begin{bmatrix} 0 & 0 \\ -1 & 0 \end{bmatrix}$, and $C_z = \begin{bmatrix} 1 & 0 \end{bmatrix}$.

2.2.2 Stability of the Pre-Filtering System

Consider again the perturbed measurement signal $v(t)$ given by (2.1), we denote by $\hat{x}(t)$ the actual state vector of the pre-filter, driven by the noisy signal $v(t)$ and evolving from an arbitrary initial condition $\hat{x}_0$ as follows:

$$\begin{cases} \dot{\hat{x}}(t) = A\hat{x}(t) + Bv(t), \\ \hat{x}_{1+n_d}(t) = C\hat{x}(t). \end{cases} \tag{2.13}$$

Introducing the error vector with respect to $x(t)$, which is driven by a choice of the filter's initial state $\hat{x}_0$ such that auxiliary signal derivative $z(t)$ matches the stationary sinusoidal behavior since the very beginning,

$$\tilde{x}(t) \triangleq \hat{x}(t) - x(t)$$

and noticing that $d(t) = v(t) - y(t)$, the dynamics of $\tilde{x}(t)$ can be written as:

$$\begin{cases} \dot{\tilde{x}}(t) = A\tilde{x}(t) + B\,d(t), \\ \tilde{x}(0) = \hat{x}_0 - x_0. \end{cases} \tag{2.14}$$

The following results can be proved:

Theorem 2.2.1 (ISS of the pre-filtering system) *Given the sinusoidal signal $y(t)$ and the perturbed measurement $v(t)$ (2.1), the error dynamic of the pre-filtering system (2.13) is ISS w.r.t. any additive disturbance signal $d(t) \in L^1_\infty$* D

Proof: Being A Hurwitz, there exists a positive matrix P that solves the the Lyapunov equation $PA + A^\top P = -I$. Let $W(\tilde{x}) \triangleq \tilde{x}^\top P \tilde{x}$, then there exist two positive scalars $\alpha_1,\ \alpha_2 \in \mathbb{R}_{>0}$ such that

$$\alpha_1 |\tilde{x}|^2 \leq \tilde{x}^\top P \tilde{x} \leq \alpha_2 |\tilde{x}|^2, \quad \forall \tilde{x}$$

The derivative of W along the system's state trajectory satisfies

$$\frac{\partial W}{\partial \tilde{x}} (A\tilde{x} + Bd) \leq -|\tilde{x}|^2 + 2\, \|P\|\, |B|\, |d|\, |\tilde{x}|.$$

For any $0 < \epsilon < 1$, let

$$\chi(s) \triangleq \frac{2\, \|P\|\, |B|}{1-\epsilon} r.$$

with $r \in \mathbb{R}_{\geq 0}$. It is easy to show that

$$|\tilde{x}| \geq \chi(|d|) \ \Rightarrow\ \frac{\partial W}{\partial \tilde{x}} (A\tilde{x} + B d) \leq -|\tilde{x}|^2,$$

and that the system is ISS with asymptotic gain

$$\gamma_x(r) = \alpha_1^{-1} \alpha_2\, \chi(r).$$

In view of the ISS property of the linear auxiliary filter (2.36), for any arbitrary $v \in \mathbb{R}_{>0}$ and for any finite-norm initial error $\tilde{x}_0$, the error vector $\tilde{x}(t)$ enters in a closed ball of radius $\gamma_x(\|d\|_\infty) + v \leq \gamma_x(\bar{d}) + v$ in finite time $T_{\tilde{x}_0, v}$. •

Now, let $\hat{z}(t)$ be the vector of the computable perturbed counterpart of $z(t)$:

$$\hat{z}(t) = \Phi[v(t)\ \ \hat{x}(t)^\top]^\top\ , \tag{2.15}$$

the boundedness of $\hat{z}(t)$ is characterized by the following corollary:

Corollary 2.2.1 *Given the sinusoidal signal $y(t)$ and the perturbed measurement $v(t)$ (2.1), if the pre-filtering system (2.6) is applied, then the available auxiliary signal vector $\hat{z}(t)$ derived by (2.15) is bounded.* □

Proof: Using (2.1) and (2.15), it is immediate to conclude that the vector $\tilde{z}(t) \triangleq \hat{z}(t) - z(t)$ enters in finite-time $T_{\delta_z} = T_{\tilde{x}_0, v}$ (for the sake of simplifying the notation, we have dropped the dependence of the reach-time T_{δ_z} on initial conditions) in a closed hyper-sphere of radius $\gamma_z(\bar{d}) + \delta$ centsred at the origin, with

$$\gamma_z(s) = \bar{\varphi}(\gamma_x(r) + r),\ \forall r \in \mathbb{R}_{\geq 0},\ \delta = \bar{\varphi} v \tag{2.16}$$

where $\bar{\varphi} \geq ||\Phi||$.

From the equality $\hat{z}(t) = \tilde{z}(t) + z(t)$, it turns out that the proven boundedness of both $\tilde{z}(t)$ and $z(t)$ implies the boundedness of the $\hat{z}(t)$, thus ending the proof. •

2.3 Estimation of a Single Sinusoidal Signal

In view of (2.12), by introducing the estimated squared-frequency $\hat{\Omega}(t) = \hat{\omega}(t)^2$, the filter output $\hat{z}(t)$ is used as the input for the following adaptive observer having internal state $\hat{\xi}(t)$:

$$\begin{cases} \dot{\hat{\xi}}(t) = (A_z - L_z C_z)\hat{\xi}(t) + L C_z \hat{z}(t) + G_z \hat{z}(t)\hat{\Omega}(t) + \hat{\xi}(t)\dot{\hat{\Omega}}(t) \\ \dot{\hat{\Omega}}(t) = -\mu \hat{\xi}(t)^\top (\hat{z}(t) - \hat{z}(t)) \end{cases}, \tag{2.17}$$

where $\mu \in \mathbb{R}_{\geq 0}$ is an arbitrary positive constant and L is the observer gain such that $(A_z - L_z C_z)$ is Hurwitz. Roughly speaking, increasing μ corresponds to an acceleration in the convergence rate of the estimation error, whereas the accuracy is degraded due to a typical trade-off between asymptotic accuracy and convergence speed (see Fig. 2.4). Finally,

$$\hat{\omega}(t) = \sqrt{\max\{0,\ \hat{\Omega}(t)\}}\,. \tag{2.18}$$

Given $\hat{\Omega}(t)$ and $\hat{z}(t)$ and assuming, for the moment, that

$$\hat{\Omega}(t) > 0,\ \forall\, t, \tag{2.19}$$

then, the filtered regime amplitude and phase (a_z, ϕ_z) defined in (2.11) are estimated by

$$\hat{a}_z(t) = \sqrt{(\hat{\Omega}(t)\hat{z}_1(t)^2 + \hat{z}_2(t)^2)/\hat{\Omega}(t)}, \tag{2.20a}$$

$$\hat{\phi}_z(t) = \angle\,[\hat{z}_2(t) + j\hat{\omega}(t)\hat{z}_1(t)]\,. \tag{2.20b}$$

Thanks to the availability of $\hat{a}_z, \hat{\omega}, \hat{\phi}_z$ related to the auxiliary signal $z_1(t)$, from (2.11), with the assumption (2.19), we obtain the following estimates of the original parameters:

$$\hat{a}(t) = \frac{\hat{a}_z(t)}{\hat{\omega}(t)^{n_d}\,|H_{1+n_d}(j\hat{\omega}(t))|}, \tag{2.21a}$$

$$\hat{\phi}(t) = \hat{\phi}_z(t) - \angle H_{1+n_d}(j\hat{\omega}(t)) - n_d\frac{\pi}{2}. \tag{2.21b}$$

After some algebra, we finally get:

$$\hat{a}(t) = \frac{\hat{a}_z(t)}{\hat{\omega}(t)^{n_d}} \left(\frac{(\omega_c^2 + \hat{\omega}(t)^2)^{\frac{1}{2}}}{\omega_c K_c} \right)^{1+n_d}, \tag{2.22a}$$

$$\hat{\phi}(t) = \hat{\phi}_z(t) + (1+n_d)\arctan\left(\frac{\hat{\omega}(t)}{\omega_c}\right) - n_d\frac{\pi}{2}. \tag{2.22b}$$

Assumption (2.19) is needed for (2.20a) and (2.21a) to be well-posed at any time-instant t. Let us remove the need for (2.19) by resorting to the following adaptive amplitude estimators. To this end, from the equality (2.20a), we define the time-varying residual that depends on the frequency estimate $\hat{\Omega}(t)$ and on the instantaneous values of the filtered signals $\hat{z}_1(t)$ and $\hat{z}_2(t)$:

$$R(\bar{a}_z(t), t) := \bar{a}_z(t)\hat{\omega}(t) - \sqrt{\hat{\Omega}(t)\hat{z}_1(t)^2 + \hat{z}_1(t)^2},$$

the following adaptation law stemming from gradient algorithm [96] can be designed

$$\begin{aligned}\dot{\bar{a}}_z(t) &= -\mu_a \frac{\partial R(\bar{a}_z, t)}{\partial \bar{a}_z} R(\bar{a}_z, t) \Big/ \left(\frac{\partial R(\bar{a}_z, t)}{\partial \bar{a}_z}\right)^2 \\ &= -\mu_a \hat{\omega}(t)\left(\hat{\omega}(t)\bar{a}_z(t) - \sqrt{\hat{\Omega}(t)\hat{z}_1(t)^2 + \hat{z}_2(t)^2}\right),\end{aligned} \tag{2.23}$$

where the estimates is clipped by: $\hat{a}_z(t) = \max\{0, \bar{a}_z(t)\}$, $\hat{a}_z(0) = \bar{a}_z(0) = 0$ and $\mu_a \in \mathbb{R}_{>0}$ is a tuning gain set by the designer to steer $R(\hat{a}_z(t), t)$ to 0 asymptotically. It is worth to point out that μ_a plays a similar role as μ does in (2.17), hence the ways of tuning are likewise referred to Fig. 2.4. Thanks to (2.23), the estimate of the filtered amplitude $\hat{a}_z(t)$ can be computed through (2.23) without the need of assuming (2.19). Using $\hat{a}_z(t)$ provided by (2.23), the following adaptive algorithm can be finally used to estimate the original amplitude:

$$\dot{\bar{a}}(t) = -\mu_a \hat{\omega}(t)^{n_d}\left(\bar{a}(t)\hat{\omega}(t)^{n_d} - \frac{\hat{a}_z(t)}{|H_{1+n_d}(\mathrm{j}\hat{\omega}(t))|}\right), \tag{2.24}$$

with a simple clipping: $\hat{a}(t) = \max\{0, \bar{a}(t)\}$ and $\hat{a}(0) = \bar{a}(0) = 0$. In Section 2.6, the amplitude estimate given by (2.24) is evaluated by simulations.

2.3.1 ISS Property of the Adaptive Estimator

In order to address the stability of the adaptive observer, let us introduce some instrumental error variables: $\tilde{z}(t) := \hat{z}(t) - z(t)$, $\tilde{\Omega}(t) := \hat{\Omega}(t) - \Omega$, and $\tilde{\zeta}(t) := \hat{z}(t) - \xi(t)\tilde{\Omega}(t)$. Then,

we have:

$$\dot{\tilde{z}}(t) = (A_z - L_z C_z)\tilde{z}(t) + (L_z C_z + \Omega G_z)\tilde{z}(t) + \tilde{\Omega}(t) G_z \hat{z}(t) + \xi(t)\dot{\hat{\Omega}}(t), \tag{2.25a}$$

$$\dot{\tilde{\Omega}}(t) = -\mu \xi(t)^\top \xi(t)\tilde{\Omega}(t) + \mu \xi(t)^\top \left(\tilde{z}(t) - \tilde{\zeta}(t)\right), \tag{2.25b}$$

$$\dot{\tilde{\zeta}}(t) = (A_z - L_z C_z)\tilde{\zeta}(t) + (L_z C_z + \Omega G_z)\tilde{z}(t). \tag{2.25c}$$

The following assumption is needed to address the convergence analysis of the estimator.

Assumption 3 *The solution $\xi(t)$ of $\dot{\xi}(t) = (A_z - L_z C_z)\xi(t) + G_z \hat{z}(t)$ is instantaneously persistently exciting (IPE) in the sense that there exist a positive constant ϵ such that*

$$\xi(t)^\top \xi(t) > \epsilon, \ \forall t \geq 0. \tag{2.26}$$

It is worth noting that, instead of the typical integral type of persistency of excitation condition (see, for instance, [8]) that requires on-line buffering by a moving time window, the exploitation of the above IPE condition in the switching algorithm presented in Section 2.3.2 greatly enhances the on-line implementation of the adaptive estimation technique, because the IPE condition is easily computable at each time instant without any delay (the reader is referred to Example 1 in Section 2.6 for an instance).

Now, the following basic stability result is given and proved.

Theorem 2.3.1 (ISS of the adaptive observer system) *Suppose that Assumption 1, 3 hold. Then, given the sinusoidal signal $y(t)$ generated by (2.2) and the perturbed measurement model (2.1), the adaptive observer as well as the frequency estimator given by (2.13), (2.15) and (2.17) are ISS with respect to any additive measurement perturbation such that $|d(t)| \leq \bar{d}$.*

D

Proof: Consider the candidate Lyapunov function $V_\zeta = \tilde{\zeta}(t)^\top Q \tilde{\zeta}(t)$, where Q is a positive definite matrix solving the linear Lyapunov's equation:

$$Q(A_z - L_z C_z) + (A_z - L_z C_z)^\top Q = -I. \tag{2.27}$$

In view of the dynamics of $\tilde{\zeta}(t)$ obeying (2.25c), the time-derivative of the Lyapunov function verifies the inequality

$$\frac{\partial V_\zeta}{\partial \tilde{\zeta}} \dot{\tilde{\zeta}}(t) \leq -|\tilde{\zeta}(t)|^2 + 2||Q||\,||L_z C_z + \Omega G_z||\,|\tilde{z}(t)|\,|\tilde{\zeta}(t)|. \tag{2.28}$$

Hence, V_ζ is an ISS-Lyapunov function for $\tilde{\zeta}(t)$ w.r.t. the $\tilde{z}(t)$. Moreover, the dynamics of $\tilde{z}(t)$ is ISS w.r.t. disturbance $d(t)$, so that $\tilde{\zeta}(t)$ is, in turn, ISS w.r.t. $d(t)$ such that $|d(t)| \leq \bar{d}$. Now, let $V_{\tilde{\Omega}} = \frac{1}{2}\tilde{\Omega}(t)^2$ be a candidate Lyapunov function of the frequency-estimation subsystem. Then, the derivative of $V_{\tilde{\Omega}}$ verifies the inequality

$$\frac{\partial V_{\tilde{\Omega}}}{\partial \tilde{\Omega}} \dot{\tilde{\Omega}}(t) \leq -\mu |\xi(t)|^2 |\tilde{\Omega}(t)|^2 + \mu |\xi(t)| |\tilde{z}(t) - \tilde{\zeta}(t)| \, |\tilde{\Omega}(t)| \,. \tag{2.29}$$

In view of (2.29), Assumption 3, and the boundedness of $|\xi(t)|$ (it is immediate to show that the dynamics of $\xi(t)$ is ISS w.r.t. the bounded input $\hat{z}(t)$), we have that $\tilde{\Omega}(t)$ is ISS w.r.t. $\tilde{\zeta}(t)$ and $\tilde{z}(t)$, which are all proven to be ISS w.r.t. $d(t)$ such that $|d(t)| \leq \bar{d}$.

Finally, the identity $\tilde{z}(t) = \tilde{\zeta}(t) + \xi(t)\tilde{\Omega}(t)$, and the boundedness of $|\xi(t)|$ together imply that also the state-estimation error $\tilde{z}(t)$ is ISS w.r.t. $d(t)$ such that $|d(t)| \leq \bar{d}$. •

Next, we are going to establish the relationship between the excitation condition and the observer poles location.

Lemma 2.3.1 (Observer Poles and Excitation) *Assume that in the noise-free mode of behaviour (that is, $d(t) = 0$), the poles of $A_z - L_z C_z$ are assigned to (p_1, p_2), where $p_1, p_2 = \sigma_1 \pm \jmath\omega_2$ with $\sigma_1 \in \mathbb{R}_{<0}$, $\omega_2 \in \mathbb{R}$, such that*

$$\omega_2^2 > \sigma_1^2, \quad \sigma_1 \in \mathbb{R}_{<0}, \quad \omega_2 \in \mathbb{R} \,. \tag{2.30}$$

Then, the IPE condition (2.26) is verified for any $t > 0$ by any sinusoidal signal.

Proof: In stationary conditions, by defining $B_\xi = [0 \;\; -1]^\top$, the dynamic equation of $\xi(t)$, in absence of noise can be rewritten as

$$\dot{\xi}(t) = (A_z - L_z C_z)\xi(t) + B_\xi \tilde{z}_1(t) \,,$$

with $\xi(0) = 0$. Then, in the Laplace domain we have $\xi_k(s) = H_{\xi,k}(s)\tilde{z}_1(s)$, $k \in \{1, 2\}$, where $H_{\xi,k}(s) = \imath_k^\top (sI - A_z + L_z C_z)^{-1} B_\xi$ and $\imath_k$ denotes the i-th unit vector.

Now, letting $p_s := p_1 + p_2$ and $p_m := p_1 p_2$, by a simple algebra we obtain

$$H_{\xi,1}(s) = -\frac{1}{s^2 - p_s s + p_m}, \quad H_{\xi,2}(s) = -\frac{s - p_s}{s^2 - p_s s + p_m},$$

and

$$\phi_{\xi,1} = \arctan \frac{p_s \omega}{p_m - \omega^2}, \quad \phi_{\xi,2} = \arctan \frac{p_s^2 \omega - p_m \omega + \omega^3}{p_s p_m} \,.$$

Owing to the structure of $H_{\xi,1}$ and $H_{\xi,2}$, the following inequality holds

$$\xi^{\top}(t)\xi(t) \geq \sum_{k=1}^{2} \bar{h}_{\xi,k}^2 a_z^2 \sin^2(\phi_z + \phi_{\xi,k}),$$

where $\bar{h}_{\xi,k} = |H_{\xi,k}(\square\omega)|$ and $\phi_{\xi,k}$ represents the phase shift of $H_{\xi,k}(s)$ at the frequency of the sinusoid.

Now, we show that $\phi_{\xi,1}(\omega) \neq \phi_{\xi,2}(\omega)$, $\forall\, \omega > 0$ by contradiction. Let us assume that there exists $\omega > 0$, such that $\phi_{\xi,1} = \phi_{\xi,2}$. The hypothesis is verified if and only if

$$\frac{p_s}{p_m - \omega^2} = \frac{p_s^2 - p_m + \omega^2}{p_s p_m},$$

which is equivalent to

$$\omega^4 + (p_s^2 - 2p_m)\omega^2 + p_m^2 = 0\,. \tag{2.31}$$

In view of (2.30), Eq. (2.31) does not admit positive roots in the variable ω (since $p_s^2 - 2p_m = p_1^2 + p_2^2 > 0$ and $p_m > 0$). Therefore, we can conclude that $\phi_{\xi,1} \neq \phi_{\xi,2}$, $\forall\, \omega > 0$. Finally, due to the phase separation property, the following inequality is verified for all $t > 0$

$$\xi^{\top}(t)\xi(t) \geq \sum_{k=1}^{2} \bar{h}_{\xi,k}^2 a_z^2 \sin^2(\phi_z + \phi_{\xi,k}) > 0$$

and there always exist a constant $\epsilon \in \mathrm{R}_{>0}$ that fulfills (2.26), thus ending the proof. •

2.3.2 Switching Mechanism Based on Excitation Level

Note that the excitation condition (2.26) might not be satisfied on certain time-instants, especially when the magnitude of the sinusoidal signal (2.2) is small compared to magnitude of disturbances and higher order harmonics. In order to avoid the estimate drift phenomena, the adaptation parameter μ is switched based on the following normalized excitation level

$$\Sigma(t) = \left(\xi(t)^{\top}\xi(t) + \rho\right)^{-1} \xi(t)^{\top}\xi(t),$$

where ρ is a given positive scalar. We introduce a pre-defined excitation threshold δ so that

$$\mu = 0 \quad \text{if} \quad \Sigma(t) < \delta \text{ (poor excitation)}.$$

The normalized IPE signal $\Sigma(t)$ is easily accessible for all t due the availability of $\xi(t)$, $\forall\, t \geq 0$, thereby permitting an switching adaptation law in correspondence with the excitation level

in real-time. In Example 1 demonstrated in Section 2.6, we will show the behavior of the estimator along with the time-varying switching signal determined by $\Sigma(t)$.

Clearly, it is important to show that the estimation error remains bounded even during the poor excitation scenarios. This is carried out in the following

Lemma 2.3.2 (Boundedness in dis-excitation phase) *Assume that* $\mu = 0$, $\forall t \geq \bar{t} > 0$, *where* $\bar{t}$ *denotes the time-instant at which the adaptation is switched off. Then, the dynamics of the adaptive observer-based sinusoidal estimator given by (2.17) is ISS w.r.t.* $d(t)$ *such that* $|d(t)| \leq \bar{d}$ *and w.r.t. the value of the frequency estimation error before the adaptation is switched off (that is,* $\tilde{\Omega}(\bar{t}^-)$*).*

D

Proof: In the suppressed identification phase, $\dot{\hat{\Omega}}(t) = \dot{\tilde{\Omega}}(t) = 0$, such that $\tilde{\Omega}(t) = \tilde{\Omega}(\bar{t}^-)$ and the error dynamics $\tilde{z}(t)$, $\tilde{\zeta}(t)$ evolve according to the following differential equations:

$$\dot{\tilde{z}}(t) = (A_z - L_z C_z)\tilde{z}(t) + (L_z C_z + \Omega G_z)\bar{\tilde{z}}(t) + \tilde{\Omega}(t) G_z \hat{z}(t),$$

$$\dot{\tilde{\zeta}}(t) = (A_z - L_z C_z)\tilde{\zeta}(t) + (L_z C_z + \Omega G_z)\bar{\tilde{z}}(t).$$

Note that the ISS properties of $\xi(t)$ and $\tilde{\zeta}(t)$ are preserved in this scenario. Due to the identity $\tilde{z}(t) = \tilde{\zeta}(t) + \xi(t)\tilde{\Omega}(t)$, we conclude that the dynamics of $\tilde{z}(t)$ admits a bound that depends on the disturbance level $\bar{d}$ and on the initial parametric error $\tilde{\Omega}(\bar{t}^-)$. •

Remark 2.3.1 (Robustness during dynamic switching) It is worth noting that some stability issues may affect the behavior of the estimator under alternate switches unless additional constraints are introduced on the minimum duration time between consecutive switching events. A detailed discussion of this subject is carried out in Chapter 3 concerning the estimation of n frequencies ($n \geq 1$), in which we prove that a simple time-based switching constraint derived from Lyapunov stability considerations guarantees the stability of the adaptive observer (a minimum finite duration between transitions is ensured).

2.4 Estimation of Fundamental Frequency of a Generic Periodic Signal

2.4.1 Problem Formulation and Preliminaries

In this section, we show that the simple adaptive observer method (2.17)-(2.18) originally conceived to estimate the frequency of a single sinusoid is valid for retrieving the fundamental

frequency of a generic periodic signal (2.3). Thanks to the analysis performed in Sec. 2.2, a 2-nd order pre-filter is enough to annihilate the dc component $a_0/2$ asymptotically, whereas we adopt the nominal pre-filter of order 3 (i.e., $n_p = 3$) herein in order to avoid a direct feedthrough from the noisy measurement, thereby giving rise to a lower sensitivity to the additive disturbance (see (2.9)).

For the sake of further analysis, let us define the bias-plus-fundamental signal

$$\eta(t) \triangleq \frac{a_0}{2} + \sqrt{a_{1,n}^2 + a_{2,n}^2}\sin(\omega t + \phi_0), \tag{2.32}$$

in order to split the pre-filtered signal $x(t)$ in two parts: $x(t) \triangleq \eta_f(t) + h_f(t)$, where $\eta_f(t) \triangleq [\eta_{f1}(t)\ \ \eta_{f2}(t)\ \ \eta_{f3}(t)]^\top$ is the state of a virtual pre-filter driven by $\eta(t)$:

$$\dot{\eta}_f(t) = A\eta_f(t) + B\eta(t) \tag{2.33}$$

with arbitrary initial conditions $\eta_{f0} \in \mathrm{R}^3$. By analogy with (2.6), it is immediate to obtain

$$A = \begin{bmatrix} -\omega_c & 0 & 0 \\ K_c\omega_c & -\omega_c & 0 \\ 0 & K_c\omega_c & -\omega_c \end{bmatrix}, \quad B = \begin{bmatrix} K_c\omega_c \\ 0 \\ 0 \end{bmatrix}, \quad C = \begin{bmatrix} 0 & 0 & 1 \end{bmatrix}.$$

Moreover, let $\eta_{f3}(t) = C\eta_f(t)$ be the output of the virtual pre-filter. Introducing the vector of auxiliary derivatives

$$z(t) = \begin{bmatrix} z_1(t) & z_2(t) \end{bmatrix}^\top \triangleq \begin{bmatrix} \dot{\eta}_{f3}(t) & \frac{d^2}{dt^2}\eta_{f3}(t) \end{bmatrix}^\top \in \mathrm{R}^2, \tag{2.34}$$

we have that $z(t)$ tends asymptotically to the stationary sinusoidal regime, which are offset-free due to differentiation. It is easy to show that the vector of stationary sinusoidal derivatives $\breve{z}(t) = [\breve{z}_1(t)\ \breve{z}_2(t)]^\top$ can be assumed to be generated by the linear marginally stable exosystem (2.12). Furthermore, let $\hat{z}(t) \triangleq [\hat{z}_1(t)\ \hat{z}_2(t)]^\top = \begin{bmatrix} \dot{\hat{x}}_3(t) & \frac{d^2}{dt^2}\hat{x}_3(t) \end{bmatrix}^\top$ be the vector of the perturbed filtered derivatives, computable from the accessible state vector of the prefilter:

$$\hat{z}(t) = \Phi\hat{x}(t), \quad \text{with} \quad \Phi = \begin{bmatrix} CA \\ CA^2 \end{bmatrix}. \tag{2.35}$$

2.4.2 ISS Property of the Adaptation Scheme

Stability of the pre-filtering scheme

From the analysis performed in the case of single sinusoidal signal, it turns out that the ISS property of the pre-filtering scheme holds inevitably due the boundedness of $h(t)$ and $d(t)$. However, the following investigations are carried out to gain a less conservative error dynamics' bound, which is also instrumental for the tuning of parameters.

First, observe that there exist an (unknown) initial state $\eta_f(0) = \bar{\eta}_0$ of the unperturbed virtual pre-filter (2.33) giving rise to an unknown state trajectory $\bar{\eta}(t)$ whose projection on the subspace containing $z(t)$ (see (2.34)) matches the stationary sinusoidal behavior since $t = 0$. Introduce the error vector $\tilde{x}(t) := \hat{x}(t) - \bar{\eta}(t)$, and owing to the fact that $h(t) + d(t) = v(t) - \eta(t)$, the dynamic of $\tilde{x}(t)$ is given by:

$$\begin{cases} \dot{\tilde{x}}(t) = A\tilde{x}(t) + B\,(h(t) + d(t)) \\ \tilde{x}(0) = \hat{x}_0 - \bar{\eta}_0 \end{cases}. \tag{2.36}$$

We can split the error in two vectors as $\tilde{x}(t) = \tilde{x}_h(t) + \tilde{x}_d(t)$, where $\tilde{x}_h(t)$ and $\tilde{x}_d(t)$ obey the two concurrent dynamic equations:

$$\dot{\tilde{x}}_h(t) = A\tilde{x}_h(t) + B\,h(t), \tag{2.37a}$$

$$\dot{\tilde{x}}_d(t) = A\tilde{x}_d(t) + B\,d(t)\,. \tag{2.37b}$$

Owing to the structure of the pre-filter, let us denote by $H_j(s)$ the transfer function from the input to the j-th state variable:

$$H_j(s) = \frac{\omega_c^j K_c^j}{(\omega_c + s)^j}, \tag{2.38}$$

such that $\mathsf{L}[\tilde{x}_{h_j}](s) = H_j(s)\mathsf{L}[h](s)$, and then by defining $\phi_n = \arctan(n\omega/\omega_c)$, in steady state we get

$$\tilde{x}_{h_j}(t) = \sum_{n=2}^{\infty} \frac{\omega_c K_c}{\sqrt{\omega_c^2 + n^2\omega^2}}^{j} [a_{1,n}\cos(n\omega t + j\phi_n) + a_{2,n}\sin(n\omega t + j\phi_n)], \quad \forall j = 1, 2, 3 \tag{2.39}$$

which can be rewritten in a compact form:

$$\tilde{x}_{h_j}(t) = \Sigma(t)^\top \mathsf{R}^j \Gamma \tag{2.40}$$

where

$$\Sigma(t) = [\cos 2\omega t \ \sin 2\omega t \ \cos 3\omega t \ \sin 3\omega t \ \cdots \ \cdots]^{\top},$$

$$\mathbf{R}^{j} = \text{block diag}[\mathbf{R}_2^{j} \ \mathbf{R}_3^{j} \ \cdots],$$

$$\mathbf{R}_n^{j} = \frac{\omega_c K_c}{\omega_c^2 + n^2\omega^2} \begin{bmatrix} \cos j\phi_n & \sin j\phi_n \\ -\sin j\phi_n & \cos j\phi_n \end{bmatrix},$$

and

$$\Gamma = [a_{1,2} \ a_{2,2} \ a_{1,3} \ a_{2,3} \ \cdots \ \cdots]^{\top}.$$

In view of (2.40) and letting $\bar{\sigma}(\mathbf{R}^j)$ be the maximum singular value of $\mathbf{R}^j$, we have:

$$|\tilde{x}_{h_j}(t)|^2 \leq \bar{\sigma}(\mathbf{R}^j)^2 |\Sigma(t)\Gamma|^2 = \bar{\sigma}(\mathbf{R}^j)^2 |h(t)|^2.$$

In order to determine an upper bound to the largest singular value of the R^j, we first compute the maximum singular value among all the sub-blocks $\mathbf{R}^j_n \forall n = 1, 2, \cdots$ as follows:

$$\bar{\sigma}(\mathbf{R}_n^j) = \sqrt{\lambda_{\max}\left(\mathbf{R}_n^{j\top}\mathbf{R}_n^j\right)} = \frac{\omega_c K_c}{\sqrt{\omega_c^2 + n^2\omega^2}} \leq \frac{\omega_c K_c}{\sqrt{\omega_c^2 + 4\omega^2}} = \bar{\sigma}(\mathbf{R}_2^j). \quad (2.41)$$

The overall high-order harmonic error vector $|\tilde{x}_h(t)|$ can be norm-bounded as shown in (2.42) below:

$$\begin{aligned} |\tilde{x}_h(t)| &= \left(\sum_{j=1}^{3} |\tilde{x}_{h_j}(t)|^2\right)^{\frac{1}{2}} \\ &\leq \left(\sum_{j=1}^{3} \bar{\sigma}(\mathbf{R}^j)^2 |h(t)|^2\right)^{\frac{1}{2}} \\ &= \left[|h(t)|^2 \sum_{j=1}^{3} \left(\frac{\omega_c K_c}{\sqrt{\omega_c^2 + 4\omega^2}}\right)^{2j}\right]^{\frac{1}{2}} \\ &= \left[|h(t)|^2 \frac{\omega_c^2 K_c^2 \left[1 - \left(\frac{\omega_c^2 K_c^2}{\omega_c^2 + 4\omega^2}\right)^3\right]}{\omega_c^2 + 4\omega^2 - \omega_c^2 K_c^2}\right]^{\frac{1}{2}} \\ &\leq \frac{\omega_c K_c}{\sqrt{\omega_c^2 + 4\omega^2 - \omega_c^2 K_c^2}} |h(t)| \end{aligned} \quad (2.42)$$

in which $\omega_c^2 + 4\omega^2 - \omega_c^2 K_c^2 > 0$ for any non-zero angular frequency ω.

As far as the dynamics of the filtered disturbance $\tilde{x}_d(t)$ is concerned, it is immediate to show that $\tilde{x}_d(t)$ is ISS, thereby it will enter in a closed ball of radius $\gamma_{x_d}(\|d\|_\infty) + \nu \leq \gamma_{x_d}(d) + \nu$ in finite time $T_{\tilde{x}_{d0},\nu}$ by analogy with the analysis given in Sec. 2.2.2. By linking the available bounds on $\tilde{x}_h(t)$ and $\tilde{x}_d(t)$, we can establish the following asymptotic bound of

the actual filtering error:

$$\begin{aligned} |\tilde{x}(t)| &\leq |\tilde{x}_h(t)| + |\tilde{x}_d(t)| \\ &= \frac{\omega_c K_c}{\omega_c^2 + 4\omega^2 - \omega_c^2 K_c^2}\bar{h} + \gamma_{x_d}(\bar{d}) + v \\ &= \gamma_x(\bar{h}, \bar{d}). \end{aligned}$$

Thanks to (2.35), the vector $\tilde{z}(t) := \hat{z}(t) - z(t)$ will enter in finite-time $T_\delta = T_{\tilde{x}_0, v}$ in a closed ball of radius $\gamma_z(\bar{h}, \bar{d}) + \delta$ centered at the origin, with

$$\delta = \bar{\varphi} v, \quad \gamma_z(r) = \bar{\varphi}\gamma_x(r), \ \forall r \in \mathbb{R}^2_{\geq 0}, \tag{2.43}$$

where $\bar{\varphi}$ is suitable upper bound on $\|\Phi\|$ such that $\|\Phi\| \leq \bar{\varphi}$. Such a bound can be expressed in terms of the tuning parameters of the algorithm and will be used to analyze the effect of the above parameters on the accuracy of the frequency estimate. In order to determine $\bar{\varphi}$, it is worth noting that

$$\|\Phi\| = \sqrt{\lambda(\Phi^\top \Phi)} \leq \sqrt{\mathrm{tr}(\Phi^\top \Phi)}.$$

The trace of $\Phi^\top \Phi$ follows that $\mathrm{tr}(\Phi^\top \Phi) = |CA|^2 + |CA^2|^2$, wherein the square-power of A can be calculated by applying the block-Jordan matrix multiplication rule. After some algebra, we obtain:

$$CA^2 = [(K_c\omega_c)^2 \ 2(K_c\omega_c)(-\omega_c) \ (-\omega_c)^2].$$

Therefore, we get the following bound:

$$\mathrm{tr}(\Phi^\top \Phi) \leq 2\omega_c^2 + 6\omega_c^4.$$

and thus, finally:

$$\|\Phi\| \leq \bar{\varphi} := \omega_c \sqrt{2 + 6\omega_c^2}. \tag{2.44}$$

Denoting by $\omega_c \kappa(\omega_c)$ the right-hand side of (2.44), the comparison function $\gamma_z(r)$ in (4.30) can be taken as

$$\gamma_z(r) = \omega_c \kappa(\omega_c)\gamma_x(r), \ \forall r \in \mathbb{R}^2_{\geq 0}. \tag{2.45}$$

In view of (2.45), the slope of the function $\gamma_z(\cdot)$ can be made arbitrarily small by reducing the parameter ω_c of the pre-filter, thus allowing to attenuate the effect of both the bounded perturbation and high-order harmonics. Note that the extra attenuation of the uncertainty is obtained at the price of decreasing the speed of convergence of the estimator.

Stability of the adaptive observer system

Analogously, we have the error variables $\tilde{z}(t) = \hat{z}(t) - z(t)$, $\tilde{\Omega}(t) = \hat{\Omega}(t) - \Omega$, $\tilde{\zeta}(t) = \tilde{z}(t) - \xi(t)\tilde{\Omega}(t)$, obey the differential equations (2.25a)-(2.25c). In order to prove the convergence of the estimation error, let us recall Assumption 3. The IPE condition (2.26) is verified in noise-free scenario with properly assigned poles, the reader is referred to Sec. 2.3.1 for a detailed discussion on this subject. In case (2.26) gets lost in a noisy environment, the robust (conservative) excitation-based switching (see Sec. 2.3.2) can be employed likewise to avoid the estimates diverge in weakly excited interval.

Theorem 2.4.1 (ISS of the adaptive observer system) *If Assumption 3 holds, then given the periodic signal $y(t)$ generated by (2.3) and the perturbed measurement $v(t)$ the adaptive observer as well as the frequency estimator given by (2.17)-(2.18) are ISS w.r.t. the bound of harmonics $|h(t)| \leq \bar{h}$ in the periodic signal and to any bounded additive measurement perturbation $|d(t)| \leq \bar{d}$.* D

Proof: Consider a Lyapunov function $V_\zeta = \tilde{\zeta}(t)^\top Q\tilde{\zeta}(t)$, where Q is a positive definite matrix that solves the linear Lyapunov's equation (2.27). In view of the $\tilde{\zeta}(t)$ dynamics (2.25c), the derivative of the Lyapunov function verifies the inequality (2.28). Hence, V_ζ is an ISS-Lyapunov function for $\tilde{\zeta}(t)$ w.r.t. $\tilde{z}(t)$. For the sake of the further analysis, let us define

$$\bar{q} \triangleq \bar{\lambda}(Q), \quad \underline{q} \triangleq \underline{\lambda}(Q)$$

and

$$p_s \triangleq (p_1 + p_2) \leq -\bar{\lambda}(L_z C_z + \Omega G_z).$$

Then we rewrite (2.28) by completing squares:

$$\begin{aligned}\frac{\partial V_\zeta}{\partial \tilde{\zeta}}\dot{\tilde{\zeta}}(t) &\leq -\frac{3}{4}|\tilde{\zeta}(t)|^2 - \frac{1}{4}|\tilde{\zeta}(t)|^2 + 2||Q||\,||L_z C_z + \Omega G_z||\,|\tilde{z}(t)|\,|\tilde{\zeta}(t)| \\ &\leq -\frac{3}{4\bar{q}}V_\zeta(t) + 4\bar{q}|p_s|\,|\tilde{z}(t)|^2 \\ &= -\beta_\zeta(V_\zeta(t) - \gamma_\zeta(\tilde{z}(t)^2))\end{aligned} \tag{2.46}$$

where we have posed $\beta_\zeta \triangleq 3/4\bar{q}$ and $\gamma_\zeta(s) \triangleq (4\bar{q}|p|)/\beta_\zeta s^2$, $\forall s \in \mathbb{R}_{\geq 0}$. By the Gronwall-Bellman Lemma, the value of the Lyapunov function V_ζ can be bounded as follows

$$V_\zeta(t) \leq e^{-\beta_\zeta t}V_\zeta(0) + (1 - e^{-\beta_\zeta t})\gamma_\zeta(\tilde{z}(t)^2)\,. \tag{2.47}$$

Now let $V_{\tilde{\Omega}} = \frac{1}{2}\tilde{\Omega}(t)^2$ be a candidate ISS-Lyapunov function for the frequency-estimation subsystem. Then the derivative of $V_{\tilde{\Omega}}$ verifies the inequality

$$\begin{aligned}\frac{\partial V_{\tilde{\Omega}}}{\partial \tilde{\Omega}}\dot{\tilde{\Omega}}(t) &\leq -\mu|\xi(t)|^2|\tilde{\Omega}(t)|^2 + \mu|\xi(t)||\tilde{z}(t) - \tilde{\zeta}(t)|\,|\tilde{\Omega}(t)| \\ &\leq -(\mu - \epsilon_1^2)|\xi(t)|^2|\tilde{\Omega}(t)|^2 - \epsilon_1^2|\xi(t)|^2|\tilde{\Omega}(t)|^2 + \mu|\xi(t)||\tilde{z}(t) - \tilde{\zeta}(t)|\,|\tilde{\Omega}(t)| \\ &\leq -(\mu - \epsilon_1^2)|\xi(t)|^2|\tilde{\Omega}(t)|^2 + \frac{\mu}{2\epsilon_1}|\tilde{z}(t) - \tilde{\zeta}(t)|^2 \\ &\leq -(\mu - \epsilon_1^2)|\xi(t)|^2|\tilde{\Omega}(t)|^2 + \frac{\mu}{\epsilon_1}(\tilde{z}(t)^2 + \frac{V_\zeta(t)}{q})\end{aligned} \tag{2.48}$$

where $\epsilon_1 \in \mathbb{R}$ such that $\epsilon_1^2 \leq \mu$. In view of (2.47) and Assumption 3, we get to:

$$\begin{aligned}\frac{\partial V_{\tilde{\Omega}}}{\partial \tilde{\Omega}}\dot{\tilde{\Omega}}(t) &\leq -(\mu - \epsilon_1^2)\epsilon|\tilde{\Omega}(t)|^2 + \frac{\mu}{\epsilon_1}\tilde{z}(t)^2 + \frac{\mu}{q\epsilon_1}[e^{-\beta_\zeta t}V_\zeta(0) + (1 - e^{-\beta_\zeta t})\gamma_\zeta(\tilde{z}(t)^2)] \\ &\leq -(\mu - \epsilon_1^2)\epsilon|\tilde{\Omega}(t)|^2 + \frac{\mu}{\epsilon_1}\tilde{z}(t)^2 + \frac{16q|p_s|}{3q|p|}\tilde{z}(t)^2 + \delta_\zeta \\ &= -(\mu - \epsilon_1^2)\epsilon|\tilde{\Omega}(t)|^2 + \frac{\mu}{\epsilon_1}\tilde{z}(t)^2 + \frac{16k_q}{3}\tilde{z}(t)^2 + \delta_\zeta,\end{aligned} \tag{2.49}$$

in which δ_ζ denotes the exponentially decaying initial condition and $k_q \triangleq \bar{q}/\underline{q}$. Hence, $V_{\tilde{\Omega}}$ is an ISS-Lyapunov function for $\tilde{\Omega}(t)$ with respect to the pre-filtered auxiliary derivative vector $\tilde{z}(t)$, which, in turn, has been proven to be ISS with respect to the higher-order harmonics $|h(t)|$ and the uncertainty $|d(t)|$. We can conclude that the overall frequency estimator is ISS with respect to h and d. Finally, $\tilde{z}(t)$ is ISS evidenced by $\tilde{z}(t) = \tilde{\zeta}(t) + \xi(t)\tilde{\Omega}(t)$ and the boundedness of $\xi(t)$. •

Although the analytical results are, in principle, similar to the counterparts in Sec. 2.3.1, proofs are reported above to gain more insights in the influence of all the parameters. According to the performed ISS analysis of the AO estimator discussed in this chapter, the accuracy of the frequency estimation is adjustable by the tuning parameters: ω_c, K_c, μ, more details pertaining the tuning of ω_c, K_c, μ are provided in the next section by simulations.

2.5 Digital implementation of the proposed method

2.5.1 Discretization of the AFP algorithm

For the sake of analysis, the main algorithm is established in continuous-time domain, which also permits flexibility in the discretization method and sample-time choice. Due to the discrete nature of the switching dynamics, it is worth to address the discretization of

the algorithm for digital implementation in order to gain more insight into this important practical aspect. In the following, we provide a counterpart in the discretized version that is obtained by Euler method with a fixed sampling time T_s as a simple instance. Thanks to Assumption 2, an admissible set of sampling time that meets the Nyquist criterion is determined, i.e., $T_s \in (0, \pi/\bar{\omega}]$.

Given a measured signal $v(t)$ sampled at $t_k = kT_s$, $k = 1, 2, \cdots$, without loss of generality, we denote by $v(k)$ the sample collected at k-th sampling instant, then the discretized on-line algorithm is given as follows with a choice of the tuning parameters K_c, ω_c, μ and ρ, δ (if the dynamic switching is adopted):

Defining $x(k) := [x_1(k) \ \cdots \ x_{n_d-1}(k)]^\top$, the pre-filter that evolves from arbitrary initial conditions $x_0 := [x_{1_0} \ \cdots \ x_{n_p 0}]^\top \in \mathbb{R}^{n_d-1}$ is

$$\begin{cases} \hat{x}(k) = \hat{x}(k-1) + T_s(A\hat{x}(k-1) + B\,v(k)) \\ \hat{x}_{n_d-1}(k) = C\hat{x}(k) \end{cases} \tag{2.50}$$

where A, B and C are give in (2.7) and (2.8). Then, we immediately get:

$$\hat{z}(k) = \begin{bmatrix} CA^{n_d}x(k) \\ CA^{n_d}(Ax(k)+Bv(k)) \end{bmatrix}.$$

The frequency is iteratively adapted by the adaptive observer in the discrete-time domain:

$$\begin{aligned} \hat{z}(k) &= \hat{z}(k-1) + T_s\big((A_z - L_z C_z)\hat{z}(k-1) + LC\hat{z}(k) + G_z\hat{z}(k)\hat{\Omega}(k-1) \\ &\qquad -\xi(k-1)\mu\xi(k-1)^\top(\hat{z}(k-1) - \hat{z}(k))\big) \\ \xi(k) &= \xi(k-1) + T_s\big((A_z - L_z C_z)\xi(k-1) + G_z\hat{z}(k)\big) \end{aligned}. \tag{2.51}$$

The excitation signal is checked at each sampling instance by

$$\Sigma(k) = \big(\xi(k)^\top\xi(k) + \rho\big)^{-1}\xi(k)^\top\xi(k),$$

which determines a switching dynamic on the adaptation gain μ

$$\mu(k) = \begin{cases} 0 & \text{if} \quad \Sigma(k) < \delta \\ \mu, & \text{otherwise} \end{cases}.$$

Thereafter, the frequency is estimated by

$$\hat{\Omega}(k) = \hat{\Omega}(k-1) - T_s\mu(k)\xi(k)^\top(\hat{z}(k) - \hat{z}(k))$$

$$\hat{\omega}(k) = \sqrt{\max\{0,\ \hat{\Omega}(k)\}}$$

with an initial frequency set to $\hat{\Omega}(0) = \hat{\omega}(0)^2$. Finally, by using $\hat{x}(t)$ and $\hat{\omega}(k)$, the amplitude and the phase are estimated straightforwardly by the discretized equations of (2.23), (2.24), (2.20b) and (2.22b).

Estimation bias due to discretization

In the practical digital implementation of the proposed continuous-time AFP methodology, a bias on the frequency estimate has to be expected due to the discretization [86]. In order to evaluate this bias, let us assume that the filter equations (2.5) are discretized by a Euler method with sampling-time T_s. We immediately get

$$X_{1+n_d}(z) = \frac{(\omega_c K_c T_s)^{1+n_d}}{(z - 1 + \omega_c T_s)^{1+n_d}} Y(z),$$

where $Y(z)$ represents the discretized measurement. After discretization and some simple algebra, the Z-transforms of the auxiliary derivatives z_1, z_2 are given by

$$Z_1(z) = (\omega_c K_c)^{1+n_d} T_s \frac{(z-1)^{n_d}}{(z - 1 + \omega_c T_s)^{1+n_d}} Y(z)$$

and

$$Z_2(z) = (\omega_c K_c)^{1+n_d} \frac{(z-1)^{1+n_d}}{(z - 1 + \omega_c T_s)^{1+n_d}} Y(z).$$

Owing to the asymptotic sinusoidal steady-state behavior, the squared frequency after discretization is computed by

$$\Omega_{\text{discr}} = -\frac{z-1}{T_s} \frac{Z_2(z)}{Z_1(z)}.$$

After some simple algebra, we get $\Omega_{\text{discr}} = -\frac{(z-1)^2}{T_s^2}$ and then, for a given measurement with true frequency ω, we have

$$\Omega_{\text{discr}} = -\frac{\text{Re}[(e^{j\omega T_s})^2]}{T_s^2} = \frac{2\cos(\omega T_s)(1 - \cos(\omega T_s))}{T_s^2}.$$

Thus, the steady-state value of the frequency after discretization is

$$\omega_{\text{discr}} = \sqrt{2\cos(\omega T_s)(1 - \cos(\omega T_s))}/T_s. \tag{2.52}$$

The relationship (2.52) may turn out to be useful in practice to correct the effects of discretization after convergence of the estimator.

2.6 Simulation and Experimental Results

2.6.1 Simulation Results

In this subsection, some numerical examples are given to illustrate the effectiveness of the proposed AO-based methodology. The Forward-Euler discretization method with sampling period $T_s = 1$ms is used in all simulations.

Example 1: Consider a biased sinusoidal measurement affected by a high-order harmonic and a bounded perturbation:

$$y(t) = 1 + a_1(t)\sin 3t + a_2(t)\sin 12t + d(t),$$

where $a_1(t)$ and $a_2(t)$ are step-wise changing amplitudes of the sinusoid and harmonic term respectively: $a_1(t) = 5$, $a_2(t) = 0.5$ for $t \in [0, 15)$, $a_1(t) = 0.5$, $a_2(t) = 2$ for $t \in [15, 30)$, $a_1(t) = 5$, $a_2(t) = 0.5$ for $t \geq 30$, while $d(t)$ is a unstructured uncertainty with uniform distribution in the interval $[-0.5, 0.5]$. With the tuning parameters set: $\omega_c = 2$, $K_c = 0.7$, $p_1 = -4$, $p_2 = -6$, the results for the algorithm without switching for $\mu = 5$ and $\mu = 2$ are depicted in Fig.2.2 (red and green dotted lines respectively). For comparison, the estimates obtained in the same situations with the switching rule characterized by $\rho = 1$ and $\delta = 0.1$, is plotted in the Fig. 2.2 as well (blue and black dotted lines respectively). In the same figure, the switching time-instants are enhanced by vertical dotted lines, while the availability of the excitation level in real-time is verified in Fig. 2.3.

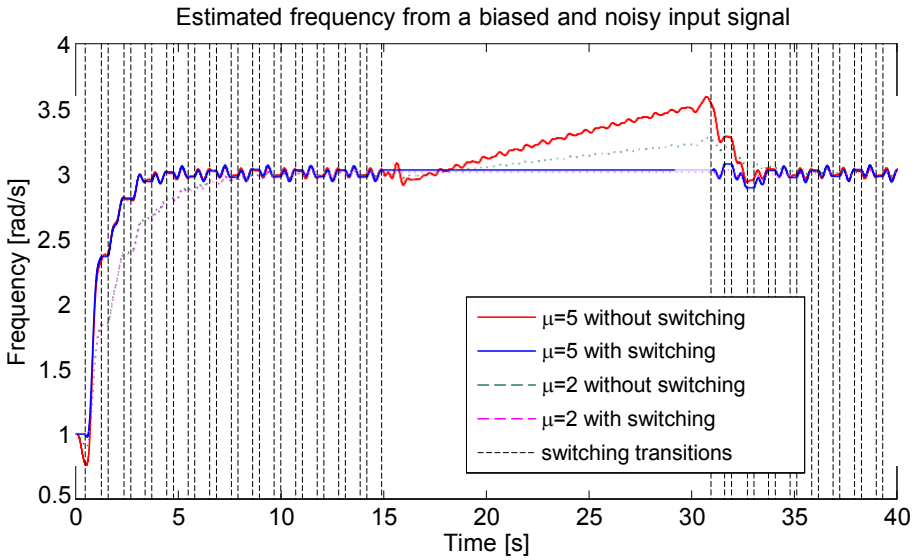

Fig. 2.2 Estimated frequency obtained by using the proposed AFP method with and without switching. The switching time-instants are shown by vertical dotted lines.

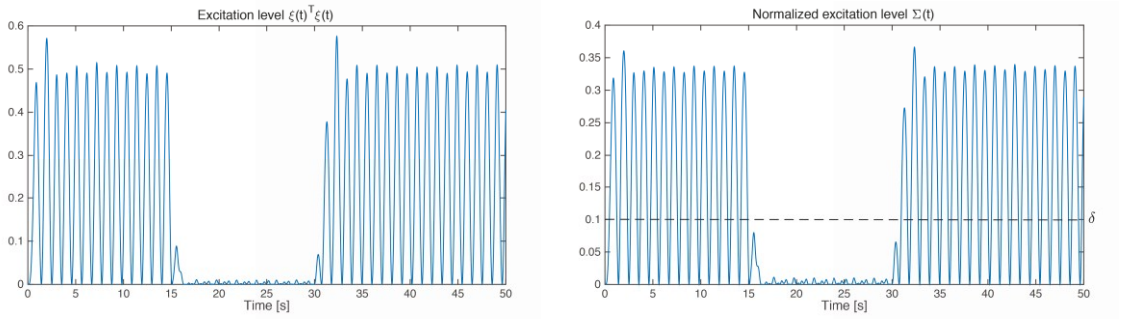

Fig. 2.3 Left: Instantaneous excitation level $\boldsymbol{\xi}(t)^T\boldsymbol{\xi}(t)$. Right: Normalized instantaneous excitation level $\boldsymbol{\Sigma}(t)$.

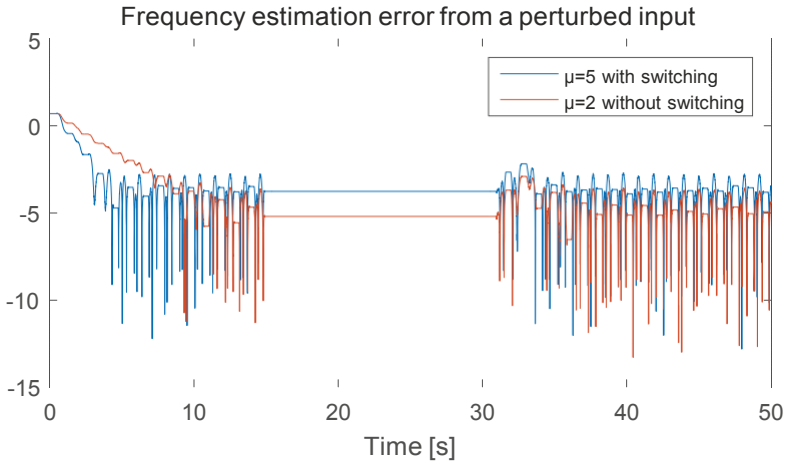

Fig. 2.4 Time-behavior of $\log|\tilde{\omega}(t)|$ in the presence of the switching.

As expected, during the time-windows in which enough excitation is present, the proposed AFP estimator is able to provide reliable estimates. On the other hand, during poorly-excited scenarios, the estimated frequency is frozen at the value taken immediately before turning-off the adaptation whereas, in case of no switching, the estimate shows a drift, as expected. Moreover, the influence of the adaptive gain μ is highlighted in Fig. 2.4, which shows that a larger value of μ improves the convergence rate at the expense of weaker noise attenuation (typical trade-off between asymptotic accuracy and convergence speed). Finally, we observe that the harmonic disturbance does not influence significantly the estimation performance due to its relatively small amplitude. Larger amplitudes clearly would have generated an attractive different equilibrium regime for the estimator.

Let us now address two important aspects, namely, guidelines for the tuning of the parameters ω_c and K_c and the effects on the estimates of the discretization.

Tuning rules for ω_c and K_c

Consider a signal $v(t) = b_1(t) + 3\sin 5t + d(t)$, where $b_1(t) = 2$ for $t \in [0, 10)$, $b_1(t) = 1$ for $t > 10$, while $d(t)$ is subject to uniform distribution in the interval $[-2.5, 2.5]$. First, we apply the nominal estimator with a constant $\mu = 5$ (no adaptation), and after we tune ω_c and K_c with the constraint of keeping constant products $\omega_c K_c = 4$ and $\omega_c K_c = 6$, respectively. The results that have been obtained are shown in Fig. 2.5. For the sake of comparison, the results obtained with the same election of parameters but without $d(t)$ are plotted as well.

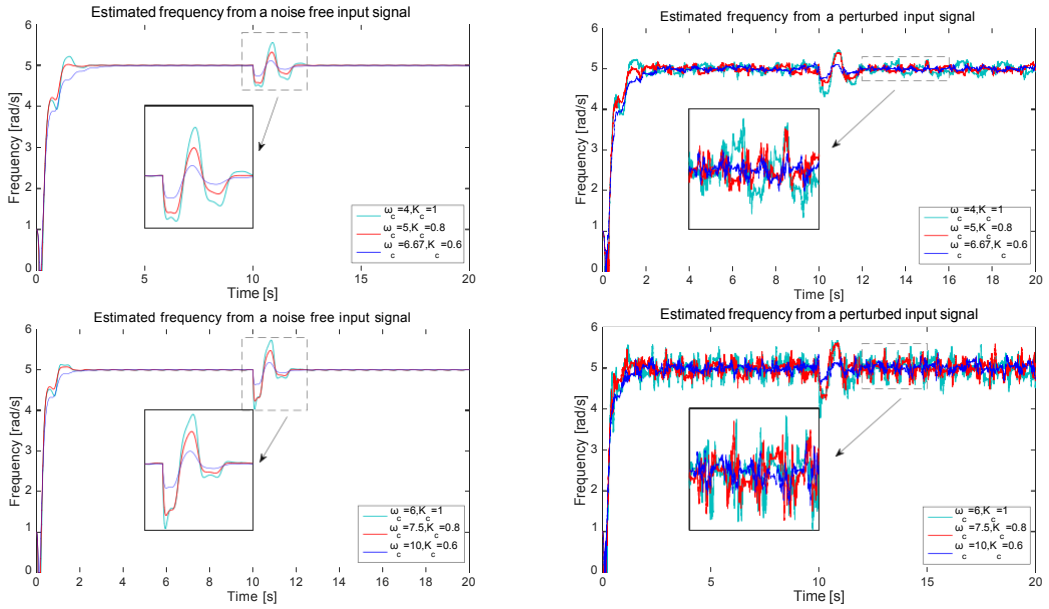

Fig. 2.5 Frequency tracking behavior based on the three sets of ω_c and K_c for a biased sinusoidal signal (top row: $\omega_c K_c = 4$, bottom row: $\omega_c K_c = 6$).

As can be noticed from the plots given in Fig. 2.5, the robustness against $d(t)$ depends on the product of ω_c and K_c: smaller values of this product give rise to better suppression of the disturbance but worse convergence speed and vice versa. Moreover, for a given value of the product of ω_c and K_c, a reduction of K_c typically yields better transient performance.

Example 2: In this example, a biased signal with two frequency steps is employed to compare the proposed AFP technique with two techniques available from the recent literature: the AFP method presented in [28] and the PLL-based technique in [58]. Let us assume that the signal that is perturbed by the same signal $d(t)$ as the one considered in the previous example:

$$v(t) = b_1(t) + 3\sin(\omega(t)t) + d(t),$$

with

$$\omega(t)=\begin{cases}4, & 0\le t<10\\ 6, & 10\le t<35\\ 2 & 35\le t<50\end{cases},\quad b_1(t)=\begin{cases}1, & 0\le t<20\\ 3 & 20\le t<50\end{cases}.$$

All the methods are initialized with the same initial condition $\hat{\omega}(0) = 1$. Method [58] is tuned with: $\mu_0 = 1$, $\mu_1 = 1$, $\mu_2 = 3$, $\mu_3 = 0.8$, while method [28] is tuned with: $K_s = 1$, $\lambda = 1$, $\omega_s = 4$, $Q_0 = (1/\lambda)I$. The adaptive parameters of the proposed method are chosen as: $\omega_c = 5$, $K_c = 0.7$, $\mu = 4$, $p_1 = -4$, $p_2 = -6$. The simulation results are shown in Fig.2.6.

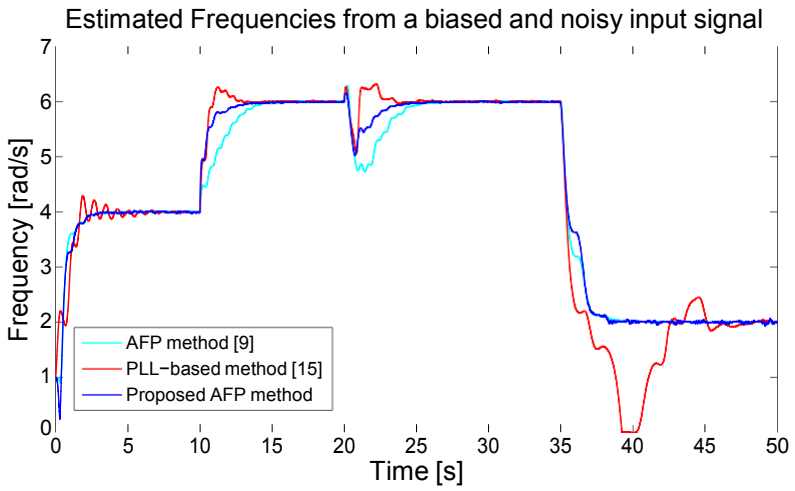

Fig. 2.6 Estimated frequencies from a biased and noisy input signal.

As can be noticed, all methods are capable to track the step-wise changing frequency with the similar response time to the first frequency value, however the PLL method [58] suffers from relatively larger overshoots for new values of the frequency and requires quite a long response time to deal with the considerable frequency drop. The AFP method [28] shows the best robustness against the disturbance at the cost of slowly tracking the intermediate frequency. Meanwhile, [28] is more sensitive to a bias variation. The proposed method shows the best transient performance and satisfactory capability of noise attenuation. In addition, it is worth noting that the PLL method is likely to be more sensitive to the adjustments of the tuning parameters than the other two methods.

For the sake of completeness, the behaviour of the amplitude adaptation scheme (2.23) is compared in Fig.2.7 with the outcome of the direct equation (2.20a). The adaptive mechanism, besides resolving the division by 0 issue of (2.20a), significantly improves the estimate in correspondence of the jumps in the frequency estimates.

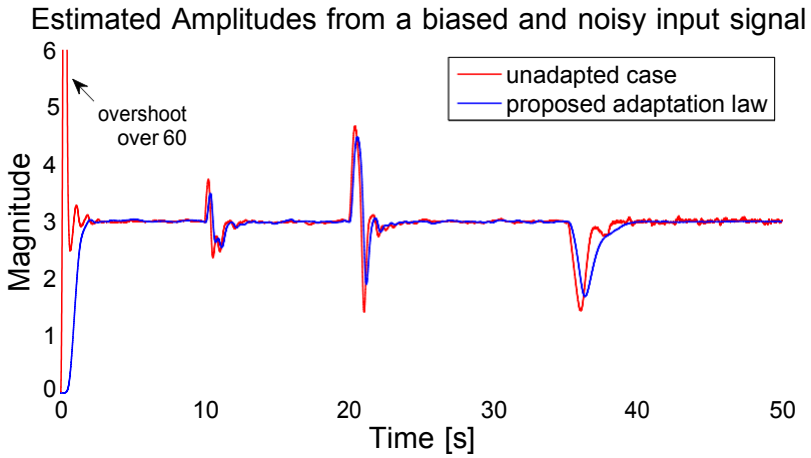

Fig. 2.7 Comparison of the behaviors in terms of amplitude estimation with adaptive mechanism (blue line) and unadapted algorithm(red line).

Example 3: Let us consider a measured signal corrupted by a drift term:

$$\hat{y}(t) = 5\sin(3t + \pi/4) + 1 + 0.5t + d(t),$$

where $d(t)$ has the same characteristics as in the previous example. The tuning coefficients are set: $\omega_c = 2.5$, $K_c = 0.6$ and $\mu = 10$, while the observer poles and initial condition are the same as given in previous example.

The results of the simulation are shown in Fig. 2.8, where we observe successful detection of the sinusoidal signal in the presence of bounded noise and an unknown drift term.

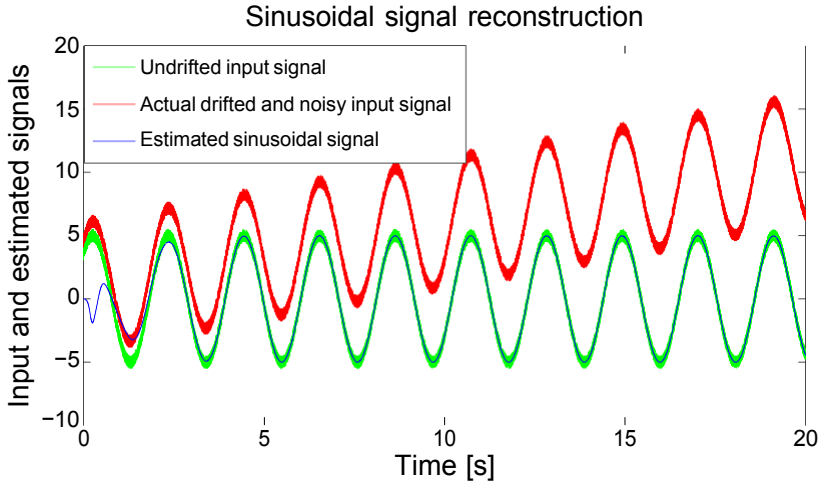

Fig. 2.8 Estimated sinusoidal signal by the proposed AFP method.

Example 4: In this example, the method presented in [69] is compared with the algorithm described in Sec. 2.4 by resorting to the same example reported in [69], with the exception of adding an unstructured perturbation term to the measurement. The periodic signal to be estimated is represented by a biased square waveform (see Fig.2.9) with unitary amplitude and frequency $\omega = 3$ rad/s:

$$\hat{y}(t) = \text{sign}(\sin(3t) - 0.5) + 1 + d(t),$$

where $d(t)$ is a bounded disturbance with uniform distribution in the interval $[-0.25, 0.25]$. The order of the prefilter for the method described in [69] is $l = 1$, yielding a total state

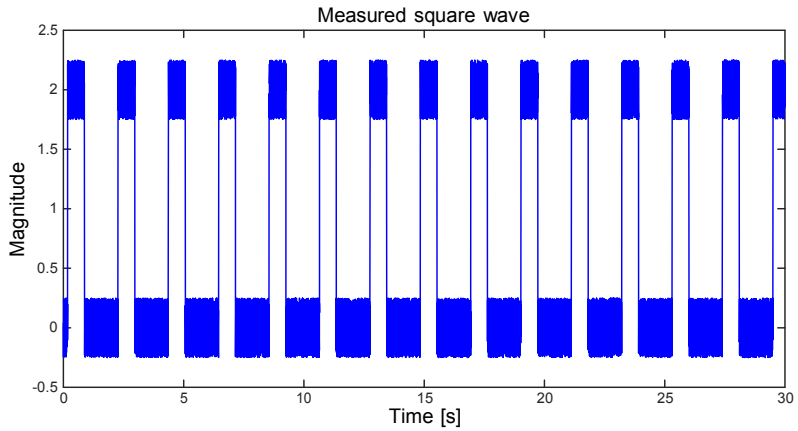

Fig. 2.9 Measured square waveform.

dimension of 10 for the overall dynamics of the adaptive observer. The adaptive coefficients of the estimator [69] take the same values reported in the Example section of [69]: $\gamma = 10000$, $d_2 = 4$, $d_3 = 5$, $d_4 = 2$, $\lambda_f = \lambda = k_0 = 1$.

The AO method presented in this chapter is tuned accordingly to $\omega_c = 1.2$, $K_c = 0.5$, $\mu = 15000$, while the poles are placed at $(-2, -1)$ to ensure that both approaches have similar response time with identical initial condition $\hat{\Omega}(0) = 0.1$. Note that the overall dimension of the proposed periodic signal estimator is 8.

According to the results illustrated in Fig.2.10, both the estimators succeeded in detecting the fundamental frequency in the presence of bounded disturbance. Indeed, the proposed estimator shows slightly better transient using a estimator characterized by a lower dynamic order.

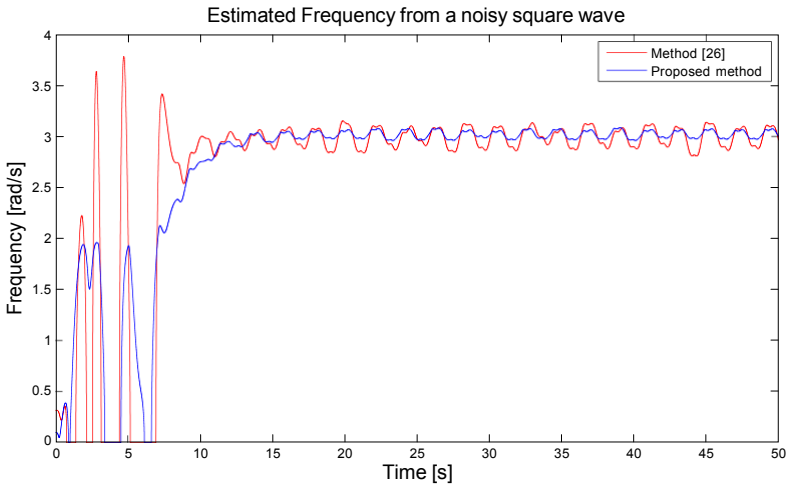

Fig. 2.10 Estimated frequency from a noisy square wave.

2.6.2 Experimental Results

Now, a practical implementation depicted in Fig.2.11 is conducted in order to evaluate the response time and accuracy of the proposed approach. Fig.2.11 also shows a picture

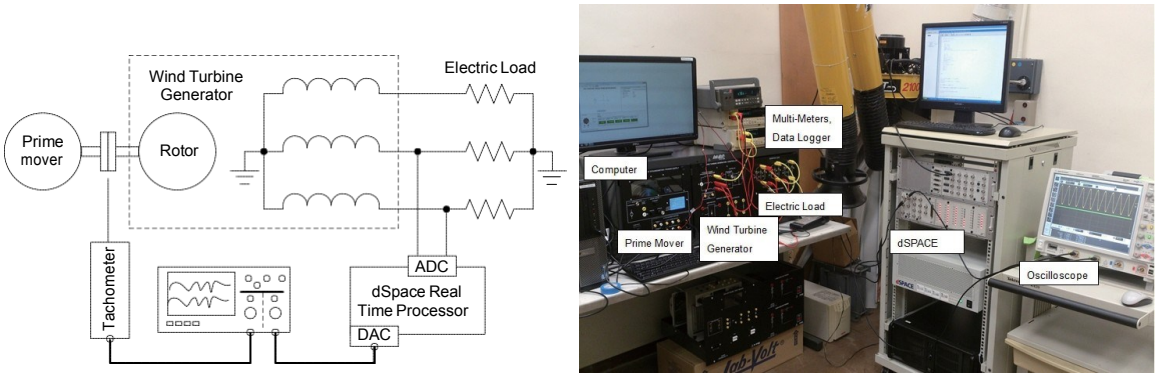

Fig. 2.11 Experimental setup and a picture of the experimental setup based on Lab-Volt Wind power training system.

of the actual setup based on the Lab-Volt wind power training system, wherein the prime mover drives the wind turbine generator with a transmission belt, thereby producing an ac voltage across the generator windings. It is worth noting that the rotational speed of the prime mover to maintain the generator output AC frequency of 50Hz is 665 rpm. During the experiment, the speed of the prime mover is programmed to emulate the intermittent nature of wind power. As a result, the generator output voltage and frequency are not constant. Moreover, the resistive load is applied as the electrical load. The instantaneous line voltage across the generator windings is measured by an analog-to-digital-converter (ADC) with

a sampling frequency of 60kHz, while a digital-to-analog-converter (DAC) is utilized to generate the estimated frequency. Such estimates are iteratively produced by the proposed estimator, which is integrated in a digital real time processor. Finally, the measured prime mover rotational speed and the estimated frequency are captured by an oscilloscope and recorded by a high precision digital-multimeter (DMM) with **5** digits resolution.

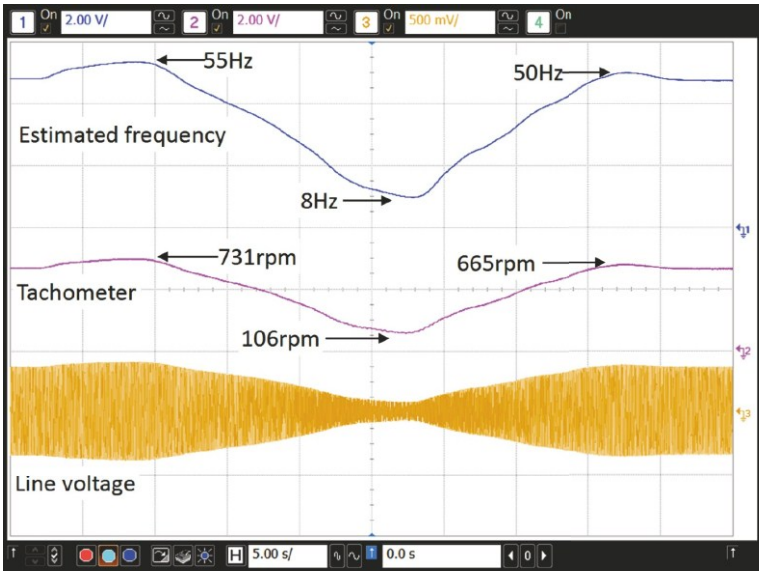

Fig. 2.12 Experimental results. Ch1. (bule) Estimated frequency obtained by using the proposed AFP method (20Hz/Div), Ch2. (pink) Output voltage from the analog tachometer (500rpm/Div), Ch3. (yellow) line voltage across the wind turbine generator (50V/Div). Time base: 5s/Div.

The dynamic behaviour of the proposed AFP algorithm is shown in Fig.2.12, where we observe that the estimated frequency tracks the fluctuating rotational speed of the wind turbine from 8Hz to 55Hz closely with almost identical profile. Fig. 2.13 shows the values of the identified frequency and prime mover rotational speed. The subtle differences between the frequency estimates and reading from tachometer (less than **0.25**mV) are due to the instrument tolerance and noise generated by the prime mover drive. Therefore, these results show that the accuracy of the proposed algorithm is limited by the resolution of the measurement equipment. It is important to note that the proposed AFP algorithm achieves high precision frequency estimation with an accuracy of **0.05**Hz resolution in this setup.

2.7 Concluding Remarks

In this chapter, a novel dual-mode adaptive observer-based technique for estimation of the amplitude, frequency and phase of sinusoidal signals from perturbed measurements has

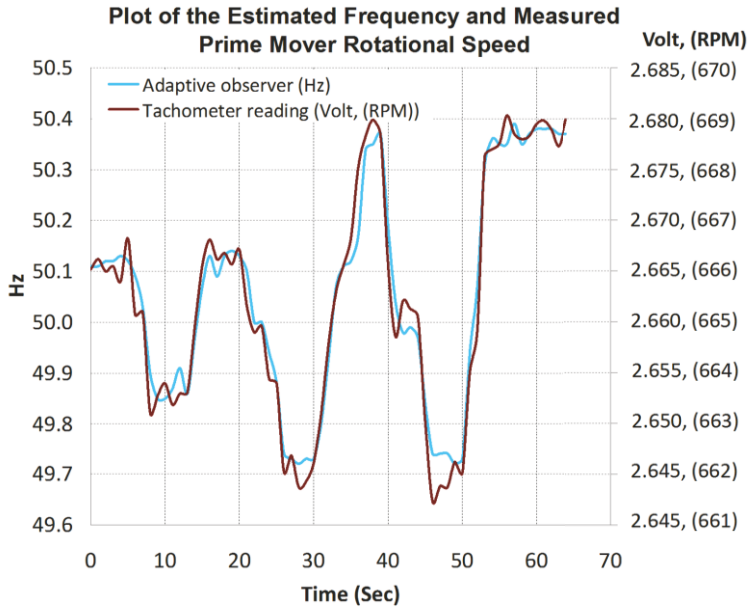

Fig. 2.13 Comparison of the estimated frequency obtained by using the proposed AFP method and measured prime mover rotational speed.

been presented. The estimator embeds a switching criterion that disables the adaptation in real-time under poor excitation conditions, thereby the behavior of the estimator in "dis-excited" time interval is characterized. The ISS analysis is carried out to enhance not only the robustness properties, but also the roles and the impacts of the adaptive parameters. This chapter also offers a comprehensive investigation on the influence of different types of perturbations, including structured, unstructured and harmonic disturbances. More specifically, the structured disturbances are modeled as a time-polynomial so as to represent bias and drift phenomena typically present in applications, whereas the unstructured disturbances are modeled as bounded noise signals. Harmonic disturbances are addressed through a fundamental frequency identification problem, where the harmonics are treated as a part of the generic periodic signal. Extensive simulations and real experiments have been carried out to show the effectiveness of the proposed adaptive algorithm.

Chapter 3

ADAPTIVE OBSERVER APPROACH: THE MULTI-SINUSOIDAL CASE

3.1 Introduction

In chapter 2, we presented an AO method for single (fundamental) frequency estimation that is one of the basic issue arising in numerous practical applications. Nevertheless, particular applications require online frequency estimates of harmonics and inter-harmonics. In this respect, various types of methods emerge in the recent literature, such as [29, 55, 75, 76], which stem from the PLL and ANF concepts. As a consequence, only local stability can be guaranteed in the most cases because of the averaging tools used for analysis. On the contrary, the AO techniques [17, 46, 80, 100, 111] relying on a system model parametrized by the coefficients of the characteristic polynomial, usually ensure global or semi-global stability. The main drawback of the AO methods is the indirect frequency estimation (computed as the zeros of the characteristic polynomial) which might result in an excessive on-line computational burden.

In this chapter, the AO method discussed in Chapter 2 is extended to a solution for multi-sinusoidal signals by proper model augmentation. In spirit of the initial results presented in [22], the presented method deals with a direct adaptation mechanism for the squares of the frequencies with semi-global stability guarantees. In contrast with [22] that is equipped by a scalar switching signal globally regulating the adaptation of the frequency parameters, the new estimator adopts a n dimensional excitation-based switching logic. Thanks to the suitable matrix decomposition techniques, this novel switching criterion enables the update of a parameter when the signal is sufficiently informative in that direction, thus enhancing the practical implementation and avoiding unnecessarily disabled adaptation in the scenario that

only parts of the directions fulfill the excitation condition (e.g. over-parametrization). The stability analysis proves the existence of a tuning parameter setting for which the estimator's dynamics are ISS with respect to bounded measurement disturbance.

The chapter is organized as follows: Section 3.2 is devoted to the formulation of the AFP problem in the multi-frequency scenario. In particular, the nominal linear multi-sinusoidal oscillator is transformed into an observable system with state-affine linear parametrization, in which the parameter-affine term depends on the unknown frequencies. In Section 3.3, the design of the adaptive observer-based estimator is treated. The embedded excitation-based switching dynamics permit the analysis in case of poor excitement by freezing the estimates under certain circumstances. Then, the stability of the presented approach is dealt with in Section 3.4 by ISS concepts. Section 3.5 gives an example of the discretized algorithm for digital implementation. Finally, in Section 3.6, simulations and practical experiments are carried out to evaluate the behavior of the algorithm.

3.2 Problem formulation and preliminaries

Consider the following perturbed multi-sinusoidal signal:

$$\begin{cases} v(t) = b + \sum_{i=1}^{n} a_i \sin(\phi_i(t)) + d(t), \\ \dot{\phi}_i(t) = \omega_i \end{cases} \tag{3.1}$$

with $\phi_i(0) = \phi_{i_0}$, where b is an unknown constant bias, the amplitudes of the sinusoids verify the inequality $a_i \geq 0,\ \forall i \in \{1, \ldots, n\}$, ϕ_{i_0} is the unknown initial phase of each sinusoid, while the term $d(t)$ and the frequencies comply with Assumption 1 and 2 (see page 19) respectively. Now, let us denote by $y(t)$ the noise-free signal

$$y(t) = b + \sum_{i=1}^{n} a_i \sin(\omega_i t + \phi_{i_0}) \tag{3.2}$$

which is assumed to be generated by the following observable autonomous marginally-stable dynamical system:

$$\begin{cases} \dot{x}(t) = A_x x(t) + \sum_{i=1}^{n} A_i x(t) \theta^*_i, \quad x(0) = x_0 \\ y(t) = C_x x(t) \end{cases} \tag{3.3}$$

with $x(t) \triangleq [x_1(t) \cdots x_{2n+1}(t)]^\top \in \mathbb{R}^{2n+1}$ and where x_0 represents the unknown initial condition which leads the output to match the stationary sinusoidal behavior since the very beginning. The new parametrization $\theta_1^*, \ldots, \theta_n^*$ used in (3.3) is related to the original frequency parameters by the relationships

$$\theta_i^* = \alpha_i + \Omega_i, \quad \forall i \in \{1, \cdots, n\}, \tag{3.4}$$

with $\Omega_i = \omega_i^2, \ \forall i \in \{1, \cdots, n\}$ and where $\alpha_1, \alpha_2, \cdots, \alpha_n$ are non-zero constants that are designed with the only requirements to satisfy $\alpha_i \neq \alpha_j$ for $i \neq j$. The matrices of the linear multi-oscillator (3.3) are given by

$$A_x = \begin{bmatrix} J_1 & 0_{2\times 2} & \cdots & 0_{2\times 2} & 0 \\ 0_{2\times 2} & J_2 & \ddots & 0_{2\times 2} & 0 \\ \vdots & \ddots & \ddots & \ddots & \vdots \\ & \ddots & \ddots & J_n & 0 \\ 0_{2\times 2} & & & & \\ 0 & \cdots & \cdots & 0 & 0 \end{bmatrix}, \quad C_x^\top = \begin{bmatrix} c_1^\top \\ c_2^\top \\ \vdots \\ c_n^\top \\ 1 \end{bmatrix}$$

where $0_{r\times s}$ represents a $r \times s$ zero matrix, for generic indexes r and s

$$J_i = \begin{bmatrix} 0 & 1 \\ \alpha_i & 0 \end{bmatrix}, \quad c_i = \begin{bmatrix} 1 & 0 \end{bmatrix}.$$

Moreover, each A_i in (3.3) is a square matrix having the $(2i, 2i-1)$th entry equal to -1. Letting

$$J_0 = \begin{bmatrix} 0 & 0 \\ -1 & 0 \end{bmatrix}$$

A_1 and A_2 for instance are given by:

$$A_1 = \begin{bmatrix} J_0 & 0_{2\times(2n-1)} \\ 0_{(2n-1)\times 2} & 0_{(2n-1)\times(2n-1)} \end{bmatrix}, \quad A_2 = \begin{bmatrix} 0_{2\times 2} & 0_{2\times 2} & 0_{2\times(2n-3)} \\ 0_{2\times 2} & J_0 & 0_{2\times(2n-3)} \\ 0_{(2n-3)\times 2} & 0_{(2n-3)\times 2} & 0_{(2n-3)\times(2n-3)} \end{bmatrix}$$

Thanks to (3.3), the noisy signal $v(t)$ can be generated by the observable system

$$\begin{cases} \dot{x}(t) = A_x x(t) + G_x(x(t))\theta^*, \ x(0) = x_0 \\ v(t) = C_x x(t) + d(t) \end{cases} \tag{3.5}$$

in which

$$G_x(x(t)) = \begin{bmatrix} G_{x_1}(x(t)) & \cdots & G_{x_i}(x(t)) & \cdots & G_{x_n}(x(t)) \end{bmatrix}, \tag{3.6}$$

$$G_{x_i}(x(t)) = [0_{1\times(2i-1)} \;\; x_{2i-1}(t) \;\; 0_{1\times(2n+1-2i)}]^\top, \; \forall i = 1, 2, \cdots, n, \tag{3.7}$$

and $\theta^* \in \mathsf{R}^n$ denotes the true parameter vector $[\theta_1^* \;\; \cdots \;\; \theta_n^*]^\top$. According to Assumption 2, there exists a known positive constant θ^*, such that $|\theta^*| \leq \theta^*$. More specifically, in the remaining parts of this chapter we consider $\theta^* \in \Theta^*$, where $\Theta^* \subset \mathsf{R}^n$ is a hypersphere of radius θ^*. It is important to stress that the constraint on θ^* is instrumental for proving the stability of the parameter adaptation law introduced in the next section, but is not needed in the actual implementation of the algorithm.

It is clear from (3.6) and (3.7) that the elements of $G_x(\cdot)$ are globally Lipschitz continuous functions due to the linearity of $G_x(\cdot)$. Moreover, the true state $x(t)$ is norm-bounded for any initial condition, i.e. $|x(t)| \leq \bar{x}, \; \forall t \in \mathsf{R}_{\geq 0}$. Both the Lipschitz condition on $G_x(\cdot)$ and the bound $\bar{x}$ allow to establish the following further bound

$$\| G_x(x(t)) \| \leq \bar{x}, \; \forall t \in \mathsf{R}_{\geq 0}.$$

Now, assuming that the estimates $\hat{x}(t)$ and $\hat{\theta}(t)$ are available, then the full AFP estimates are obtained by

$$\hat{\Omega}_i(t) = \max\{0, \hat{\theta}(t) - \alpha_i\}, \qquad \hat{\omega}_i(t) = \begin{cases} \hat{\Omega}_i(t), & \text{if } \hat{\Omega}_i(t) \geq \omega_{\min} \\ \omega_{\min}, & \text{otherwise} \end{cases}, \tag{3.8}$$

$$\hat{a}_i(t) = \begin{cases} \left(\hat{\Omega}_i(t) \hat{x}_{2i-1}(t)^2 + \hat{x}_{2i}(t)^2 \right) / \hat{\Omega}_i(t), & \text{if } \hat{\Omega}_i(t) \geq \omega_{\min} \\ 0, & \text{otherwise} \end{cases}, \tag{3.9}$$

and

$$\hat{\phi}_i(t) = \angle \left(\hat{x}_{2i}(t) + \mathrm{j}\, \hat{\omega}_i(t)\, \hat{x}_{2i-1}(t) \right), \quad i = 1, 2, \cdots, n. \tag{3.10}$$

In addition, the estimates of the offset is obtained directly by $\hat{b} = \hat{x}_{2n+1}$. Note that the possible singularity issue $\hat{\Omega}_i(t) = 0$ affecting (3.9) is addressed by the following adaptive amplitude estimators (3.11) in spirit of the previous treatment reported in Section 2.3 on the estimation of a single sinusoidal signal:

$$\begin{aligned} \dot{\bar{a}}_i(t) &= -\mu_a \hat{\omega}_i(t) \left(\hat{\omega}_i(t) \bar{a}_i(t) - \left(\hat{\Omega}_i(t) \hat{x}_{2i-1}(t)^2 + \hat{x}_{2i}(t)^2 \right) \right), \\ \hat{a}_i(t) &= \max\{0, \bar{a}_i(t)\} \end{aligned} \tag{3.11}$$

where $\hat{a}_i(0) = \bar{a}_i(0) = 0$, $\mu_a \in \mathrm{R}_{>0}$ is an adjustable gain subject to the trade-off between accuracy and convergence speed (see Fig. 2.4).

3.3 Filtered-augmentation-based adaptive observer

Recall the biased multi-oscillator (3.5), in which n unknown frequencies are embedded. In order to address the frequency estimation task by means of an adaptive observer approach (see [84] for a special case), let us first augment the dynamics of the observed system with a synthetic low-pass filter driven by the noisy measurement:

$$\dot{v}_f(t) = A_f v_f(t) + B_f v(t), \tag{3.12}$$

where A_f and B_f are set by the designer such that A_f is Hurwitz and the pair (A_f, B_f) is controllable. $v_f(t) \in \mathrm{R}^{n_f}$ denotes the accessible state vector and with arbitrary initial condition v_{f0}, such that the dimension n_f of the augmented dynamics verifies $n_f = n - 1$.

For the sake of the forthcoming analysis, it is convenient to split the filtered output into two components:

$$v_f(t) \triangleq y_f(t) + d_f(t),$$

where $y_f(t)$ and $d_f(t)$ can be thought as produced by two virtual filters, driven by the unperturbed output and by the measurement disturbance, respectively:

$$\dot{y}_f(t) = A_f y_f(t) + B_f y(t), \quad \dot{d}_f(t) = A_f d_f(t) + B_f d(t). \tag{3.13}$$

Consequently, in view of (3.5), (3.13), the overall augmented system dynamics with the extended perturbed output measurement equation can be written as follows:

$$\begin{cases} \dot{z}(t) = A_z z(t) + G_z(z(t))\theta \\ \eta(t) = C_z z(t) \\ \tilde{\eta}(t) = \eta(t) + d_\eta(t) \end{cases}, \tag{3.14}$$

with $z(0) = z_0 \in \mathrm{R}^{n_z}$, $n_z = 2n + 1 + n_f = 3n$, and $z(t) \triangleq [x^\top(t)\ y_f^\top(t)]^\top$, $z_0 \triangleq [x_0^\top\ \hat{y}_{f0}^\top]^\top$, $\tilde{\eta}(t) \triangleq [v(t)\ v_f^\top(t)]^\top$, $d_\eta(t) \triangleq [d(t)\ d_f^\top(t)]^\top$,

$$A_z \triangleq \begin{bmatrix} A_x & 0_{(2n+1)\times(n-1)} \\ B_e C_x & A_f \end{bmatrix}, \quad C_z \triangleq \begin{bmatrix} C_x & 0_{1\times(n-1)} \\ 0_{(n-1)\times(2n+1)} & I_{(n-1)} \end{bmatrix},$$

and

$$G_z(z(t)) \triangleq \begin{bmatrix} G_x(T_{zx}z(t)) \\ 0_{(n-1)\times n} \end{bmatrix},$$

with the transformation matrix given by $T_{zx} \triangleq [I_{2n+1}\ 0_{(2n+1)\times(n-1)}]$. It is worth noting that $G_z(z(t))$ is also Lipschitz, with unitary Lipschitz constant as $G_x(x(t))$, and can be norm-bounded by $\bar{x}$. Moreover, the assumed norm-bound $\bar{d}$ on the output noise implies the existence of $\bar{d}_\eta$ such that $\bar{d}_\eta > 0 : |d_\eta(t)| \leq \bar{d}_\eta,\ \forall t \in \mathbb{R}_{\geq 0}$.

Now, we introduce the structure of the adaptive observer for obtaining estimates of the unknown parameter vector θ^*, and in turn frequency estimates $\hat{\Omega}_i,\ i = 1, \cdots, n$. Besides the measured output filter (3.12), the architecture of the estimator also includes three dynamic components (3.15), (3.16) and (3.18), which are described below:

1) Augmented state estimator:

$$\dot{\hat{z}}(t) = (A_z - LC_z)\hat{z}(t) + L\eta(t) + G_z(\hat{z}(t))\hat{\theta}(t) + \Xi(t)\dot{\hat{\theta}}(t) \tag{3.15}$$

with $\hat{z}(0) = \hat{z}_0$ and where $\Xi(t)$ is defined in (3.17). The gain matrix L is given by

$$L \triangleq \begin{bmatrix} L_x & 0_{(2n+1)\times(n-1)} \\ 0_{(n-1)\times 1} & 0_{(n-1)\times(n-1)} \end{bmatrix}$$

where L_x is a suitable gain matrix such that $(A_x - L_xC_x)$ is Hurwitz. Additional constraints on the poles' selection are discussed in Theorem 3.4.1.

2) Parameter-affine state-dependent filters:

Let $G_{z_1}(z(t)), \cdots, G_{z_n}(z(t))$ be the columns of $G_z(z(t))$, that is

$$G_z(z(t)) = \begin{bmatrix} G_{z_1}(z(t)) & \cdots & G_{z_i}(z(t)) & \cdots & G_{z_n}(z(t)) \end{bmatrix}.$$

Then, we introduce a set of auxiliary signal $\xi_i(t),\ i = 1, \cdots, n$, whose dynamics obeys the following differential equations driven by the available (estimated) counterpart of $G_z(z(t))$:

$$\dot{\xi}_i(t) = (A_z - LC_z)\xi_i(t) + G_{z_i}(\hat{z}(t)),\ \forall i = 1, \cdots, n, \tag{3.16}$$

with $\xi_i(0) = 0_{n_z\times 1}$. By collecting all the filters' states, we get the auxiliary signal matrix

$$\Xi(t) = [\xi_1(t) \cdots \xi_i(t) \cdots \xi_n(t)], \tag{3.17}$$

used in (3.15).

3) Frequency adaptation unit:

Herein, an projection operator P is utilized to confine the estimated parameter $\hat{\theta}(t)$ to the predefined convex region Θ^*

$$\dot{\hat{\theta}}(t) = \mathsf{P}\left(\dot{\hat{\theta}}_{pre}(\Psi(t), t)\right)_{|\leq \bar{\theta}^*} \tag{3.18}$$

with $\hat{\theta}(0) = \hat{\theta}_0$ set arbitrarily, and where $\dot{\hat{\theta}}_{pre}$ is the unconstrained parameter's derivative, whose explicit expression is given in (3.21); $\Psi(t) \in \mathsf{R}^{n\times n}$ represents a diagonal matrix consisting of binary (1: on, 0: off) on-off switching signals which enable or disable the adaptation of a specific parameter:

$$\Psi(t) \mathrel{/\!\!:=} \mathrm{diag}[\psi_1(t), \cdots, \psi_i(t), \cdots, \psi_n(t)]. \tag{3.19}$$

The adaptation-enabling signals $\psi_i(t),\ \forall i = 1, 2, \cdots, n$ will be specified later on. For the sake of brevity, we write $\hat{\theta}_{pre}(t)$ instead of $\hat{\theta}_{pre}(\Psi(t), t)$, dropping the dependence of $\hat{\theta}_{pre}$ on $\Psi(t)$ in the rest of the section. The parameters' derivative projection operator in (3.18) is defined as [52]:

$$\mathsf{P}\left(\dot{\hat{\theta}}_{pre}(t)\right)_{|\leq \bar{\theta}^*} \mathrel{/\!\!:=} \dot{\hat{\theta}}_{pre}(t) - \mathsf{I}(\theta)\frac{\hat{\theta}(t)\hat{\theta}^{\top}(t)}{\bar{\theta}^{*2}}\dot{\hat{\theta}}_{pre}(t) \tag{3.20}$$

where $\mathsf{I}(\theta)$ denotes the indicator function, defined as:

$$\mathsf{I}(\theta) \mathrel{/\!\!:=} \begin{cases} 1, & \text{if } |\hat{\theta}(t)| = \bar{\theta}^* \text{ and } \hat{\theta}^{\top}(t)\dot{\hat{\theta}}_{pre}(t) > 0, \\ 0, & \text{otherwise}. \end{cases}$$

Now, the unconstrained derivative is given by:

$$\dot{\hat{\theta}}_{pre}(t) \mathrel{/\!\!:=} -\mu U_{\Psi}(t)\left(\Psi(t)S_{\Psi}(t)\right)U_{\Psi}^{\top}(t)U_{\Xi}(t)\breve{S}_{\Xi}(t)U_{\Xi}^{\top}(t)\Xi^{\top}(t)C_z^{\top}(C_z\hat{x}(t) - \hat{\eta}(t)), \tag{3.21}$$

with U_{Ψ}, S_{Ψ}, U_{Ξ}, $\breve{S}_{\Xi}$ defined in the following. The matrices U_{Ψ} and S_{Ψ} are obtained by the SVD of $\Sigma_{\Psi}(\Xi(t))$:

$$\begin{aligned}\Sigma_{\Psi}(\Xi(t)) \mathrel{/\!\!:=} &\left(\Xi^{\top}(t)\Xi(t) + \rho^2 I\right)^{-1}\Xi^{\top}(t)C_z^{\top}C_z\Xi(t) \\ &= U_{\Psi}(t)S_{\Psi}(t)U_{\Psi}^{\top}(t)\end{aligned}$$

in which $S_{\Psi}(t)$ is a diagonal matrix comprising all the eigenvalues of $\Sigma_{\Psi}(\Xi(t))$. Analogously, U_{Ξ} and S_{Ξ} are obtained by the SVD of the matrix $\Sigma_{\Xi}(\Xi)$ defined as:

$$\Sigma_{\Xi}(\Xi(t)) \mathrel{/\!\!:=} \Xi^{\top}(t)C_z^{\top}C_z\Xi(t) = U_{\Xi}(t)S_{\Xi}(t)U_{\Xi}^{\top}(t).$$

Thanks to the above decomposition, let us define the matrix $S_{\Xi}(t) \triangleq \mathrm{diag}\{S_{\Xi_i}(t)\}$ where

$$S_{\Xi_i}(t) = \begin{cases} \lambda_i(S_{\Xi}(t))^{-1}, & \text{if } \psi_i(t) = 1, \\ 0, & \text{if } \psi_i(t) = 0 \end{cases}. \tag{3.22}$$

The binary switching signal $\psi_i(t)$, $i = 1, 2, \ldots, n$ that determines the activation/suppression of the parameter adaptation possesses the following hysteretic property:

$$\psi_i(t) = \begin{cases} 1, & \text{if } \lambda_i(\Sigma(\Xi(t))) \geq \bar{\delta} \\ 0, & \text{if } \lambda_i(\Sigma(\Xi(t))) < \underline{\delta} \\ \psi_i(t^-), & \text{if } \underline{\delta} \leq \lambda_i(\Sigma(\Xi(t))) < \bar{\delta} \end{cases} \tag{3.23}$$

The transition thresholds $\underline{\delta}$, $\bar{\delta}$ are fixed by the designer such that $0 < \underline{\delta} < \bar{\delta} < 1$. The introduction of the hysteresis is motivated by the need to ensure a minimum finite duration between transitions (see Fig. 3.11).

Remark 3.3.1 To avoid the possible interference between the estimators (e.g., two or more estimators to converge to the same frequency value), we may apply distinct frequency 'clips' in different ranges of frequency based on a priori knowledge on the nominal frequency values (a similar idea of frequency separation can be found in [76]).

3.4 Stability analysis

Before we carry out the stability analysis, let us define the augmented state-estimation error vector

$$\tilde{z}(t) \triangleq \hat{z}(t) - z(t).$$

Moreover, in order to address the case of overparametrization (that is, the number of model parameters n is larger than the number of sinusoids $n_e(t) \in \mathbb{N} : 0 \leq n_e(t) \leq n$ that at time t are adapted), it is convenient to define two parameter estimation errors, one accounting for all the parameters

$$\tilde{\theta}(t) \triangleq \hat{\theta}(t) - \theta^* \in \mathbb{R}^n,$$

and the other considering the $n_e(t)$ components that are adapted at a given instant

$$\tilde{\theta}_{n_e(t)}(t) \triangleq \hat{\theta}_{n_e(t)}(t) - \theta^*_{n_e(t)} \in \mathbb{R}^{n_e(t)},$$

where $\hat{\theta}_{n_e(t)}(t)$ and $\theta^*_{n_e(t)}$ collect all and only those scalar components of the estimated and true parameter vectors for which $\psi_i(t) = 1$. In this connection, let $E_{n_e(t)} \in \mathbb{N}^{n_e(t)}$ be a set

containing the integer indexes of all and only those components for which the adaptation is enabled at time t.

As said above, the case of overparametrization herein corresponds to a situation in which the number of frequency parameters of the observer, n, is larger than $n_e(t)$, the number of dominant sinusoids in terms of amplitude with unique frequency forming the measured signal[1] (more details of overparametrization in the context of adaptive control can be found in [104]). In this case a minimal realization of the generator of the measured signals is a multi-harmonic oscillator of order $2n_e$, composed by the collection of exactly n_e unique harmonic oscillators [37]. Accordingly, a non-minimal realization for such a signal generator can be taken as the union of the said minimal multi-harmonic oscillator with an augmented dynamics formed by $(n - n_e)$ harmonic oscillators with null-states and arbitrary frequencies. The possibility to assign arbitrarily the frequency of the augmented null-amplitude multi-oscillator is the key for proving the stability in this context. For the sake of the further discussion, without loss of generality, let us take the frequency parameters of the augmented dynamics equal to the present estimates produced by the filter for the components not adapted due to poor excitation, achieved by

$$\theta_i^* = \hat{\theta}(t), \ \forall i \in \{1, 2, \cdots, n\} \backslash E_{n_e(t)}, \tag{3.24}$$

which implies

$$\tilde{\theta}(t) \ /'. \ \hat{\theta}(t) - \theta_i^* = 0, \ \forall i \in \{1, 2, \cdots, n\} \backslash E_{n_e(t)}. \tag{3.25}$$

For the sake of the further discussion let us also define the linear time-varying combination of state and parameter vectors $\tilde{\zeta}(t) \ /'. \ \sum_{i=1}^{n} \xi_i(t)\tilde{\theta}(t) - \tilde{z}(t)$, The state-estimation error evolves according to the differential equation:

$$\begin{aligned}\dot{\tilde{z}}(t) &= (A_z - LC_z)\tilde{z}(t) + Ld_\eta(t) + G_z(\tilde{z}(t))\tilde{\theta}(t) + G_z(\tilde{z}(t))\theta^* + \sum_{i=1}^{n} \xi_i(t)\dot{\hat{\theta}}(t) \\ &= (A_z - LC_z)\tilde{z}(t) + Ld_\eta(t) + G_z(\tilde{z}(t))\theta^* + \sum_{i \in E_{n_e(t)}} G_{z_i}(\tilde{z}(t))\tilde{\theta}(t) + \Xi(t)\dot{\hat{\theta}}(t),\end{aligned} \tag{3.26}$$

where $G_z(\tilde{z}(t)) \ /'. \ G_z(\tilde{z}(t)) - G_z(z(t))$. Meanwhile, the auxiliary variable $\tilde{\zeta}(t)$ evolves according to

$$\dot{\tilde{\zeta}}(t) = \sum_{i \in E_{n_e(t)}} \dot{\xi}_i(t)\tilde{\theta}(t) + \Xi(t)\dot{\tilde{\theta}}(t) - \dot{\tilde{z}}(t), \tag{3.27}$$

[1]The residual sinusoidal signals not accounted for by the adaptation are masked and implicitly treated as a disturbance.

which, after some algebra, leads to

$$\begin{aligned}\dot{\tilde{\zeta}}(t) = & \sum_{i \in E_{ne(t)}} \Big((A_z - LC_z)\xi_i(t)\tilde{\theta}(t) + G_z(\tilde{z}(t))\tilde{\theta}(t) \Big) + \Xi(t)\dot{\tilde{\theta}}(t) - (A_z - LC_z)\tilde{z}(t) \\ & - G_z(\tilde{z}(t))\tilde{\theta}(t) - Ld_\eta(t) - G_z(z(t))\tilde{\theta}(t) - G_z(\tilde{z}(t))\theta^* - \Xi(t)\dot{\tilde{\theta}}(t) \\ = & (A_z - LC_z)\tilde{\zeta}(t) - Ld_\eta(t) - G_z(\tilde{z}(t))\theta^* .\end{aligned} \tag{3.28}$$

In Fig. 3.1, we draw the overall excitation-based switching scheme, which is instrumental for the forthcoming analysis. In principle, the adaptation is deemed activated as long as $n_e \neq 0$, which means at least one component is updating. An active identification interval always starts from a transition to active identification time-interval, and ends up with a transition to dis-excitation time-interval, while the dis-excitation interval is the opposite. More specifically, let $k_e(t)$ be a counter for the transitions to excitation, described by the

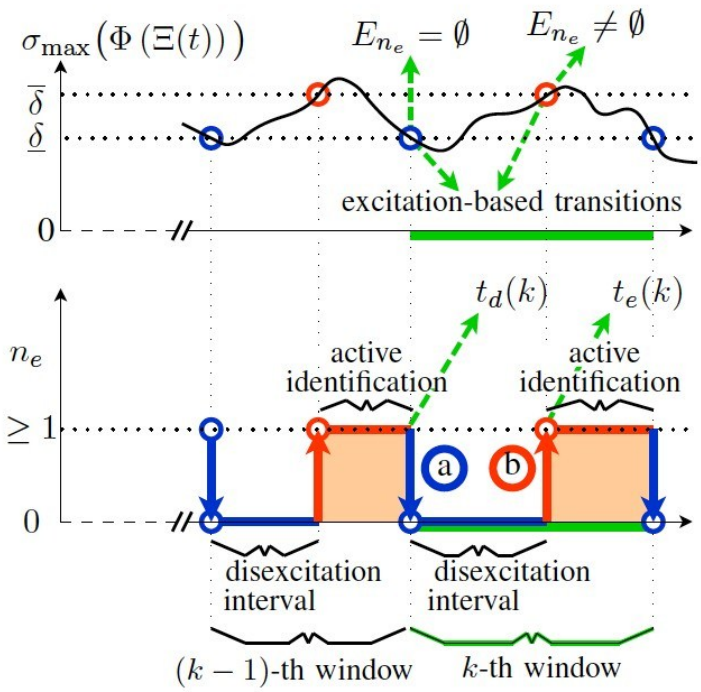

Fig. 3.1 Scheme of the excitation-based switching scheme for enabling/disabling the parameter adaptation. The transitions to dis-excitation (a) and to active identification phases (b) have been highlighted.

jump dynamics given below:

$$k_e(t) = \begin{cases} k_e(t^-) + 1, & \text{if } E_{n_e}(t^-) = \emptyset \text{ and } E_{n_e}(t) \neq \emptyset, \\ k_e(t^-), & \text{if } E_{n_e}(t^-) \neq \emptyset \text{ and } E_{n_e}(t) = \emptyset. \end{cases}$$

Analogously, let $k_{1\to 0}(t)$ be a counter with respect to the transition from excitation to dis-excitation:

$$k_d(t) = \begin{cases} k_d(t^-) + 1, & \text{if } E_{n_e}(t^-) \neq \emptyset \text{ and } E_{n_e}(t) = \emptyset, \\ k_d(t^-), & \text{if } E_{n_e}(t^-) = \emptyset \text{ and } E_{n_e}(t) \neq \emptyset. \end{cases}$$

Moreover, let $t_d(k)$ and $t_e(k)$ denote the transition time-instants:

$$t_e(k) \triangleq \inf(t \geq 0 : k_e(t) = k), \quad t_d(k) \triangleq \inf(t \geq 0 : k_d(t) = k).$$

Without loss of generality and taking into account that the system starts from zero-excitement, then

$$t_e(k) > t_d(k), \forall k \in \mathbb{Z}_{>0}.$$

and the counters are initialised by $k_e(0) = 0$, $k_d(0) = 1$. Hence, the integer k always identifies a two-phase time-window made of a dis-excitation interval followed by an active estimation interval (see Fig. 3.1).

Since $(A_z - LC_z)$ is Hurwitz, for any positive definite matrix Q, there exist a positive definite matrix P that solves the linear Lyapunov equation

$$(A_z - LC_z)^\top P + P(A_z - LC_z) = -2Q.$$

In the following, we analyze the behaviour of the adaptive observer in two situations by a Lyapunov candidate that accounts for all the parameters:

$$V(t) \triangleq \frac{1}{2}\left(\tilde{z}^\top(t)P\tilde{z}(t) + \tilde{\theta}^\top(t)\tilde{\theta}(t) + g\tilde{\zeta}^\top(t)P\tilde{\zeta}(t)\right), \tag{3.29}$$

where $g \in \mathbb{R}_{>0}$.

i) *Active adaptation interval of finite duration*, i.e. in which $n_e(t) \geq 1 = n_e, \forall t \in [t_e(k), t_d(k+1)]$ (we omit the time-dependence of n_e assuming that for the whole interval it remains constant). In this case the set $E_{n_e}(t)$ is non-empty, $V(t)$ defined in (3.29) shrinks to the following positive definite function, considering the sole components actively adapted:

$$V_{n_e}(t) \triangleq \frac{1}{2}\left(\tilde{z}^\top(t)P\tilde{z}(t) + \tilde{\theta}_{n_e}^\top(t)\tilde{\theta}_{n_e}(t) + g\tilde{\zeta}^\top(t)P\tilde{\zeta}(t)\right). \tag{3.30}$$

In this interval, we prove that V_{n_e} is an ISS-Lyapunov function for the system comprising all states and only the parameters undergoing adaptation, that will converge to the true values. The present scenario comprises, besides the overparametrization case, also the full-parametrization case, which yields to the ISS of the whole dynamics.

ii) *Total dis-excitation*, i.e., none of the parameters is adapted due to poor excitation. In this scenario the set $E_{n_e(t)}$ is empty. In this case we show that the overall function (3.29) remains bounded.

After that, the Lyapunov analysis in these two scenarios are linked properly and we are able to prove that the alternate occurrence of active identification phases and poorly excited phases yields to convergence, provided that the active identification phases have a sufficient duration. To simplify the analysis, we will consider that the number of adapted sinusoids n_e is fixed (i.e., $E_{n_e(t)}$ is an invariant set) within a whole excitation/dis-excitation interval (see Fig. 3.1), that is the set $E_{n_e(t)}$ may be either the empty set $\{0\}$ during the dis-excitation phase, either a set $E_{n_e} \neq \emptyset$ for an arbitrary active adaptation interval. Note that this assumption does not limit the applicability of the adaptive observer to this very special case, being it just a technicality needed to render the problem tractable in a simple analytical way (an active adaptation phase with time-varying $n_e(t)$ can be regarded as a combination of multiple excited intervals).

3.4.1 Active adaptation interval of finite duration

Consider an arbitrary active identification phase $t_e(k) \leq t < t_d(k+1)$ (see Fig. 3.1) and let $\Psi_{n_e}(t)$ be the binary matrix in this scenario with only $\psi_i(t) = 1,\ \forall i \in E_{n_e}$. The upcoming analysis is carried out in order to exhibit the benefit of using the derivative projection on the parameters' estimates. Thanks to (3.20), in the presence of the projection $\mathrm{I}(\theta) = 1$ and $|\hat{\theta}(t)| = \bar{\theta}^*$, we have

$$\tilde{\theta}^{\top}(t)\dot{\hat{\theta}}(t) = \tilde{\theta}^{\top}(t)\dot{\hat{\theta}}(t) - \tilde{\theta}^{\top}(t)\frac{\hat{\theta}(t)\hat{\theta}^{\top}(t)}{\bar{\theta}^{*2}}\dot{\hat{\theta}}(t)$$

$$= \tilde{\theta}^{\top}(t)\dot{\hat{\theta}}_{pre}(t) - \frac{1}{\bar{\theta}^{*2}}\tilde{\theta}^{\top}(t)\hat{\theta}(t)\hat{\theta}^{\top}(t)\dot{\hat{\theta}}_{pre}(t).$$

Owing to the convexity of the admissible set, it holds that $\tilde{\theta}^{\top}(t)\hat{\theta}(t) = \left(\hat{\theta}^{\top}(t) - \theta^{*\top}\right)\hat{\theta}(t) \geq 0$. Now, we recall the triggering condition of projection $\hat{\theta}^{\top}(t)\dot{\hat{\theta}}_{pre}(t) > 0$, which implies that

$$\frac{1}{\bar{\theta}^{*2}}\tilde{\theta}^{\top}(t)\hat{\theta}(t)\hat{\theta}^{\top}(t)\dot{\hat{\theta}}_{pre}(t) \geq 0.$$

Finally, we can bound the scalar product $\tilde{\theta}^{\top}(t)\dot{\tilde{\theta}}(t)$ by:

$$\tilde{\theta}^{\top}(t)\dot{\tilde{\theta}}(t) = \tilde{\theta}^{\top}(t)\dot{\hat{\theta}}(t) \leq \tilde{\theta}^{\top}(t)\dot{\hat{\theta}}_{pre}(t).$$

For instance, a 2-dimensional pictorial representation of the projection-based adaptation is shown in Fig. 3.2 to enhance the influence of the derivative projection on the parameters estimates. In virtue of the fact that

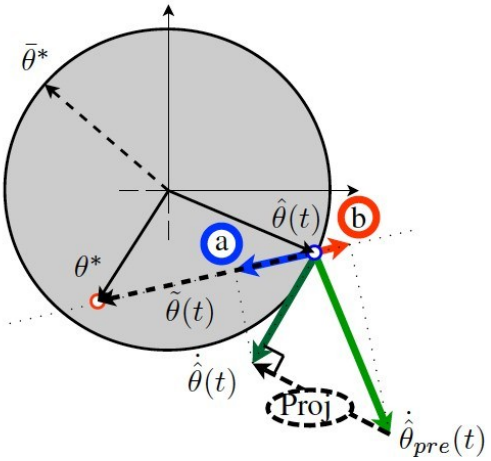

Fig. 3.2 A 2D pictorial representation of the projection-based adaptation. When $|\hat{\theta}(t)| = \theta^*$ and $\dot{\theta}_{pre}(t)$ points out of the feasible region, then the derivative of the parameter vector is obtained by projecting $\dot{\hat{\theta}}_{pre}(t)$ to the tangential hyperplane. To visually compare the values of the scalar products $-\tilde{\theta}^{\top}\dot{\hat{\theta}}_{pre}(t)$ and $-\tilde{\theta}^{\top}\dot{\hat{\theta}}(t)$, consider the projected vectors (a) and (b) respectively.

$$U_{\Psi}(t)\left(\Psi_{n_e}(t)S_{\Psi}(t)\right)U_{\Psi}^{\top}(t) = \left(\Xi^{\top}(t)\Xi(t)+\rho^2 I\right)^{-1} U_{\Xi}(t)\left(\Psi_{n_e}(t)S_{\Xi}(t)\right)U_{\Xi}^{\top}(t)$$

the unconstrained derivative $\dot{\hat{\theta}}_{pre}(t)$ can be expanded as follows:

$$\begin{aligned}\dot{\hat{\theta}}_{pre}(t) &= -\mu\left(\Xi^{\top}(t)\Xi(t)+\rho^2 I\right)^{-1} U_{\Xi}(t)\left(\Psi_{n_e}(t)S_{\Xi}(t)\right)U_{\Xi}^{\top}(t)U_{\Xi}(t)\check{S}_{\Xi}(t)U_{\Xi}^{\top}(t)\\ &= -\mu\left(\Xi^{\top}(t)\Xi(t)+\rho^2 I\right)^{-1}\Psi(t)\Xi^{\top}(t)C_z^{\top}\left(C_z\Xi(t)\tilde{\theta}(t) - d_{\eta}(t) - C_z\tilde{\zeta}(t)\right).\end{aligned} \tag{3.31}$$

Thanks to (3.25), the following inequality holds in the presence of overparametrization:

$$\frac{d}{dt}\left(\tilde{\theta}_{n_e}^{\top}(t)\tilde{\theta}_{n_e}(t)\right) \leq -\underline{\mu}\delta|\tilde{\theta}_{n_e}(t)|^2 + \frac{\mu\bar{c}}{2\rho}|\tilde{\theta}_{n_e}(t)||d_{\eta}(t)| \frac{\mu\bar{c}^2}{2\rho}|\tilde{\theta}_{n_e}(t)||\tilde{\zeta}(t)|,$$

where $\bar{c} \triangleq \|C_z\|$.

The following result can now be proven.

Theorem 3.4.1 (ISS of the dynamic estimator) *If Assumption 2 holds, given the sinusoidal signal $y(t)$ defined in (3.2) and the perturbed measurement (3.1), then in an active adaptation interval $t_e(k) \leq t < t_d(k+1)$, there exist poles of $(A_x - L_x C_x)$, $\mu \in \mathbb{R}_{>0}$ and $\rho \in \mathbb{R}_{>0}$ such that $V_{n_e}(t)$ is an ISS Lyapunov function with respect to any bounded disturbance d_η and in turn ISS w.r.t. bounded measurement disturbance $|d(t)| \leq \bar{d}$. Thus $\tilde{z}(t)$ and $\tilde{\theta}_{n_e}(t)$ are ISS w.r.t. d.* □

Proof: In view of (3.24), we immediately have $|\tilde{\theta}(t)| = |\tilde{\theta}_{n_e}|$, which implies $V(t) = V_{n_e}(t)$, and makes it possible to study the time-derivative of $V_{n_e}(t)$ in place of $V(t)$:

$$\dot{V}_{n_e}(t) = \frac{1}{2}\left(\tilde{z}^\top(t)P\dot{\tilde{z}}(t) + \dot{\tilde{z}}^\top(t)P\tilde{z}(t)\right) + \tilde{\theta}_{n_e}(t)^\top \dot{\theta}_{n_e}(t) + \frac{g}{2}\left(\tilde{\zeta}^\top(t)P\dot{\zeta}(t) + \dot{\zeta}^\top(t)P\tilde{\zeta}(t)\right). \tag{3.32}$$

By letting $\bar{l} \triangleq \|L\|$, $\underline{q} \triangleq \underline{\lambda}(Q)$, $\bar{p} \triangleq \bar{\lambda}(P)$, after some algebra, $\dot{V}(t)$ can be bounded as follows:

$$\begin{aligned}
\dot{V}_{n_e}(t) \leq\ & -\underline{q}|\tilde{z}(t)|^2 - g\underline{q}|\tilde{\zeta}(t)|^2 - \underline{\mu\delta}|\tilde{\theta}_{n_e}(t)|^2 + \bar{p}\bar{l}|\tilde{z}(t)||d_\eta(t)| + \bar{p}|\tilde{z}(t)|^2|\tilde{\theta}(t)| \\
& + \overline{px}|\tilde{z}(t)||\tilde{\theta}(t)| + \bar{p}\bar{\theta}^*|\tilde{z}(t)|^2 + \mu\bar{p}\bar{c}^2|\tilde{z}(t)|^2 + \mu\bar{p}\bar{c}|\tilde{z}(t)||d_\eta(t)| \\
& + \mu\frac{\bar{c}}{2\rho}|\tilde{\theta}_{n_e}(t)||d_\eta(t)| + \mu\frac{\bar{c}^2}{2\rho}|\tilde{\theta}_{n_e}(t)||\tilde{\zeta}(t)| + g\bar{p}\bar{l}|\tilde{\zeta}(t)||d_\eta(t)| + g\bar{p}\bar{\theta}^*_{n_e}|\tilde{z}(t)||\tilde{\zeta}(t)|.
\end{aligned}$$

In view of the inequality $|\tilde{\theta}_{n_e}(t)| = |\tilde{\theta}(t)| \leq 2\bar{\theta}^*$ and by re-arranging the above inequality to put in evidence the square monomial and the binomial terms, we get:

$$\begin{aligned}
\dot{V}_{n_e}(t) \leq\ & -(\underline{q} - \mu\bar{p}\bar{c}^2 - 3\bar{p}\bar{\theta}^*)|\tilde{z}(t)|^2 + \bar{p}\left(\bar{l} + \mu\bar{c}\right)|\tilde{z}(t)||d_\eta(t)| - \frac{g\underline{q}}{2}|\tilde{\zeta}(t)|^2 - \frac{g\underline{q}}{4}|\tilde{\zeta}(t)|^2 \\
& + g\bar{p}\bar{\theta}^*|\tilde{z}(t)||\tilde{\zeta}(t)| - \frac{\underline{\mu\delta}}{6}|\tilde{\zeta}(t)|^2 + g\bar{p}\bar{l}|\tilde{\zeta}(t)||d_\eta(t)| - \frac{\underline{\mu\delta}}{2}|\theta_{n_e}(t)| - \frac{\underline{\mu\delta}}{6}|\theta_{n_e}(t)| \\
& + \overline{px}|\tilde{z}(t)||\tilde{\theta}_{n_e}(t)| - \frac{\underline{\mu\delta}}{6}|\tilde{\theta}_{n_e}(t)|^2 + \mu\frac{\bar{c}}{2\rho}|\tilde{\theta}_{n_e}(t)||d_\eta(t)| - \frac{\underline{\mu\delta}}{6}|\tilde{\theta}_{n_e}(t)| \\
& + \mu\frac{\bar{c}^2}{2\rho}|\tilde{\theta}_{n_e}(t)||\tilde{\zeta}(t)|.
\end{aligned}$$

Now, we complete the squares, thus obtaining

$$\begin{aligned}
\dot{V}_{n_e}(t) \leq\ & -\frac{(\underline{q} - \mu\bar{p}\bar{c}^2 - 3\bar{p}\bar{\theta}^*)}{2} - \frac{g}{q}\bar{p}^2\theta^*\left(-\right)_2 - \frac{3(\overline{px})^2}{2\underline{\mu\delta}}|\tilde{z}(t)|^2 - \left(\frac{g\underline{q}}{2} - \frac{3\mu\bar{c}^4}{8\rho^2\underline{\delta}}\right)|\tilde{\zeta}(t)|^2 \\
& - \frac{\underline{\mu\delta}}{2}|\tilde{\theta}_{n_e}(t)|^2 + \frac{\bar{p}^2\left(\bar{l} + \mu\bar{c}\right)^2}{2(\underline{q} - \mu\bar{p}\bar{c}^2 - 3\bar{p}\bar{\theta}^*)} + \frac{3\mu\bar{c}^2}{8\rho^2\underline{\delta}} + \frac{g}{q}\bar{p}^2\bar{l}^2|d_\eta(t)|^2.
\end{aligned}$$

Finally, the following inequality can be established:

$$\dot{V}_{ne}(t) \leq -\beta_1 \left| V_{ne}(t) - \gamma_1(\bar{d}_\eta) \right|, \tag{3.33}$$

where

$$\beta_1 := \min \left(\frac{(\underline{q} - \mu\bar{p}\bar{c}^2 - 3\bar{p}\bar{\theta}^*)}{2\bar{p}} - \frac{\underline{g}(-)_2}{\underline{q}\bar{p}\,\theta^*} - \frac{3\bar{x}^2\bar{p}}{2\mu\underline{\delta}}, \frac{\mu\underline{\delta}}{2}, \frac{\underline{q}}{2\bar{p}} - \frac{3\mu\bar{c}^4}{8g\rho^2\underline{\delta}\bar{p}} \right) \tag{3.34}$$

and

$$\gamma_1(r) := \frac{1}{\beta_1} \frac{\bar{p}^2(\bar{l} + \mu\bar{c})^2}{2(\underline{q} - \mu\bar{p}\bar{c}^2 - 3\bar{p}\bar{\theta}^*)} + \frac{3\mu\bar{c}^2}{8\rho^2\underline{\delta}} + \frac{\underline{g}\bar{p}\,\bar{l}^2}{\underline{q}} r^2, \forall r \in \mathbb{R}_{\geq 0}. \tag{3.35}$$

Hence, the proof is concluded if

$$\beta_1 > 0. \tag{3.36}$$

In view of (3.36), all the components involved in (3.34) should be positive, wherein $\mu\underline{\delta}/2 > 0$ can be immediately verified by choosing a positive μ. Now, we set the excitation threshold $\underline{\delta}$ and the Q matrix arbitrarily, determining $\underline{q}$. Then, assume the poles of $(A_x - L_xC_x)$ are placed such that $\bar{p}$ is sufficient small. Letting $\bar{p} \leq \mu$, we determine a sufficient condition to ensure the positiveness of the first term in (3.34):

$$\frac{(\underline{q} - \mu^2\bar{c}^2 - 3\mu\bar{\theta}^*)}{2} - \mu\frac{\underline{g}(-)_2}{\underline{q}\,\theta^*} - \mu\frac{3\bar{x}^2}{2\underline{\delta}} > 0. \tag{3.37}$$

Being the Lyapunov parameter $g > 0$ arbitrary, let us fix $g = 1$ for simplicity. At this point, with any fixed regularization parameter $\rho \in \mathbb{R}_{>0}$ (we do not pose limits on ρ now) we can always determine a sufficiently small value of μ for which the inequality holds true. Next, by suitably allocating the poles, we compute the output-injection gain L that realizes the needed $\bar{p}$. Finally, to render β_1 strict-positive, we choose a sufficient large ρ such that

$$\frac{\underline{q}}{2\bar{p}} - \frac{3\mu\bar{c}^4}{8g\bar{p}\rho^2\underline{\delta}} > 0.$$

thus ending the proof. ∎

Remark 3.4.1 (Parameter tuning) To avoid the increase of the worst-case sensitivity to bounded noises, instead of excessively reducing the value of $\bar{p}$ that leads high-gain output injection through L, and high values of $\bar{l}$ and γ_1 correspondingly, we can set $\bar{p} = \mu$ and increase the regularization parameter ρ.

3.4.2 Total dis-excitation phase

Clearly, it is important to show that the estimation error remains bounded also during the time-intervals in which no excitation is present (e.g., $t_d(k) \leq t < t_e(k)$ as illustrated in Fig. 3.1). This is carried out in the following result.

Lemma 3.4.1 (Boundedness in dis-excitation phase) *Under the same assumptions of Theorem 3.4.1, consider an arbitrary dis-excitation interval $t_d(k) \leq t < t_e(k)$ in which $E_{n_e}(t) = \emptyset$. Then, under suitably chosen $\mu \in \mathbb{R}_{>0}$, $\rho \in \mathbb{R}_{>0}$ and the poles of $(A_x - L_x C_x)$, $V(t)$ is an ISS Lyapunov function w.r.t. $d(t)$ (where $|d(t)| \leq d$) and w.r.t. $V(t_d(k))$.* □

Proof: In the considered dis-excitation scenario, the estimation is totally unexcited in all directions, i.e. $\sum_{i=1}^{n} \psi_i(t) = 0,\ \forall t \geq t_d(k) > 0$, thus yielding $\dot{\tilde{\theta}}(t) = 0_{n\times 1}$, and $\tilde{\theta}(t) = \tilde{\theta}(t_d^-)$. In this respect, the time-derivative of the Lyapunov function $V(t)$ satisfies

$$\dot{V}(t) \leq -(\underline{q} - 3\bar{p}\bar{\theta}^*)|\tilde{z}(t)|^2 + \bar{p}\bar{l}|\tilde{z}(t)||d_\eta(t)| - \frac{g\underline{q}}{2}|\tilde{\zeta}(t)|^2 - \frac{g\underline{q}}{4}|\tilde{\zeta}(t)|^2 + g\bar{p}\bar{\theta}^*|\tilde{z}(t)||\tilde{\zeta}(t)| - \frac{g\underline{q}}{4}|\zeta(t)|^2 + g\bar{p}\bar{l}|\zeta(t)||d_\eta(t)| + \bar{p}\bar{x}|\tilde{z}(t)||\theta(t)|.$$

Applying the inequality $|\tilde{\theta}(t_d(k))|^2 \leq 2V(t_d(t)),\ \forall t \geq t_d(k)$, we have:

$$\dot{V}(t) \leq -(\underline{q} - 3\bar{p}\bar{\theta}^*)|\tilde{z}(t)|^2 + \bar{p}\bar{l}|\tilde{z}(t)||d_\eta(t)| - \frac{g\underline{q}}{2}|\tilde{\zeta}(t)|^2 - \frac{g\underline{q}}{4}|\tilde{\zeta}(t)|^2 + g\bar{p}\bar{\theta}^*|\tilde{z}(t)||\tilde{\zeta}(t)| - \frac{g\underline{q}}{4}|\zeta(t)|^2 + g\bar{p}\bar{l}|\zeta(t)||d_\eta(t)| - |\theta(t)|^2 + 2V(t_d(k)) + \bar{p}\bar{x}|\tilde{z}(t)||\theta(t)|.$$

By completing squares, we obtain the following upper bound for $\dot{V}(t)$:

$$\dot{V}(t) \leq -\frac{(\underline{q} - 3\bar{p}\bar{\theta}^*)}{2} - \frac{g}{q}\bar{p}^2(\bar{\theta}^*)^2 - \frac{3(\bar{p}\bar{x})^2}{2}|\tilde{z}(t)|^2 - \frac{5}{6}|\tilde{\theta}(t)|^2 - \frac{g\underline{q}}{2}|\tilde{\zeta}(t)|^2 + 2V(t_d(k)) + \frac{\bar{p}^2\bar{l}^2}{2(\underline{q} - 3\bar{p}\bar{\theta}^*)} + \frac{g}{\underline{q}}\bar{p}^2\bar{l}^2|d_\eta(t)|^2$$

and hence, after some algebra, it follows that

$$\dot{V}(t) \leq -\beta_0\left(V(t) - L_0 V(t_d(k)) - \gamma_0(\bar{d}_\eta(t))\right) \tag{3.38}$$

where $L_0 := 2/\beta_0$,

$$\beta_0 := 2\min\left(\frac{(\underline{q} - 3\bar{p}\bar{\theta}^*)}{2\bar{p}} - \frac{g}{q}\bar{p}(\bar{\theta}^*)^2 - \frac{3\bar{p}\bar{x}^2}{2},\ \frac{5}{6},\ \frac{\underline{q}}{2\bar{p}}\right)$$

and

$$\gamma_0(r) \triangleq \frac{1}{\beta_0}\left(\frac{\bar{p}^2\bar{l}^2}{2(\underline{q}-3\bar{p}\bar{\theta}^*)}+\frac{g\,\bar{p}^2\bar{l}^2}{\underline{q}}\right)r^2,\ \forall r\in\mathbb{R}_{\geq 0}.$$

The positiveness of β_0 can be justified by following the same steps taken in Section 3.4.1. It is easy to show that $\beta_0 > 0$ is ensured through a suitable design of μ and ρ, thus concluding the proof. ∎

3.4.3 Robustness Under Alternate Switching

At this stage, the stability of the adaptive observer under alternate switching is characterized by linking the results obtained for the two excitation phases. Thanks to the Bellman Gronwall lemma, we are able to prove that the alternate occurrence of active identification phases and poorly excited phases may yield to convergence provided that the active identification phases have a sufficient duration.

Theorem 3.4.2 *Under the same assumptions of Theorem 3.4.1, consider the adaptive observer (3.12), (3.15)- (3.18) equipped with the excitation-based switching strategy defined in (3.42). Then, the discrete dynamics induced by sampling the adaptive observer in correspondence of the switching transitions has the asymptotic ISS property if the excitation phases last longer than* $\beta_1^{-1}\ln(L_0)$. □

Proof: By the B-G Lemma, the value of the Lyapunov function (3.38) within the dis-excitation intervals can be bounded as follows:

$$V(t)\leq V(t_d(k))+\left(1-e^{-\beta_0(t-t_d)}\right)\left(L_0V(t_d^-(k))+\gamma_0(\bar{d}_\eta)-V(t_d(k))\right),$$
$$\forall t\in[t_d(k),t_e(k)),\ \forall k\in\mathbb{Z}_{>0}.$$

Instead, during the excitation phases, the Lyapunov function (3.33) can be bounded as

$$V(t)\leq V(t_e(k))+\left(1-e^{-\beta_1(t-t_e(k))}\right)\left(\gamma_1(\bar{d}_\eta)-V(t_e(k))\right),$$
$$\forall t\in[t_e(k),t_d(k+1)),\ \forall k\in\mathbb{Z}_{>0}.$$

In order to link the two modes of behaviour, let us denote by $V_k = V(t_d(k))$ the value of the Lyapunov function sampled at the k-th transition to dis-excitement, occurring at time $t_d(k)$ (or equivalently, at the end of the $(k-1)$-th active identification phase).

Due to the poor excitation during the interval $[t_d(k), t_e(k))$, at the transition time $t_e(k)$ we can establish the (possibly conservative) bound

$$V(t_e(k))\leq L_0V_k+\gamma_0(\bar{d}_\eta).$$

Such a bound holds for any duration the disexcitation phase. For any subsequent active identification time $t = t_e(k) + \Delta t$ with $\Delta t < t_d(k+1) - t_e(k)$, we get the inequality:

$$\begin{aligned} V(t) &\leq V(\underline{t_e}(k)) + \left(1 - e^{-\beta_1(t-t_e(k))}\right)\left(\gamma_1(\bar{d}_\eta) - V(t_e(k))\right) \\ &= \gamma_1(d_\eta) - e^{-\beta_1(t-t_e(k))}\gamma_1(\bar{d}_\eta) + e^{-\beta_1(t-t_e(k))}V(t_e(k)) \\ &\leq \gamma_1(\bar{d}_\eta) - e^{-\beta_1(t-t_e(k))}\gamma_1(\bar{d}_\eta) + e^{-\beta_1(t-t_e(k))}\left(\gamma_0(\bar{d}_\eta) + L_0 V_k\right) \\ &= \gamma_1(\bar{d}_\eta) + e^{-\beta_1\Delta t}\left(\gamma_0(\bar{d}_\eta) - \gamma_1(\bar{d}_\eta) + L_0 V_k\right). \end{aligned}$$

Now, let us arbitrarily set $0 < \kappa < 1$ and let $\Delta T_e = -\beta_1^{-1}\ln\left(L_0^{-1}\kappa\right)$. If the active identification phase is long enough to verify the inequality $t_d(k+1) - t_e(k) > \Delta T_e$, then we can guarantee the following difference bound on the discrete (sampled) Lyapunov function sequence:

$$V_{k+1} \leq \gamma_1(\bar{d}_\eta) + \frac{\kappa}{L_0}\left(\gamma_0(\bar{d}_\eta) - \gamma_1(\bar{d}_\eta)\right) + \kappa V_k$$

which can be rewritten in the following compact form:

$$V_{k+1} - V_k \leq -(1-\kappa)V_k + \gamma(\bar{d}_\eta),$$

where $\gamma(s) = \gamma_1(s) + \kappa L_0^{-1}(\gamma_0(s) - \gamma_1(s))$, $\forall s \geq 0$.

We can conclude that V_k is a discrete ISS Lyapunov function for the sampled sequence, with samples taken at the end of the excitation phases assumed always to last longer than $\beta^{-1}\ln(L_0)$.

Now, we recover the ISS properties for the continuous-time system by studying the inter-sampling behaviour of $V(t)$. Let $k(t)$, $\forall t > 0$ denote the index of the current time-window: $k(t) = k : t \in [t_d(k), t_d(k+1))$ and consider two positive constants Δt_1, Δt_2, such that $\Delta t_1 \leq t_e(k) - t_d(k)$, $\Delta t_2 \leq t_d(k+1) - t_e(k)$. Between two samples, the Lyapunov function is bounded by:

$$\begin{aligned} V(t) &\leq \max_{\Delta t_1 \in \mathbb{R}_{\geq 0}} \left\{ V_{k(t)} + \left(1 - e^{-\beta_0\Delta t_1}\right)\left(L_0 V_{k(t)} + \gamma_0(\bar{d}_\eta) - V_{k(t)}\right) \right\} \\ &\quad + \max_{\Delta t_2 \in \mathbb{R}_{\geq 0}} \left\{ \gamma_1(\bar{d}_\eta) - e^{-\beta_1\Delta t_2}\left(\gamma_1(\bar{d}_\eta) - \gamma_0(\bar{d}_\eta) - L_0 V_{k(t)}\right) \right\} \\ &\leq (1+L_0)V_{k(t)} + \gamma_0(\bar{d}_\eta) + \gamma_1(\bar{d}_\eta) + \gamma_0(\bar{d}_\eta) + L_0 V_{k(t)} \\ &= (1+2L_0)V_{k(t)} + \gamma_1(d_\eta) + 2\gamma_0(d_\eta). \end{aligned} \tag{3.39}$$

If we let $k(t) \xrightarrow[t\to\infty]{} \infty$ (i.e., an infinite number of active identification phases occurs asymptotically or a single excitation phase lasts indefinitely), then the estimation error in the inter-sampling times converges to a region whose radius depends only on the assumed disturbance bound. •

Remark 3.4.2 It is worth noting that the thresholds $\bar{\delta}$ and $\underline{\delta}$ play important roles in the behavior of the estimator under alternate switches. Because of the hysteretic property, the values of $\bar{\delta}$ and $\underline{\delta}$ have to be properly set to avoid the excitation signals of the adapted frequencies being confined in the transient interval (i.e., $[\underline{\delta}, \bar{\delta}]$). Suitable choices can be found off-line by a priori information of the inputs.

Remark 3.4.3 In practical applications, in order to the improve the speed of convergence, a robust provision can be adopted consisting in re-initializing the parameter-vector with the value estimated by a previous sufficiently long identification phase (i.e. $t_d(k+1) - t_e(k) \geq \beta_1^{-1} \ln(L_0)$) after any insufficiently long excitation interval. In this respect, let k^* be a counter for the sole active identification phases lasting more than the minimal duration $\beta_1^{-1} \ln(L_0)$ and consider $V_{k^*} = V(t_d(k^*))$. In this case, V_{k^*} is a discrete ISS Lyapunov function for the sampled adaptive observer, with samples collected at the end of the sole excitation phases lasting longer than $\beta_1^{-1} \ln(L_0)$.

3.5 Digital implementation of the proposed method

In this section, we show a counterpart of this switched algorithm in the discrete-time domain to enhance the applicability. Similar to the one presented in Section 2.5, the first step consists in selecting a set of parameters A_f, B_f, α_1, α_2, μ, ρ, μ_A, $\bar{\delta}$, $\underline{\delta}$; after that, Euler method is employed with a sampling period is T_s, thus resulting in a discretized algorithm given as follows, provided a measurement $v(k)$, $k = 1, 2, \cdots$

$$v_f(k) = v_f(k-1) + T_s (A_f v_f(k-1) + B_f v(k)) , \tag{3.40a}$$

$$\hat{z}(k) = \hat{z}(k-1) + T_s \big((A_z - LC_z)\hat{z}(k-1) + L\hat{\eta}(k) + G_z(\hat{z}(k-1))\hat{\theta}(k-1) \tag{3.40b}$$

$$+ \Xi(k-1)(\hat{\theta}(k-1) - \hat{\theta}(k-2)) \big) , \tag{3.40c}$$

$$\Xi(k) = \Xi(k-1) + T_s ((A_z - LC_z)\Xi(k-1) + G_z(\hat{z}(k))) , \tag{3.40d}$$

$$\hat{\theta}_{pre}(k) = \hat{\theta}_{pre}(k-1) \tag{3.40e}$$

$$+ T_s \big(-\mu U_\Psi(k) (\Psi(k) S_\Psi(k)) \, U_\Psi^\top(k) U_\Xi(k) \check{S}_\Xi(k) U_\Xi^\top(k) \Xi^\top(k) C_z^\top (C_z \hat{z}(k) - \hat{\eta}(k)) \big) , \tag{3.40f}$$

$$\hat{\theta}(k) = \hat{\theta}(k-1) + \hat{\theta}_{pre}(k) - \hat{\theta}_{pre}(k-1) - \mathrm{I}(\theta) \left(\frac{\hat{\theta}(k-1)\hat{\theta}^\top(k-1)}{\hat{\theta}^{*2}} \right) \tag{3.40g}$$

$$\times \big(\hat{\theta}_{pre}(k) - \hat{\theta}_{pre}(k-1) \big) , \tag{3.40h}$$

where $\tilde{\eta}(k) := [v(k)\ v_f^\top(k)]^\top$, $U_\Psi(k)$, $S_\Psi(k)$, $U_\Xi(k)$, $\check{S}_\Xi(k)$ are obtained by the SVD of $\Sigma_\Psi(\Xi(k))$ and $\Sigma_\Xi(\Xi(k))$ at the corresponding sampling instant, that is

$$\Sigma_\Psi(\Xi(k)) = \left(\Xi^\top(k)\Xi(k) + \rho^2 I\right)^{-1} \Xi^\top(k) C_z^\top C_z \Xi(k) = U_\Psi(k) S_\Psi(k) U_\Psi^\top(k)$$

$$\Sigma_\Xi(\Xi(k)) := \Xi^\top(k) C_z^\top C_z \Xi(k) = U_\Xi(k) S_\Xi(k) U_\Xi^\top(k).$$

Furthermore, in view of (3.22), we have $\check{S}_\Xi(k) = \mathrm{diag}\{\check{s}_{\Xi_i}(k)\}$ where

$$\check{s}_{\Xi_i}(k) = \begin{cases} \lambda_i(S_\Xi(k))^{-1}, & \text{if } \psi_i(k) = 1, \\ 0, & \text{if } \psi_i(k) = 0 \end{cases}, \tag{3.41}$$

and the binary switching signal $\psi_i(k)$, $i = 1, 2, \ldots, n$ is determined by

$$\psi_i(k) = \begin{cases} 1, & \text{if } \lambda_i(\Sigma(\Xi(k))) \geq \bar{\delta} \\ 0, & \text{if } \lambda_i(\Sigma(\Xi(k))) < \underline{\delta} \\ \psi_i(k-1), & \text{if } \underline{\delta} \leq \lambda_i(\Sigma(\Xi(k))) < \bar{\delta} \end{cases}. \tag{3.42}$$

The indicator function is given by

$$I(\theta) := \begin{cases} 1, & \text{if } |\hat{\theta}(k-1)| = \bar{\theta}^* \text{ and } \hat{\theta}^\top(k-1)\dot{\hat{\theta}}_{pre}(k) > 0, \\ 0, & \text{otherwise}. \end{cases}$$

Thereafter, the estimates of the frequencies are obtained as follow by using $\hat{\theta}(k)$:

$$\hat{\omega}_i(k) = \max\{0, \hat{\theta}_i(k) - \alpha_i\}, \tag{3.43}$$

Finally, the amplitude and the phase of the sinusoids as well as the offset are estimated by

$$\begin{aligned} &\bar{a}_i(k) = \bar{a}_i(k-1) - T_s \mu_a \hat{\omega}_i(k) \quad \hat{\omega}_i(k) \bar{a}_i(k) - \left(\hat{\Omega}_i(k) \hat{x}_{2i-1}(k)^2 + \hat{x}_{2i}(k)^2\right), \\ &\hat{a}_i(k) = \max\{0, \bar{a}_i(k)\} \end{aligned} \tag{3.44}$$

and

$$\hat{\phi}_i(k) = \angle(\hat{x}_{2i}(k) + \hat{\omega}_i(k)\hat{x}_{2i-1}(k)), \quad i = 1, 2, \cdots, n. \tag{3.45}$$

In addition, the offset is estimated directly by

$$\hat{b}(k) = \hat{x}_{2n+1}(k).$$

3.6 Simulation and Experimental Results

3.6.1 Simulation Results

In this subsection, some numerical examples are given to illustrate the effectiveness of the proposed multi-sinusoidal estimator. The Forward-Euler discretization method with sampling period $T_s = 3 \times 10^{-4}$s is employed in all simulations.

Example 1: In this example, we compare the proposed method with two techniques available from the literature: the adaptive observer method [67] and the parallel AFLL method [29], all fed by the following signal composed by two sinusoids:

$$y(t) = \sin 2t + \sin 5t.$$

All the methods are initialized with the same initial conditions $\hat{\omega}_1(0) = 3$ and $\hat{\omega}_2(0) = 4$. Method [67] is tuned with: $\gamma_1 = \gamma_2 = 8 \times 10^3$, $k = 1$, $d_2 = 9$, $d_3 = 27$, $d_4 = 27$, while method [29] is tuned with: $K_{s_1} = K_{s_2} = 1$, $\gamma_{s_1} = 0.3$, $\gamma_{s_2} = 0.5$, $\omega_{s_1} = 3$, $\omega_{s_2} = 4$. The tuning gains of the proposed method are chosen as: $\alpha_1 = 0$, $\alpha_2 = -0.5$, $A_f = -5$, $B_f = 4.5$, $\mu = 6$, $\rho = 0.2$, $\mu_A = 0.15$ with the poles placed at $(-2, -0.7, -0.5, -0.2)$. The simulation results are reported in Fig.3.3.

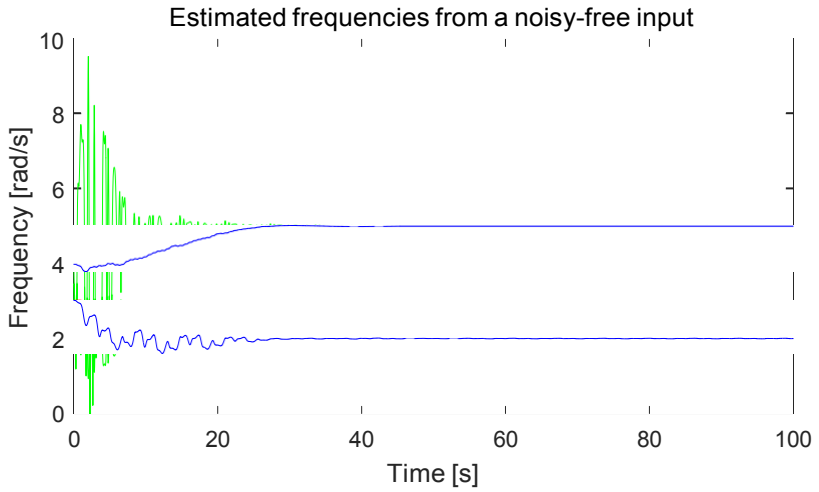

Fig. 3.3 Time-behavior of the estimated frequencies obtained by using the proposed method (blue) compared with the time behaviors of the estimated frequencies by [67] (green) and [29] (red).

It is worth noting from Fig. 3.3 that all the estimators succeeded in detecting the frequencies in a noise-free scenario, after a similar transient behavior (throuhg a suitable choice of the tuning gains), though method [67] is subject to a slightly larger overshoot.

Let us now consider the input signal $y(t)$ corrupted by a bounded perturbation $d(t)$ uniformly distributed in the interval $[-0.5, 0.5]$. As shown in Fig. 3.4, the stationary performance of method [67] deteriorates due to the injection of the perturbation. Moreover, as shown in Fig. 3.5, where we plot $\log|\tilde{\omega}(t)|$ with respect to one frequency $\omega = 5$ rad/s as an example to appreciated the behavior of [29] and the proposed observer in detail, the presented method exhibits a slightly better immunity to the bounded uncertainty.

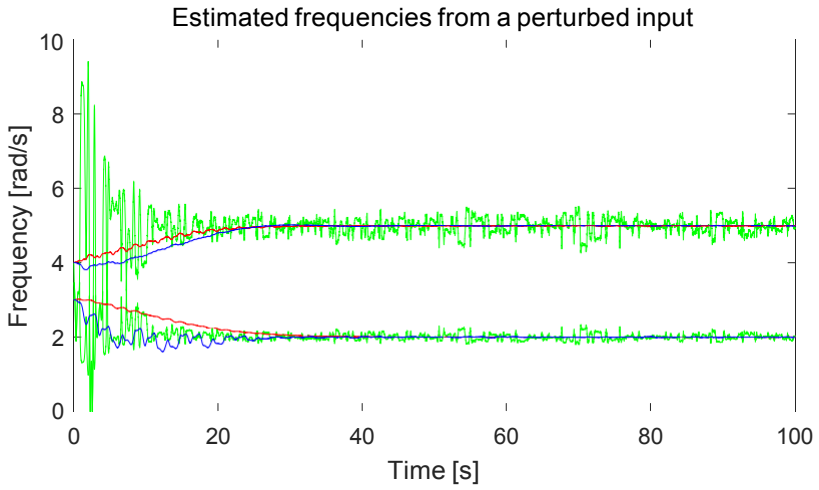

Fig. 3.4 Time-behavior of the estimated frequencies by using the proposed method (blue line) compared with the time behaviors of the estimated frequencies by the method [67] (green line) and the method [29] (red line).

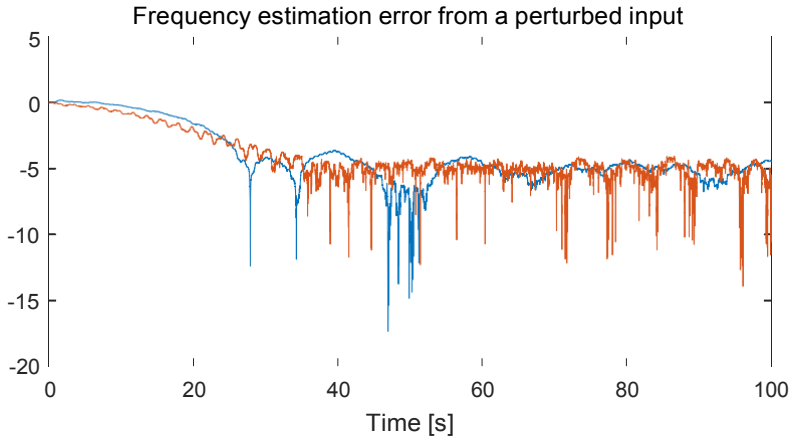

Fig. 3.5 Time-behavior of $\log|\tilde{\omega}(t)|$ with $\omega = 5$ rad/s by using the proposed method (blue line) compared with the time behaviors of the estimated frequencies by the method [29] (red line).

The estimated amplitudes obtained by applying [29] are compared with the outcome of the proposed adaptive observer in Fig. 3.6 and 3.7 (the algorithm proposed in [67] is

not considered here, since it deals with frequency estimation only). Thanks to the adaptive scheme (3.11), the proposed method offers enhanced transient and steady state behavior with a similar convergence speed in the presence of $d(t)$.

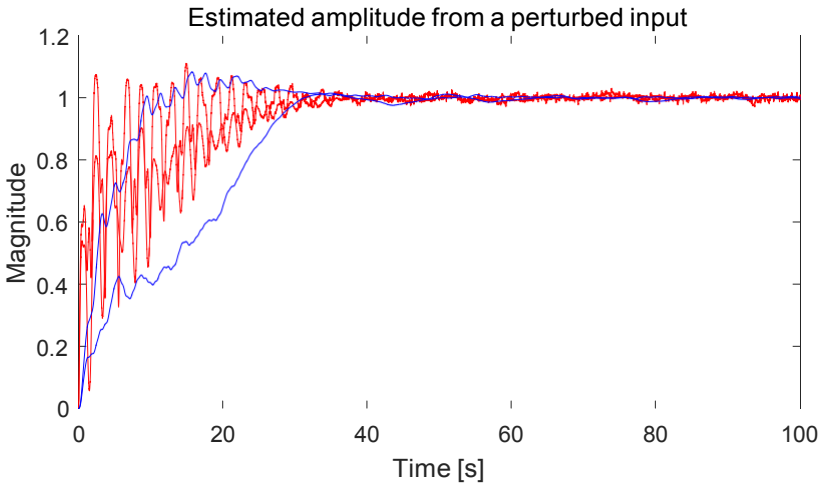

Fig. 3.6 Time-behavior of the estimated amplitudes by using the proposed method (blue lines) compared to the estimates by the method [29] (red lines).

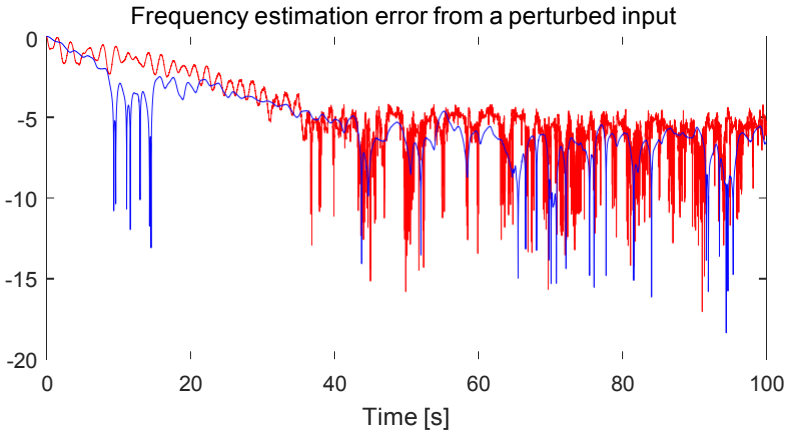

Fig. 3.7 Time-behavior of $\log|\tilde{a}_1(t)|$ with $a_1 = 1$ rad/s by using the proposed method (blue lines) compared to the estimates by the method [29] (red lines).

Moreover, resorting to the estimated amplitudes and phases, the input is reconstructed by the next equation

$$\hat{y}(t) = \hat{a}_1(t)\sin\hat{\phi}_1(t) + \hat{a}_2(t)\sin\hat{\phi}_2(t).$$

Some periods of the estimates are plotted for observation in Figure 3.8, where the accuracy of the phase estimation is verified.

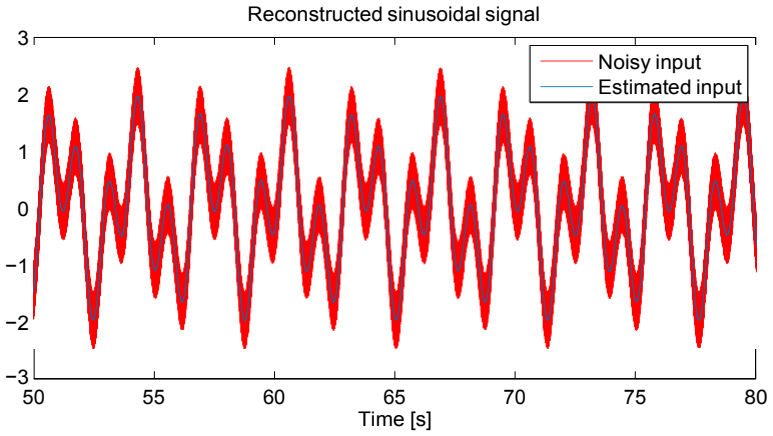

Fig. 3.8 Estimated sinusoidal signal by the proposed AFP method.

Now, we instead consider a more aggressive disturbance $d(t)$ that obeys uniform distribution in the interval $[-2.5, 2.5]$ in order to observer the influence of the coefficients ρ and μ. The results are given in Fig. 3.9, and for the sake of comparison, the root mean square of the frequency estimation error within a time-interval in steady state is calculated and presented in Table 3.1. As can be seen, for a fixed value of either ρ or μ, the tuning of other parameter is subject to the typical trader-off between accuracy and convergence speed.

Table 3.1 Comparison of frequency estimation with different valued coefficents.

Tuning Parameters		Root mean square of the frequency estimation error (60s-100s)			
fixed μ	$\rho = 0.25$	frequency 1	0.0141	frequency 2	0.0107
	$\rho = 0.15$		0.0282		0.0324
fixed ρ	$\mu = 4$	frequency 1	0.0135	frequency 2	0.0095
	$\mu = 8$		0.0264		0.0183

Example 2: In order to evaluate the performance of the method in the presence of a DC offset and of a partial dis-excitation, consider a biased signal consisting of two sine waves that turn into a pure single sinusoid after a certain time instant:

$$v(t) = 4\sin 3t + A_2(t)\sin 2t + 1 + d(t)$$

where $A_2(t)$ obeys a step-wise change: $A_2(t) = 3,\ 0 \le t < 120,\ A_2(t) = 0,\ t \ge 120$ and $d(t)$ has the same characteristics as in the previous example. The behavior of the proposed estimator is recorded in Figs. 3.10-3.12 with the tuning gains chosen as follows: $A_f = -6,\ B_f = 6,\ \alpha_1 = -2,\ \alpha_2 = -1,\ \mu = 70,\ \rho = 0.3,\ \mu_A = 0.1,\ \bar{\delta} = 3\times 10^{-4},\ \underline{\delta} = 3\times 10^{-5}$ and the poles' location $[-0.6, -0.5, -0.3, -1, -10]$.

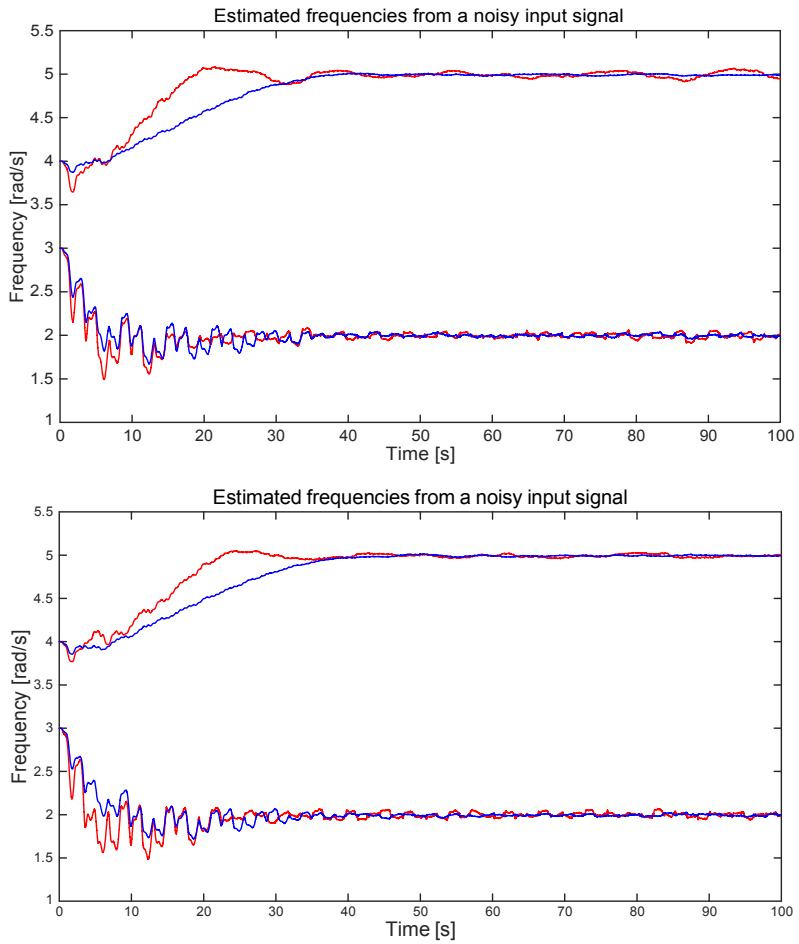

Fig. 3.9 Frequency tracking behavior with different values of ρ and μ for a noisy input. Top: $\rho = 0.25$ (blue lines), $\rho = 0.15$ (red lines). Bottom: $\mu = 4$ (blue lines), $\rho = 8$ (red lines).

More specifically, in Fig. 3.10 the excitation signals $\lambda_1(\Phi(\Xi(t)))$, $\lambda_2(\Phi(\Xi(t)))$ are shown together with the correspondent switching signals $\psi_1(t)$, $\psi_2(t)$, to enhance the availability of the individual excitation level in real-time, thus in turn allowing to disable the parameter adaptation in directions with poor excitation conditions.

Moreover, it follows from Fig. 3.11 and Fig. 3.12 that all the initialized parameters including the offset are successfully estimated. After time $t = 120\mathrm{s}$, the system is characterized by overparametrization. The vanishing of the second sinusoid is captured by the associated amplitude estimate, that fades to 0 eventually, though the frequency estimate is non-zero. Conversely, the parameters of the excited sinusoidal components remains at the accurate estimates after a transient response.

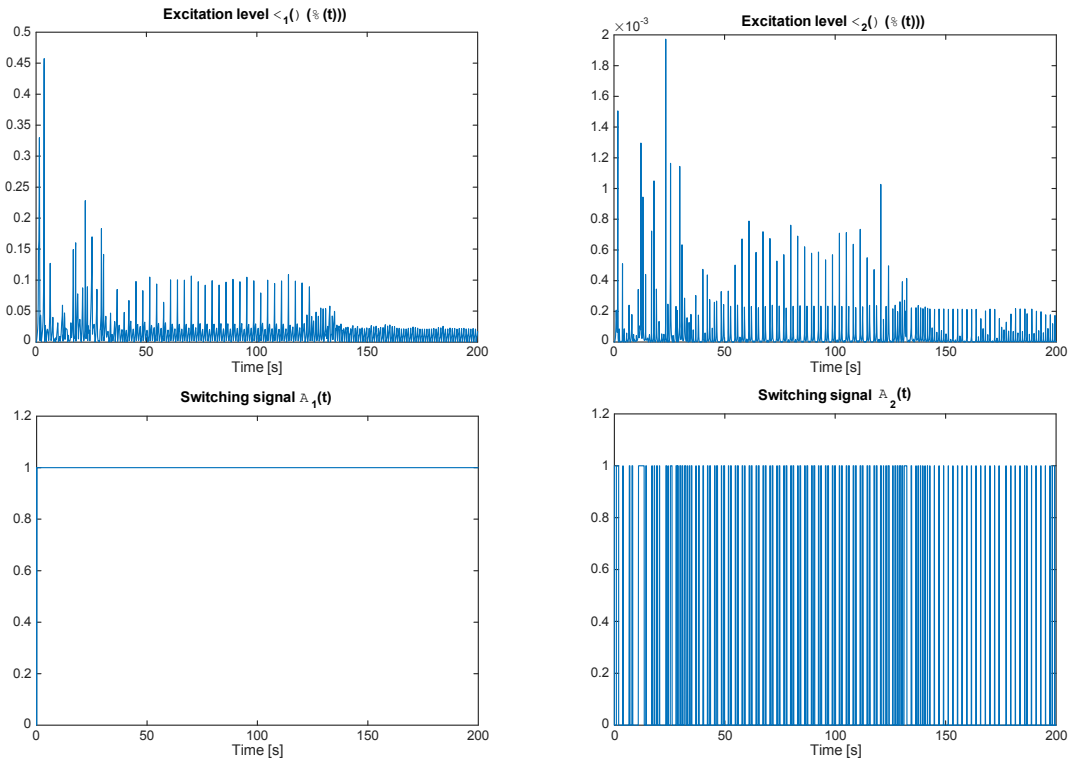

Fig. 3.10 (a) Excitation level $\lambda_1(\Phi(\Xi(t)))$; (b) Excitation level $\lambda_2(\Phi(\Xi(t)))$; (c) Switching signal $\psi_1(t)$; (d) Switching signal $\psi_2(t)$.

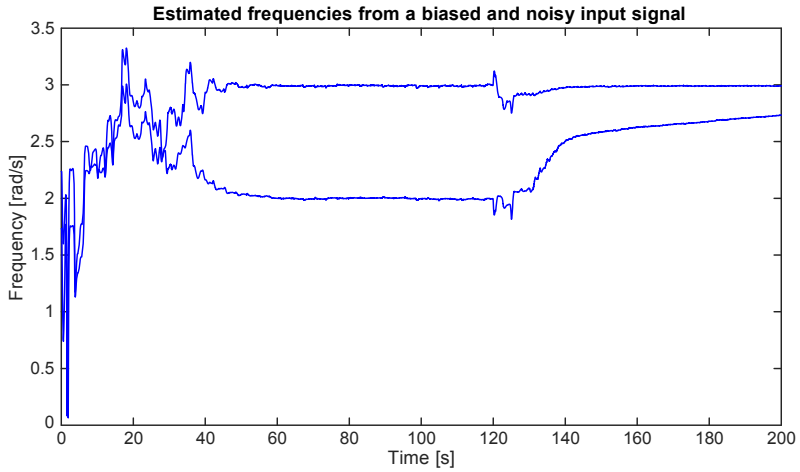

Fig. 3.11 Time-behavior of the estimated frequencies by using the proposed method. One of frequency estimates diverges after 120s due to the loss of excitation in one direction after 120s (see the description on page 77).

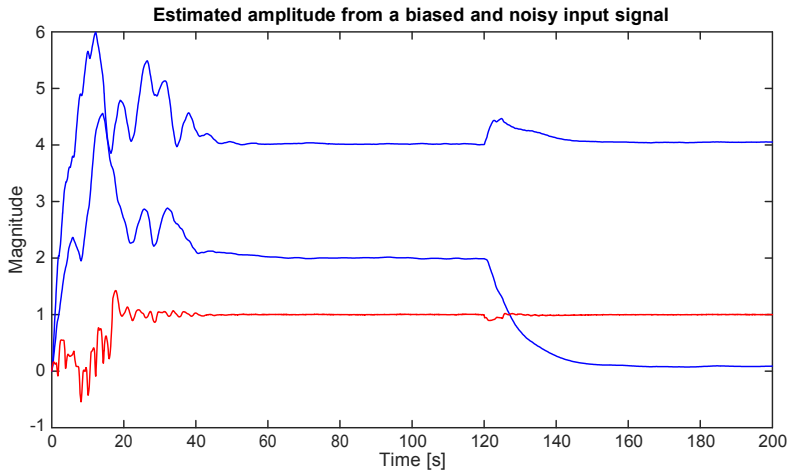

Fig. 3.12 Time-behavior of the estimated amplitudes (blue lines) and the estimated bias (red line) by using the proposed method. One of the sinusoid vanishes after 120s, therefore its amplitude decays to 0, resulting in a dis-excitation phase in one direction (see the description on page 77).

3.6.2 Experimental Results

In this section, an experimental example is illustrated to investigate the behavior of the approach in a real-time digital implementation. The proposed method has been deployed on a dSpace board connected to a programmable electrical signal generator (see Fig. 3.13): *Tektronix AFG3102 dual channel function generator*, which produces a voltage signal, given by

$$y(t) = 4\sin 7t + 2\sin 5t$$

affected by unknown bounded uncertainties. Fig. 3.14 shows some periods of the noisy sinusoidal signal generated by the programmable source. Computation burden is one the most important aspects of implementation in practice. For the sake of simplicity, all the dynamic equations of the estimator are discretized by the forward Euler method, avoiding an excessive load for the dSpace system. The parameters of the estimator (4th order for two frequencies) is set to $\alpha_1 = 0$, $\alpha_2 = -1$, $A_f = -2$, $B_f = 1$, $\mu = 20$, $\rho = 1$, $\mu_A = 0.2$ with the poles placed at $(-0.7, -0.4, -0.5, -1)$.

The dSpace board computes the estimates in real-time with a fixed sampling rate of 10KHz based on the Maltab/Simulink platform. The results are captured by an oscilloscope with 4 channels respectively allocated to dual frequencies and amplitudes. The measured signals are then imported in Matlab for carrying out the post-analysis. As shown in Fig. 3.15 and 3.16, the estimator is capable to gather the frequency and amplitude contents with great accuracy, despite the unavoidable measurement noise due the limitation of the measurement

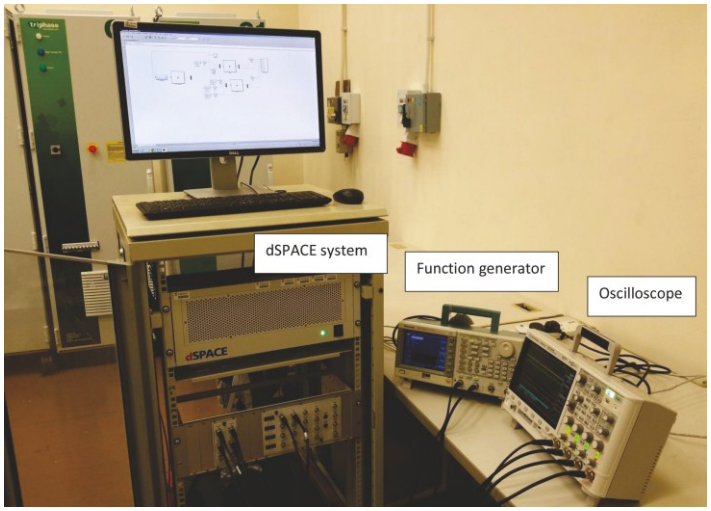

Fig. 3.13 The experimental setup.

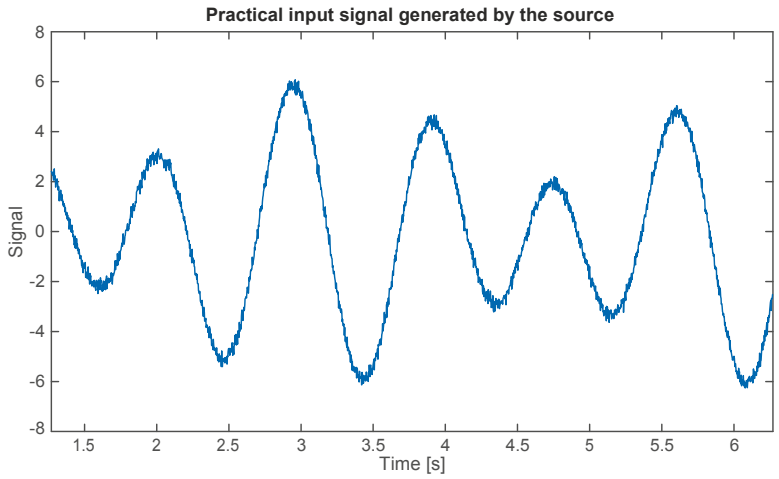

Fig. 3.14 A real-time noisy signal generated by the electrical signal generator.

devices. Note that the limitation on the dSpace processor puts a restriction on the practical comparisons, since the computing power is not enough to handle more than one algorithms simultaneously.

3.7 Concluding Remarks

The problem of estimating the amplitudes, frequencies and phases of a biased multi-sinusoidal signal is discussed in this chapter. A typical signal generator is formulated, thus allowing *direct* frequency adaptation by a novel adaptive observer approach that is based on the AO technique for singular frequency (see Chapter 2). Compared to other adaptive

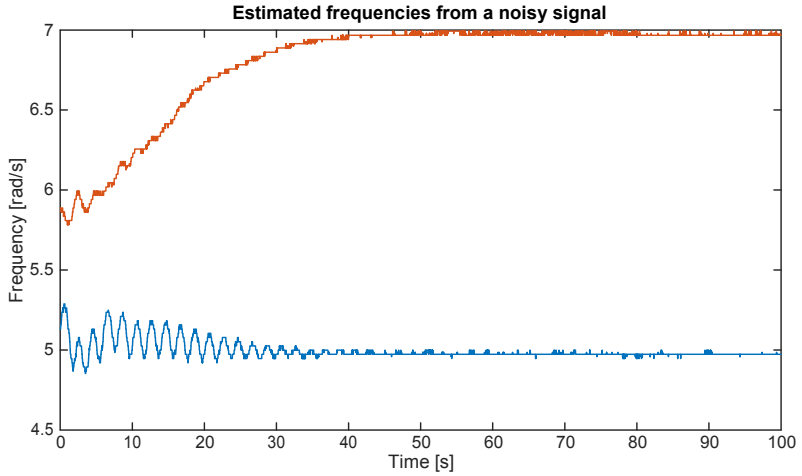

Fig. 3.15 Real-time frequency detection of a single with two frequency contents by using the proposed method.

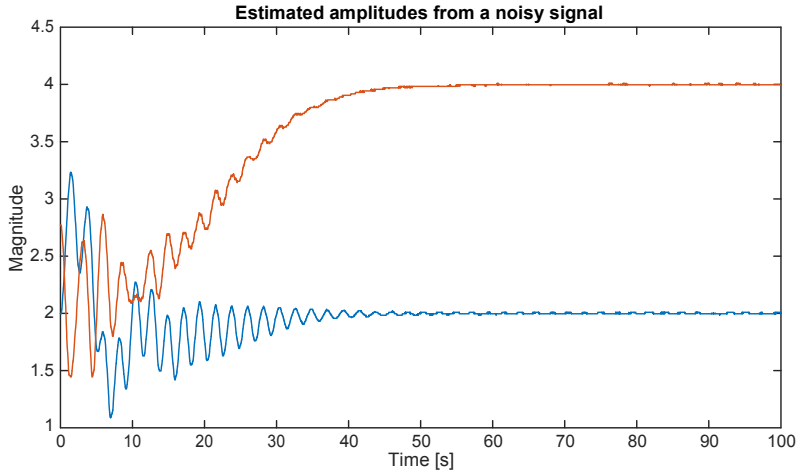

Fig. 3.16 Real-time amplitude detection of a single with two frequency contents by using the proposed method.

observer methods (e.g., [47, 67]) that estimate the characteristic polynomial's coefficients of the signal-generator system, the proposed algorithm significantly enhances an on-line implementation feature, thereby addressing one of the challenging issues in multi-frequency estimation. On the other hand, thanks to the excitation-based switching dynamics that freeze the estimates as long as a weak excitation condition is detected in real-time, the phenomenon of poor excitation is approached, and the proposed estimator is proven to be ISS with respect to bounded disturbances and overparametrization. The tuning criteria of the adaptation parameters of the estimator are obtained analytically as a result of the ISS based analysis.

The effectiveness of the proposed algorithm has been shown by extensive simulations and real-time experiments.

Chapter 4

STATE-VARIABLE FILTERING-BASED APPROACH

4.1 Introduction

In this chapter, following the treatment introduced in Chapter 2, we also use a pre-filtering technique in order to obtaining a set of signals, independent of the structured perturbation, for the constructions of the frequency adaptation law. Nevertheless, the pre-filtered signals are *directly* exploited for AFP estimation to achieve a simpler algorithm in terms of dynamic order. Consider

$$v(t) = y(t) + b + d(t), \quad t \in \mathbb{R}_{\geq 0} \tag{4.1}$$

where $y(t)$ is the stationary sinusoid given in (2.2), and the order of the structured perturbation n_d is set to 1 without loss of generality. In fact, in the next section, we show that the arbitrarily higher order perturbation (compared to (2.1)) can be addressed by augmenting the order of the pre-filters by analogy to the nominal pre-filtering system given in Sec. 2.2.1.

Recent works [86, 89] have shown that the derivative signals generated by the single pre-filtering action (2.6) of order 4 can be *directly* used for robust frequency detection from biased measurement (4.1). Let us choose from [86] the frequency adaptation law for the reader's convenience:

$$\dot{\hat{\Omega}}(t) = -\mu \left[z_0(t) z_2(t) + z_1(t) z_3(t) \right] \left(\hat{\Omega}(t) z_0(t) - z_2(t) \right) z_0(t) + \left((z_0(t))^2 + (z_1(t))^2 \right) \left(\hat{\Omega}(t) z_1(t) - z_3(t) \right) z_1(t), \tag{4.2}$$

where the vector of auxiliary derivatives are defined w.r.t. the filtered signals $x_4(t)$ generated by a 4th order pre-filter in the form of (2.6):

$$z(t) = [\, z_0(t),\, z_1(t),\, z_2(t),\, z_3(t) \,]^\top \;/'. \quad \dot{x}_4(t),\, -\frac{d^2}{dt^2}x_4(t),\, -\frac{d^3}{dt^3}x_4(t),\, \frac{d^4}{dt^4}x_4(t) \;^\top \quad . \quad (4.3)$$

The method presented in [86], where the pre-filter was conceived as a cascade of first-order low-pass (LP) filters, is generalized by proposing a *parallel pre-filtering scheme* in which two LP filters with different pole locations are used to generate auxiliary signals that are directly used to estimate the parameters of the sinusoid. This enhanced structure allows to simplify the adaptation law (4.2) without violating the ISS property against the exogenous disturbance $d(t)$. In contrast with other methods [2, 8, 21, 90] that are also based on a single pre-filter system, this novel mechanism permits the squared-frequency parameter to be adapted directly without resorting to intermediate variables or tools as in [2, 8, 21, 90]. The ISS analysis also makes it possible to obtain useful tuning guidelines, since the dissipation rate and the ISS-asymptotic-gain are both expressed in terms of the estimator's parameters. Finally, the effectiveness of the proposed technique is shown by comparative numerical simulations and by a real experiment addressing the estimation of the frequency of the electrical mains from a noisy voltage measurement.

This chapter is organized as follows: In Section 4.2, we introduce the parallel pre-filtering scheme with dual filters characterized by distinct poles. Starting from the generalized parallel pre-filtering estimator presented in Section 4.3, a minimum order configuration characterized via a specific stability analysis is introduced in Section 4.4. The associated amplitude and phase detection method is given in Sec. 4.5. Section 4.6 gives an example of the discretized algorithm for digital implementation. Finally, Section 4.7 is dedicated to the simulations and the real-time experiments.

4.2 Parallel Pre-Filtering System

The parallel pre-filtering scheme consists in combining a pair of independent low-pass filters (2.5) and indexed by $k \in \{1, 2\}$. The architecture is shown in Fig. 4.1 by a block diagram. Without loss of generality, assuming we adopt a n_p-th order pre-filter, in such case let us denote by

$$x_k(t) = \begin{bmatrix} x_{k,1}(t) & \cdots & x_{k,n_p}(t) \end{bmatrix}^\top \in \mathrm{R}^{n_p},\, k \in \{1, 2\}$$

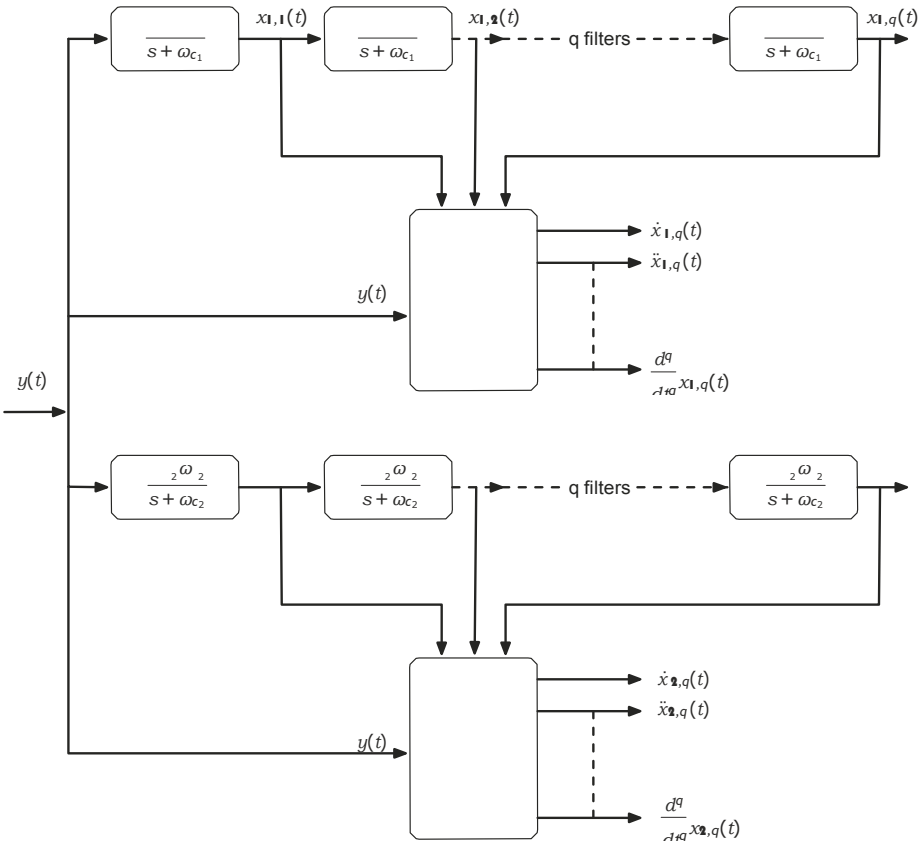

Fig. 4.1 Detailed scheme of the proposed pre-filtering system.

two "virtual" state vectors (i.e., not implemented in practice but instrumental to carry out the stability analysis) of the k-th filter, driven by $y(t)$!:. $\breve{y}(t) + b$ (not measurable) in place of $v(t)$ and evolving from arbitrary initial conditions:

$$\begin{cases} \dot{x}_k(t) = A_k x_k(t) + B_k y(t), \quad \forall k = 1,2 \; t \in \mathbb{R}_{\geq 0} \\ x_k(0) = x_{k_0} \end{cases}, \tag{4.4}$$

where $A_k \in \mathbb{R}^{n_p \times n_p}$ and $B_k \in \mathbb{R}^{n_p}$, $\forall k \in \{1,2\}$ are given by

$$A_k = \begin{bmatrix} -\omega_{c_k} & 0 & \cdots & \cdots & 0 \\ K_{c_k}\omega_{c_k} & -\omega_{c_k} & \ddots & \ddots & \vdots \\ 0 & \ddots & \ddots & \ddots & 0 \\ \vdots & \ddots & \ddots & & \\ \vdots & \ddots & \ddots & \ddots & \\ 0 & \cdots & 0 & K_{c_k}\omega_{c_k} & -\omega_{c_k} \end{bmatrix}, \; B_k = \begin{bmatrix} K_{c_k}\omega_{c_k} \\ 0 \\ \vdots \\ 0 \end{bmatrix}, \; \forall k \in \{1,2\}.$$

The parameters $\omega_{c_1}, \omega_{c_2} \in \mathbb{R}_{>0}$, with $\omega_{c_1} \neq \omega_{c_2}$ represent the poles of the low-pass filters, while $K_{c_1}, K_{c_2} \in (0, 1]$ play the role of damping gains. For the sake of further analysis, let us introduce the combined virtual state vector $x(t) = [x_1(t)\ x_2(t)]^\top$, which is governed by the following differential equation, taking on the same form as in the nominal case (2.6):

$$\dot{x}(t) = A_p x(t) + B_p y(t), \quad t \in \mathbb{R}_{\geq 0}, \tag{4.5}$$

with $x(0) = [x_{1_0}^\top, x_{2_0}^\top]^\top$ and

$$A_p = \begin{bmatrix} A_1 & 0 \\ 0 & A_2 \end{bmatrix}, \quad B_p = \begin{bmatrix} B_1 \\ B_2 \end{bmatrix}.$$

Following the same procedure as in Sec 2.2.1, it is readily seen that in the time-domain the derivatives $\frac{d^i}{dt^i} x_{k,n_p}(t)$, $1 \leq i \leq n_p$ are available and tend asymptotically to the sinusoidal regime as $t \to \infty$. Let us consider the stationary sinusoidal conditions

$$\frac{d^i}{dt^i} x_{k,n_p}(t) \approx a_{k,i} \sin(\phi_{k,i}(t)), \ \forall t >> 0, \quad k \in \{1, 2\}, \tag{4.6}$$

where

$$a_{k,i} = a\omega^i |H_{k,n_p}(\square\omega)|, \quad \phi_{k,i}(t) = \phi(t) + \angle H_{k,n_p}(\square\omega) + \frac{\pi}{2} i, \tag{4.7}$$

with

$$H_{k,n_p}(s) = \frac{\omega_{c_k}^{n_p} K_{c_k}^{n_p}}{(s + \omega^{c_k})^{n_p}}.$$

Clearly, the derivative signals (4.6) are directly computable from the filters' states (see (2.9)) and can be used as auxiliary signals to retrieve the frequency, the amplitude, and the phase of the input sinusoid. It is clear that a high order perturbation can be dealt with by a sufficient large n_p following the same procedure (see Section 2.2 for more details).

Theorem 4.2.1 (ISS of the parallel pre-filtering system) *Given the sinusoidal signal $y(t)$ and the perturbed measurement $v(t)$ (2.1), the error dynamics of the parallel pre-filtering system (4.5) is ISS w.r.t. any additive disturbance signal $d(t) \in L^1_\infty$* D

Proof: The proof is trivial due to the fact that $A_p < 0$. It is thus omitted here (the reader is referred to the single-filter case dealt with in Sec 2.2.2). •

Although the selection of n_p is not unique, the use of higher-order filters is not advisable unless needed (e.g., in the presence of higher order perturbation, see Chapter 2) because of the drawbacks of the higher order filtering (stated on page 27 in Sec. 2.2). To this end, in the rest of this chapter, we first characterize the stability properties of a generalized parallel

pre-filtering-based estimation scheme, where each filter has order equal to n_p; the order can be minimized to a 3 + 3 configuration characterized by the same unified convergence analysis. Then, in Section 4.4, we further reduce the order yielding to a simplified 2 + 2 scheme the stability analysis of which has to be carried out in a different way. Practically, the choice of pre-filter's configuration is determined by the designer depending on the performance requested to the estimator. Indeed, in Section 4.7, we show that, at the cost of increasing the order of the pre-filter, the 3 + 3 algorithm can provide an enhanced noise immunity in contrast with the 2 + 2 technique.

4.3 Generic Order $n_p + n_p$ Pre-Filtering-Based Frequency Estimator

4.3.1 Underlying Idea

Without loss of generality, let us start from considering a parallel pre-filtering stage having two pre-filters each of order n_p, where $n_p \geq 3$. In correspondence to the available auxiliary vectors

$$\hat{z}_1(t) = \begin{bmatrix} \frac{d^{n_p-2}}{dt^{n_p-2}}\hat{x}_{1,n_p}(t) & \frac{d^{n_p-2}}{dt^{n_p-2}}\hat{x}_{2,n_p}(t) \end{bmatrix}^\top, \quad \hat{z}_2(t) = \begin{bmatrix} \frac{d^{n_p}}{dt^{n_p}}\hat{x}_{1,n_p}(t) & \frac{d^{n_p}}{dt^{n_p}}\hat{x}_{2,n_p}(t) \end{bmatrix}^\top, \tag{4.8}$$

formed by the derivatives of the internal pre-filter's states, we introduce the counterparts in the noise-free conditions:

$$z_1(t) = \begin{bmatrix} \frac{d^{n_p-2}}{dt^{n_p-2}}x_{1,n_p}(t) & \frac{d^{n_p-2}}{dt^{n_p-2}}x_{2,n_p}(t) \end{bmatrix}^\top, \quad z_2(t) = \begin{bmatrix} \frac{d^{n_p}}{dt^{n_p}}x_{1,n_p}(t) & \frac{d^{n_p}}{dt^{n_p}}x_{2,n_p}(t) \end{bmatrix}^\top,$$

which have the sinusoidal regime $\tilde{z}_1(t)$, $\tilde{z}_2(t)$. For simplicity, let us create the combined vectors $\hat{z}(t) = [\hat{z}_1(t)\ \hat{z}_2(t)]^\top$, $\tilde{z}(t) = [\tilde{z}_1(t)\ \tilde{z}_2(t)]^\top$, and the error vector in the presence of $d(t)$: $\tilde{z}(t) = \hat{z}(t) - \tilde{z}(t)$. The vector of auxiliary signals $\hat{z}(t)$ can be expressed directly in terms of the available input $y(t)$ and the n_p-th order filter's states, $\hat{x}_1(t)$ and $\hat{x}_2(t)$:

$$\hat{z}(t) = \Phi_{n_p} \begin{bmatrix} y(t) & \hat{x}_1(t)^\top & \hat{x}_2(t)^\top \end{bmatrix}^{1_\top}, \tag{4.9}$$

with

$$\Phi_{n_p} = \begin{bmatrix} 0_{n_p-1} & CA_1^{n_p-2} & 0_{n_p} & 0_{n_p} \\ CA_1^{n_p-1}B_1 & CA_1^{n_p-2} & 0_{n_p} & 0_{n_p} \\ CA_2^{n_p-1}B_2 & 0_{n_p} & CA_2^{n_p-2} & 0_{n_p} \\ 0_{n_p} & 0_{n_p} & 0_{n_p} & CA_2^{n_p-2} \end{bmatrix}.$$

Accordingly, the "virtual" combined auxiliary derivatives $\mathbf{z}(t) = \begin{bmatrix} \mathbf{z}_1(t)^\top & \mathbf{z}_2(t)^\top \end{bmatrix}^\top$ can be expressed as

$$\mathbf{z}(t) = \Phi_{n_p} \begin{bmatrix} y(t) & \mathbf{x}_1(t)^\top & \mathbf{x}_2(t)^\top \end{bmatrix}^\top. \tag{4.10}$$

Moreover, the stationary sinusoids $\mathbf{z}_1(t)$, $\mathbf{z}_2(t)$ defined in (4.10) satisfy the equality

$$\Omega \mathbf{z}_1(t) + \dot{\mathbf{z}}_2(t) = 0.$$

We propose to obtain the unknown frequency of the measured signal by enforcing the above constraint on the estimated one. To this end, the following gradient-based adaptation law represents the core of the methodology, which exploits the available pre-filtered signals $\hat{\mathbf{z}}_1(t)$, $\hat{\mathbf{z}}_2(t)$ in place of the unavailable pure sinusoids $\mathbf{z}_1(t)$ and $\dot{\mathbf{z}}_2(t)$:

$$\dot{\hat{\Omega}}(t) = -\mu \hat{\mathbf{z}}_1(t)^\top \left(\hat{\Omega}(t) \hat{\mathbf{z}}_1(t) + \dot{\hat{\mathbf{z}}}_2(t) \right). \tag{4.11}$$

Besides the frequency-adaptation mechanism just described, the pre-filter-based AFP scheme also involves an amplitude and phase estimation method that will be described later on in Section 4.5.

4.3.2 Stability Analysis of the Frequency Estimator

Assume the unknown sinusoidal regime $\mathbf{x}(t)$ induced by the initial filter's state $\mathbf{x}_0$ gives rise to a "virtual" signal vector $\mathbf{z}(t)$ that matches the stationary sinusoidal behavior since the very beginning, when driven by the unperturbed sinusoid $y(t)$, that is:

$$\mathbf{x}(t) : \Phi_{n_p} \begin{bmatrix} y(t) & \mathbf{x}(t)^\top \end{bmatrix}^\top = \mathbf{z}(t) = \begin{bmatrix} \mathbf{z}_1(t)^\top & \mathbf{z}_2(t)^\top \end{bmatrix}^\top, \ \forall t \in \mathbb{R}_{\geq 0}. \tag{4.12}$$

The ISS of the error dynamics $\tilde{\mathbf{x}}(t)$ claimed in Theorem 4.2.1 immediately implies that $\tilde{\mathbf{z}}(t) \,/\!'\!. \, \hat{\mathbf{z}}(t) - \mathbf{z}(t)$ is ISS due to the identities (4.9) and (4.10). The error trajectory will enter in finite-time in a closed ball of radius $\gamma_z(d) + \delta$ centered at the origin, where

$$\gamma_z(r) = \bar{\Phi}_{n_p}(\gamma_x(r) + r), \ \forall r \in \mathbb{R}_{\geq 0}, \ \delta = \bar{\Phi}_{n_p} u \tag{4.13}$$

and where $\overline{\Phi}_{n_p} \geq \|\Phi_{n_p}\|$.

Introducing the frequency estimation error $\tilde{\Omega}(t) := \hat{\Omega}(t) - \Omega$, and applying the identity $\dot{z}_2(t) = -\Omega z_1(t)$, the dynamics of the frequency estimation error $\tilde{\Omega}(t)$ evolves according to

$$\begin{aligned}\dot{\tilde{\Omega}}(t) &= -\mu(z_1(t)+\tilde{z}_1(t))^\top \left(\hat{\Omega}(t)(z_1(t)+\tilde{z}_1(t)) - \Omega z_1(t) + \tilde{z}_2(t)\right) \\ &= -\mu\tilde{\Omega}z_1(t)^\top z_1(t) + \mu\tilde{\Omega}f_1(t,\tilde{z}) + \mu f_2(t,\tilde{z}),\end{aligned} \tag{4.14}$$

where

$$\begin{aligned}f_1(t,\tilde{z}) &= -2z_1(t)^\top\tilde{z}_1(t) - \tilde{z}_1(t)^\top\tilde{z}_1(t) \\ f_2(t,\tilde{z}) &= \Omega(f_1(t,\tilde{z}) + \tilde{z}_1(t)^\top z_1(t)) - \hat{z}_1(t)^\top\tilde{z}_2(t).\end{aligned}$$

Note that the functions $f_1(t,\tilde{z})$ and $f_2(t,\tilde{z})$ verify $f_1(t,0)=0$, $f_2(t,0)=0$ for all $t \in \mathbb{R}_{\geq 0}$. Moreover, owing to the boundedness of $z(t)$, there exist two $\mathcal{K}_\infty$-functions $\gamma_{f,1}(\cdot)$ and $\gamma_{f,2}(\cdot)$ such that

$$|f_1(t,\tilde{z})| \leq \gamma_{f,1}(|\tilde{z}|), \quad |f_2(t,\tilde{z})| \leq \gamma_{f,2}(|\tilde{z}|). \tag{4.15}$$

The following assumption is needed to prove the convergence of the estimation error.

Assumption 4 *The signal $z_1(t)$ is persistently exciting in the sense that there exist a constant $\varepsilon > 0$ such that*

$$z_1(t)^\top z_1(t) \geq \varepsilon, \ \forall t > 0. \tag{4.16}$$

In the following derivations, we show that Assumption 4 is verified under a suitable choice of ω_{c_1} and ω_{c_2} in the nominal (noise-free) condition. Let us expand $z_1(t)^\top z_1(t)$ as follows:

$$\begin{aligned}z_1(t)^\top z_1(t) &= \left(\frac{d^{n_p-2}x_{1,n_p}}{dt^{n_p-2}}(t)\right)^2 + \left(\frac{d^{n_p-2}x_{2,n_p}}{dt^{n_p-2}}(t)\right)^2 \\ &= \sum_{k=1}^{2} a_{k,n_p-2}\sin^2\left(\phi(t) + \phi_{k,n_p} + \frac{\pi}{2}(n_p-2)\right),\end{aligned}$$

where $a_{k,n_p-2} = a\omega^{n_p-2}|H_{k,n_p}(j\omega)|$ and ϕ_{k,n_p} denotes the phase of $H_{k,n_p}(j\omega)$. After some algebra, we get

$$\phi_{1,n_p} = n_p \arctan\left(-\frac{\omega}{\omega_{c_1}}\right), \quad \phi_{2,n_p} = n_p \arctan\left(-\frac{\omega}{\omega_{c_2}}\right).$$

Thanks to the fact that $|\phi_{1,n_p} - \phi_{2,n_p}| < \frac{n_p\pi}{2}$, $\forall \omega > 0$, $z_1(t)^\top z_1(t)$ is strictly positive for $t > 0$ if

$$|\phi_{1,n_p} - \phi_{2,n_p}| \neq j\pi, j \in [0, 1, 2, \ldots \lfloor n_p/2 \rfloor), \ \forall \omega \in \mathbb{R}_{>0} \tag{4.17}$$

with $\lfloor \cdot \rfloor$ being the floor operator.

In view of (4.17), it is readily seen that $|\phi_{1,n_p} - \phi_{2,n_p}| = 0$, i.e., $\phi_{1,n_p} = \phi_{2,n_p}$, $\forall \omega > 0$ as long as ω_{c_1} and ω_{c_2} are distinct. Next, we show a choice of the pre-filters' parameters such that

$$\omega_{c_1}^2 + \omega_{c_2}^2 - (2 + 4\alpha^2)\omega_{c_1}\omega_{c_2} < 0, \tag{4.18}$$

where $\alpha = \tan(\pi/n_p)$, implies that the condition $|\phi_{1,n_p} - \phi_{2,n_p}| = j\pi, j \in [1, 2, ... \lfloor n_p/2 \rfloor)$, $\forall \omega > 0$ is satisfied. Let us suppose that there exists $\omega \in \mathrm{R}_{>0}$, such that $|\phi_{1,n_p} - \phi_{2,n_p}| = j\pi$. Such hypothesis holds if and only if

$$\arctan\left(\frac{\omega}{\omega_{c_1}}\right) - \arctan\left(\frac{\omega}{\omega_{c_2}}\right) = \pm\frac{j\pi}{n_p}.$$

Taking $\tan(\cdot)$ on both hand side of the above equation, and owing to the property of trigonometric functions, we get

$$\left(\frac{\omega}{\omega_{c_1}} - \frac{\omega}{\omega_{c_2}}\right) \Big/ \left(1 + \frac{\omega^2}{\omega_{c_1}\omega_{c_2}}\right) = \pm \tan(j\pi/n_p)$$

which can be rearranged as follows:

$$\tan(j\pi/n_p)\omega^2 \pm (\omega_{c_1} - \omega_{c_2})\omega + \tan(j\pi/n_p)\omega_{c_1}\omega_{c_2} = 0. \tag{4.19}$$

Note that equation (4.19) does not admit any real root in the variable ω as long as

$$\omega_{c_1}^2 + \omega_{c_2}^2 - (2 + 4\tan(j\pi/n_p)^2)\omega_{c_1}\omega_{c_2} < 0,$$

which is always true if (4.18) holds since $0 < \tan(\pi/n_p) \leq \tan(j\pi/n_p) < \tan(\pi/2)$. Therefore, by contradiction, the condition

$$|\phi_{1,n_p} - \varphi_{2,n_p}| = j\pi, j \in [0, 1, 2, ... \lfloor n_p/2 \rfloor), \forall \omega \in \mathrm{R}_{>0}$$

can be ensured by proper selection of ω_{c_1}, ω_{c_2}. Finally, due to the phase separation property, there always exist a positive constant ε, such that excitation condition (4.16) is verified for all $t > 0$.

Theorem 4.3.1 (ISS of the adaptive frequency identifier) *Under Assumption 4, given the sinusoidal signal $y(t)$ and the perturbed measurement model (4.1), the frequency estimation system made up of the two filters (4.4) of order n ($n \geq 3$) and by the adaptation law (4.9)*

and (4.11) is ISS w.r.t. any additive disturbance signal $d(t) \in \mathsf{L}^1_\infty$ *such that*

$$\|d\|_\infty < \bar{d} < \gamma_z^{-1}\left(\gamma_{f,1}^{-1}(\varepsilon)\right), \tag{4.20}$$

where γ_z *and* $\gamma_{f,1}$ *are given by (4.13) and (4.15), respectively.* D

Proof: According to (4.13), for any positive $\delta \in \mathsf{R}_{>0}$ there exists a finite time-instant T_δ such that $|\tilde{z}(t)| \le \gamma_z(d) + \delta$, $\forall\, t \ge T_\delta$, which implies

$$\gamma_{f,1}(|\tilde{z}(t)|) \le \gamma_{f,1}(\gamma_z(\bar{d}) + \delta), \quad \forall\, t \ge T_\delta. \tag{4.21}$$

If the bound (4.20) on the disturbances holds, then, for some $\delta \in \mathsf{R}_{>0}$, the following inequality is satisfied

$$\varepsilon - \gamma_{f,1}(\gamma_z(\bar{d}) + \delta) > 0. \tag{4.22}$$

Thus, in view of (4.14), (4.15) and Assumption 4, the following bound on the derivative of candidate Lyapunov function $V = \frac{1}{2}\tilde{\Omega}^2$ can be established for any $t > T_\delta$:

$$\begin{aligned} \frac{\partial V}{\partial \tilde{\Omega}}\dot{\tilde{\Omega}}(t) &\le -\mu\left(\varepsilon - \gamma_{f,1}(\gamma_z(\bar{d}) + \delta)\right)|\tilde{\Omega}(t)|^2 + \mu\gamma_{f,2}(|\tilde{z}(t)|)|\tilde{\Omega}(t)| \\ &\le -\Delta_\mu |\tilde{\Omega}(t)|^2 + \mu\gamma_{f,2}(|\tilde{z}(t)|)|\tilde{\Omega}(t)|, \; t \ge T_\delta, \end{aligned} \tag{4.23}$$

where $\Delta_\mu := \mu\left(\varepsilon - \gamma_{f,1}(\gamma_z(\bar{d}) + \delta)\right)$ is a positive constant. Thus, $\tilde{\Omega}(t)$ is ISS w.r.t. $\tilde{z}(t)$ and in turn, ISS w.r.t. d. •

4.3.3 Pre-Filter of Order $3+3$

In this paragraph, we specialize the previous scheme to the case $n_p = 3$. Considering $n_p = 3$ in (4.8), the auxiliary vectors are:

$$\hat{z}_1(t) = \begin{bmatrix} \dot{\hat{x}}_{1,3}(t) & \dot{\hat{x}}_{2,3}(t) \end{bmatrix}^\top, \quad \hat{z}_2(t) = \begin{bmatrix} \frac{d^3}{dt^3}\hat{x}_{1,3}(t) & \frac{d^3}{dt^3}\hat{x}_{2,3}(t) \end{bmatrix}^\top,$$

formed by the derivatives of the internal pre-filter's states of order 3. For simplicity, let us consider the combined vector of auxiliary signals $\hat{z}(t) = [\hat{z}_1(t)\ \hat{z}_2(t)]^\top$ which can be expressed directly in terms of the available measurement $v(t)$ and the pre-filter's states $\hat{x}_k(t) \in \mathsf{R}^3$, $k = 1, 2$:

$$\hat{z}(t) = \Phi_3 \begin{bmatrix} v(t) & \hat{x}_1(t)^\top & \hat{x}_2(t)^\top \end{bmatrix}^\top, \tag{4.24}$$

with

$$\Phi_3 = \begin{bmatrix} 0 & CA_1 & 0 \\ 0 & 0 & CA_2 \\ CA_1^2B_1 & CA_1^3 & 0 \\ CA_2^2B_2 & 0 & CA_2^3 \end{bmatrix}$$

Finally, the frequency is estimated by the recursive algorithm (4.11) on the basis of the updated $\hat{z}_1(t)$ and $\hat{z}_2(t)$. The stability analysis of the 3 + 3 frequency estimator is a special case of the one given in Section 4.3.2 and is therefore omitted.

4.4 Order 2 + 2 Pre-Filtering-Based Frequency Estimator

4.4.1 Underlying Idea

In this section, we aim to further reduce the dynamic order of the estimator, by decreasing the order of the two pre-filters to $n_p = 2$. Let us choose $K_{c_1} = K_{c_2} = K_c$ and then introduce the auxiliary signals $z_1(t) = x_{1,2}(t) - x_{2,2}(t)$ and $z_2(t) = \frac{d^2 x_{1,2}}{dt^2}(t) - \frac{d^2 x_{2,2}}{dt^2}(t)$. It is easy to show that both z_1 and z_2 tend asymptotically to a sinusoidal regime given by:

$$\begin{aligned} z_1(t) &\xrightarrow{t\to\infty} \hat{z}_1(t) = a_{1,0}\sin(\phi_{1,0}(t)) - a_{2,0}\sin(\phi_{2,0}(t)), \\ z_2(t) &\xrightarrow{t\to\infty} \hat{z}_2(t) = -\Omega \hat{z}_1(t), \end{aligned} \tag{4.25}$$

with $\Omega = \omega^2$ is the true (unknown) squared-frequency, and where

$$a_{k,0} = a\,|H_{k,2}(\Box\omega)|, \quad \phi_{k,0}(t) = \phi(t) + \angle H_{k,2}(\Box\omega). \tag{4.26}$$

with

$$H_{k,2}(s) = \frac{\omega_{c_k}^2 K_c^2}{(s+\omega_{c_k})^2}.$$

In view of (4.25), $\hat{z}_1(t)$ turns out to be a pure single sinusoidal signal having frequency ω and amplitude

$$a_{z_1} = \sqrt{y_p^2 + y_q^2}, \tag{4.27}$$

in which

$$\begin{aligned} y_p &= a_{1,0}\cos\angle H_{1,2}(\Box\omega) - a_{2,0}\cos\angle H_{2,2}(\Box\omega), \\ y_q &= a_{1,0}\sin\angle H_{1,2}(\Box\omega) - a_{2,0}\sin\angle H_{2,2}(\Box\omega). \end{aligned}$$

Similar to the order $n_p + n_p$ algorithm, the following gradient-based adaptation law that exploits the available pre-filtered signals $\hat{z}_1(t)$, $\hat{z}_2(t)$ in place of the unavailable pure sinusoids

$\hat{z}_1(t)$ and $\hat{z}_2(t)$, is adopted for the frequency estimation:

$$\dot{\hat{\Omega}}(t) = -\mu \hat{z}_1(t) \left(\hat{\Omega}(t)\hat{z}_1(t) + \hat{z}_2(t) \right), \tag{4.28}$$

with $\mu > 0$ being a user-defined adaptation gain aimed at tuning the convergence speed of the estimator.

4.4.2 Stability Analysis of the Frequency-Adaptation Scheme with 2+2 Pre-Filter

Let us introduce the combined vector $\hat{z}(t) = [\hat{z}_1(t)\ \hat{z}_2(t)]^\top$ that can be expressed as

$$\hat{z}(t) = \Phi_2 \left[v(t) \quad \hat{x}_1(t)^\top \quad \hat{x}_2(t)^\top \right]^\top, \tag{4.29}$$

where $\hat{x}_1(t) = [\hat{x}_{1,1}(t) \ \cdots \ \hat{x}_{1,2}(t)]^\top$, $\hat{x}_2(t) = [\hat{x}_{2,1}(t) \ \cdots \ \hat{x}_{2,2}(t)]^\top$ and

$$\Phi_2 = \begin{bmatrix} 0 & CB & -CB \\ C(A_1B_1 - A_2B_2) & CA_1^2 & -CA_2^2 \end{bmatrix}.$$

By analogy to the foregoing analysis illustrated in Section 4.3.2, we immediately conclude that the trajectory of $\tilde{z}(t)$ will enter in a closed ball of radius $\gamma_z(\bar{d}) + \delta$ centered at the origin in finite-time, where

$$\gamma_z(r) = \bar{\Phi}_2(\gamma_x(r) + r),\ \forall r \in \mathbb{R}_{\geq 0},\ \delta = \bar{\Phi}_2 v, \tag{4.30}$$

being $\bar{\Phi}_2 \geq ||\Phi_2||$. Thanks to the relationship $\hat{z}_2(t) = -\Omega \hat{z}_1(t)$, let us rewrite (4.28) in terms of the errors $\tilde{z}_1$ and $\tilde{z}_2$:

$$\begin{aligned} \dot{\tilde{\Omega}}(t) &= -\mu \left(\hat{z}_1(t) + \tilde{z}_1(t) \right)\left(\hat{\Omega}(t)(\hat{z}_1(t) + \tilde{z}_1(t)) - \Omega \hat{z}_1(t) + \tilde{z}_2(t) \right) \\ &= -\mu \tilde{\Omega} \hat{z}_1(t)^2 + \mu \tilde{\Omega} f_1(t, \tilde{z}) + \mu f_2(t, \tilde{z}), \end{aligned} \tag{4.31}$$

where

$$\begin{aligned} f_1(t, \tilde{z}) &= -2\hat{z}_1(t)\tilde{z}_1(t) - \tilde{z}_1(t)^2, \\ f_2(t, \tilde{z}) &= \Omega(f_1(t, \tilde{z}) + \tilde{z}_1(t)\tilde{z}_1(t)) - (\hat{z}_1(t) + \tilde{z}_1(t))\tilde{z}_2(t). \end{aligned}$$

It is not difficult to see that there exist two $\mathcal{K}_\infty$-functions $\gamma_{f,1}(\cdot)$ and $\gamma_{f,2}(\cdot)$ such that

$$|f_1(t, \tilde{z})| \leq \gamma_{f,1}(|\tilde{z}|), \quad |f_2(t, \tilde{z})| \leq \gamma_{f,2}(|\tilde{z}|). \tag{4.32}$$

The following result characterizes the stability properties of the frequency estimator.

Theorem 4.4.1 (ISS of the adaptive frequency identifier) *Given the sinusoidal signal $v(t)$ and the perturbed measurement model (2.1), let the bound on the measurement disturbance d verify the inequality:*

$$||d||_\infty < \bar{d} < \gamma_z^{-1}\left(\gamma_{f,1}^{-1}\left(\frac{\omega\kappa a_{z_1}^2 \ln((1-\kappa_\Delta)/\kappa)}{\mu\pi\kappa a_{z_1}^2 - 2\omega\ln(1/\kappa)}\right)\right), \tag{4.33}$$

where a_{z_1} is given by (4.27), $\kappa : \kappa \in (0,1)$ is chosen arbitrarily, $\kappa_\Delta \in \mathbb{R}_{>0}$ is such that $1-\kappa_\Delta > \kappa$, and μ is chosen large enough to verify the following two inequalities:

$$\omega \ln(1/\kappa)/(\mu\kappa a_{z_1}^2) < \pi \tag{4.34}$$

and

$$\cos^2\left(\frac{\omega\ln(1/\kappa)}{2\mu\kappa a_{z_1}^2}\right) - \kappa \geq \frac{\omega\kappa\ln((1-\kappa_\Delta)/\kappa)}{\mu\pi\kappa a_{z_1}^2 - 2\omega\ln(1/\kappa)}. \tag{4.35}$$

Then, the frequency estimation system given by the two filters (4.5) with $n=2$ and by (4.28) and (4.29) is ISS w.r.t. $d(t)$. D

Proof: Consider the following candidate Lyapunov function $V(\tilde{\Omega}) = \frac{1}{2}\tilde{\Omega}^2$. In view of (4.31) and (4.32), the time-derivative of $V(t)$ along the system's trajectory satisfies:

$$\frac{\partial V}{\partial \tilde{\Omega}}\dot{\tilde{\Omega}}(t) = \tilde{\Omega}(t)\dot{\tilde{\Omega}}(t) \leq -\mu\left(z_1(t)^2 - \gamma_{f,1}(|\tilde{x}(t)|)\right)\tilde{\Omega}(t)^2 + \mu\gamma_{f,2}(|\tilde{x}(t)|)|\tilde{\Omega}(t)|, \tag{4.36}$$

in which the stationary sinusoidal signal $z_1(t)$ appears explicitly. Now, under the assumption of $\bar{d}$ given by (4.33) and the inequalities (4.34) and (4.35), then the period of the squared sinusoid $z_1^2(t)$ can be partitioned in three intervals: P_2, in which it holds that

$$\left(z_1(t)^2 - \gamma_{f,1}(\gamma_z(\bar{d}) + \delta)\right) \geq \kappa a_{z_1}^2$$

and P_1, P_3, in which this inequality is not guaranteed. In the following, we denote by t_0, t_1 and t_2 the transition time-instants between the aforementioned modes of behavior, as described in Fig.4.2. Without loss of generality, the duration of P_2 is denoted by T_e that is subject to $T_e \leq \frac{\pi}{\omega}$, while the duration of P_1 and P_3 are identical denoted by $T_d = \frac{\pi}{2\omega} - \frac{T_e}{2}$. We prove that there exist a suitably specified constant, such that if the interval P_2 lasts for more than $\bar{T}_e$, then the discrete-time Lyapunov function obtained by sampling the continuous-time Lyapunov function at the end of the three phases is a discrete-ISS Lyapunov function.

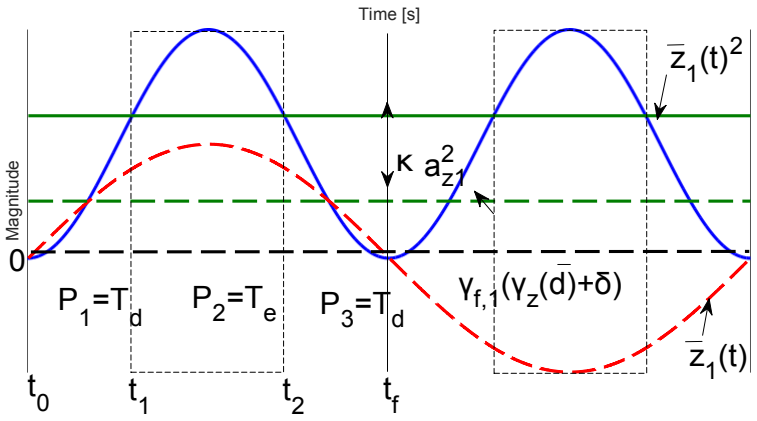

Fig. 4.2 An example plot of the excitation signal $\bar{z}_1^2(t)$ (blue line) induced by the stationary sinusoidal signal $\bar{z}_1(t)$ with amplitude a_{z_1} (dotted red line), as well as two horizontal thresholds $\gamma_{f,1}(\gamma_z(d)+\delta)$ (dotted green line) and $\gamma_{f,1}(\gamma_z(d)+\delta)+\kappa a_{z_1}^2$ (green line).

Moreover, we show that the required duration $\bar{T}_e$ of P_2 can be guaranteed if the disturbance verifies inequality (4.33) reported in the statement of the theorem.

During P_2, we have:

$$\dot{V}(t) \leq -\mu\kappa a_{z_1}^2 \tilde{\Omega}(t)^2 + \mu\gamma_{f,2}(|\tilde{z}(t)|)|\tilde{\Omega}(t)|\,. \tag{4.37}$$

By completing squares, we get:

$$\begin{aligned} \dot{V}(t) &\leq -\mu\frac{\kappa a_{z_1}^2}{2}\tilde{\Omega}(t)^2 + \frac{\mu}{2\kappa a_{z_1}^2}\gamma_{f,2}(|\tilde{z}(t)|)^2 \\ &\leq -\mu\kappa a_{z_1}^2(V(t)-\gamma_e(d))\,, \end{aligned} \tag{4.38}$$

with $\gamma_e(\bar{d}) = (2\kappa^2 a_{z_1}^4)^{-1}\gamma_{f,2}(|\tilde{z}(t)|)^2$. Analogously, during P_1 and P_3, we obtain the following upper bound for $\dot{V}(t)$

$$\dot{V}(t) \leq \mu\gamma_{f,1}(|\tilde{z}(t)|)\left(V(t)+\gamma_d(\bar{d})\right), \tag{4.39}$$

where $\gamma_d(r)$ is a K-function such that $\gamma_d(r)\gamma_{f,1}(r)^2 \geq \frac{\gamma_{f,2}(r)^2}{2}$, $\forall\, r \geq 0$.

Applying the Gronwall-Bellman Lemma to (4.38), the value of the Lyapunov function during P_2 ($t_1 \leq t < t_2$) can be bounded as follows:

$$\begin{aligned} V(t) &\leq V(t_1) + (1-e^{-\mu\kappa a_{z_1}^2(t-t_1)})(\gamma_e(\bar{d}) - V(t_1)) \\ &= e^{-\mu\kappa a_{z_1}^2(t-t_1)}V(t_1) + \gamma_e(\bar{d})(1-e^{-\mu\kappa a_{z_1}^2(t-t_1)}),\ \forall\, t \in [t_1, t_2)\,. \end{aligned} \tag{4.40}$$

Taking the same steps as above, we obtain a further bound of $V(t)$ during the "dis-excited" intervals P_1 and P_3:

$$V(t) \leq V(t_p)e^{\mu\gamma_{f,1}(|\tilde{x}(t)|)(t-t_p)} + (e^{\mu\gamma_{f,1}(|\tilde{x}(t)|)(t-t_p)} - 1)\gamma_d(\bar{d}),$$
$$\forall t \in [t_0, t_1), \text{ if } p = 0 \text{ or } \forall t \in [t_2, t_0 + \frac{\pi}{\omega}), \text{ if } p = 2. \quad (4.41)$$

Due to the poor excitation during P_1 and P_3, at the end of these intervals we can establish a (possibly) conservative bound

$$V(t_e) \leq e^{\mu\gamma_{f,1}(|\tilde{x}(t)|)T_d}(V(t_p) + \gamma_d(\bar{d})), \; t_e = t_1, \text{ if } p = 0 \text{ (i.e., in } P_1)$$
$$\text{or } t_e = t_0 + \frac{\pi}{\omega}, \text{ if } p = 2 \text{ (i.e., in } P_3). \quad (4.42)$$

Then, in view of (4.40), assuming that the mode P_2 occurs for a time T_e (we do not pose a lower-bound on T_e at this point, possibly $T_e = 0$), we get the inequality:

$$V(t_2) \leq e^{-\mu\kappa a_{z_1}^2 T_e}|e^{\mu\gamma_{f,1}(|\tilde{x}(t)|)T_d}(V(t_0) + \gamma_d(\bar{d}))| + \gamma_e(\bar{d})(1 - e^{-\mu\kappa a_{z_1}^2 T_e}). \quad (4.43)$$

Finally, denoting by $V_k := V(t_0 + k\frac{\pi}{\omega})$ the value of the Lyapunov function at the end of each k-th P_3 interval, and considering that t_0 is arbitrary within the set $t_0 \in \{t : \tilde{z}_1^2(t) = 0\}$, from inequalities (4.42) and (4.43), we can easily get the following expression:

$$V_{k+1} \leq e^{2\mu\gamma_{f,1}(|\tilde{x}(t)|)T_d - \mu\kappa a_{z_1}^2 T_e} V_k + \gamma_e(\bar{d})(1 - e^{-\mu\kappa a_{z_1}^2 T_e})e^{\mu\gamma_{f,1}(|\tilde{x}(t)|)T_d}$$
$$+ (e^{2\mu\gamma_{f,1}(|\tilde{x}(t)|)T_d - \mu\kappa a_{z_1}^2 T_e} + e^{\mu\gamma_{f,1}(|\tilde{x}(t)|)T_d})\gamma_d(\bar{d}). \quad (4.44)$$

We now show that a minimum time-duration of phase P_2, denoted by $\bar{T}_e$, is ensured as long as the bound (4.33) is verified. Indeed (4.33) implies that

$$\gamma_{f,1}(\gamma_z(\bar{d}) + \delta) < \frac{\omega\kappa a_{z_1}^2 \ln((1 - \kappa_\Delta)/\kappa)}{\mu\pi\kappa a_{z_1}^2 - 2\omega \ln(1/\kappa)} = \frac{\ln((1 - \kappa_\Delta)/\kappa)}{2\mu(\pi/2\omega - \ln(1/\kappa)/\mu\kappa a_{z_1}^2)}. \quad (4.45)$$

Then, thanks to (4.35), there exists a positive constant $\bar{T}_d$ that bounds the length of the dis-excitation interval ($T_d \leq \bar{T}_d$) :

$$\bar{T}_d := \min\left\{t \leq \frac{\pi}{\omega} : \tilde{z}_1(t_0 + t)^2 \geq a_{z_1}^2 \cos^2\frac{\omega \ln(1/\kappa)}{2\mu\kappa a_{z_1}^2}\right\}.$$

Owing to the fact that $z_1(t_0+\overline{T}_d)^2 = a_{z_1}^2 \sin^2(\omega(t_0+\overline{T}_d))$, then $\overline{T}_d$ can be computed as the minimum positive solution of the equation:

$$a_{z_1}^2 \sin_2(\overline{\omega T}_d) = a_{z_1}^2 \cos^2 \frac{\omega \ln(1/\kappa)}{2\mu\kappa a_{z_1}^2}.$$

From (4.34), it holds that

$$\overline{T}_d = \frac{\pi}{2\omega} - \frac{\ln(1/\kappa)}{2\mu\kappa a_{z_1}^2}.$$

Hence,

$$T_e \geq \frac{\pi}{\overline{\omega}} - 2\overline{T}_d \geq \frac{\ln(1/\kappa)}{\mu\kappa a_{z_1}^2} = \overline{T}_e.$$

Combining $\overline{T}_d$ and (4.45), we also get

$$e^{2\mu\gamma_{f,1}(|z(t)|)T_d} < e^{2\mu\gamma_{f,1}(|z(t)|)\overline{T}_d} < \frac{(1-\kappa_\Delta)}{\kappa}.$$

Next, we prove that the Lyapunov function with discrete dynamics induced by sampling the frequency estimator in correspondence of the transitions is ISS with respect to the measurement disturbance $d(t)$. Since

$$t_2 - t_1 = T_e \geq \frac{\ln(1/\kappa)}{\mu\kappa a_{z_1}^2},$$

picking $\epsilon \in \mathbb{R}_{>0}$ such that $1-\kappa_\Delta < \epsilon < 1$, then we can guarantee the following bound on the discrete (sampled) Lyapunov function sequence:

$$V_{k+1} \leq \epsilon V_k + \gamma_e(\overline{d})(1-\kappa)\frac{1}{\sqrt{\kappa}} + (1+\frac{1}{\sqrt{\kappa}})\gamma_d(\overline{d}).$$

In compact form:

$$V_{k+1} - V_k \leq -(1-\epsilon)V_k + \gamma_v(\overline{d}),$$

where the function $\gamma_v(\cdot)$ is a $\mathcal{K}$-function defined as

$$\gamma_v(r) = \gamma_e(r)(1-\kappa)\frac{1}{\sqrt{\kappa}} + (1+\frac{1}{\sqrt{\kappa}})\gamma_d(r), \quad \forall r \in \mathbb{R}_{\geq 0}.$$

Hence, we are able to conclude that V_k is a discrete ISS Lyapunov function for the sampled sequence.

Finally, we show the ISS for the continuous-time system by using the continuity of $V(t)$ and the boundedness of its time-derivative in the inter-sampling. Thanks to the periodicity

of the excitation signal $z_1(t)^2$, let us denote by $t_0(k)$, $t_1(k)$ and $t_2(k)$ the transition time-instants of the k-th period of $z_1(t)^2$, and $k(t)$ the index of the current period: $k(t) = k : t \in [t_0(k), t_0(k+1))$. Between two samples, the Lyapunov function can be bounded (possibly in a conservative way) by,

$$\begin{aligned} V(t) &\le \left(\frac{1}{\sqrt{\kappa}}\right)^2 \left(V(t_0) + \gamma_d(\bar{d})\right)^2 + \left(\sqrt{\kappa}\left(V(t_0) + \gamma_d(\bar{d})\right) + \gamma_e(\bar{d})\right)^2 \\ &\quad + V(t_0) + \frac{1}{\sqrt{\kappa}}\gamma_e(\bar{d}) + \left(1 + \frac{1}{\sqrt{\kappa}}\right)\gamma_d(\bar{d}) \\ &= \frac{1 + \sqrt{\kappa} + \kappa}{\sqrt{\kappa}} V_{k(t)} + \left(1 + \frac{1}{\sqrt{\kappa}}\right)\gamma_e(\bar{d}) + \left(2 + \frac{2}{\sqrt{\kappa}}\right)\gamma_d(\bar{d}). \end{aligned} \quad (4.46)$$

Since $k(t) \xrightarrow{t\to\infty} \infty$, an infinite number of excited phases with length T_e occurs asymptotically; the estimation error in the inter-sampling times converges to a compact region whose radius depends on the bound on the disturbance (assumed to exist), hence concluding the proof. •

4.5 Amplitude and Phase Estimation

Finally, we propose a unified algorithm for estimating the amplitude and the phase that applies to all the $n_p + n_p$ ($n_p \ge 2$) methods presented in this chapter. Following the same procedure carried out in Section 2.3, the amplitude and phase ($a_{k,q}$, $\phi_{k,q}$) of the q-th derivative of the n_p-th state variable of the k-th pre-filter (see (4.6) and (4.7)) can be estimated as follows by using $\hat{\omega}(t)$ obtained by either methods illustrated in this chapter:

$$\hat{a}_{k,q}(t) = \sqrt{\hat{\Omega}(t)^{q-1} \left(\frac{d^{q-1}}{dt^{q-1}}\hat{x}_{k,n_p}(t)\right)^2 + \left(\frac{d^q}{dt^q}\hat{x}_{k,n_p}(t)\right)^2}, \quad (4.47a)$$

$$\hat{\phi}_{k,q}(t) = \angle\left(\frac{d^q}{dt^q}\hat{x}_{k,n_p}(t) + \mathrm{i}\,\hat{\omega}(t)^q \frac{d^{q-1}}{dt^{q-1}}\hat{x}_{k,n_p}(t)\right), \ \forall q \le n_p, \quad (4.47b)$$

and

$$\hat{a}(t) = \frac{\hat{a}_{k,q}(t)}{\hat{\omega}(t)^q}\left(\sqrt{\omega_{c_k}^2 + \hat{\omega}(t)^2/(K_{c_k}\omega_{c_k})}\right)^{n_p}, \quad (4.48a)$$

$$\hat{\phi}(t) = \hat{\phi}_{k,q}(t) + n_p \arctan(\hat{\omega}(t)/\omega_{c_k}) - \frac{\pi}{2}q. \quad (4.48b)$$

The "ill" defined non-adaptive formulas (4.47a) and (4.48a) (they are not defined when $\hat{\omega}(t) = 0$) are amended by the following adaptive mechanisms:

$$\dot{\hat{a}}_{k,q}(t) = -\mu_a \left[\hat{a}_{k,q}(t) - \frac{\Omega(t)}{\hat{\omega}} \left(\frac{d^{q-1}}{dt^{q-1}} \hat{x}_{k,n_p}(t) \right)^2 + \left(\frac{d^q}{dt^q} \hat{x}_{k,n_p}(t) \right)^2 \right] \tag{4.49}$$

and

$$\dot{\hat{a}}(t) = -\mu_a \hat{\omega}(t)^q \left(\hat{\omega}(t)^q \hat{a}(t) - \hat{a}_{k,q}(t) \left(\sqrt{\omega_{c_k}^2 + \hat{\omega}(t)^2 / (K_{c_k} \omega_{c_k})} \right)^{n_p} \right) \tag{4.50}$$

with initial condition $\hat{a}_{k,q}(0) = 0$, $\hat{a}(0) = 0$ and tunable parameters $\mu_a \in \mathbb{R}_{>0}$ that determine the rate of convergence. The above adaption laws makes it easy to enforce, simply by a clipping (e.g., (3.11)), the positivity constraints $\hat{a} \geq 0$.

4.6 Digital implementation of the proposed method

In this section, we briefly illustrate the digital implementation of the introduced algorithms. Consider a measured signal $v(k)$, $k = 1, 2, \cdots$ sampled by T_s, we firstly make a choice of the tunable parameters ω_{c1}, ω_{c2}, K_{c1}, K_{c2}, μ. It is worth noting that both methods rely on the filtered signals obtained by the parallel pre-filtering system (4.5), which in the discrete-time domain is represented by

$$x(k) = x(k-1) + T_s \left(A_p x(k-1) + B_p v(k) \right), \tag{4.51}$$

where $x(t) = [x_1(t)\ x_2(t)]^\top$, $\hat{x}_1(t) = [\hat{x}_{1,1}(t)\ \cdots\ \hat{x}_{1,2}(t)]^\top$, $\hat{x}_2(t) = [\hat{x}_{2,1}(t)\ \cdots\ \hat{x}_{2,2}(t)]^\top$. Thanks to (4.51), the auxiliary signal $\hat{z}(k)$ for the method 1 (see Section 4.3.3) is obtained by

$$\hat{z}(k) = \Phi_3 \left(v(k)\ \hat{x}_1(k)^\top\ \hat{x}_2(k)^\top \right)^\top,$$

with

$$\Phi_3 = \begin{bmatrix} 0 & CA_1 & 0 \\ 0 & 0 & CA_2 \\ CA_1^2 B_1 & CA_1^3 & 0 \\ CA_2^2 B_2 & 0 & CA_2^3 \end{bmatrix}.$$

On the other side, for method 2 (see Section 4.4), we get

$$\hat{z}(k) = \Phi_2 \left(v(k)\ \hat{x}_1(k)^\top\ \hat{x}_2(k)^\top \right)^\top,$$

with

$$\Phi_2 = \begin{bmatrix} 0 & C & -C \\ C(A_1B_1 - A_2B_2) & CA_1^2 & -CA_2^2 \end{bmatrix}.$$

The frequency adaptation laws for both methods have the same representation, which in the discrete-time domain writes:

$$\hat{\Omega}(k) = \hat{\Omega}(k-1) - T_s\mu\tilde{z}_1(k)\left(\hat{\Omega}(k-1)\tilde{z}_1(k) + \tilde{z}_2(k)\right),$$

$$\hat{\omega}(k) = \max\{0,\ \hat{\Omega}(k)\}$$

where $z_1(k)$, $z_2(k)$ for method 1 are vectors, however for method 2 they are scalars.

Finally, by using $\tilde{x}(t)$ and $\hat{\omega}(k)$, it is straightforward to estimate the amplitude and the phase by the discretized equations of (4.49), (4.50), (4.47b) and (4.48b).

4.7 Simulation and Experimental Results

4.7.1 Simulation Results

In this subsection, the behaviour of the proposed methods are evaluated and compared with three recently proposed AFP techniques [58], [28] and [90]. All the algorithms are discretized by Forward-Euler discretization method with fixed sampling period 1×10^{-3}s. The algorithms considered in the comparative analysis have been tuned to have a similar response time when fed by a unitary-amplitude sinusoid of frequency $1/(2\pi)$, when initialized with zero initial conditions (indeed, the initial transient of the frequency-estimates shown in Fig.4.3 put in evidence that the considered methods share the same rise-time). The evaluations are conducted in the case of a biased sinusoidal signal, undergoing both frequency and offset steps-wise variations.

Let us consider a sinusoidal measurement corrupted by a bounded disturbance:

$$v(t) = b(t) + 3\sin(\omega(t)t + \pi/4) + d(t), \tag{4.52}$$

with

$$\omega(t) = \begin{cases} 4, & 0 \le t < 10 \\ 8, & 10 \le t < 35 \\ 2 & 35 \le t < 50 \end{cases}, \quad b(t) = \begin{cases} 1, & 0 \le t < 20 \\ 3 & 20 \le t < 50 \end{cases}.$$

$d(t)$ is a bounded disturbance with uniform distribution in the interval [-0.5, 0.5]. All the methods are initialized with the same initial condition $\hat{\omega}(0) = 1$. Method [58] is tuned with: $\mu_0 = 1.5$, $\mu_1 = 3$, $\mu_2 = 3$, $\mu_3 = 0.8$, while method [28] is tuned with: $K_s = 1$, $\lambda =$

1, $\omega_s = 4$, $Q_0 = (1/\lambda)I$. For method [90], we set $\gamma_0 = \lambda_0^2 = 8$, $\gamma_1 = 6$, $k = 0.18$. Finally, the tuning parameters of the proposed methods are selected by: $\omega_{c_1} = 6$, $\omega_{c_2} = 3$, $K_{c_1} = 0.6$, $K_{c_2} = 0.8$, $\mu = 1$ and $\omega_{c_1} = 9$, $\omega_{c_2} = 2$, $K_{c_1} = K_{c_2} = 0.6$, $\mu = 4$ respectively (heuristic tuning guidelines of the pre-filtering parameters ω_{c_k}, K_{c_k} and the adaptive gain μ can be referred to the Figure 2.4 and 2.5). The frequency-estimation trends obtained by the simulations are depicted in Fig.4.3.

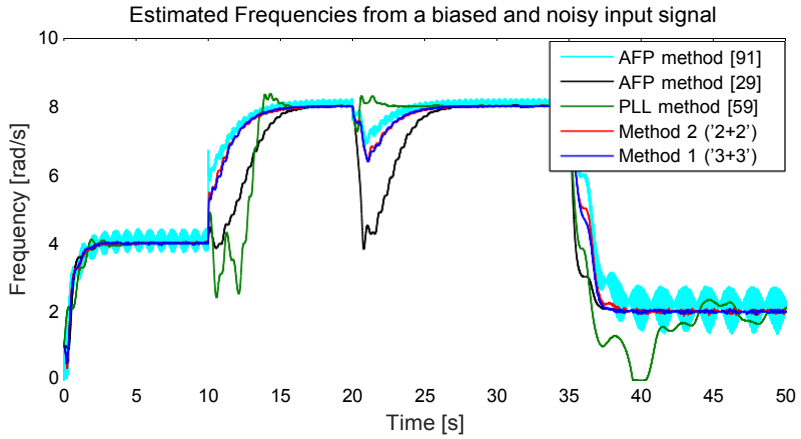

Fig. 4.3 Time-behavior of the estimated frequency by using the proposed AFP methods (blue and red line respectively) compared with the time behaviors of the estimated frequency by the AFP methods [28] (black line), [58] (green line) and [90] (cyan line).

All the methods are capable to track the initial frequency satisfactorily, with similar response time (the constraint for choosing parameters). The PLL method [58] exhibits a good noise immunity in stationary conditions, but is quite slow to track frequency variations, specially in the low-frequency range. The AFP method [28] is the more sensitive to the bias change, however, it performs the best noise attenuation at the cost of slow reaction to a significant frequency change. The proposed methods can handle considerable frequency variations with relatively fast response time and acceptable robustness against noise. Compared to the single pre-filter-based method [90] (note that the switching dynamic consists in this algorithm is switched off in order to consider the time-varying frequency), in this example the presented methods equipped with parallel pre-filters show certain improvements in terms of noise immunity without deteriorating the transient performance.

The amplitude estimates of each method are reported in Fig.4.4 ([90] is excluded, since it only deals with frequency estimation). Among the three recursive algorithms, the PLL method [58] is the simplest in terms of dynamic order, but it is prone to be affected by the parametric perturbations. On the other hand, the proposed methods estimate the amplitude in a relatively smoother manner, in particular, method 1 (see Section 4.3) provides the best noise immunity in the stationary phases.

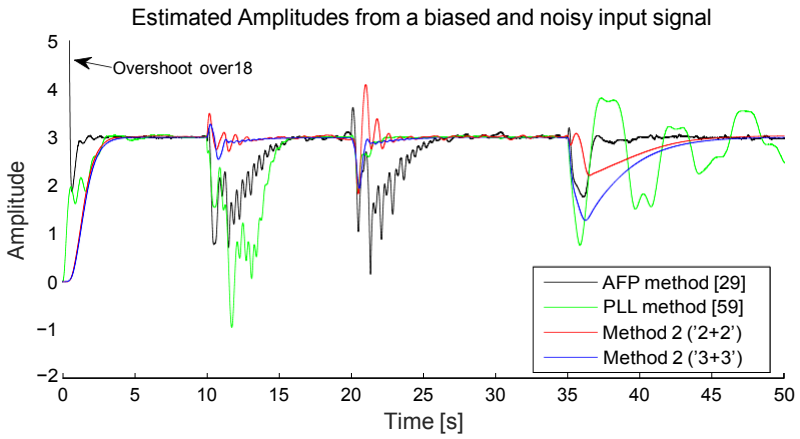

Fig. 4.4 Time-behavior of the estimated amplitude by using the proposed AFP methods (blue and red line respectively) compared with the time behaviors of the estimated frequency by the AFP methods [28] (black line) and [58] (green line).

Thanks to the availability of the phase estimation, the sinusoidal signal reconstructed by the proposed method is depicted in Fig.4.5, in which the unbiased signal is recovered successfully in a smooth manner even the input is affected by a bounded uncertainty.

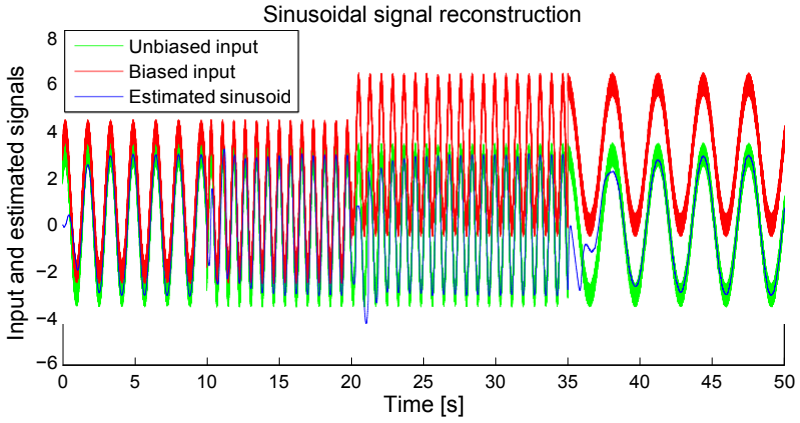

Fig. 4.5 Estimated sinusoidal signal by the proposed AFP method 2 (blue line). To appreciate the time-behavior of the estimated signal, the biased noisy input is depicted (red line), as well as the same signal without the time-varying bias term (green line).

In order to complete the comparison of the proposed methods, in Fig.4.6, the time-behaviors of the estimated frequency are shown in another case in which higher level of noise affects the input. It can be observed that method 1 with an order 3 + 3 configuration (see Section 4.3) offers slightly better steady state performance at the expense of increased complexity.

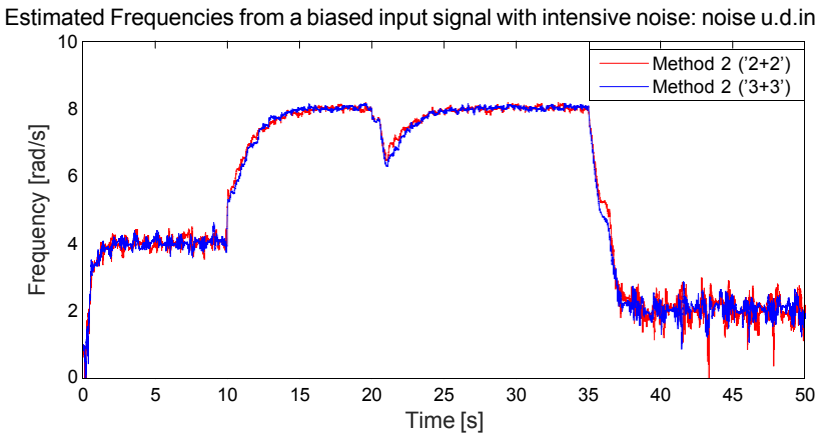

Fig. 4.6 Comparison of the behaviors of the proposed AFP method 1 (blue line) and 2 (red line) in the presence of a bounded perturbation within the interval $[-5, 5]$.

4.7.2 Experimental Results

In order to evaluate the robustness of the proposed algorithm in practice, we have deployed the method 2 introduced in Section 4.4 on a dSpace system. In order to confirm the simulation results on an experimental test-rig, the two prior methods [58] and [28] have been implemented in the same system, with the task of estimating the frequency, the phase and amplitude of an electrical voltage signal generated by a programmable power supply able to reproduce the perturbations typically experienced in micro-grids. Note that all the methodologies are discretized by Euler method with sampling rate set to 60kHz. Fig. 4.7 shows some periods of the noisy sinusoidal signal generated by the programmable power supply. The large voltage ripples superimposed on the measured sinusoid correspond to the perturbations that may arise from the switching actions of grid-connected power electronic devices. On the other side, voltage-injected spikes are used to reproduce the large voltage transients due to the sudden change of electric loads or to severe radio frequency interference such as those caused by lightning.

In the first test, the frequency of the supply is varied according to the following pattern: 50-48-50-52-48Hz (which is likely to occur on a small-scale power system such as a micro-grid). In particular, the frequency changes are composed of multiple steps in order to imitate the inertia of electro-mechanical generators. The tuning gains of the methods [58] and [28] are set to the following values: $\mu_0 = 15$, $\mu_1 = \mu_2 = 300$, $\mu_3 = 0.07$ and $K_s = 1$, $\lambda = 10$, $\omega_s = 2\pi 50$, $Q_0 = (1/\lambda)\mathbf{I}$, while the parameters of the proposed estimator are: $\omega_{c_1} = 320$, $\omega_{c_2} = 250$, $K_{c_1} = K_{c_2} = 0.6$, $\mu_1 = 50$. The dSpace board computes the frequency estimates in real-time and converts them to analog signals that are collected by an

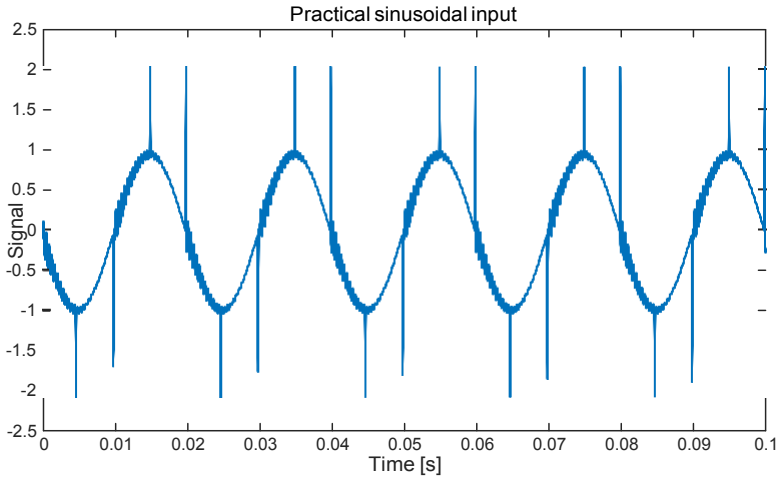

Fig. 4.7 A real-time 50 Hz sinusoidal voltage signal corrupted by ripples reproducing the perturbation due to a typical switching device and 4 large spikes per cycle to reproduce RF interference.

oscilloscope whose plot is given in Fig. 4.8. The estimates show that all the methods can be adjusted to achieve a similar response time to the given frequency step-wise variations.

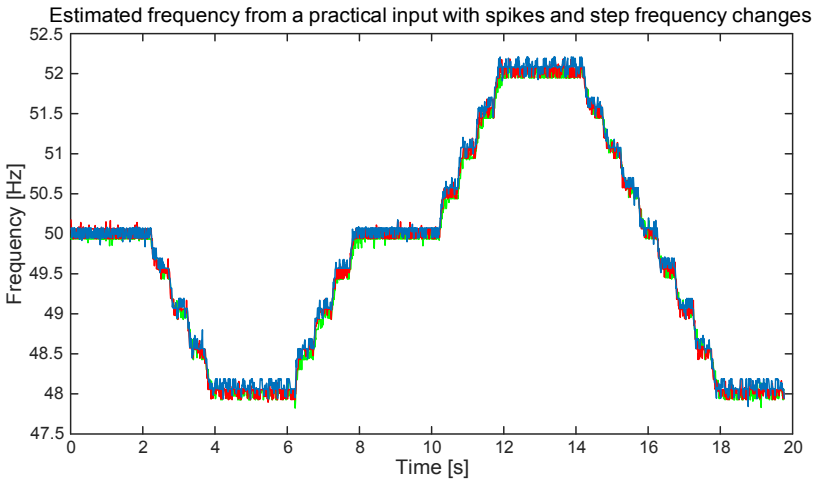

Fig. 4.8 Real-time frequency tracking of a sinusoidal signal with a step-wise changing frequency (50-48-50-52-48 Hz): the time behaviors of the estimated frequency by the AFP methods [28] (greed line), [58] (red line) and the proposed method 2 (blue lines).

For the sake of completeness, with the fixed parameter setting the robustness against bias variations is tested by introducing a measurement offset with step-wise changes (0-0.5-0) over the alternating current voltage signal given in Fig. 4.7 . According to the results shown

in Fig. 4.9, the proposed method shows an enhanced transient behavior with only minor loss on the stationary accuracy compared with the other two approaches.

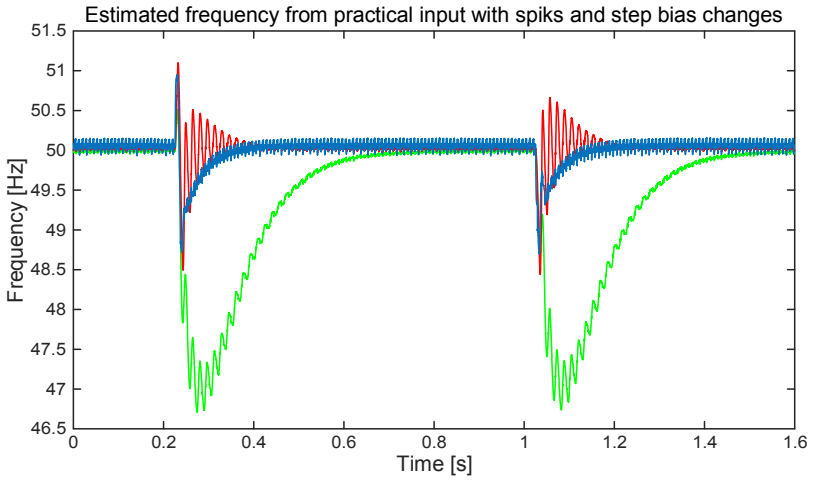

Fig. 4.9 Real-time frequency tracking of a sinusoidal signal with a step-wise changing offset: the time behaviors of the estimated frequency by the AFP methods [28] (greed line), [58] (red line) and the proposed method 2 (blue lines).

4.8 Concluding Remarks

This chapter deals with an AFP scheme based on the parallel pre-filtering paradigm with the aim of reducing the dynamic order of the adaptive observer approach introduced in Chapter 2. The parallel pre-filtering methodology consists in filtering a noisy-biased sinusoid with a pair of two low-pass filters of a given order, whose inner states are used to estimate the frequency, the phase and the amplitude of the original sinusoid. The robust stability properties of the presented methods with respect to additive measurement perturbations are characterized by an Input-to-State stability analysis, which also provides basic tuning rules for the parameters of the adaptation laws. Numerical simulations and practical experiments on a laboratory test-rig confirm that the proposed method is robust with respect to additive measurement noise and is able to track large and sudden frequency variations. Finally, the ease of implementation of the pre-filter-based method makes it a valid alternative to existing AFP methodologies for the task of electrical network monitoring and synchronization with mains.

Part II

NON-ASYMPTOTIC ESTIMATORS

Chapter 5

FINITE-TIME PARAMETRIC ESTIMATION OF A SINUSOIDAL SIGNAL

5.1 Introduction

In the previous chapters, we elaborated a few types of AFP techniques which ensure asymptotic convergence of the estimates. The purpose of this chapter is to present a method that can accomplish finite-time parameter estimation of a single sinusoidal signal possibly corrupted by an offset.

Let us consider

$$y(t) = b + a\sin(\phi(t)), \quad \dot{\phi}(t) = \omega, \quad \phi(0) = \phi_0 \tag{5.1}$$

where $b \in \mathrm{R}_{>0}$, $a \in \mathrm{R}_{>0}$, ϕ and $\omega \in \mathrm{R}_{>0}$ are the unknown offset, amplitude, phase and frequency, respectively. Our objective consists in providing the AFP estimates of the sinusoidal signal (5.1) in a deadbeat manner. After that, we also show that the estimation error is ISS with respect to the measurement noise, provided a noisy signal, i.e., $v(t) = y(t) + d(t)$, in which $d(t)$ is a bounded disturbance.

Substantial numbers of tools are currently available in the literature for estimating the characteristics of a biased sinusoidal signal (referred to Sec. 1.2 for more details). However, only a few of the algorithms are capable to achieve the convergence of the estimates to the true values within an arbitrarily small *finite time*, which is a very desirable feature in several application contexts like, for example, micro-grids power systems that are affected by severe frequency fluctuations due to low inertia of generators, and vibration suppression in high-value mechanical systems. Typically, algebraic derivatives (see e.g. [66, 106]) and modulating functions [33] represent two main tools for constructing a non-asymptotic

estimator. Nevertheless, a comprehensive investigation concerning the stability properties in a noisy environment is still missing so far.

In this chapter, we propose a robust parametric finite-time estimation methodology for biased sinusoidal signals by employing a class of kernel based-linear integral operators. The use of such integral operators allows to annihilate the effects of the unknown initial conditions, which produce an asymptotic behavior in terms of estimation error convergence. In the spirit of preliminary work on the sole frequency estimation problem (see [85]), this chapter deals with a finite-time convergent estimation scheme in which the frequency, amplitude and phase of a sinusoidal signal are estimated in finite-time. Volterra integral operators [83] with suitably designed kernels are exploited and, in contrast with existing works, the behavior of the estimator in the presence of a bounded additive measurement disturbance is rigorously characterized by ISS arguments as well. To the best of the author's knowledge, this is the first finite-time convergent sinusoidal estimator the behavior of which is analyzed also in the presence of unstructured and bounded measurement perturbations.

This chapter is organized as follows: Section 5.2 introduces several useful notations and basic definitions regarding a typical linear integral operator. In Section 5.3, the Volterra integral operators are characterized whereas in Section 5.4, the finite-time estimation technique is illustrated. In Section 5.5, the stability and robustness properties of the proposed estimation tool are dealt with. Section 5.6 gives an example of the discretized algorithm for digital implementation. Extensive simulation results are provided in Section 5.7 and Section 5.8 draws some concluding remarks.

5.2 Preliminaries

In the following, for the reader's convenience, some basic concepts of linear integral operators' algebra (see [14] and the references therein) are recalled. More specifically, we use transformations acting on the Hilbert space $\mathsf{L}^2_{loc}(\mathsf{R}_{\geq 0})$ of locally square-integrable functions with domain $\mathsf{R}_{\geq 0}$ and range R (*i.e.*, $u(\cdot) \in \mathsf{L}_{loc}(\mathsf{R}_{\geq 0}) \Leftrightarrow (u(\cdot) : \mathsf{R}_{\geq 0} \to \mathsf{R}) \wedge \left(\int_B |u(t)|^2\, dt < \infty,\ \forall \text{ compact } B \subset \mathsf{R}_{\geq 0}\right)$. Given a function $u \in \mathsf{L}_{loc}(\mathsf{R}_{\geq 0})$, its image through the Volterra (linear, integral) operator V_K induced by a Hilbert-Schmidt HS *Kernel Function* $K(\cdot, \cdot) : \mathsf{R} \times \mathsf{R} \to \mathsf{R}$ is usually denoted by $[\mathsf{V}_K u](\cdot)$, and is defined by the inner product:

$$[\mathsf{V}_K u](t) := \int_0^t K(t, \tau) u(\tau) d\tau, \quad t \in \mathsf{R}_{\geq 0}. \tag{5.2}$$

Any explicit function of time $u(t) : t \to u(t) \in \mathsf{R}$, such that $u(\cdot) \in \mathsf{L}^2_{loc}(\mathsf{R}_{\geq 0})$ will be addressed in this paper as a signal. Then, given two scalars $a, b \in \mathsf{R}_{\geq 0}$, with $a < b$, let us

denote by $u_{[a,b]}(\cdot)$ and $u_{(a,b]}(\cdot)$ the restriction of a signal $u(\cdot)$ to the closed interval $[a, b]$ and to the left open interval $(a, b]$, respectively. Moreover, let $u(t) \in \mathsf{R}$, $\forall t \geq 0$ be an i-times differentiable signal, we denote by $u^{(1)}$ the i-th order time-derivative signal. The operator $\text{sign}(\cdot)$ used in this chapter is defined by

$$\text{sign}(u) \; /'. \; \begin{cases} 1 & \text{if } x > 0\,, \\ -1 & \text{if } x < 0\,, \\ \in [-1, 1] & \text{if } x = 0\,. \end{cases} \tag{5.3}$$

Given a kernel function $K(\cdot\,,\cdot)$ in two variables, its i-th order weak derivative with respect to the second argument will be denoted as $K^{(i)}$, $i \in \mathsf{Z}_{\geq 0}$. For obvious practical implementability reasons, it is convenient to devise a differential form for the operators. By applying the Leibniz differentiation rule to the Volterra integral, the transformed signal $[\mathsf{V}_k x](t)$, for $t \geq 0$, can be obtained as the output of a dynamic system described by the following scalar integro-differential equation:

$$\begin{cases} \dot{\xi}(t) = K(t, t)x(t) + \displaystyle\int_0^t \frac{\partial}{\partial t} K(t, \tau) \quad x(\tau)d\tau, \; t \in \mathsf{R}_{\geq 0} \\ [\mathsf{V}_K x]\,(t) = \xi(t) \end{cases}, \tag{5.4}$$

with $\xi(0) = \xi_0 = \displaystyle\int_0^0 K(0, \tau)x(\tau)d\tau$. Now, we introduce some useful results dealing with the application of Volterra operators to the derivatives of a signal.

Lemma 5.2.1 (Volterra image of a signal's derivative) *For a given $i \geq 0$, consider a signal $u(\cdot) \in \mathsf{L}^2(\mathsf{R}_{\geq 0})$ that admits a i-th weak derivative in $\mathsf{R}_{\geq 0}$ and a kernel function $K(\cdot\,,\cdot) \in \mathsf{HS}$ that admits the i-th derivative (in the conventional sense) with respect to the second argument, $\forall t \in \mathsf{R}_{\geq 0}$. It holds that:*

$$\begin{aligned} \left[\mathsf{V}_K u^{(i)}\right](t) = & \sum_{j=0}^{i-1} (-1)^{i-j-1} u^{(j)}(t) K^{(i-j-1)}(t, t) \\ & + \sum_{j=0}^{i-1} (-1)^{i-j} u^{(j)}(0) K^{(i-j-1)}(t, 0) + (-1)^i \left[\mathsf{V}_{K^{(i)}} u\right](t), \quad \forall t \in \mathsf{R}_{\geq 0}, \end{aligned} \tag{5.5}$$

that is, $\left[\mathsf{V}_K u^{(i)}\right](\cdot)$ is non-anticipative with respect to $u(\cdot)$ and its first (i-1)-th derivatives $u^{(1)}(\cdot), \ldots, u^{(i-1)}(\cdot)$. D

Proof: Integrating by parts, we have:

$$\left|\mathcal{V}_K u^{(i)}\right|(t) = \int_0^t K(t,\tau)u^{(i)}(\tau)d\tau$$
$$= u^{(i-1)}(t)K(t,t) - u^{(i-1)}(0)K(t,0) - \int_0^t K^{(1)}(t,\tau)u^{(i-1)}(\tau)d\tau\,. \quad (5.6)$$

The integral operator on the right-hand side of (5.6) can be further split by parts:

$$-\int_0^t K^{(1)}(t,\tau)u^{(i-1)}(\tau)d\tau$$
$$= -u^{(i-2)}(t)K^{(1)}(t,t) + u^{(i-2)}(0)K^{(1)}(t,0) + \int_0^t K^{(2)}(t,\tau)u^{(i-2)}(\tau)d\tau\,.$$

Proceeding by induction we obtain

$$\int_0^t K(t,\tau)u^{(i)}(\tau)d\tau = \sum_{j=1}^{i}(-1)^{j+1}u^{(i-j)}(t)K^{(j-1)}(t,t) +$$
$$\sum_{j=1}^{i}(-1)^{j}u^{(i-j)}(0)K^{(j-1)}(t,0) + (-1)^{i}\int_0^t K^{(i)}(t,\tau)u(\tau)d\tau, \quad (5.7)$$

that is, the function obtained by applying the Volterra operator to the i-th derivative is non-anticipative with respect to lower-order derivatives. The identity (5.5) can be verified by rearranging indexing of the summation in (5.7), thus completing the proof. •

Lemma 5.2.1 allows to identify a class of kernels such that for each derivative $u^{(i)}$, $i \in \{0, \cdots, n-1\}$, the image signal $\left|\mathcal{V}_k u^{(i)}\right|(t)$, $t > 0$ is independent from the initial states $u(0)$, $u^{(1)}(0)$, $\cdots$, $u^{(i-1)}(0)$, according to the following definition.

Definition 5.2.1 (i-th order non-asymptotic kernel) *Consider a function $K(\cdot,\cdot)$ satisfying the assumptions of Lemma 5.2.1; if, in addition, for a given $i \geq 1$, the kernel verifies the condition*

$$K^{(j)}(t,0) = 0\,,\ \forall t \in \mathbb{R}_{\geq 0},\quad \forall j \in \{0,\ldots,i-1\}, \quad (5.8)$$

then, it is called an i-th order non-asymptotic kernel. D

Assuming that $K(\cdot,\cdot)$ is an n-th order non-asymptotic kernel function, (5.7) can be further simplified by removing the initial condition-dependent term on the right hand side, it

holds that:

$$\mathsf{I}\mathsf{V}_K\, u^{(i)}\mathsf{I}\,(t) = \sum_{j=0}^{i-1} (-1)^{i-1-j} u^{(j)}(t) K^{(i-j-1)}(t,t) + (-1)^i [\mathsf{V}_{K^{(i)}} u](t),\ i \in \{1, \ldots, n-1\}. \tag{5.9}$$

Considering the case $i = 1$, by some trivial manipulation of (5.9) we have that

$$\mathsf{I}\mathsf{V}_K u^{(1)}\mathsf{I}\,(t) = u(t)K(t,t) - [\mathsf{V}_{K^{(1)}} u]\,(t)\,. \tag{5.10}$$

Moreover, changing the kernel K with $K^{(j)}$ and and performing the substitution of $u^{(i)}$ for u, for any $j \in \{1, \ldots, n-1\}$ we have that also the following integral equation holds

$$\mathsf{I}\mathsf{V}_{K^{(j)}} u^{(i+1)}\mathsf{I}\,(t) = u^{(i)}(t)K^{(j)}(t,t) - \mathsf{I}\mathsf{V}_{K^{(j+1)}} u^{(i)}\mathsf{I}\,(t)\,. \tag{5.11}$$

5.3 Bivariate Feedthrough Non-asymptotic Kernels

At this stage, we introduce a typical non-asymptotic kernel for the sake of further discussion.

Definition 5.3.1 (i-th Order BF-NK) *[87] A kernel $K(\cdot\,,\cdot) \in \mathsf{HS}$ that satisfies the assumptions given in Lemma 5.2.1 and that, for a given $i \geq 1$, also verifies the conditions*

$$K^{(j)}(t,t) = 0,\ \forall t = 0,\ \forall j \in \{0, \ldots, i-1\}, \tag{5.12}$$

is called i-th Order Bivariate Feedthrough Non-asymptotic (BF-NK) kernel.

Here, we introduce a BF-NK that fulfils (5.12), expressed in the following lines:

$$F(t,\tau) = e^{-\beta(t-\tau)}(1 - e^{-\bar{\beta}\tau})^n, \tag{5.13}$$

which is parametrized by the constants $\beta \in \mathsf{R}_{>0}$ and $\bar{\beta}$. In view of (5.13), all the non-asymptotic conditions up to the n-th order are met by the factor $\left(1 - e^{-\bar{\beta}\tau}\right)^n$ regardless of the choice of β and $\bar{\beta}$. For any $i \in \{0, 1, \cdots, n\}$, the τ derived kernel functions read (an exmaple of BF-NK is depicted in Fig. 5.1 showing the behavior of the kernel and its derivatives):

$$F^{(i)}(t,\tau) = e^{-\beta t} \frac{d^i}{d\tau^i} e^{\beta\tau}(1 - e^{-\bar{\beta}\tau})^n\,. \tag{5.14}$$

Specializing (5.4) to the kernel (5.14) with respect to the sinusoidal signal $y(t)$, we have that the transformed signal $[\mathsf{V}_{F^{(i)}} y]\,(t)$, for any $i \in \{1, 2, \cdots, n\}$ can be obtained as the output of

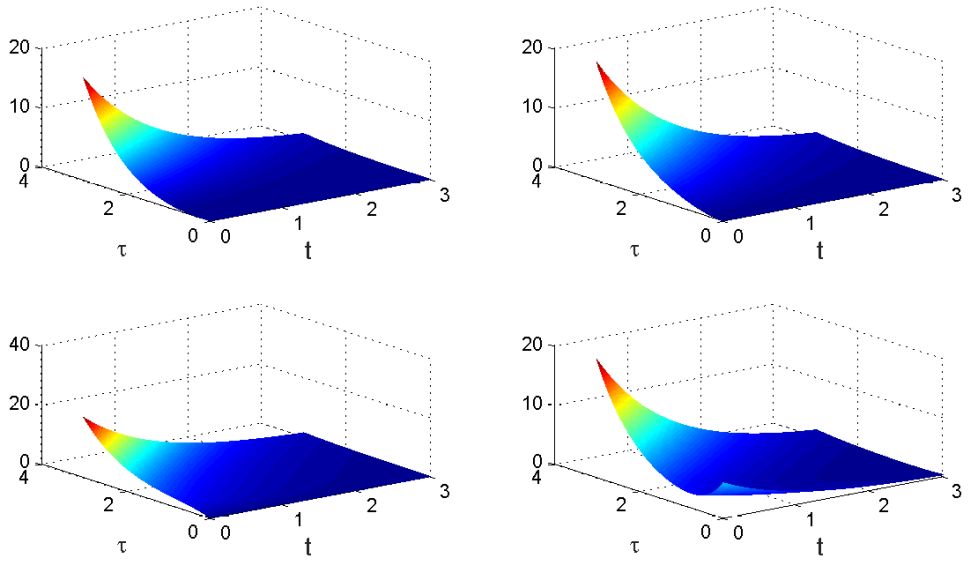

Fig. 5.1 Plots of the Bivariate Feedthrough Non-asymptotic Kernels and its derivatives (see (5.14)), for $\beta = \bar{\beta} = 1$ and $n = 3$.

a linear time-varying scalar system. Letting $\xi(t) = [\mathsf{V}_{F^{(i)}} y](t)$, we have that

$$\begin{aligned} \dot{\xi}(t) &= F^{(i)}(t,t)y(t) + \int_0^t \frac{\partial}{\partial t} F^{(i)}(t,\tau)\; y(\tau)d\tau \\ &= F^{(i)}(t,t)y(t) - \beta\xi(t),\ t \in \mathsf{R}_{\geq 0} \end{aligned} \tag{5.15}$$

with $\xi(0) = \xi_0 = 0$. Being $F^{(i)}(t,t)$ bounded, and β strictly positive, it holds that the scalar dynamical system realization of the Volterra operators induced by the proposed kernels is BIBO stable with respect to $y(t)$.

5.4 Finite-time AFP estimation in the presence of bias

It is worth noting that the biased sinusoidal signal $y(t)$ given in (5.1) is generated by the undamped linear oscillator:

$$y^{(3)}(t) = -\Omega y^{(1)}(t), \tag{5.16}$$

where $\Omega = \omega^2$. Taking the Volterra linear integral operator on both sides of (5.16), we obtain

$$\left|\mathsf{V}_K y^{(3)}\right|(t) = -\Omega \left|\mathsf{V}_K y^{(1)}\right|(t)\,. \tag{5.17}$$

In view of (5.11), we can expand both sides of (5.17) by

$$\begin{aligned}\mathsf{V}_{Ky^{(3)}}(t) &= y^{(2)}(t)K(t,t) - \mathsf{V}_{K^{(1)}y^{(2)}}(t)\\ &= \mathsf{V}_{K^{(2)}y^{(1)}}(t) - y^{(1)}(t)K^{(1)}(t,t) + y^{(2)}(t)K(t,t)\\ &= y(t)K^{(2)}(t,t) - [\mathsf{V}_{K^{(3)}}y](t) - y^{(1)}(t)K^{(1)}(t,t) + y^{(2)}(t)K(t,t)\end{aligned}$$

and

$$\mathsf{V}_{Ky^{(1)}}(t) = y(t)K(t,t) - [\mathsf{V}_{K^{(1)}}y](t).$$

After some algebra, we get

$$\begin{aligned}[\mathsf{V}_{K^{(3)}}y](t) - K^{(2)}(t,t)y(t) + K^{(1)}(t,t)y^{(1)}(t)\\ - K(t,t)y^{(2)}(t) + \Omega([\mathsf{V}_{K^{(1)}}y](t) - K(t,t)y(t)) = 0. \quad (5.18)\end{aligned}$$

Consider three BF-NKs (5.13) denoted by F_1, F_2 and F_3 with $n = 3$, that is

$$F_h(t,\tau) = e^{-\beta_h(t-\tau)}(1 - e^{-\bar{\beta}_h\tau})^3,$$

where $\beta_h \in \mathsf{R}_{>0}$, $\forall h = \{1, 2, 3\}$ and $\bar{\beta}_h$ are set by the designers such that

$$\beta_i \neq \beta_j, \quad \text{for } i \neq j \quad (5.19)$$

while $\bar{\beta}_i$ and $\bar{\beta}_j$ may possibly coincide. Then let us rewrite (5.18) with respect to F_1, F_2 and F_3, obtaining the following three equations:

$$\begin{aligned}&\mathsf{V}_{F_1^{(3)}y}(t) - F_1^{(2)}(t,t)y(t) + F_1^{(1)}(t,t)y^{(1)}(t) - F_1(t,t)y^{(2)}(t)\\ &\quad + \Omega\left(\mathsf{V}_{F_1^{(1)}y}(t) - F_1(t,t)y(t)\right) = 0, \quad (5.20a)\\ &\mathsf{V}_{F_2^{(3)}y}(t) - F_2^{(2)}(t,t)y(t) + F_2^{(1)}(t,t)y^{(1)}(t) - F_2(t,t)y^{(2)}(t)\\ &\quad + \Omega\left(\mathsf{V}_{F_2^{(1)}y}(t) - F_2(t,t)y(t)\right) = 0, \quad (5.20b)\\ &\mathsf{V}_{F_3^{(3)}y}(t) - F_3^{(2)}(t,t)y(t) + F_3^{(1)}(t,t)y^{(1)}(t) - F_3(t,t)y^{(2)}(t)\\ &\quad + \Omega\left(\mathsf{V}_{F_3^{(1)}y}(t) - F_3(t,t)y(t)\right) = 0. \quad (5.20c)\end{aligned}$$

Now, it is convenient to introduce the following auxiliary signals that are kernel-dependent (and thus *a-priori* known functions of time) and are computable by processing the measure-

ment by the Volterra operators:

$$\begin{aligned} \kappa_{a,h}(t) &:= \mathrm{V}_{F_h^{(3)}} y(t) - F_h^{(2)}(t,t)y(t), \\ \kappa_{b,h}(t) &:= F_h^{(1)}(t,t), \\ \kappa_{c,h}(t) &:= -F_h(t,t), \\ \kappa_{d,h}(t) &:= \mathrm{V}_{F_h^{(1)}} y(t) - F_h(t,t)y(t), \ \forall h = 1,2,3. \end{aligned} \tag{5.21}$$

In the following, we show that the signals $\mathrm{V}_{F_h^{(3)}} y(t)$ and $\mathrm{V}_{F_h^{(1)}} y(t)$ appearing in $\kappa_{a,h}(t)$ and $\kappa_{d,h}(t)$, respectively, can be obtained as the output of a linear time-varying system. To this end, let us define the internal state vector

$$\xi(t) := \left[\xi_{\beta_1}(t)^\top \ \xi_{\beta_2}(t)^\top \ \xi_{\beta_3}(t)^\top\right]^\top \in \mathrm{R}^6$$

with $\xi_{\beta h}(t) \in \mathrm{R}^3, \ \forall h \in \{1,2,3\}$ in turn defined as

$$\xi_{\beta_h}(t) := \left[\mathrm{V}_{F_h^{(1)}} y(t) \ \ \mathrm{V}_{F_h^{(3)}} y(t)\right]^\top.$$

In view of (5.15), the time evolution of the internal state vector $\xi(t)$ of (5.15) is described by

$$\dot{\xi}(t) = G_\xi \xi(t) + E_\xi(t) y(t), \tag{5.22}$$

with $\xi(0) = 0$ and where G_ξ is a diagonal, time invariant and Hurwitz matrix. More specifically, $G_\xi = \mathrm{blockdiag}[G_{\xi_h}, \ h = 1,2,3] \in \mathrm{R}^{6\times 6}$, with $G_{\xi_h} = \mathrm{diag}(-\beta_h) \in \mathrm{R}^{2\times 2}$, while the time-varying input matrices $E_\xi(t) \in \mathrm{R}^6$ can be expressed as

$$E_\xi(t) = \left[E_{\xi_1}(t)^\top \ \ E_{\xi_2}(t)^\top \ \ E_{\xi_3}(t)^\top\right]^\top,$$

where $E_{\xi_h}(t) \in \mathrm{R}^2$ are given by: $E_{\xi_h}(t) = \left[F_h^{(1)}(t,t) \ \ F_h^{(3)}(t,t)\right]^\top$. Finally, $\kappa_{a,h}(t)$ and $\kappa_{d,h}(t)$ can be expressed in terms of the scalar elements of $\xi(t) = [\xi_1(t), \ \xi_2(t), \ \cdots, \ \xi_6(t)]^\top \in \mathrm{R}^6$:

$$\begin{aligned} \kappa_{a,h}(t) &:= \xi_{2h}(t) - F_h^{(2)}(t,t)y(t) \\ \kappa_{d,h}(t) &:= \xi_{2h-1}(t) - F_h(t,t)y(t), \ \forall h = 1,2,3. \end{aligned} \tag{5.23}$$

Substituting (5.21) into (5.20a)-(5.20c), after some algebra we can eliminate the variables, $y^{(1)}(t)$ and $y^{(2)}(t)$ from the system, obtaining equation (5.24) that has Ω as the only unknown

(for brevity, we have dropped the dependence of all variables on t):

$$\begin{aligned}\kappa_{a,3}\kappa_{b,2}\kappa_{c,1}^2 - \kappa_{a,3}\kappa_{b,1}\kappa_{c,1}\kappa_{c,2} + \kappa_{a,1}\kappa_{b,3}\kappa_{c,1}\kappa_{c,2} - \kappa_{a,2}\kappa_{b,3}\kappa_{c,1}^2 + \kappa_{a,2}\kappa_{b,1}\kappa_{c,1}\kappa_{c,3} \\ - \kappa_{a,1}\kappa_{b,2}\kappa_{c,1}\kappa_{c,3} + \Omega^2(\kappa_{b,3}\kappa_{c,1}\kappa_{c,2}\kappa_{d,1} - \kappa_{b,3}\kappa_{c,1}^2\kappa_{d,2} + \kappa_{b,1}\kappa_{c,1}\kappa_{c,3}\kappa_{d,2} \\ - \kappa_{b,2}\kappa_{c,1}\kappa_{c,3}\kappa_{d,1} + \kappa_{b,2}\kappa_{c,1}^2\kappa_{d,3} - \kappa_{b,1}\kappa_{c,1}\kappa_{c,2}\kappa_{d,3}) = 0\,. \quad (5.24)\end{aligned}$$

Let us rearrange the left-hand-side of (5.24) by extracting the variables indexed by a and d respectively, thereby getting

$$\begin{aligned}\kappa_{a,1}(\kappa_{b,3}\kappa_{c,1}\kappa_{c,2} - \kappa_{b,2}\kappa_{c,1}\kappa_{c,3}) + \kappa_{a,2}(\kappa_{b,1}\kappa_{c,1}\kappa_{c,3} - \kappa_{b,3}\kappa_{c,1}^2) + \kappa_{a,3}(\kappa_{b,2}\kappa_{c,1}^2 - \kappa_{b,1}\kappa_{c,1}\kappa_{c,2}) \\ + \Omega^2(\kappa_{d,1}(\kappa_{b,3}\kappa_{c,1}\kappa_{c,2} - \kappa_{b,2}\kappa_{c,1}\kappa_{c,3}) + \kappa_{d,2}(\kappa_{b,1}\kappa_{c,1}\kappa_{c,3} - \kappa_{b,3}\kappa_{c,1}^2) \\ + \kappa_{d,3}(\kappa_{b,2}\kappa_{c,1}^2 - \kappa_{b,1}\kappa_{c,1}\kappa_{c,2})) = 0\,,\end{aligned}$$

which, in turn, can be rearranged in vector form as follows:

$$\kappa_a^\top(t)\mathsf{F}(t,t) = -\Omega\kappa_d^\top(t)\mathsf{F}(t,t)\,, \quad (5.25)$$

with $\kappa_a(t) = [\kappa_{a,1}\ \kappa_{a,2}\ \kappa_{a,3}]^\top$, $\kappa_d(t) = [\kappa_{d,1}\ \kappa_{d,2}\ \kappa_{d,3}]^\top$ and

$$\mathsf{F}(t,t) = \begin{bmatrix} \mathsf{F}_1(t,t) \\ \mathsf{F}_2(t,t) \\ \mathsf{F}_3(t,t) \end{bmatrix} - \begin{bmatrix} \kappa_{b,3}\kappa_{c,1}\kappa_{c,2} - \kappa_{b,2}\kappa_{c,1}\kappa_{c,3} \\ \kappa_{b,1}\kappa_{c,1}\kappa_{c,3} - \kappa_{b,3}\kappa_{c,1}^2 \\ \kappa_{b,2}\kappa_{c,1}^2 - \kappa_{b,1}\kappa_{c,1}\kappa_{c,2} \end{bmatrix}$$

that depends only on the kernels $F_h(t,t)$, $h = 1, 2, 3$ in correspondence with $\kappa_{b,h}(t)$ and $\kappa_{c,h}(t)$ defined in (5.21). By rewriting (5.25) in a compact form, we finally obtain the following equality:

$$\kappa_1(t) = -\Omega\kappa_2(t) \quad (5.26)$$

with $\kappa_1(t) = \kappa_a^\top(t)\mathsf{F}(t,t)$, $\kappa_2(t) = \kappa_d^\top(t,t)\mathsf{F}(t,t)$. Note that, due to the positivity of the squared frequency, it also holds that:

$$|\kappa_1(t)| = \Omega|\kappa_2(t)|\,. \quad (5.27)$$

Applying to both sides of (5.27) the linear operator V_{K_g}, with kernel $K_g(t,\tau) = e^{-g(t-\tau)}$, $g \in \mathsf{R}_{>0}$, we have that

$$\Omega[\mathsf{V}_{K_g}|\kappa_2(t)|](t) = [\mathsf{V}_{K_g}|\kappa_1(t)|](t)\,. \quad (5.28)$$

Defining $\gamma_1(t) \triangleq [\mathrm{V}_{K_g}|\kappa_1(t)|](t)$ and $\gamma_2(t) \triangleq [\mathrm{V}_{K_g}|\kappa_2(t)|](t)$, it follows that $\gamma_1(t)$ and $\gamma_2(t)$ obey the differential equations:

$$\dot{\gamma}_i(t) = |\kappa_i(t)| - g\gamma_i(t),\ i = 1, 2 \tag{5.29}$$

with $\gamma_i(0) = 0,\ i = 1, 2$. Finally, in view of (5.28) we have that Ω verifies the following constraint for any t:

$$\gamma_1(t) = \gamma_2(t)\Omega.$$

When an estimate $\hat{\Omega}(t)$ of the squared frequency is available, we have that the constraint is not met when $\hat{\Omega} = \Omega$ and a residual term can be introduced:

$$R_\Omega(t) = \gamma_1(t) - \gamma_2(t)\hat{\Omega}(t).$$

The following assumption is needed in order to propose a sliding mode-based adaptation law for frequency estimation. Note that a modified excitation condition is employed instead of the standard PE condition (see, for instance, [96]) to facilitate the upcoming analysis only.

Assumption 5 (Persistency of Excitation) *The signal κ_2 is persistently exciting in R with a level of excitation $\epsilon > 0$, i.e. $\exists t_\epsilon > 0$ such that*

$$\frac{1}{t_\epsilon}\int_{t-t_\epsilon}^{t} |\kappa_2(\tau)|d\tau \geq \epsilon,\ \forall t \geq t_\epsilon. \tag{5.30}$$

Under Assumption 5, thanks to (5.29), $\gamma_2(t)$, driven by $|\kappa_2(t)|$, is ensured to be positive for all $t \geq t_\epsilon$, as follows:

$$\begin{aligned}\gamma_2(t) &= \int_{t-t_\epsilon}^{t} e^{-g(t-\tau)}|\kappa_2(\tau)|d\tau \\ &\geq e^{-gt_\epsilon}\int_{t-t_\epsilon}^{t} |\kappa_2(\tau)|d\tau \\ &\geq t_\epsilon\epsilon e^{-gt_\epsilon}.\end{aligned} \tag{5.31}$$

Let $\delta_\epsilon \triangleq t_\epsilon\epsilon e^{-gt_\epsilon}$, then the following adaptation law on the basis of the second order sliding mode technique, exploiting the residual signal $R(\hat{\Omega}, t)$, is proposed:

$$\begin{aligned}\Omega(t) &= \begin{cases}\gamma_2(t)^{-1}\left(\eta_\Omega(t) + L_1\sqrt{|R_\Omega(t)|}\,\mathrm{sign}(R_\Omega(t)) - \hat{\Omega}(t)\dot{\gamma}_2(t) + \dot{\gamma}_1(t)\right), & \text{if } \gamma_2(t) \geq \delta_\epsilon, \\ 0, \quad \text{otherwise.}\end{cases} \\ \dot{\eta}_\Omega(t) &= L_2\,\mathrm{sign}(R_\Omega(t))\end{aligned} \tag{5.32}$$

with $\hat{\Omega}(0) > 0$ set arbitrarily and $\eta_\Omega(0) = 0$, $L_1, L_2 \in \mathbb{R}_{>0}$ are constant gains set by the designer, such that $L_1 \geq 8L_2$. The operator $\text{sign}(\cdot)$ is defined by (5.3) and the solution of (5.32) is understood in the Filippov sense [36] (this applies to all the sliding mode algorithms introduced in this chapter).

Later, in Section 5.5, we will show that the frequency adaptation algorithm (5.32) is able to identify the squared-frequency in finite-time in a noise-free scenario, while the estimation error is ISS in the presence of measurement noise. Compared to the preliminary work [85] that exploits a first order sliding mode-based adaptation law, the use of a second order sliding mode (see [78] and [114]) allows a significant suppression of the chattering phenomenon, which will be highlighted in the simulation results provided in Section 5.7. Moreover, the time-based switching condition in [85] is enhanced by a more robust switching mechanism that depends on a known signal and the above excitation condition.

Remark 5.4.1 The constraint $L_1 \geq 8L_2$ is imposed in order to facilitate the forthcoming convergence analysis only. In fact L_1 and L_2 can be set as arbitrary positive constants, which is sufficient to ensure the stability of the estimator.

Now, with the aim of estimating the amplitude of the sinusoid in finite time, we exploit a further structural constraint verified by the derivatives of the measured signal. Indeed, thanks to (5.20a)-(5.20c) and introducing the signals

$$\rho_h(\Omega, t) = \kappa_{a,h}(t) + \Omega\kappa_{d,h}(t), \quad h = 1, 2, 3,$$

it follows that the derivatives verify the following identities:

$$\begin{cases} y^{(1)}(t) = \dfrac{F_1(t,t)\rho_2(\Omega,t) - F_2(t,t)\rho_1(\Omega,t)}{F_1^{(1)}(t,t)F_2(t,t) - F_1(t,t)F_2^{(1)}(t,t)}, \\ y^{(2)}(t) = \dfrac{F_1^{(1)}(t,t)\rho_2(\Omega,t) - F_2^{(1)}(t,t)\rho_1(\Omega,t)}{F_1^{(1)}(t,t)F_2(t,t) - F_1(t,t)F_2^{(1)}(t,t)} \end{cases} \tag{5.33}$$

if $F_1^{(1)}(t,t)F_2(t,t) - F_1(t,t)F_2^{(1)}(t,t) \neq 0$, and

$$\begin{cases} y^{(1)}(t) = \dfrac{F_1(t,t)\rho_3(\Omega,t) - F_3(t,t)\rho_1(\Omega,t)}{F_1^{(1)}(t,t)F_3(t,t) - F_1(t,t)F_3^{(1)}(t,t)}, \\ y^{(2)}(t) = \dfrac{F_1^{(1)}(t,t)\rho_3(\Omega,t) - F_3^{(1)}(t,t)\rho_1(\Omega,t)}{F_1^{(1)}(t,t)F_3(t,t) - F_1(t,t)F_3^{(1)}(t,t)} \end{cases} \tag{5.34}$$

if $F_1^{(1)}(t,t)F_2(t,t) - F_1(t,t)F_2^{(1)}(t,t) = 0$.

It is worth noting that the above expressions are always well-posed (singularity-free) for any $t > 0$ thanks to the condition (5.19) on the parameters of the three kernels.

By deriving (5.1) twice with respect to time, we obtain that the true squared-frequency Ω verifies the following structural constraint:

$$\Omega y^{(1)}(t)^2 + y^{(2)}(t)^2 = a^2\Omega^2 . \tag{5.35}$$

Applying to both sides of (5.35) the linear operator $V_{K_{g_a}}$, with kernel $K_{g_a}(t, \tau) = e^{-g_a(t-\tau)}$, $g_a \in \mathbb{R}_{>0}$, we have that

$$V_{K_{g_a}}\left[\sqrt{\Omega y^{(1)}(t)^2 + y^{(2)}(t)^2}\right](t) = a[V_{K_g}\Omega](t). \tag{5.36}$$

We have that the constraint (5.36) is in general not met unless $\hat{a}(t) = a$, when only the estimates $\hat{\Omega}(t)$ of Ω, $\hat{a}(t)$ of a and $\hat{y}^{(i)}(t)$ of $y^{(i)}(t)$ are available. Assuming that the frequency estimation error vanishes within a finite time, bounded by $\bar{T}_\Omega$ (see the proof in Section 5.5), the estimated derivatives can be obtained from (5.33), (5.34) by using $\hat{\Omega}(t)$ in place of Ω, thus becoming exact in finite time after $\hat{\Omega}(t)$ has converged to Ω. Following the same steps taken for the frequency adaptation, we introduce a time-varying residual that depends on the frequency estimate $\hat{\Omega}(t)$ and on the signals $\hat{y}^{(1)}(t)$ and $\hat{y}^{(2)}(t)$ obtained by (5.33) and (5.34)

$$\begin{aligned} R_a(t) := V_{K_{g_a}}\left[\sqrt{\hat{\Omega}(t)\hat{y}^{(1)}(t)^2 + \hat{y}^{(2)}(t)^2}\right](t) - \hat{a}(t)[V_{K_g}\hat{\Omega}(t)](t) \\ = \gamma_{a_1}(t) - \hat{a}(t)\gamma_{a_2}(t), \quad \forall t \geq t_\epsilon + \bar{T}_\Omega \end{aligned}$$

in which

$$\begin{aligned} \dot{\gamma}_{a_1}(t) &= \psi(t)\left(\sqrt{\hat{\Omega}(t)\hat{y}^{(1)}(t)^2 + \hat{y}^{(2)}(t)^2} - g_a\gamma_{a_1}(t)\right), \\ \dot{\gamma}_{a_2}(t) &= \psi(t)\left(\hat{\Omega}(t) - g_a\gamma_{a_2}(t)\right), \end{aligned}$$

with $\gamma_{a_1}(0) = \gamma_{a_2}(0) = 0$, $\psi(t)$ a binary on-off switching signals: $\psi(t) = 1$, $\forall t \geq t_\epsilon + \bar{T}_\Omega$, $\psi(t) = 0$, $\forall t < t_\epsilon + \bar{T}_\Omega$. The following adaptation law based on the second order sliding mode is designed

$$\begin{aligned} \dot{\hat{a}}(t) &= \psi(t)\gamma_{a_2}(t)^{-1}\left(\eta_a(t) + L_3\left|R_a(t)\right|^{\frac{1}{2}}\operatorname{sign}(R_a(t)) - \hat{a}(t)\dot{\gamma}_{a_2}(t) + \dot{\gamma}_{a_1}(t)\right), \\ \dot{\eta}_a(t) &= L_4\operatorname{sign}(R_a(t)) \end{aligned} \tag{5.37}$$

with $\hat{a}(0) = 0$ and where L_3, $L_4 \in \mathbb{R}_{>0}$ are tuning gains set by the designer to steer the residual term $R_a(t)$ to 0 in finite-time. Note that the invertibility of $\gamma_{a_2}(t)$ is verified for any

$t > t_\epsilon + \overline{T_\Omega}$ due to the positiveness of $\hat{\Omega}(t)$. Finally, the phase of the sinusoidal signal can be easily estimated as follows:

$$\hat{\vartheta}(t) = \angle \begin{pmatrix} \hat{y}^{(2)}(t) + j\hat{\omega}(t)\hat{y}^{(1)}(t) \\ 1 \end{pmatrix}, \quad \forall t \geq t_\epsilon + \overline{T_\Omega}. \tag{5.38}$$

5.5 Finite-time convergence and robustness analysis

In this section, we first address the convergence properties of the proposed estimator in absence of external perturbations. Subsequently, the stability properties in the presence of a bounded measurement disturbance are analyzed.

5.5.1 Finite-time convergence

The main result consists in the following theorem.

Theorem 5.5.1 *If Assumption 5 holds, given the pure sinusoidal signal $y(t)$, the estimated frequency $\hat{\Omega}(t)$ that is governed by the adaptation law given by (5.32) converges to the true value Ω in finite time.* □

Proof: Assuming that the noise-free measurement $y(t)$ is available, we show that the residuals R_Ω and R_A converge to zero in finite-time. Under the P.E. condition (see Assumption 5), the finite-time convergence of the residuals implies also the deadbeat convergence of $\hat{\Omega}(t)$ and $\hat{A}(t)$ to Ω and A, respectively. The dynamics of $R_\Omega(t)$ obeys the following differential equation:

$$\dot{R}(\hat{\Omega}, t) = \dot{\gamma}_1(t) - \dot{\gamma}_2(t)\hat{\Omega}(t) - \gamma_2(t)\dot{\hat{\Omega}}(t). \tag{5.39}$$

For $t \geq t_\epsilon$, by substituting the adaptation law in (5.39), we have

$$\dot{R}_\Omega(t) = -\eta_\Omega(t) - L_1 \quad \overline{|R_\Omega(t)|}\,\mathrm{sign}(R_\Omega(t)). \tag{5.40}$$

Consider an auxiliary variable vector $\zeta(t) = [\zeta_1(t) \;\; \zeta_2(t)]^\top$, where

$$\zeta_1(t) = \quad \overline{|R_\Omega(t)|}\,\mathrm{sign}(R_\Omega(t)), \quad \zeta_2(t) = \eta_\Omega(t),$$

then:

$$\dot{\zeta}(t) = \frac{1}{\overline{|R_\Omega(t)|}} M\zeta(t), \quad \forall R_\Omega(t) = 0 \tag{5.41}$$

where

$$M = \begin{bmatrix} -\frac{1}{2}L_1 & -\frac{1}{2} \\ L_2 & 0 \end{bmatrix}, \tag{5.42}$$

with spectrum $\lambda\{M\} = \frac{-L_1 \pm \sqrt{L_1 - 8L_2}}{4}$. Being M Hurwitz, there always exists a positive symmetric matrix P that solves the linear Lyapunov equation $M^\top P + PM = -2qI$. Resorting to the following upper bound on the maximum solution P of the Lyapunov equation $X^\top P + PX = -Q$, for X Hurwitz and $Q > 0$ (see [112]):

$$\bar{p} \triangleq \bar{\lambda}(P) \leq \frac{1}{2}\bar{\lambda}(-QX^{-1}),$$

in our case we have

$$\bar{p} \leq q\bar{\lambda}(-M^{-1}) = \frac{q}{\underline{\alpha}},$$

where $\underline{\alpha} \triangleq \min \operatorname{eig}(-M)$. Now, let us introduce a quadratic function $V_\Omega = \zeta^\top P \zeta$, which can be expanded as

$$V_\Omega(t) = p_{11}|R_\Omega(t)| + p_{22}\eta_\Omega(t)^2 + 2p_{12}\sqrt{|R_\Omega(t)|}\operatorname{sign}(R_\Omega(t))\eta_\Omega(t), \tag{5.43}$$

with p_{ij} the components of the matrix P. Note that, by taking the limit

$$\lim_{\zeta_1 \to 0} V_\Omega(\zeta) = p_{22}\eta_\Omega(t)^2$$

we can rewrite (5.43) as follows:

$$V_\Omega(\zeta) = \begin{cases} \zeta^\top P \zeta, & \text{if } \zeta_1(t) \neq 0 \\ p_{22}\zeta_2^2, & \text{if } \zeta_1(t) = 0 \end{cases}.$$

After some algebra, the time-derivative of $V_\Omega(t)$ along the trajectories of the system (5.41) can be written as:

$$\dot{V}_\Omega(t) = \begin{cases} -\dfrac{2q}{\sqrt{|R_\Omega(t)|}}|\zeta(t)|^2, & \text{if } \zeta_1(t) \neq 0, \\ 0, & \text{if } \zeta_1(t) = 0. \end{cases}$$

Clearly, $\zeta_1(t)$ will stay in 0 when it crosses zero. In case $\zeta_1(t) \neq 0$, using the facts that $|R_\Omega(t)|^{-1/2} = |\zeta_1(t)|^{-1} > |\zeta(t)|^{-1}$ and $V_\Omega(t) \leq p^{\top}|\zeta(t)|^2$, $\dot{V}_\Omega(t)$ can be bounded as

$$\begin{aligned} \dot{V}_\Omega(t) &\leq -\frac{2q}{|\zeta(t)|}|\zeta(t)|^2 \\ &\leq -\frac{2q}{\sqrt{p}}V_\Omega(t)^{\frac{1}{2}} \\ &\leq -2\sqrt{\alpha q}V_\Omega(t)^{\frac{1}{2}}. \end{aligned} \tag{5.44}$$

In view of the Lyapunov-based finite-time convergence result presented in [4], then (5.44) implies that $\zeta(t) \to 0$ with a guaranteed reaching-time $T_\Omega(V_\Omega(t_\epsilon))$ verifying the inequality:

$$T_\Omega(V_\Omega(t_\epsilon)) \leq \frac{V_\Omega(t_\epsilon)}{\sqrt{\alpha q}} \triangleq T_\Omega. \tag{5.45}$$

Finally, noting that $\zeta(t) \to 0$ implies $R_\Omega(t) \to 0$, then we can conclude that $\hat{\Omega}(t) \to \Omega$ in finite-time. •

In the noise-free condition, the frequency estimate coincides with the true frequency, i.e. $\hat{\Omega}(t) = \Omega$ for all $t > t_\epsilon + T_\Omega(V_\Omega(t_\epsilon))$, which makes it possible to prove the finite-time convergence of the estimated amplitude $\hat{a}(t)$ ruled by (5.37) to a. By defining

$$\zeta_a(t) = [\quad \sqrt{|R_a(t)|}\,\mathrm{sign}(R_a(t)),\ \eta_a(t)]^{\top},$$

then

$$\dot{\zeta}_a(t) = \frac{1}{\sqrt{|R_a(t)|}} M_a \zeta_a(t), \quad \forall R_a \neq 0,$$

where

$$M_a = \begin{bmatrix} -\frac{1}{2}L_3 & -\frac{1}{2} \\ L_4 & 0 \end{bmatrix}. \tag{5.46}$$

Consider a positive symmetric matrix P_a that solves the Lyapunov equation

$$M_a^{\top} P_a + P_a M_a = -2q_a I,$$

and $\alpha_a \triangleq \min \mathrm{eig}(-M_a)$. The convergence time verifies the upper bound:

$$T_a(V_a(t_\epsilon + T_\Omega(V_\Omega(t_\epsilon)))) \leq \frac{V_a(t_\epsilon + T_\Omega(V_\Omega(t_\epsilon)))}{\sqrt{\alpha_a q_a}}. \tag{5.47}$$

Thus, the finite time convergence of the amplitude estimate occurs at time:

$$t = t_\epsilon + T_\Omega(V_\Omega(t_\epsilon)) + T_a(V_a(t_\epsilon + T_\Omega(V_\Omega(t_\epsilon)))).$$

This result can be proved by following the same steps taken to prove the finite-time convergence of the frequency estimate and is therefore omitted.

5.5.2 Robustness in the presence of a bounded measurement disturbance

Now, we consider the scenario in which the sinusoidal measurement is corrupted by a norm-bounded additive noise $d(t)$: $|d(t)| \leq \bar{d}$, such that $v(t) \triangleq y(t) + d(t)$.

Let us rewrite (5.22) introducing the noise term $d(t)$:

$$\dot{\hat{\xi}}(t) = G_\xi \hat{\xi}(t) + E_\xi(t)(y(t) + d(t)) \tag{5.48}$$

and the error $\tilde{\xi}(t) = \hat{\xi}(t) - \xi(t)$. Then, the error dynamics can be expressed by

$$\dot{\tilde{\xi}}(t) = G_\xi \tilde{\xi}(t) + E_\xi(t)d(t). \tag{5.49}$$

Being the matrix G_ξ Hurwitz, and $E_\xi(t)d(t)$ bounded, $\tilde{\xi}(t)$ is ISS w.r.t. $E_\xi(t)d(t)$. Each component in the vector variable $\tilde{\xi}(t) \triangleq [\tilde{\xi}_1(t) \;\; \tilde{\xi}_2(t) \;\; \cdots \;\; \tilde{\xi}_6(t)]^\top$ verifies the inequality:

$$\begin{aligned} |\tilde{\xi}_{h\times i}(t)| &\leq e^{-\beta_h t}\tilde{\xi}_{h\times i}(0) + \frac{1 - e^{-\beta_h t}}{\beta_h} \sup_{0\leq\tau<t} E_{h\times i}(\tau)\bar{d} \\ &\leq e^{-\beta_h t_\epsilon}\tilde{\xi}_{h\times i}(0) + \frac{1}{\beta_h} \sup_{0\leq\tau<t} K_h^{(i)}(\tau,\tau)\bar{d}, \;\; \forall h, i \in \{1,2,3\}\times\{1,2\}, \; \forall t \geq t_\epsilon. \end{aligned}$$

Let us denote the upper bound of $|\tilde{\xi}_{h\times i}(t)|$ by $\overline{\tilde{\xi}_{h\times i}}$, such that

$$\overline{\tilde{\xi}_{h\times i}} \triangleq e^{-\beta_h t_\epsilon}\tilde{\xi}_{h\times i}(0) + \frac{1}{\beta_h} \sup_{0\leq\tau<t} K_h^{(i)}(\tau,\tau)\bar{d}.$$

From (5.23), introducing the error signals $\tilde{\kappa}_{a,h}(t) \triangleq \hat{\kappa}_{a,h}(t) - \kappa_{a,h}(t)$, $\tilde{\kappa}_{d,h}(t) \triangleq \hat{\kappa}_{d,h}(t) - \kappa_{d,h}(t)$, it follows that

$$\begin{aligned} |\tilde{\kappa}_{a,h}(t)| &= |\tilde{\xi}_{2h}(t) - F_h^{(2)}(t,t)d(t)| \leq \tilde{\xi}_{2h} + \sup_{0\leq\tau<t} F_h^{(2)}(\tau,\tau)\bar{d} \\ |\tilde{\kappa}_{d,h}(t)| &= |\tilde{\xi}_{2h-1}(t) - F_h(t,t)d(t)| \leq \tilde{\xi}_{2h-1} + \sup_{0\leq\tau<t} F_h(\tau,\tau)\bar{d} \end{aligned}$$

and then $|\tilde{\kappa}_1(t)|$, $|\tilde{\kappa}_2(t)|$ are ISS bounded with respect to $\tilde{\xi}(t)$ because

$$\begin{aligned}
|\tilde{\kappa}_1(t)| &= |\hat{\kappa}_1(t) - \kappa_1(t)| \\
&= |\tilde{\kappa}_a^{\top}(t)\mathrm{F}(t,t)| \\
&\le |\tilde{\kappa}_a(t)|_1 |\mathrm{F}(t,t)|_1 \\
&= \sum_{h=1}^{3} \tilde{\xi}_{2h} + \sup_{0\le\tau<t} F_h^{(2)}(\tau,\tau)\bar{d}^3 \prod_{h=1}^{3} \sup_{0\le\tau<t} \mathrm{F}_h(\tau,\tau), \\
|\tilde{\kappa}_2(t)| &= |\hat{\kappa}_2(t) - \kappa_2(t)| \\
&= |\tilde{\kappa}_d^{\top}(t)\mathrm{F}(t,t)| \\
&\le |\tilde{\kappa}_d(t)|_1 |\mathrm{F}(t,t)|_1 \\
&= \sum_{h=1}^{3} \tilde{\xi}_{2h-1} + \sup_{0\le\tau<t} F_h(\tau,\tau)\bar{d}^3 \prod_{h=1}^{3} \sup_{0\le\tau<t} \mathrm{F}_h(\tau,\tau).
\end{aligned}$$

Moreover, $\xi(t)$ and the kernels are bounded, thus implying the boundedness of $\kappa_1(t)$, $\kappa_2(t)$ and $\hat{\kappa}_1(t)$, $\hat{\kappa}_2(t)$. For the sake of further analysis, let

$$\bar{\tilde{\kappa}}_1(\bar{d}) := \sum_{h=1}^{3} \tilde{\xi}_{2h} + \sup_{0\le\tau<t} F_h^{(2)}(\tau,\tau)\bar{d}^3 \prod_{h=1}^{3} \sup_{0\le\tau<t} \mathrm{F}_h(\tau,\tau)$$

and

$$\bar{\tilde{\kappa}}_2(\bar{d}) := \sum_{h=1}^{3} \tilde{\xi}_{2h-1} + \sup_{0\le\tau<t} F_h(\tau,\tau)\bar{d}^3 \prod_{h=1}^{3} \sup_{0\le\tau<t} \mathrm{F}_h(\tau,\tau).$$

Under Assumption 5, for all $t \ge t_\epsilon$ it holds that

$$\begin{aligned}
\frac{1}{t_\epsilon}\int_{t-t_\epsilon}^{t} |\hat{\kappa}_2(\tau)|d\tau &\ge \frac{1}{t_\epsilon}\int_{t-t_\epsilon}^{t} |\kappa_2(\tau)| - |\tilde{\kappa}_2(\tau)|d\tau \\
&\ge \epsilon - \frac{1}{t_\epsilon}\int_{t-t_\epsilon}^{t} |\tilde{\kappa}_2(\tau)|d\tau \\
&\ge \epsilon - \bar{\tilde{\kappa}}_2(\bar{d}) \\
&= \epsilon - \sigma(\bar{d})
\end{aligned}$$

where

$$\sigma(\bar{d}) := \bar{\tilde{\kappa}}_2(\bar{d}). \tag{5.50}$$

Now, consider $\hat{\gamma}_1(t)$ and $\hat{\gamma}_2(t)$ (i.e., the noisy counterparts of $\gamma_1(t)$, $\gamma_2(t)$). The following dynamic filters driven by the norm of the noisy auxiliary signals $|\hat{\kappa}_1(t)|$ and $|\hat{\kappa}_2(t)|$, respectively, are introduced:

$$\dot{\hat{\gamma}}_i(t) = |\hat{\kappa}_i(t)| - g\hat{\gamma}_i(t), \quad i = 1, 2. \tag{5.51}$$

By analogy with (5.31), we have

$$\hat{\gamma}_2(t) = \int_{t-t_\epsilon}^{t} e^{-g(t-\tau)}|\dot{\hat{\kappa}}_2(\tau)|\,d\tau \geq t_\epsilon e^{-gt_\epsilon}(\epsilon - \sigma(\bar{d})),\ \forall t \geq t_\epsilon .$$

To make $\hat{\gamma}_2(t)$ strictly positive for $t \geq t_\epsilon$, we impose another constraint on the noise bound: $\bar{d} < \sigma^{-1}(\epsilon)$. Let us denote by $\tilde{\alpha} \stackrel{\Delta}{=} t_\epsilon e^{-gt_\epsilon}(\epsilon - \sigma(\bar{d}))$ the transition threshold that determines the triggering time of the adaptation. Then, the following frequency adaptation law in the noisy case with respect to realizable signals is proposed:

$$\begin{cases} \dot{\hat{\gamma}}_2(t) = -\hat{\gamma}_2(t) + L_1 |\hat{R}_\Omega(t)|\,\mathrm{sign}(\hat{R}_\Omega(t)) - \hat{\Omega}(t)\dot{\hat{\gamma}}_2(t) + \dot{\hat{\gamma}}_1(t) & \text{, if } \hat{\gamma}_2(t) \geq \tilde{\alpha}, \\ \Omega(t) = 0, & \text{otherwise.} \end{cases}$$

$$\dot{\hat{\eta}}_\Omega(t) = L_2 \mathrm{sign}(\hat{R}_\Omega(t)) \tag{5.52}$$

where $\hat{R}_\Omega(t) = \hat{\gamma}_1(t) - \hat{\gamma}_2(t)\hat{\Omega}(t)$.

The following result characterises the stability properties of the adaptive estimation law(5.52).

Theorem 5.5.2 *If Assumption 5 holds, then, given the sinusoidal signal $y(t)$ and the perturbed measurement $v(t)$, the estimated frequency $\hat{\Omega}(t)$ that evolves according to the adaptation law given by (5.52), converges in finite-time into a closed interval that contains Ω and the frequency estimation error $\tilde{\Omega}(t) = \hat{\Omega}(t) - \Omega$ is ISS, with respect to any disturbance signal $d(t) \in \mathsf{L}_\infty^1$ such that $\bar{d} < \sigma^{-1}(\epsilon)$, where $\sigma(\cdot)$ is defined in (5.50).*

□

Proof: Consider the error variables: $\tilde{\gamma}_1(t) \stackrel{\Delta}{=} \hat{\gamma}_1(t) - \gamma_1(t)$ and $\tilde{\gamma}_2(t) \stackrel{\Delta}{=} \hat{\gamma}_2(t) - \gamma_2(t)$. (5.29) implies that the dynamics of the error variables obeys the following differential equations:

$$\dot{\tilde{\gamma}}_i(t) = |\kappa_i(t) + \tilde{\kappa}_i(t)| - |\kappa_i(t)| - g\tilde{\gamma}_i(t),\ i = 1, 2 .$$

By using the triangle inequality, we obtain

$$\dot{\tilde{\gamma}}_i(t) \leq |\tilde{\kappa}_i(t)| - g\tilde{\gamma}_i(t),\ i = 1, 2$$

that, in turn, lead to the following bounds $\forall t \geq t_\epsilon$:

$$|\tilde{\gamma}_i(t)| \leq e^{-gt_\epsilon}\tilde{\gamma}_i(0) + \frac{1}{g}\bar{\tilde{\kappa}}_i(\bar{d}),\ i = 1, 2.$$

Finally, it turns out that $\tilde{\gamma}_1(t)$ and $\tilde{\gamma}_2(t)$ are ISS with respect to $\tilde{\xi}(t)$ and $\bar{d}$.

Following the same steps taken in the noise-free condition, we introduce the noisy counterpart of the auxiliary variable vector $\hat{\zeta}(t) = [\hat{\zeta}_1(t),\ \hat{\zeta}_2(t)]^\top$, where

$$\hat{\zeta}_1(t) = \sqrt{|\hat{R}_\Omega(t)|}\,\mathrm{sign}(\hat{R}_\Omega(t)),\quad \hat{\zeta}_2(t) = \hat{\eta}_\Omega(t),$$

and $\hat{\zeta}(t)$ obey the differential equations:

$$\dot{\hat{\zeta}}(t) = \frac{1}{\sqrt{|\hat{R}_\Omega(t)|}} M\hat{\zeta}(t),\ \ \forall \hat{R}_\Omega(t) \neq 0. \tag{5.53}$$

Analogously, the residual $\hat{R}_\Omega(t)$ can be proved bounded and decays to 0 with a constant rate. From the equality $\hat{R}_\Omega(t) = \hat{\gamma}_1(t) - \hat{\gamma}_2(t)\hat{\Omega}(t)$, we have that

$$\hat{\Omega}(t) = \frac{\hat{\gamma}_1(t)}{\hat{\gamma}_2(t)},\ \ \forall t \geq t_\epsilon + T_\Omega(V_\Omega(t_\epsilon)),$$

in which $T_\Omega(V_\Omega(t_\epsilon))$ is the time of convergence. It turns out that the proven boundedness of $\hat{\gamma}_1(t)$, $\hat{\gamma}_2(t)$ and Assumption 5 implies the boundedness of $\hat{\Omega}(t)$ for all $t > 0$. Moreover, the frequency estimates $\hat{\Omega}(t)$ will enter into the compact region

$$\hat{\Omega}(t) \in \left[\inf_{0\leq\tau<t} \frac{\hat{\gamma}_1(\tau)}{\hat{\gamma}_2(\tau)},\ \sup_{0\leq\tau<t} \frac{\hat{\gamma}_1(\tau)}{\hat{\gamma}_2(\tau)}\right],\ \forall t \geq t_\epsilon + T_\Omega(V_\Omega(t_\epsilon)).$$

which contains Ω. Hence, the estimation error $\tilde{\Omega}(t) = \hat{\Omega}(t) - \Omega$ is ISS with respect to $\bar{d}$. •

Concerning the amplitude estimation in noisy conditions, analogously to the noise-free case, we introduce the perturbed residual signal

$$\hat{R}_a(t) := V_{K_{ga}}\sqrt{\hat{\Omega}(t)\hat{y}^{(1)}(t)^2 + \hat{y}^{(2)}(t)^2}\ (t) - \hat{a}(t)[V_{K_g}\hat{\Omega}(t)](t)$$
$$= \hat{\gamma}_{a_1}(t) - \hat{a}(t)\hat{\gamma}_{a_2}(t),\ \ \forall t \geq t_\epsilon + T_\Omega(V_\Omega(t_\epsilon))$$

with

$$\dot{\hat{\gamma}}_{a_1}(t) = \psi(t)\left(\sqrt{\hat{\Omega}\hat{y}^{(1)}(t)^2 + \hat{y}^{(2)}(t)^2} - g_a\hat{\gamma}_{a_1}(t)\right),$$
$$\dot{\hat{\gamma}}_{a_2}(t) = \psi(t)\left(\hat{\Omega}(t) - g_a\hat{\gamma}_{a_2}(t)\right),$$

and $\hat{y}^{(1)}(t)$, $\hat{y}^{(2)}(t)$, computed by (5.33)-(5.34) with the substitution of $\hat{\rho}_h(\hat{\Omega}, t) := \hat{\kappa}_{a,h}(t) + \hat{\Omega}(t)\hat{\kappa}_{d,h}(t)$, $h = 1, 2, 3$ in place of $\rho_h(\Omega, t)$.

Then, the amplitude adaptation law in the presence of noise $d(t)$ is given by

$$\begin{cases} \dot{\hat{a}}(t) = \psi(t)\hat{\gamma}_{a_2}(t)^{-1}\left[\hat{\eta}_a(t) + L_3\sqrt{|\hat{R}_a(t)|}\,\mathrm{sign}(\hat{R}_a(t)) - \hat{a}(t)\dot{\hat{\gamma}}_{a_2}(t) + \dot{\hat{\gamma}}_{a_1}(t)\right], \\ \dot{\hat{\eta}}_a(t) = L_4\,\mathrm{sign}(R_a(t)) \end{cases} \tag{5.54}$$

with $\hat{a}(0) = 0$.

Thanks to the boundedness of the $\hat{\Omega}(t)$, $\hat{\kappa}_{a,h}$ and $\hat{\kappa}_{d,h}$, it is straightforward to show that $\hat{y}^{(1)}(t)$, $\hat{y}^{(2)}(t)$ are bounded when the input is perturbed. Following the same stability analysis with respect to the frequency estimation, we immediately prove that $\hat{a}(t)$ converges to $\hat{\gamma}_{a_1}(t)/\hat{\gamma}_{a_2}(t)$ in finite-time, which is bounded due to the boundedness of $\hat{y}^{(1)}(t)$ and $\hat{y}^{(2)}(t)$.

5.6 Digital implementation of the proposed method

Herein, we provide a discrete-time counterpart of this algorithm, which is sampled by Euler method with a fixed sampling period T_s. More sophisticated discretization methods may be chosen depending on the computation power and the required accuracy (see Sec. 5.7 for more details).

It is worth noting that, kernels to be used at each time sampling instants can be computed off-line, thus alleviating the on-line computation burden. By choosing a set of tuning parameters β_h, $\bar{\beta}_h$, $h = 1, 2, 3$, g, g_a, L_1, L_2, L_3, L_4 and δ_ϵ, then the discretized on-line algorithm is described as follows, given a measurement $y(k)$, $k = 1, 2, \cdots$

$$\xi(k) = \xi(k-1) + T_s\left(G_\xi \xi(k-1) + E_\xi(k) y(k)\right),$$

with

$$E_\xi(k) = \begin{bmatrix} E_{\xi_1}(k)^\top & E_{\xi_2}(k)^\top & E_{\xi_3}(k)^\top \end{bmatrix}^\top,$$

where $E_{\xi_h}(t) \in \mathbb{R}^2$ are given by: $E_{\xi_h}(k) = \begin{bmatrix} F_h^{(1)}(k,k) & F_h^{(3)}(k,k) \end{bmatrix}^\top$. Then, we immediately have

$$\begin{aligned} \kappa_{a,h}(k) &:= \xi_{2h}(k) - F_h^{(2)}(k,k) y(k), \\ \kappa_{b,h}(k) &:= F_h^{(1)}(k,k), \\ \kappa_{c,h}(k) &:= -F_h(k,k), \\ \kappa_{d,h}(k) &:= \xi_{2h-1}(k) - F_h(k,k) y(k), \quad \forall h = 1, 2, 3. \end{aligned}$$

After that, $\kappa_1(k) = \kappa_a^{\top}(k)\mathsf{F}(k,k)$, $\kappa_2(k) = \kappa_d^{\top}(k,k)\mathsf{F}(k,k)$ are available thanks to the relations

$$\kappa_a(k) = [\kappa_{a,1}(k)\ \kappa_{a,2}(k)\ \kappa_{a,3}(k)]^{\top},\ \kappa_d(k) = [\kappa_{d,1(k)}\ \kappa_{d,2}(k)\ \kappa_{d,3}(k)]^{\top}$$

and

$$\mathsf{F}(k,k) = \begin{bmatrix} \mathsf{F}_1(k,k) \\ \mathsf{F}_2(k,k) \\ \mathsf{F}_3(k,k) \end{bmatrix} = \begin{bmatrix} \kappa_{b,3}(k)\kappa_{c,1}(k)\kappa_{c,2}(k) - \kappa_{b,2}(k)\kappa_{c,1}(k)\kappa_{c,3}(k) \\ \kappa_{b,1}(k)\kappa_{c,1}(k)\kappa_{c,3}(k) - \kappa_{b,3}(k)\kappa_{c,1}(k)^2 \\ \kappa_{b,2}(k)\kappa_{c,1}(k)^2 - \kappa_{b,1}(k)\kappa_{c,1}(k)\kappa_{c,2}(k) \end{bmatrix}$$

Moreover, the auxiliary signals γ_1 and γ_2 are computed by

$$\gamma_i(k) = \gamma_i(k-1) + T_s\left(|\kappa_i(k)| - g\gamma_i(k-1)\right),\ i = 1, 2,$$

which gives rise to the residual term

$$R_{\Omega}(k) = \gamma_1(k) - \gamma_2(k)\hat{\Omega}(k-1).$$

The estimated frequency adapts according to

$$\hat{\Omega}(k) = \begin{cases} \hat{\Omega}(k-1) + T_s\gamma_2(k)^{-1}\left(\eta_{\Omega}(k-1) + L_1 R_{\Omega}(k)|\text{sign}(R_{\Omega}(k))\right) \\ -\hat{\Omega}(k-1)(\gamma_2(k) - \gamma_2(k-1)) + (\gamma_1(k) - \gamma_1(k-1)),\ \text{if}\ \gamma_2(k) \geq \delta_{\epsilon}, \\ \hat{\Omega}(k-1),\quad \text{otherwise.} \end{cases}$$

$$\eta_{\Omega}(k) = \eta_{\Omega}(k-1) + T_s L_2 \text{sign}(R_{\Omega}(k))$$

By using the frequency estimates at each sampling instant, the estimated signal derivatives $\hat{y}^{(1)}(k)$ and $\hat{y}^{(2)}(k)$ are obtained from the discretized version of (5.33) and (5.34), that is

$$\begin{bmatrix} \hat{y}^{(1)}(k) \\ \hat{y}^{(2)}(k) \end{bmatrix} = \begin{bmatrix} \dfrac{F_1(k,k)\rho_2(\hat{\Omega},k) - F_2(k,k)\rho_1(\hat{\Omega},k)}{F_1^{(1)}(k,k)F_2(k,k) - F_1(k,k)F_2^{(1)}(k,k)} \\ \dfrac{F_1^{(1)}(k,k)\rho_2(\Omega,k) - F_2^{(1)}(k,k)\rho_1(\Omega,k)}{F_1^{(1)}(k,k)F_2(k,k) - F_1(k,k)F_2^{(1)}(k,k)} \end{bmatrix},$$

if $F_1^{(1)}(k,k)F_2(k,k) - F_1(k,k)F_2^{(1)}(k,k) = 0$, and

$$\hat{y}^{(1)}(k) = \frac{F_1(k,k)\rho_3(\hat{\Omega},k) - F_3(k,k)\rho_1(\hat{\Omega},k)}{F_1^{(1)}(k,k)F_3(k,k) - F_1(k,k)F_3^{(1)}(k,k)},$$

$$\hat{y}^{(2)}(k) = \frac{F_1^{(1)}(k,k)\rho_3(\Omega,k) - F_3^{(1)}(k,k)\rho_1(\Omega,k)}{F_1^{(1)}(k,k)F_3(k,k) - F_1(k,k)F_3^{(1)}(k,k)}$$

if $F_1^{(1)}(k,k)F_2(k,k) - F_1(k,k)F_2^{(1)}(k,k) = 0$, and where

$$\rho_h(\hat{\Omega},k) = \kappa_{a,h}(k) + \Omega\kappa_{d,h}(k), \quad h = 1,2,3.$$

The following steps are carried out for amplitude and phase estimation

$$\gamma_{a_1}(k) = \gamma_{a_1}(k-1) + T_s\psi(k)\left[\hat{\Omega}(k)\hat{y}^{(1)}(k)^2 + \hat{y}^{(2)}(k)^2 - g_a\gamma_{a_1}(k-1)\right],$$

$$\gamma_{a_2}(k) = \gamma_{a_2}(k-1) + T_s\psi(k)\left[\hat{\Omega}(k) - g_a\gamma_{a_2}(k-1)\right],$$

in which $\psi(k) = 1, \ \forall k \geq (t_\epsilon + \overline{T}_\Omega)/T_s$, $\psi(k) = 0, \ \forall k < (t_\epsilon + \overline{T}_\Omega)/T_s$. Based on the residual depending on $\gamma_{a_1}(k), \ \gamma_{a_2}(k)$

$$R_a(k) = \gamma_{a_1}(k) - \hat{a}(k-1)\gamma_{a_2}(k), \quad \forall k \geq (t_\epsilon + \overline{T}_\Omega)/T_s,$$

the amplitude is adaptively calculated by

$$\hat{a}(k) = \hat{a}(k-1) + \psi(k)\left[T_s\gamma_{a_2}(k)^{-1}\left[\eta_a(k-1) + L_3\left[\overline{R_a(k)|}\mathrm{sign}(R_a(k)) - \hat{a}(k-1)(\gamma_{a_2}(k) - \gamma_{a_2}(k-1)) + (\gamma_{a_1}(k) - \gamma_{a_1}(k-1))\right]\right],$$

$$\eta_a(k) = \eta_a(k-1) + T_sL_4\mathrm{sign}(R_a(k))$$

with $\hat{a}(0) = 0$. Finally, the phase of the sinusoidal signal is identified as follows:

$$\hat{\vartheta}(k) = \angle\left[\hat{y}^{(2)}(k) + j\hat{\omega}(k)\hat{y}^{(1)}(k)\right]^{-1}, \quad \forall k \geq (t_\epsilon + \overline{T}_\Omega)/T_s.$$

5.7 Simulation results

Three numerical examples are given to illustrate the effectiveness of the proposed AFP methodology.

Example 1: Let us consider the following measured sinusoidal signal:

$$v(t) = 2 + 3\sin 5t + d(t),$$

where $d(t)$ is a bounded disturbance with uniform distribution in the interval $[-0.25, 0.25]$.

In this first example, we compare the proposed method with the very recent one (based on first order sliding mode) given in [85]. In addition to show the performance, we also address the effects of discretization enhancing the superiority of the algorithm in the case of a simple digital implementation. More specifically, we let $T_s = 1 \times 10^{-4}$s and evaluate two discretization procedures:

1. Euler method
2. 4-th order Runge-Kutta

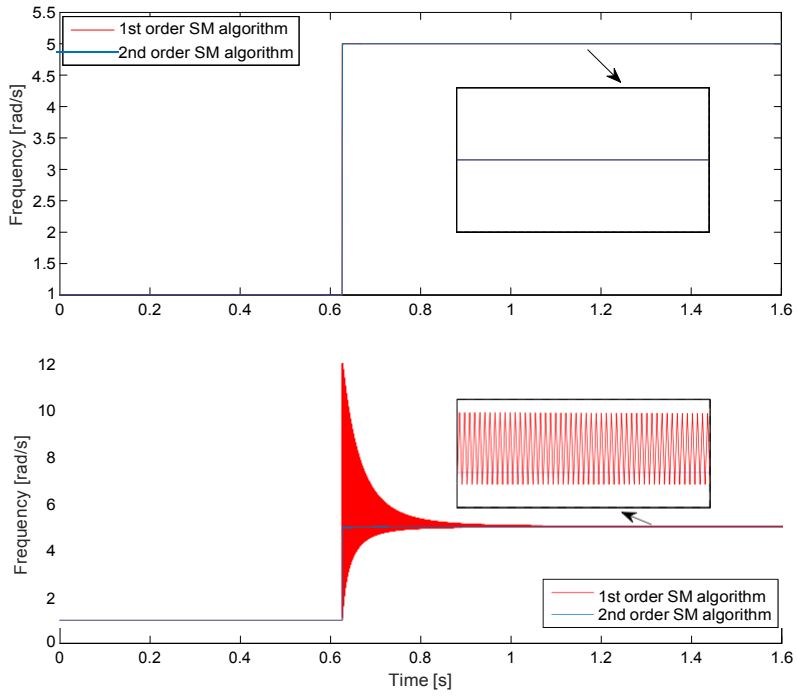

Fig. 5.2 Time-behavior of the estimated frequency by using the proposed method and the method [85] in noise-free scenario: Top: 4-th order Runge-Kutta method, Bottom: Euler method.

The proposed method is equipped with three BF-NKs having parameters: $\beta_1 = 1$, $\beta_2 = 2$, $\beta_3 = 3$, $\bar{\beta}_h = 2.5$, $h = 1, 2, 3$ also we let $g = g_a = 25$, $L_1 = 30$, $L_2 = 2$, $L_3 = 300$, $L_4 = 5$ and $\delta_\epsilon = 1e-5$, while the algorithm considered in [85] is tuned by the same

initial condition and similar transient under Runge-Kutta discretization in absence of noise (i.e. $d(t) = 0$). The following facts are used for tuning this deadbeat AFP approach: 1) In view of (5.49), large values of β_h, $h = 1, 2, 3$ that result in a fast convergence of the error variable $\tilde{\xi}(t)$, correspond to a higher noisy sensitivity because of (5.5.2); 2) In order to increase the convergence speed, we can instead enforce the eigenvalue of M and M_a (defined in (5.42) and (5.46)) respectively) far away from the imaginary axis by manipulating $L_1 L_2 L_3$, L_4, thanks to the analysis carried out in Section 5.5.

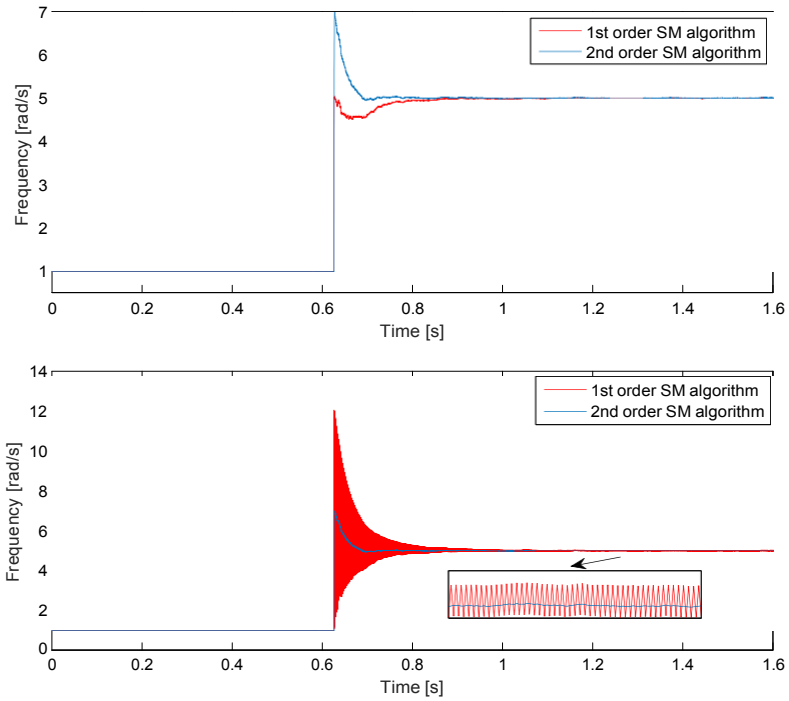

Fig. 5.3 Time-behavior of the estimated frequency by using the proposed method and the method [85] in noisy scenario: Top: 4-th order Runge-Kutta method, Bottom: Euler method.

With reference to the results reported in Figs. 5.2 and 5.3, the proposed technique shows superior performance compared to the one in [85] when a simple Euler discretization is employed whereas using a Runge-Kutta discretization, the two algorithms show similar performance.

In Figs. 5.4, the estimated sinewave reconstructed by $\hat{y}(t) = \hat{A}\sin\hat{\phi}(t)$ are shown using the Runge-Kutta discretization procedure. It is worth noting that the proposed method succeeds in detecting the amplitude and the phase, thereby recovering the pure sinusoidal signal by the amplitude and phase estimates within a very short transient period and a high level of noise immunity in the presence of bounded disturbance .

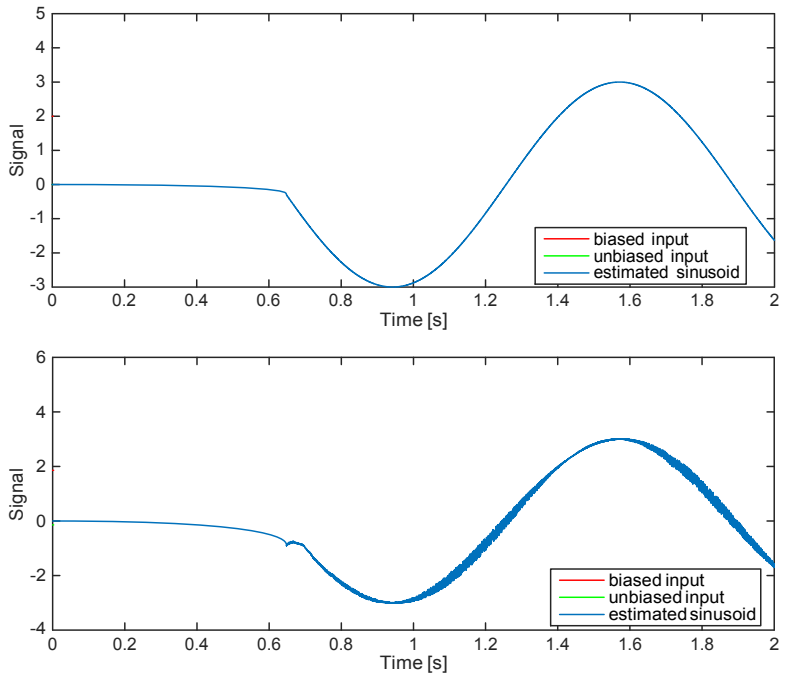

Fig. 5.4 Time-behavior of the reconstructed pure sine-wave by using the proposed method in noise-free and noisy scenarios.

Example 2: In this second more challenging example, the behavior of the proposed method is compared with the modulating function-based estimator proposed in [33] and the first order sliding mode approach [85].

Consider a biased and noisy sinusoidal signal

$$v(t) = A_0(t) + A(t)\sin(2\pi f(t)\, t) + d(t),$$

where the amplitude, frequency and the offset change over time according to the following pattern: $A(t) = 10$, $f(t) = 50$Hz, $A_0(t) = 1$, $0 \leq t < 0.5$, $A(t) = 12$, $f(t) = 52$Hz, $A_0(t) = 0.8$, $0.5 \leq t < 1$. $d(t)$ is a signal with uniform distribution in the interval $[-0.5, 0.5]$. The parameters of the method in [33] are set as $T = \pi/10$, $n = 500$, $\mu = 0.99$, $K = 6$. Method [85] implements three kernels having parameters: $\beta_1 = 50$, $\beta_2 = 80$, $\beta_3 = 100$, $\bar{\beta} = 60$, while $g = 30$, $L = 1.2 \times 10^6$. The proposed method is equipped with the same kernels as the 1-st order SM algorithm [85], whereas $g = 30$, $g_a = 100$, $L_1 = 2 \times 10^4$, $L_2 = 20$, $L_3 = 1 \times 10^5$ and $L_4 = 50$.

In principle, the method given in [33] identifies the true frequency “instantaneously" as it is enabled, whereas the proposed method achieves finite-time convergence with tunable convergence rate determined by the parameter L_1, L_2. It is worth noting from Fig. 5.5 that

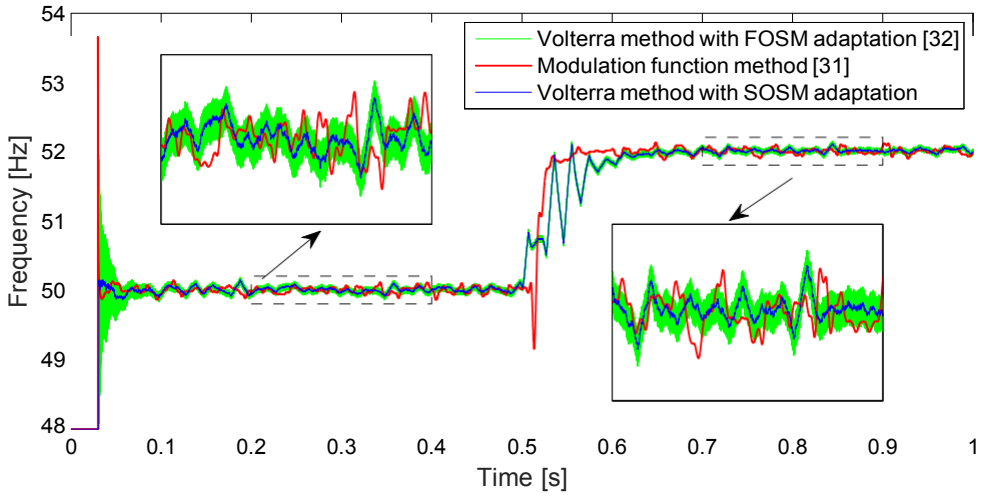

Fig. 5.5 Time-behavior of the estimated frequency by using the proposed method (blue line) compared with the time behaviors of the estimated frequency by the finite-time method [33] (red line) and the 1-st order SM method [85] (green line) respectively.

they are tuned with similar response to the initial frequency and the same initial condition $\hat{f}(0) = 48\text{Hz}$ for fair comparison. Although all the methods deal with the frequency step in a very fast manner, the proposed estimator performs slightly better in terms of robustness against bounded disturbances. Indeed, the chattering phenomenon in steady state is significantly mitigated by using a higher order sliding mode adaptation scheme.

Example 3: In this example, a comparison concerning the frequency estimation is carried out between the presented method and a recently proposed method [79] also addressing finite-time frequency estimation. Consider the biased signal used in the example reported in [79]

$$y(t) = 2 + 3\sin(4t + \pi/4) \tag{5.55}$$

with unknown sinusoidal parameters. The adaptation law of method [79] is initialized by $\hat{\Theta}_1(0) = [0, 0, 0]^\top$, while the learning gain and other coefficients are set as $\Gamma_1 = \text{diag}([50, 500, 500])$, $\lambda_1 = 2.5$, $\lambda_2 = 5$, $l = 1$, $\kappa = 0.001$. On the other hand, the proposed method is tuned by $\beta_1 = 1$, $\beta_2 = 2$, $\beta_3 = 3$, $\bar{\beta} = 2.5$, $g = 3$, $L_1 = 30$, $L_2 = 2$, $\delta_\epsilon = 1 \times 10^{-4}$ and the same initial frequency estimate $\hat{\omega}(0) = \sqrt{5}$. The behavior of both methods is shown in a noise-free scenario and in the case of noisy measurements where the noise has the same characteristics as in the previous example (see Fig. 5.6). As can be noticed, the proposed method compares favorably with the one in [79].

Unlike the algorithm illustrated in [79] where the (unknown) initial conditions of the signal generators' state significantly affect the estimates during the transient, the proposed

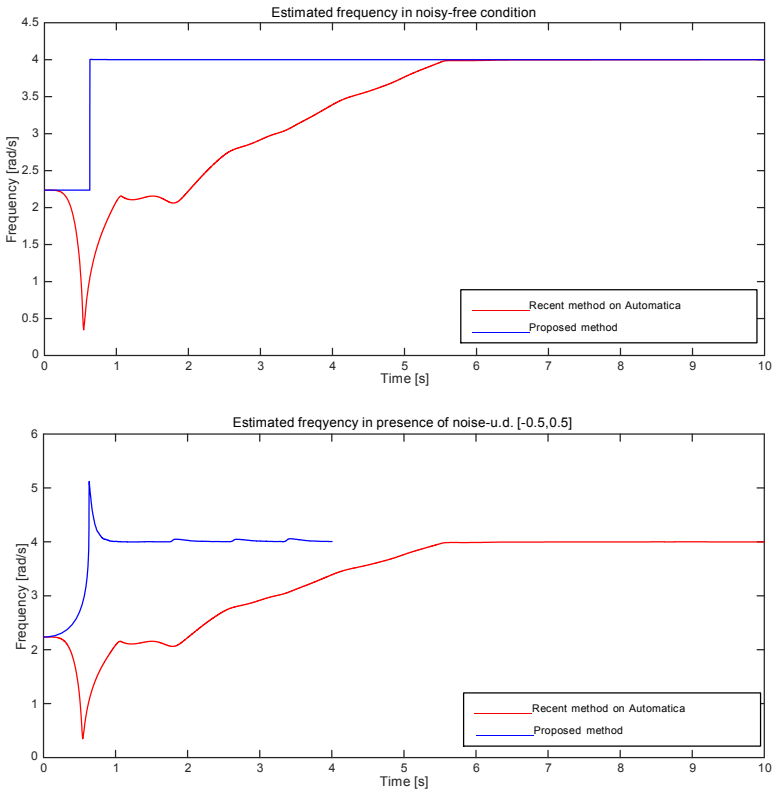

Fig. 5.6 Time-behavior of the estimated frequency by using the proposed method (blue line) compared with the time behaviors of the estimated frequency obtained by the method [79] (red line) respectively. Top: noise-free case. Bottom: noisy case.

estimation methodology inherently annihilates the initial conditions. To enhance this significant feature, in Fig. 5.6 two simulations referred to different initial conditions but using the same input signal (5.55) are reported. As can be noticed, the proposed method yields in finite-time the same estimate of the frequency, irrespective of the initial conditions.

5.8 Concluding Remarks

In the this chapter, the problem of AFP identification from a noisy and biased measurement has been addressed. With the aim of addressing the challenging issue, we introduce a novel deadbeat estimator, which can provide reliable frequency estimates within an arbitrary small finite time. The method consists in processing the measured signal with Volterra operators, to obtain auxiliary signals that are used in combination with second-order sliding mode adaptation laws to estimate the frequency, the amplitude and the phase of the original signal. This algorithm has been proved to be finite-time convergent in nominal condition and enjoys

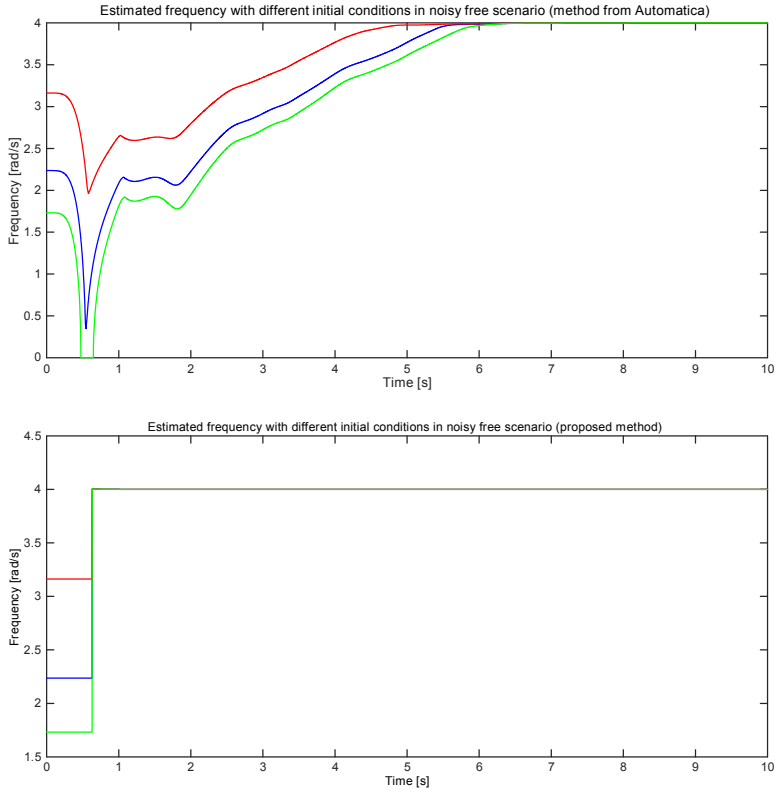

Fig. 5.7 Time-behavior of the estimated frequency with different initial conditions and in a noise-free scenario. Left: the estimator proposed in [79]. Right: the proposed method.

ISS stability properties with respect to bounded measurement perturbations. Numerical examples have been reported showing the effectiveness of the proposed method compared to recently published results.

Chapter 6

CONCLUSIONS AND FUTURE PROSPECTS

6.1 Concluding Remarks

Parameter estimation of a sinusoidal signal perturbed by additive disturbances has been accomplished by a wide variety of techniques in the literature including extended Kalman filters, phase locked loop tools, adaptive notch filtering and internal model based techniques. This thesis first of all provides a thorough review of the literature with special emphasis on several representative approaches, such as KF, PLL, ANF, SVF and AO, which are all characterized by asymptotic convergence. On the other hand, AFP estimators that can converge within a (possibly very small) finite time represent a special category that is seldom discussed and solved so far. The available methods are mainly devised by two strategies: algebraic derivative and modulating functions, whereas there is a lack of the theoretical investigation for the convergence properties in the presence of bounded measurement noise. Besides, as mentioned in Chapter 1.3 research challenges also consist in other aspects (e.g., global stability, accuracy, multi-frequency estimation), which are studied herein.

In this thesis, the problem of adaptive estimation of the characteristics of a single sinusoidal signal from a measurement affected by structured and unstructured disturbances is addressed. Thanks to the proposed pre-filtering technique, the structured disturbances that belong to a class of time-polynomial signals incorporating both bias and drift phenomena can be tackled in a unified manner. We basically propose two *asymptotic* methods designed respectively by adaptive observer and state variable filtering tools. In the estimation context presented in the thesis, the "instantaneous" persistency of excitation condition is embedded in the proposed algorithms rather than the standard "integral" type PE condition. This is a very

significant feature in terms of on-line implementation, since it makes it possible to enhance the performance when the system is weakly excited resorting a typical excitation-based switching algorithm without the need for on-line approximate computation of integrals. The stability of the devised AFP systems are analyzed by an ISS analysis, whereby we induce a few tuning guidelines for the adjustable parameters of the proposed algorithms, depending on the assumed noise level and on the required asymptotic accuracy. More specifically, the AO scheme has been shown robust even in the presence of multi-harmonics, while the ISS bound depends on the power of the total harmonic contents. The SVF approach provides advantages in terms of implementation due to the reduced complexity. From a practical perspective, the discretized algorithm is subject to a steady-state bias, motivated by which a post-correction formula is devised for the compensation under Euler discretization method.

The AO system for a single sine wave has also been extended into a generic structure for estimating amplitudes, frequencies and phases of biased multi-sinusoidal signals in the presence of bounded perturbations on the measurement. The key aspect of advantages over existing tools is the realization of direct detection of the unknown frequencies with ISS stability guarantee. On the other hand, thanks to the individual excitation-based switching logic embedded in the update laws regarding each frequency component, the problem of overparametrization is addressed.

Finally, a novel *finite-time* convergent estimation technique is proposed for AFP identification of a single sinusoidal signal. Resorting to Volterra integral operators with suitably designed kernels, the measured signal is processed, yielding a set of auxiliary signals, in which the influence of the unknown initial conditions is removed. A second-order sliding mode-based adaptation law–fed by the aforementioned auxiliary signals–is designed for finite-time estimation of the frequency, amplitude, and phase. The main contribution lies in the characterization of the worst case behavior in the presence of the bounded additive disturbances by ISS arguments.

The effectiveness of the proposed estimation approaches has been examined and compared with other existing tools via extensive numerical simulations. Experimental results are provided as well for the sake of evaluation in real-time.

6.2 Future Work

This section is devoted to highlight possible extensions of the presented methodologies. These extensions can be explored in two directions: more comprehensive theory and possible applications. From a theoretical point of view, the robustness characterization carried out so far only accounts for the measurements corrupted by bounded disturbances. Future research

efforts could be devoted to a probabilistic analysis of the algorithms with respect to white and colored noises with the aim of establishing a relationship between the accuracy and signal-to-noise ratio (SNR). Moreover, it is worth to establish the discrete-time counterparts of the devised algorithms in an entire discrete-time framework, so that we can avoid problems due to discretization (e.g., discretization error in state state, performance discrepancy due to distinct discretization policy). In the context of deadbeat AFP estimation, future work includes the design of novel kernels as well as the comparative analysis in terms of few aspects, such as robustness, tuning of weighting factors and complexity. This may lead to the evaluation in some real-world scenarios.

Concerning the potential application of the proposed techniques, two main research directions can be pursued in the future: output regulation of a linear or nonlinear system and condition (vibration) monitoring of mechanical systems. More specifically, in many practical situations, the frequencies of the external signals are not precisely available, for example, the periodic disturbances in rotational machinery. In this respect, it turns out that an adaptive learning scheme for updating the profiles of unknown sinusoidal or periodic signals is a premise of disturbance cancellation strategies, thus motivating us to embed the proposed estimators in regulators, such as internal model principle and feedforward compensator. On the other hand, the process of oscillations of a machine in operation is described by mechanical vibrations, which reflect the condition of the system. A typical example is a ball bearing that is a type of rolling-element bearing widely used in various of machinery. The healthy monitoring of a ball bearing system consists in identifying the bearing faults induced by different factors, such as excessive loads, over heating and corrosion. The cornerstone behind this idea is the vibration analysis based on the on-line frequency detection that can be dealt with by the multi-sinusoidal estimator. Finally, in the specific applications that require the estimates to converge in a neighborhood of the true values within a predetermined finite time, independently from the unknown initial conditions, the deadbeat AFP estimator may turns out to be very useful by providing nearly instantaneous estimates.

References

[1] Aranovskii, S. V., Bobtsov, A. A., Kremlev, A. S., and Luk'yanova, G. V. (2007). A robust algorithm for identification of the frequency of a sinusoidal signal. *Journal of Computer and Systems Sciences International*, 46(3):371–376.

[2] Aranovskiy, S., Bobtsov, A., Kremlev, A., Nikolaev, N., and O.Slita (2010). Identification of frequency of biased harmonic signal. *European J. Control*, 2:129–139.

[3] Best, R. E. (1999). *Phase-Locked Loops, Design, Simulation, and Applications*. New York: McGraw-Hill, 4th edition.

[4] Bhat, S. P. and Bernstein, D. S. (2000). Finite-time stability of continuous autonomous systems. *SIAM J. Control Optim.*, 38(3):751–766.

[5] Bittanti, S., Campi, M., and Savaresi, S. (1997). Unbiased estimation of a sinusoid in colored noise via adapted notch filters. *Automatica*, 33(2):209–215.

[6] Bittanti, S. and Savaresi, S. (2000). On the parametrization and design of an extended kalman filter frequency tracker. *IEEE Trans. on Automatic Control*, 45(9):1718–1724.

[7] Bobtsov, A. A. (2008). New approach to the problem of globally convergent frequency estimator. *Int. J. of Adaptive Control and Signal Processing*, 22(3):306–317.

[8] Bobtsov, A. A., Efimov, D., Pyrkin, A. A., and Zolghadri, A. (2012). Switched algorithm for frequency estimation with noise rejection. *IEEE Trans. on Automatic Control*, 57(9):2400–2404.

[9] Bodson, M. and Douglas, S. (1997). Adaptive algorithms for the rejection of sinusoidal disturbances with unknown frequency. *Automatica*, 33(12):2213–2221.

[10] Bodson, M., Jensen, J. S., and Douglas, S. C. (2011). Active noise control for periodic disturbances. *IEEE Trans. on Control System Technology*, 9(1):200–205.

[11] Bollen, M. (2011). *The Smart Grid: Adapting the power system to new challenges (Synthesis Lectures on Power Electronics)*. Morgan and Claypool Publishers.

[12] Brown, L. J. and Zhang, Q. (2003). Identification of periodic signals with uncertain frequency. *IEEE Trans. on Signal Processing*, 51(6):1538–1545.

[13] Brown, L. J. and Zhang, Q. (2004). Periodic disturbance cancellation with uncertain frequency. *Automatica*, 40(4):631–637.

[14] Burton, T. (2005). *Volterra Integral and Differential Equations*. Elsevier.

[15] Carnevale, D. and A.Astolfi (2008). A minimal dimension observer for global frequency estimation. In *Proc. IEEE American Control Conference*, pages 5269–5274, Seattle, WA.

[16] Carnevale, D. and Astolfi, A. (2009). Hybrid observer for global frequency estimation of saturated signals. *IEEE Trans. on Automatic Control*, 54(10):2461–2464.

[17] Carnevale, D. and Astolfi, A. (2011). A hybrid observer for frequency estimation of saturated multi-frequency signals. In *Proc. of the IEEE Conf. on Decision and Control and European Control Conference*, pages 2577–2582, Orlando, FL, USA.

[18] Carnevale, D., Galeani, S., and A.Astolfi (2010). Hybrid observer for multi-frequency signals. In *Proc.of IFAC workshop Adaptation and Learning in Control and Signal Processing (ALCOSP)*, Bogazici University, Turkey.

[19] Chen, B., Pin, G., Ng, W. M., Hui, S. Y. R., and Parisini, T. (2015a). A parallel prefiltering approach for the identification of a biased sinusoidal signal: Theory and experiments. *Int. J. Adapt. Control Signal Process*.

[20] Chen, B., Pin, G., Ng, W. M., Lee, C. K., Hui, S. Y. R., and Parisini, T. (2014a). An adaptive observer-based switched methodology for the identification of a perturbed sinusoidal signal: Theory and experiments. *IEEE Trans. on Signal Processing*, 62(24):6355–6365.

[21] Chen, B., Pin, G., and Parisini, T. (2013). Adaptive observer-based sinusoid identification: structured and bounded unstructured measurement disturbances. In *Proc. of the IEEE European Control Conference*, pages 2645–2650, Zurich, Switzerland.

[22] Chen, B., Pin, G., and Parisini, T. (2014b). An adaptive observer-based estimator for multi-sinusoidal signals. In *Proc. IEEE American Control Conference*, Portland, OR, USA.

[23] Chen, B., Pin, G., and Parisini, T. (2014c). Robust parametric estimation of biased sinusoidal signals: a parallel pre-filtering approach. In *Proc. of the IEEE Conf. on Decision and Control*, Los Angeles.

[24] Chen, B., Pin, G., and Parisini, T. (2015b). Frequency estimation of periodic signals: an adaptive observer approach. In *Proc. IEEE American Control Conference*, Chicago, IL, USA.

[25] de Souza Ribeiro, L., Saavedra, O., de Lima, S., and de Matos, J. (2011). Isolated microgrids with renewable hybrid generation: The case of lencois island. *IEEE Transactions on Sustainable Energy*, 20(1):1–11.

[26] Delille, G., Francois, B., and Malarange, G. (2012). Dynamic frequency control support by energy storage to reduce the impact of wind and solar generation on isolated power system's inertia. *IEEE Transactions on Sustainable Energy*, 3(4):931–939.

[27] D.L., M.-V., Rodriguez-Angeles, A., and Sira-Ramirez, H. (10-13 Jan. 2009). Robust gpi observer under noisy measurements. *Electrical Engineering, Computing Science and Automatic Control, CCE 2009 6th International Converence*, pages 1–5.

[28] Fedele, G. and Ferrise, A. (2012). Non adaptive second order generalized integrator for identification of a biased sinusoidal signal. *IEEE Trans. on Automatic Control*, 57(7):1838–1842.

[29] Fedele, G. and Ferrise, A. (2014). A frequency-locked-loop filter for biased multi-sinusoidal estimation. *IEEE Trans. on Signal Processing*, 62(5):1125–1134.

[30] Fedele, G., Ferrise, A., and Frascino, D. (2009a). Multi-sinusoidal signal estimation by an adaptive sogi-filters bank. In *15th IFAC Symposium on System Identification*, pages 402–407.

[31] Fedele, G., Ferrise, A., and Muraca, P. (2011). An adaptive quasi-notch filter for a biased sinusoidal signal estimation. In *IEEE International Conference on Control and Automation (ICCA)*, pages 1060–1065, Santiago.

[32] Fedele, G., Ferrise, A., and Muraca, P. (2014). An adaptive "quasi" repetitive controller for the fundamental frequency estimation of periodic signals. In *19th World Congress the International Federation of Automatic Control*, pages 12098–12103.

[33] Fedele, G. and L.Coluccio (2010). A recursive scheme for frequency estimation using the modulating function method. *Applied Mathematics and Computation* , 216(5):1393–1400.

[34] Fedele, G., Picardi, C., and Sgro, D. (2009b). A power electrical signal tracking strategy based on the modulating functions method. *IEEE Transactions on Industrial Electronics*, 56(10):4079–4087.

[35] Feola, L., Langella, R., and Testa, A. (2013). On the effects of unbalances, harmonics and interarmonics in pll systems. *IEEE Trans. on Instrum. and Meas.*, 62(9):2399–2409.

[36] Filippov, A. F. (1988). *Differential equations with discontinuous right-hand sides*. Dordrecht, Boston, London: Kluwer Academic Publishers.

[37] Francis, B. and Wonham, B. (1976). The internal model principle of control theory. *Automatica*, 12(5):457–465.

[38] Francis, B. and Wonham, W. (1975). The internal model principle for linear multivariable regulators. *Applied Mathematics and Optimization*, 2:170–194.

[39] Fu, H. and Kam, P. Y. (2007). Map/ml estimation of the frequency and phase of a single sinusoid in noise. *IEEE Trans. on Signal Processing*, 55(3):834–845.

[40] Furthmüller, C., Colaneri, P., and Re, L. D. (2012). Adaptive robust stabilization of continuous casting. *Automatica*, 48(1):225–232.

[41] Gardner, F. (2005). *Phaselock Techniques*. New York/Oxford: Wiley Blackwell.

[42] Goebel, R. and Teel, A. R. (2006). Solutions to hybrid inclusions via set and graphical convergence with stability theory applications. *Automatica*, pages 573–587.

[43] Guo, X. and Bodson, M. (2003). Frequency estimation and tracking of multiple sinusoidal components. In *Proc. of the IEEE Conf. on Decision and Control*, Maui, Hawaii, USA.

[44] Hajimolahoseini, H., Taban, M. R., and Soltanian-Zadeh, H. (2012). Extended kalman filter frequency tracker for nonstationary harmonic signals. *Measurement*, 45(1):126–132.

[45] Hou, M. (2005). Amplitude and frequency estimation of a sinusoid. *IEEE Trans. on Automatic Control*, 50(6):855–858.

[46] Hou, M. (2007). Estimation of sinusoidal frequencies and amplitudes using adaptive identifier and observer. *IEEE Trans. on Automatic Control*, 52(3):493–499.

[47] Hou, M. (2012). Parameter identification of sinusoids. *IEEE Trans. on Automatic Control*, 57(2):467–472.

[48] Hsieh, G. C. and Hung, J. C. (1996). Phase-locked loop techniques-a survey. *IEEE Trans. on Industrial Electronics*, 43(6):609–615.

[49] Hsu, L., Ortega, R., and Damm, G. (1999). A globally convergent frequency estimator. *IEEE Trans. on Automatic Control*, 44(4):698–713.

[50] Huang, C. H., Ch.H. Lee, K. S., and Wang, Y. (2008). Frequency estimation of distorted power system signals using a robust algorithm. *IEEE Trans. on Power Delivery*, 23(1):41–51.

[51] Ioannou, P. and Fidan, B. (2006). *Adaptive Control Tutorial*. SIAM, Boston, MA.

[52] Ioannou, P. and Sun, J. (1996). *Robust Adaptive Control*. Pretice Hall, Boston, MA.

[53] Karimi, H., Karimi-Ghartemani, M., and Iravani, M. R. (2004). Estimation of frequency and its rate of change for applications in power systems. *IEEE Trans. on Power Delivery*, 19(2):472–480.

[54] Karimi-Ghartemani, M. and Iravani, M. R. (2002). A nonlinear adaptive filter for online signal analysis in power systems: Applications. *IEEE Trans. on Power Delivery*, 17(2):617–622.

[55] Karimi-Ghartemani, M. and Iravani, M. R. (2005). Measurement of harmonics/inter-harmonics of time-varying frequencies. *IEEE Trans. on Power Delivery*, 20(1):23–31.

[56] Karimi-Ghartemani, M., Karimi, H., and Bakhshai, A. R. (2009). A filtering technique for three-phase power systems. *IEEE Trans. on Instrum. and Meas.*, 58(2):389–396.

[57] Karimi-Ghartemani, M., Karimi, H., and Iravani, M. R. (2004a). A magnitude/phase-locked loop system based on estimation of frequency and in-phase/quadrature-phase amplitudes. *IEEE Trans. on Industrial Electronics*, 51(2):511–517.

[58] Karimi-Ghartemani, M., Khajehoddin, S. A., Jain, P. K., Bakhshai, A., and Mojiri, M. (2012). Addressing dc component in pll and notch filter algorithms. *IEEE Trans. on Power Electronics*, 27(1):78–86.

[59] Karimi-Ghartemani, M., Mokhtari, H., and Iravani, M. R. (2000). Wavelet based on-line disturbance detection for power quality applications. *IEEE Trans. on Power Delivery*, 15(4):1212–1220.

[60] Karimi-Ghartemani, M., Mokhtari, H., Iravani, M. R., and Sedighy, M. (2004b). A signal processing system for extraction of harmonics and reactive current of single-phase systems. *IEEE Trans. on Power Delivery*, 19(3):979–986.

[61] Karimi-Ghartemani, M. and Ziarani, A. K. (2003). Periodic orbit analysis of two dynamical systems for electrical engineering applications. *Journal of Engineering Mathematics*, 45(2):135–154.

[62] Karimi-Ghartemani, M. and Ziarani, A. K. (2004). A nonlinear time-frequency analysis method. *IEEE Trans. on Signal Processing*, 52(6):1585–1595.

[63] Khalil, H. (2001). *Nonlinear Systems*. Prentice Hall.

[64] Kim, S. and Y.Park (1999). Active control of multi-tonal noise with reference generator based on on-line frequency estimator. *Journal of Sound and Vibration*, 227(3):646–666.

[65] Liu, D., Gibaru, O., and Perruquetti, W. (2011). Parameters estimation of a noisy sinusoidal signal with time-varying amplitude. In *Proc. 19th Mediterranean conference on Control and automation (MED'11)*, pages 570 – 575, Corfu.

[66] Luviano-Juarez, A., Cortes-Romero, J., and Sira-Ramirez, H. (2015). Parameter identification of a discretized biased noisy sinusoidal signal. *Measurement*, 60:129–138.

[67] Marino, R. and P.Tomei (2002). Global estimation of n unknown frequencies. *IEEE Trans. on Automatic Control*, 47(8):1324–1328.

[68] Marino, R., Santosuosso, G. L., and Tomei, P. (2003). Robust adaptive compensation of biased sinusoidal disturbances with unknown frequency. *Automatica*, 39:1755–1761.

[69] Marino, R. and Tomei, P. (2014). Frequency estimation of periodic signals. In *Proc. of the IEEE European Control Conference*, Strasbourg.

[70] Mark, J. G., Steele, J. R., and Hansen, C. C. (1982). Residual mode phase locked loop. *U.S. Patent*.

[71] Mojiri, M. and Bakhshai, A. (2007a). Stability analysis of periodic orbit of an adaptive notch filter for frequency estimation of a periodic signal. *Automatica*, 43(3):450–455.

[72] Mojiri, M. and Bakhshai, A. R. (2004). An adaptive notch filter for frequency estimation of a periodic signal. *IEEE Trans. on Automatic Control*, 49(2):314–318.

[73] Mojiri, M. and Bakhshai, A. R. (2007b). Estimation of n frequencies using adaptive notch filter. *IEEE Trans. on Circuits and Systems-II*, 54(4):338–342.

[74] Mojiri, M., Karimi-Ghartemani, M., and Bakhshai, A. (2007a). Estimation of power system frequency using an adaptive notch filter. *IEEE Trans. on Instrum. and Meas.*, 56(6):2470–2477.

[75] Mojiri, M., Karimi-Ghartemani, M., and Bakhshai, A. (2007b). Time-domain signal analysis using adaptive notch filter. *IEEE Trans. on Signal Processing*, 55(1):85–93.

[76] Mojiri, M., Karimi-Ghartemani, M., and Bakhshai, A. (2010a). Processing of harmonics and interharmonics using an adaptive notch filter. *IEEE Trans. on Power Delivery*, 25(2):534–542.

[77] Mojiri, M., Yazdani, D., and Bakhshai, A. (2010b). Robust adaptive frequency estimation of three-phase power systems. *IEEE Trans. on Instrum. and Meas.*, 59(7):1793–1802.

[78] Moreno, J. A. and Osorio, M. (2012). Strict lyapunov functions for the super-twisting algorithm. *IEEE Trans. on Automatic Control*, 57(4):1035–1040.

[79] Na, J., Yang, J., Wu, X., and Guo, Y. (2015). Robust adaptive parameter estimation of sinusoidal signals. *Automatica*, 53:376–384.

[80] Obregon-Pulido, G., Castillo-Toledo, B., and Loukianov, A. (2002). A globally convergent estimator for n-frequencies. *IEEE Trans. on Automatic Control*, 47(5):857–863.

[81] Pei, S.-C. and Chien-ChengTseng (1994). Real time cascade adaptive notch filter scheme for sinusoidal parameter estimation. *Signal Processing*, 39(1-2):117–130.

[82] Pin, G. (2010). A direct approach for the frequency-adaptive feedforward cancellation of harmonic disturbances. *IEEE Trans. on Signal Processing*, 58(7):3513–3530.

[83] Pin, G., Assalone, A., Lovera, M., and Parisini, T. (2015 (to appear)). Non-asymptotic kernel-based parametric estimation of continuous-time linear systems. *IEEE Trans. on Automatic Control*.

[84] Pin, G., Chen, B., and Parisini, T. (2013a). A nonlinear adaptive observer with excitation-based switching. In *Proc. of the 52nd Conference on Decision and Control*, pages 4391–4398, Florence.

[85] Pin, G., Chen, B., and Parisini, T. (2015). Deadbeat kernel-based frequency estimation of a biased sinusoidal signal. In *Proc. of the IEEE European Control Conference*, Linz.

[86] Pin, G., Chen, B., Parisini, T., and Bodson, M. (2014). Robust sinusoid identification with structured and unstructured measurement uncertainties. *IEEE Trans. on Automatic Control*, 59(6):1588–1593.

[87] Pin, G., Lovera, M., Assalone, A., and Parisini, T. (2013b). Kernel-based non-asymptotic state estimation for linear continuous-time system. In *Proc. of the IEEE American Control Conference*, pages 3123 – 3128, Washing, DC.

[88] Pin, G. and Parisini, T. (2011). A direct adaptive method for discriminating sinusoidal components with nearby frequencies. In *Proc. of the IEEE American Control Conference*, pages 2994–2999, O'Farrell Street, San Francisco, CA, USA.

[89] Pin, G., Parisini, T., and Bodson, M. (2011). Robust parametric identification of sinusoisal signals: an input-to-state stability approach. In *Proc. of the IEEE Conf. on Decision and Control*, pages 6104–6109, Orlando, FL.

[90] Pyrkin, A. A., Bobtsov, A. A., Efimov, D., and Zolghadri, A. (2011). Frequency estimation for periodical signal with noise in finite time. In *Proc. of the IEEE Conf. on Decision and Control*, pages 3646–3651, Orlando, FL.

[91] Ramos, P. M. and Serra, A. C. (2009). Comparison of frequency estimation algorithms for power quality assessment. *Measurement*, 42:1312–1317.

[92] Regalia, P. (1991). An improved lattice-based adaptive iir notch filter. *IEEE Trans. on Signal Processing*, 39(9):2124–2128.

[93] Regalia, P. A. (2010). A complex adaptive notch filter. *IEEE Signal Processing Letters*, 17(11):937–940.

[94] Rodríguez, P., J. Pou, J. B., Candela, J. I., Burgos, R. P., and Boroyevich, D. (2007). Decoupled double synchronous reference frame pll for power converters control. *IEEE Trans. on Power Electronics*, 22(2):584–592.

[95] Routray, A., Pradhan, A., and Rao, P. (2002). A novel kalman filter for frequency estimation of distorted signal in power systems. *IEEE Trans. on Instrum. and Meas.*, 51(3):469–479.

[96] Sastry, S. and Bodson, M. (1994). *Adaptive Control: Stability, Convergence, and Robustness*. Prentice-Hall.

[97] Scala, B. L. and Bitmead, R. (1996). Design of an extended kalman filter frequency tracker. *IEEE Trans. on Signal Processing*, 44(3):739–742.

[98] Scala, B. L., Bitmead, R., and James, M. R. (1995). Conditions for stability of the extended kalman filter and their application to the frequency tracking problem. *Math. Control, Signals, and Syst.*, 8(1):1–26.

[99] Scala, B. L., Bitmead, R., and Quinn, B. (1996). An extended kalman filter frequency tracker for high-noise environments. *IEEE Trans. on Signal Processing*, 44(2):431–434.

[100] Sharma, B. B. and Kar, I. N. (2008). Design of asymptotically convergent frequency estimator using contraction theory. *IEEE Trans. on Automatic Control*, 53(8):1932–1937.

[101] Snyder, D. L. (1969). *The State-Variable Approach to Continuous Estimation with Applications to Analog Communications Theory*. MIT Press, Boston, MA.

[102] So, H. C., Chan, F. K. W., and Sun, W. (2011). Subspace approach for fast and accurate single-tone frequency estimation. *IEEE Trans. on Signal Processing*, 59(2):827–831.

[103] Stephens, D. R. (1998). *Phase-Locked Loops for Wireless Communications, Digital and Analog Implementations*. Dordrecht, The Netherlands: Kluwer.

[104] Tao, G. and Ioannou, P. A. (1990). Persistency of excitation and overparametrization in model reference adaptive control. *IEEE Trans. on Automatic Control*, 35(2):254–256.

[105] Tedesco, F., Casavola, A., and Fedele, G. (2013). Discrete-time frequency-locked-loop filters for parameters estimation of sinusoidal signals. In *Proc. of the 52nd Conference on Decision and Control*, pages 4399–4404, Florence.

[106] Trapero, J. R., Sira-Ramirez, H., and Battle, V. F. (2007a). An algebraic frequency estimator for a biased and noisy sinusoidal signal. *Signal Processing*, 87(6):1188–1201.

[107] Trapero, J. R., Sira-Ramirez, H., and Battle, V. F. (2007b). A fast on-line frequency estimator of lightly damped vibrations in flexible structures. *Journal of Sound and Vibration*, 307(1-2):365–378.

[108] Trapero, J. R., Sira-Ramirez, H., and Battle, V. F. (2008). On the algebraic identification of the frequencies, amplitudes and phases of two sinusoidal signals from their noisy sum. *International Journal of Control*, 81(3):507–518.

[109] Tsao, T., Qian, Y., and Nemani, M. (2000). Repetitive control for asymptotic tracking of periodic signals with an unknown period. *J. Dyn. Syst. Meas. Contr.*, 122(2):364–369.

[110] Wu, B. and Bodson, M. (2003). A magnitude/phase-locked loop approach to parameter estimation of periodic signals. *IEEE Trans. on Automatic Control*, 48(4):612–618.

[111] Xia, X. (2002). Global frequency estimation using adaptive identifiers. *IEEE Trans. on Automatic Control*, 47(7):1188–1193.

[112] Yasuda, K. and Hirai, K. (1979). Upper and lower bounds on the solution of the algebraic matrix riccati and lyapunov equation. *IEEE Trans. on Automatic Control*, 24(6):483–487.

[113] Zhang, Q. and Brown, L. J. (2006). Noise analysis of an algorithm for uncertain frequency identification. *IEEE Trans. on Automatic Control*, 51(1):103–110.

[114] Zhao, L., Huang, J., Liu, H., Li, B., and Kong, W. (2014). Second-order sliding-mode observer with online parameter identification for sensorless induction motor drives. *IEEE Transactions on Industrial Electronics*, 61(10):5280–5289.

[115] Ziarani, A. K. and Karimi-Ghartemani, M. (2005). On the equivalence of three independently developed phase-locked loops. *IEEE Trans. on Automatic Control*, 50(2):2021–2027.

[116] Ziarani, A. K. and Konrad, A. (2004). A method of extraction of nonstationary sinusoids. *Signal Processing*, 84(8):1323–1346.